On Cooperation, Energy Harvesting, and Security in Cognitive Radio Networks

A Thesis Submitted

in Partial Fulfillment of the Requirements

for the Degree of

Doctor of Philosophy

by

Sanket Sanjay Kalamkar

to the

DEPARTMENT OF ELECTRICAL ENGINEERING

INDIAN INSTITUTE OF TECHNOLOGY,KANPUR

May 2016

CERTIFICATE

It is certified that the work contained in the thesis entitled "*On Cooperation, Energy Harvesting, and Security in Cognitive Radio Networks*" by *Sanket Sanjay Kalamkar* has been carried out under my supervision and that this work has not been submitted elsewhere for a degree.

May 2016

Adrish Banerjee
Associate Professor,
Department of Electrical Engineering,
Indian Institute of Technology,
Kanpur-208016.

Abstract

Due to the limited availability and rigid allocation of the spectrum, it has become difficult to accommodate the emerging wireless applications. This thesis explores one of the key enablers of the next-generation wireless networks leveraging the dynamic spectrum sharing, namely cognitive radio. To show the effectiveness of cognitive radio and the challenges associated with it, this thesis forays into three aspects of cognitive radio: 1) Cooperation; 2) energy harvesting; 3) security. Based on spectrum sharing modes in cognitive radio, we organize this thesis in three parts.

The first part of the thesis focuses on the overlay mode, where an energy harvesting secondary network helps the primary network relay the information and in turn gets the spectrum access as a reward for the cooperation. With only information cooperation between primary and secondary networks, we first provide the optimal resource allocation policy that maximizes the secondary user sum-throughput and address the issue of fairness at the user level. We then consider information as well as energy cooperation between primary and secondary networks over a finite horizon, where we show the improvement in rate regions due to this two-level cooperation.

The second part of the thesis focuses on the underlay mode, where secondary users seek help from an intermediate node to facilitate their communication under the primary's interference constraint. We first analyze the outage performance of the secondary network with the cooperation from energy harvesting relays. We then investigate the secure communication via an untrusted energy harvesting relay and provide design insights to obtain positive secrecy rate. Third, in a non-energy harvesting scenario, we perform outage analysis for the secondary network with direct-link assisted relaying under the primary's interference.

The third part of the thesis focuses on the interweave mode. We first study conventional energy detection based cooperative spectrum sensing in the presence of malicious users that send falsified spectrum sensing data. We propose an outlier method based on Dixon's test to find a malicious user and remove it from the cooperation. We then consider improved energy detection, where a positive power operation p replaces the squaring operation in conventional energy detection. We analyze its spectrum sensing performance with multiple-antennas and study the effect of antenna correlation on the optimum value of p.

To Late Mrs. Shukla Madam..

Acknowledgements

This has been a long and sometimes an arduous journey. It would have been longer or even impossible without the support from many individuals.

I would like to express my gratitude towards my advisor Prof. Adrish Banerjee for providing me complete freedom to pursue my research interests. I thank him for his invaluable guidance throughout my thesis. He has gone out of his way to ensure that I had every opportunity: to learn, travel, and present at conferences. His support went beyond academic.

I would also like to thank Prof. Ketan Rajawat, Prof. Aditya Jagannatham, and Prof. Ajit K. Chaturvedi for insightful technical discussions and feedback on my work. I thank Prof. Rajawat for drawing on his wealth of knowledge to give high-level ideas that led to the work on resource allocation in wireless powered cognitive radio (Chapter 2). I also thank Prof. Jagannatham for the excellent course on Wireless Communications he taught me and for the memorable time I had with him during our basketball games. I would also like to thank all my coauthors and collaborators during my PhD thesis: Prof. Rajawat, Jeya Pradha J, Abhishek K. Gupta, Hrusikesha Pradhan, Subhajit Majhi, Praveen K. Singh, Vipul Gupta, and Ananya Roychowdhury.

Wireless Communications, Coding, and Cognitive radio laboratory (WC3 Lab) has been my academic home during PhD. I am particularly indebted to three individuals, Jeya Pradha J, Kedar Kulkarni, and Kalpant Pathak, who have been always ready to have technical and non-technical discussions, and for putting up with my idiosyncrasies. Jeya has been my main collaborator over the past three years. The collaboration was always enjoyable and fruitful. Kedar has provided encouragement when the going got tough. I am thankful to Kalpant for his insightful thoughts on optimization techniques, and he has been awesome in keeping lively environment in the lab. I also want to thank other members of WC3 Lab including Onkar Pandit, Ravikiran Bhonagiri, Partha Swain, Anirudh Palle, Hrusikesha Pradhan, Nitish Gupta, Pranav Sakulkar, Vivek G, Praveen Singh, Gaurav Agarwal, Abhishek Gupta, Chandrashekar Goud, Abhishek Srivastava, Manoj Gowda, Shailendra Kumar, Sudhakar Reddy, Ayush Kumar, Gourab Ghatak, Ayush Agrawal, Swarup Suman Patra, Yogesh Dharmwal, Rahul Joon, Prachi Bansal, and Kusum Kalyani.

My PhD experience has been significantly enhanced through the interactions with other

students of the Department of Electrical Engineering including Ekant Sharma, Prem Rawat, Sachin Kadam, Pushpendra Singh, Om Prakash, Chandrakant Gaikwad, Amrita Mishra, Gayathri R, Abhay Sah, Naveen DV, Adarsh Patel, Sateesh Dhuli, Sinnu Thomas, Sandeep Kumar, Amrit Singh Bedi, Javed Akhtar, Chirag Arora, and Vipul Arora. Thanks to Nikhil Joshi and Ravikant Patil who convinced me to come to IIT Kanpur for the post-graduation studies; otherwise, this acknowledgement and PhD thesis would have never appeared.

I would also like to thank Mrs. Neeru Chabbra and Mr. Vijay Yadav. Mrs. Chhabra has always been kind to inquire about my well-being. Vijay kept lab devices free from technical glitches and his humour maintained a cheerful environment.

I gratefully acknowledge the research fellowship from Tata Consultancy Services (TCS). The generous funding from TCS, Resources and Alumni Office of IIT Kanpur, Department of Science and Technology, and IEEE Communications Society gave me several opportunities to attend and speak at conferences from all over the world.

The members from non-academic life had an enormous role to play to make IIT Kanpur my second home in last seven years. They not only kept me floating through my PhD but also enriched my life with their amazing company. Prachita and Sonali need a special mention who provided tremendous support when they were at IIT Kanpur, and continued it even after they graduated. I got wonderful company to explore travel opportunities. Thanks to my travel guru Prashant. The time with Jalidar, Sushant, Nikhil, Sandeep, Chetan, Prasad, Adwait, Aditya, Nishigandha, Tushar, and Sandip at canteens was one of the most memorable times I spent at IIT Kanpur. Yogesh, Amita, and Gaikwad vahini fed me with delicious Maharashtrian dishes whenever I craved for the home food. Thanks to Navya, Reshma, Soniya, Khushboo, Ilesha, Ranjana, Juhi, and Swamy for being such great friends in a short duration at the end of PhD. I am grateful to employees of Hall 8 mess for the excellent food they provided and for accommodating me in their great team of Cricket.

I am extremely grateful to my parents and sister Sampada for their support through all my endeavors. I envy my parents' patience while I delay adulthood. I am greatly indebted to my aunt Vanita, uncle Raju, cousin Sushil, and in-laws for their unwavering support. And, thank you Jeya, my wife, for everything.

Contents

List of Figures

List of Tables

List of Acronyms

AF	Amplify-and-Forward
AWGN	Additive White Gaussian Noise
BSS	Best SU Selection
BPSK	Binary Phase Shift Keying
BWS	Bi-weight Scale
CCRN	Cooperative Cognitive Radio Network
CDF	Cumulative Distribution Function
CED	Conventional Energy Detector
CR	Cognitive Radio
CSI	Channel State Information
CSS	Cooperative Spectrum Sensing
DAP	Data Access Point
DF	Decode-and-Forward
DPC	Dirty Paper Coding
EAP	Energy Access Point
EE	Energy Efficiency
EH	Energy Harvesting
ETA	Equal Time Allocation
FCC	Federal Communications Commission
HAP	Hybrid Access Point
IED	Improved Energy Detector
KKT	Karush-Kuhn-Tucker

MIMO	Multiple Input Multiple Output
MRC	Maximum Ratio Combining
MTM	Minimum Throughput Maximization
PD	Primary Destination
PDF	Probability Density Function
PS	Power Splitting
PSD	Power Spectral Density
PT	Primary Transmitter
PTA	Proportional Time Access
PU	Primary User
QoS	Quality of Service
QPSK	Quadrature Phase Shift Keying
RF	Radio Frequency
ROC	Receiver Operating Characteristics
RSS	Random SU Selection
ST	Secondary Transmitter
SD	Secondary Destination
SINR	Signal-to-Interference-Noise Ratio
SIR	Signal-to-Interference Ratio
SNR	Signal-to-Noise Ratio
SR	Secondary Relay
SSDF	Spectrum Sensing Data Falsification Attack
STORA	Sum Throughput Optimal Resource Allocation
SU	Secondary User
TDMA	Time Division Multiple Access
TS	Time Switching
WPCN	Wireless Powered Communication Network
WP-CCRN	Wireless Powered Cooperative Cognitive Radio Network
WSPRT	Weighted Sequential Probability Ratio Test

List of Notation

$\triangleq$	defined as equal to ($x \triangleq y$: x is defined as y)
$\approx$	approximately equal to
$\ll$	much less than
$\gg$	much greater than
$\bar{R}_{\mathrm{p}}$	target primary user rate
$\bar{R}_{\mathrm{s}}$	target secondary user rate
η	energy conversion/transfer efficiency
h	channel coefficient
g	channel power gain
N_0	noise Power
Θ_{p}	primary user's outage probability threshold
$\mathbb{P}$	probability
$[x]^+$	$\max(x, 0)$
P_{pk}	peak power
$\mathcal{G}$	SNR gap
$B_{\max}$	finite battery capacity
$\ln(x)$	natural log of x
$\log_2(x)$	the log, base 2, of x
$Q(x)$	Gaussian Q-function
$\mathrm{erfc}(x)$	complementary error function
H_0	null hypothesis

H_1	alternative hypothesis
$\|x\|$	absolute value (amplitude) of x
$\|\mathcal{S}\|$	cardinality of set $\mathcal{S}$
$\mathbb{E}[\cdot]$	expectation operator
$\mathbb{E}[\cdot\|\cdot]$	conditional expectation operator
Ω	mean channel gain
$f_X(x)$	probability density function of random variable X
$F_X(x)$	cumulative distribution function of random variable X
$x!$	factorial of x
$\frac{\partial x}{\partial y}$	derivative of x with respect to y
P_D	probability of detection
P_M	probability of miss detection
P_F	probability of false alarm
$\exp(x)$	e^x
$\mathrm{E}_1(\cdot)$	exponential integral
$\mathcal{B}(\cdot,\cdot)$	Beta function
$\Gamma(\cdot)$	Gamma function
$\Gamma(\cdot,\cdot)$	upper incomplete Gamma function
$\Upsilon(\cdot,\cdot)$	lower incomplete Gamma function
$\mathcal{N}(x,y)$	Gaussian distribution with mean x and variance y
$\mathcal{W}(\cdot)$	Lambert W function

Chapter 1

Introduction

1.1 Introduction to Cognitive Radio

The dramatic advancements in wireless technology in last two decades have given birth to enormous number of new wireless applications in both licensed and unlicensed frequency bands. While on one hand, the current spectrum regulations allow only licensed users to access licensed bands, on the other hand, the unlicensed bands are limited and thus getting too much crowded. Thus the exponential growth in wireless applications at the backdrop of rigid spectrum assignment has created spectrum scarcity. Also the studies by the regulatory bodies like Federal Communications Commission (FCC) have shown that the fixed allocation of spectrum causes its inefficient use and thus underutilizes it in space, time, and frequency domains [1]. This has led to the flurry of research in devising the efficient spectrum management policies.

Given the great variation in the spectrum usage with time and location, the most appropriate way seems to be the dynamic spectrum access policies, as identified in [2, 3, 4, 5]. Out of this need to adjust to the surrounding dynamic radio environment was born the idea of cognitive radio [6]. Cognitive radio adapts its certain operating parameters (e.g., transmit power, carrier frequency, and modulation strategy) by learning in real time [2]. Using advanced radio and signal processing techniques along with flexible and novel spectrum allocation strategies, cognitive radio aims to accommodate new wireless applications in the crowded spectrum without degrading the performance of established wireless users [5]. Thus,

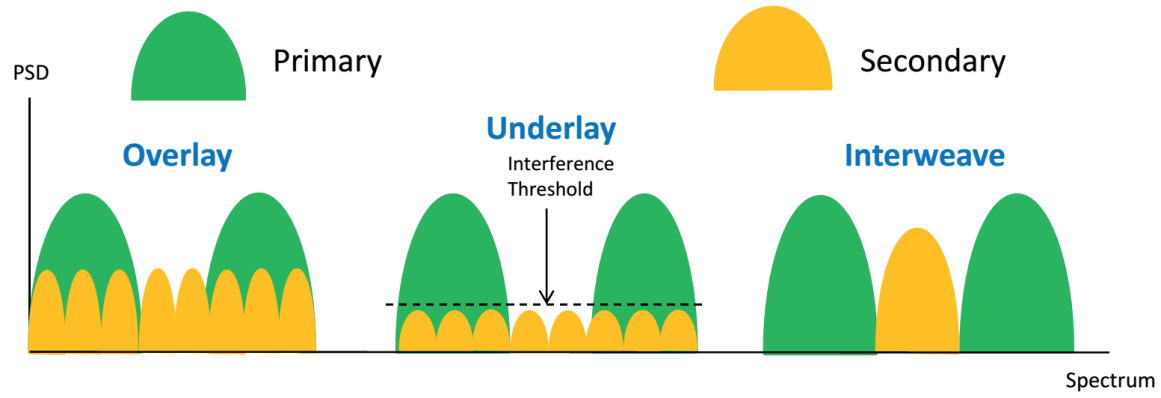

Figure 1.1: Three modes of spectrum sharing in cognitive radio.

cognitive radio can facilitate efficient use of the scarce spectrum by allowing unlicensed users (also called secondary users) to share the spectrum with the licensed user (also called primary user).

The protagonists of this thesis are secondary users (SUs) and primary users (PUs). The SUs wish to access the spectrum that belongs to PUs. There are mainly three modes in which SUs can share the spectrum with PUs [5]:

(a) *Overlay mode*: An SU gets the spectrum access if it maintains or improves PU's quality-of-service (QoS).

(b) *Underlay mode*: An SU can share the spectrum with PU if the interference caused by the former to the latter is below the predefined threshold.

(c) *Interweave mode*: An SU can opportunistically access the vacant spectrum, provided its communication does not interrupt other transmissions.

Fig. 1.1 depicts the aforementioned three modes of cognitive radio, where y-axis corresponds to the power spectral density (PSD) of PU and SU. As Fig. 1.1 shows, the overlay and underlay modes allow both PU and SU to coexist, while the interweave mode allows SU to access only the vacant spectrum. The following section gives a brief overview of these three modes.

1.2 Overview of Cognitive Radio Modes

1.2.1 Overlay Mode

In overlay mode, SU has the knowledge of PU's codebook or message. The information about codebook can be obtained if PU follows standard publicized codebooks for its communication. Also PU itself can periodically broadcast the codebook information. Thus SU can obtain PU message by hearing it for some time and then decoding it. Basically, the enabling premise for the overlay mode is that the SU has PU's message before its transmission begins. Exploiting such knowledge, SU can coexist with PU than competing with it for the spectrum access. For example, the knowledge of PU message can be utilized to eliminate the interference at the secondary destination (SD) by using techniques such as Dirty Paper Coding (DPC) [7, 8, 9]. The other way to exploit PU message knowledge is to improve the quality of PU's communication by transmitting (relaying) it to the primary destination (PD) using a part of the available power [10, 11, 12, 13]. The rest of the power can be used for SU's own transmission. In this case, SU cooperates with PU to maintain or enhance the latter's QoS. As a reward of this cooperation, SU can access the spectrum to transmit its own data. The scenario where SU relays PU message is also called as cooperative cognitive radio network (CCRN).

1.2.2 Underlay Mode

The governing factor in underlay mode is the permissible interference level at PD, which is assumed to be known to SU. Thus SU can have concurrent transmission with that of PU, provided the interference caused to PD by SU's transmission remains below a predefined threshold. To ensure that the interference threshold is met at PD, SU can spread the signal over large bandwidth, as in ultrawideband systems. Also multiple antennas can be used to steer SU's signal away from PD [14]. As shown in Fig. 1.1, due to the unavoidable interference constraint, an SU usually needs to transmit with low power, thus having short communication range.

1.2.3 Interweave Mode

Unlike overlay and underlay modes, the interweave mode requires SU to access the spectrum only if PU is absent, i.e., SU needs to access the spectrum opportunistically. As shown in [1], a major portion of the spectrum is unused in time, frequency, and space domains. Such a vacant spectrum is called *spectrum hole*. These spectrum holes vary with frequency, time, and geographical location, and can be used by SU to access the spectrum without causing interference to legitimate users. For example, depending on the traffic, PU can be busy or idle at a given time. If PU is idle, SU can access the spectrum for its communication. The prerequisite for such opportunistic access is the periodic detection of the spectrum hole. This process of detecting a spectrum hole is known as *spectrum sensing* [15]. Spectrum usage is thus enhanced through the frequency reuse in the spectrum hole. Spectrum sensing needs to be accurate to avoid the miss detection of PU, as it causes interference to the active PU. Similarly, the false alarm denies the spectrum access opportunity to SU even if PU is absent, wasting the spectrum.

In the following section, we discuss the background related to the thesis and the motivation behind this thesis.

1.3 Background and Motivation

Since two heterogeneous networks (primary and secondary networks) coexist in the same frequency band, there can be inter-network as well as intra-network cooperation to facilitate the spectrum sharing between these networks. One of our goals in this thesis is to exploit the possibility of such cooperation. But the cooperation among nodes also raises security concerns. Two security issues that we consider in this thesis are eavesdropping and presence of malicious users. The third goal is to incorporate energy harvesting in cognitive radio. Energy harvesting has potential to avoid the frequent battery replacement and facilitate mobility for wireless users. We aim to integrate energy harvesting in cognitive radio while incorporating cooperation and addressing aforementioned security concerns. Overall, this thesis focuses on aforementioned spectrum sharing modes in cognitive radio mainly from three aspects:

(i) Cooperation

(ii) Security

(iii) Energy Harvesting

We elaborate on these three aspects in detail in the following subsections.

1.3.1 Cooperation in Cognitive Radio

There are a variety of ways in which the cooperation among nodes can be formed in cognitive radio. We discuss below the possible cooperation strategies in the aforementioned spectrum sharing modes.

1.3.1.1 Cooperation in Overlay Mode

As discussed in Section 1.2.1, an SU helps PU relay its message to PD which improves QoS of the primary network. As a reward for this cooperation, the secondary network gets the spectrum access for its transmissions. The reward could be a fraction of PU's bandwidth or time-slot. For example, suppose PU has some fixed amount of data to deliver in a time slot. If SU assists PU relay the data, by exploiting the spatial diversity, the latter could finish its transmission earlier than the intended time. Thus the remaining time of the slot can be rewarded to the secondary network for its use. This cooperation-generated time period creates a spectrum access opportunity for the secondary network, while maintaining QoS of the primary network. Thus the inter-network cooperation brings a win-win situation for both primary and secondary networks.

1.3.1.2 Cooperation in Underlay Mode

Recall that, in underlay mode, the transmit power of an SU is restricted by the interference threshold at PD. Thus, a secondary transmitter (ST) may not be able to reliably send data to its destination due to low power and path-loss if the latter is located far from ST. In such case, ST can seek help from an intermediate node belonging to the secondary network,

called a relay node, to send data to SD.[1] The use of relay node reduces the distance between two nodes and thus allows ST to send data over a longer distance reliably under primary's interference constraint. Thus this intra-network cooperation from the relay improves the coverage and the reliability of the communication.

1.3.1.3 Cooperation in Interweave Mode

In interweave mode, the spectrum sensing (PU detection process) becomes challenging due to fading and shadowing. For example, an SU attempting to sense the spectrum may experience a deep fade channel to the primary transmitter (PT). As a result, SU cannot detect the presence of PU. Thus it decides that the spectrum is vacant even if PT is present and begins the transmission, which interferes with PU communication. An obvious solution to improve the quality of spectrum sensing is the cooperation among multiple SUs. The basic idea is that each SU senses the spectrum using a detection technique (e.g., using energy detection [15]), and then the local decisions/spectrum sensing data are combined in a centralized/distributed manner to make a cooperative decision on the presence or absence of PU. This cooperative spectrum sensing—as an intra-network cooperation—exploits the spatial diversity and thus combats fading/shadowing in a better way than the case where a single SU senses the spectrum [16].

In the absence of cooperation from multiple SUs, an SU can use multiple antennas to improve the spectrum sensing performance. If separated by sufficient spacing, each of the antennas can virtually act as a separate node. Thus, by combining the sensing data received by each antenna, the spectrum sensing performance can be improved significantly [17, 18, 19]. But, in practice, if PT is located far from the sensing terminal (antenna in this case), it creates a small received channel-angular spread, which makes antennas correlated. The correlation among sensing data in turn deteriorates the spectrum sensing performance [20, 21].

Overall, the cooperation in all cognitive radio modes increases the chances of the spectrum sharing and in turn improves spectrum utilization. But the cooperation involves the

[1]The relay node may belong to some other network different from the secondary network. To show how intra-network cooperation can be realized in underlay mode, for instance, we consider that the relay node belongs to the secondary network.

interaction among nodes and thus raises security concerns. In this regard, we discuss below the security threats that come along with cooperation.

1.3.2 Security Concerns in Cooperation

1.3.2.1 Untrusted Relaying

The first security threat is *eavesdropping*, where a non-legitimate node attempts to hear the communication between two legitimate nodes. Such a non-legitimate node is called an eavesdropper. The eavesdropper can be an external node (from a different network) as well as an internal node (from the same network). Since the wireless medium is a broadcast medium, the users not belonging to the secondary network can listen to secondary transmissions and try to decode the information that is being communicated. Often, the eavesdropping node could be the one that belongs to the secondary network itself. For example, in underlay mode, ST and SD—the legitimate nodes—wish to keep the confidential information secret from the relaying node despite its cooperation in forwarding the information [22]. Thus the relay is trusted in forwarding the information, but untrusted out of the concern that the relay might attempt to decode the confidential information that is being relayed. In this case, the relaying node is considered as an eavesdropper. In practice, such scenario occurs in defence and government intelligence networks, where all nodes do not possess the same right to access the information. For example, if two nodes having access to confidential information wish to exchange the information, but do not have a direct link due to severe fading and shadowing, they might need to take help from an intermediate node that does not have privilege to access the confidential information.

One way to foil eavesdropping is to use physical-layer security approach, where the random nature of the physical medium is exploited to achieve positive secrecy rate.[2] For example, jamming signals can be used to deteriorate the eavesdropping channel of the untrusted relay. This reduces the chances of relay decoding the confidential information that is being relayed.

[2]The secrecy rate is the number of bits that could be transmitted in a secure manner per unit time.

1.3.2.2 Spectrum Sensing Data Falsification Attack

The second security threat that we consider is the spectrum sensing data falsification (SSDF) attack, which occurs in cooperative spectrum sensing (interweave mode) [23, 24, 25].[3] In cooperative spectrum sensing, when multiple SUs cooperate for spectrum sensing, a few SUs that deliberately manipulate the local sensing data and report these falsified data can easily influence the cooperative decision about the presence or absence of PU. Such users are called *malicious users*. Malicious SUs can get spectrum access by falsely reporting the sensing data that indicate the presence of PU even if PU is absent. Since the spectrum sensing data is falsified in this attack, this is called *spectrum sensing data falsification attack*. To have a reliable cooperative spectrum sensing decision, it is important to detect malicious users and possibly remove them from the cooperation.

The local spectrum sensing data reported by malicious users differ from the actual sensed data. Thus malicious users reporting the falsified spectrum sensing data can be considered as outliers and detected using outlier detection techniques [27].[4]

1.3.3 Energy Harvesting in Cognitive Radio

The third goal of this thesis is to investigate the effects of energy harvesting nodes on spectrum sharing. Energy harvesting is the process where nodes acquire energy from external sources. In the design of future wireless networks, energy harvesting has gained importance due to its ability to furnish energy to wireless devices while endowing the freedom of mobility. Also energy harvesting can virtually provide perpetual energy, which avoids the frequent replacement of battery. With the ever-increasing demand for wireless services along with a need for green communications, spectral efficiency and energy efficiency have become important criteria in the design of wireless systems. Energy harvesting (EH) cognitive radio [28, 29, 30, 31, 32, 33, 34] is a promising solution to improve the spectrum utilization; in particular, spectral efficiency is improved by spectrum sharing, while achieving self-sustaining green communications.

[3] We direct the reader to [26] for the details of other attacks in cognitive radio such as primary emulation attack, control channel jamming attack, etc.

[4] An outlier is the data that appear to be inconsistent with rest of the data.

The external sources of energy could be from nature or belong to man-made phenomena. The sources from nature include: solar, wind, thermal, vibration, etc [35]. Also the man-made sources can provide energy through wireless energy transfer, where the energy is transferred from one node to other node via radio-frequency (RF) signals in a controlled manner [36]. Wireless energy transfer has facilitated energy sharing among nodes, which has applications in wireless networks [37].

In wireless energy transfer, the source can be a dedicated node for the energy broadcast or just a information transmitting node. In the former case, the source broadcasts energy signals from which wireless nodes harvest energy, which can be further used to transmit their data. In the latter case, since RF signals can carry information and energy simultaneously, the receiver uses incoming RF signals to harvest energy [38, 39, 40]. We briefly discuss below these two cases.

1.3.3.1 Dedicated Energy Source

The uncertain and intermittent energy arrivals can make energy sources from nature unreliable for wireless applications with strict QoS requirements. This limitation has motivated the use of dedicated RF signals radiated by an access point in a controlled manner to power wireless devices, giving rise to wireless powered communication networks (WPCNs) [41, 42, 43]. The RF power transfer is the backbone of WPCN, where a hybrid access point (HAP)[5] broadcasts energy to devices via RF signals. The devices use harvested energy to transmit their data back to HAP.

The WPCN offers multiple advantages over harvesting energy from ambient RF signals that are not intended for energy transfer, such as co-channel interference. First, the energy broadcast by HAP is controllable in terms of system design (e.g., number of antennas), waveform design, and transmit power level. This allows HAP to supply stable and continuous energy to wireless devices [43, 44]. Contrary, ambient RF signals are uncontrollable as other RF sources may not be always transmitting. The second advantage is the flexibility in deployment of HAP [45, 46]. An HAP can be placed at a convenient location to reduce losses

[5]The term *hybrid* comes from the fact that HAP can act as an energy access point (EAP) as well that data access point (DAP) [44]. However, EAP and DAP may be located separately.

in energy transfer due to path-loss and shadowing.

Currently, using dedicated energy broadcast, it is possible to transfer energy in order of microwatts over a distance of 10 meters [47], which is sufficient for several low-power wireless nodes [48] such as medical implants and wireless sensors. With the recent technological advancements like low-power electronics [48], massive MIMO (tens to hundreds of antennas) providing sharp energy beams towards users to improve energy transfer efficiency [49], and small-cell deployment reducing inter-nodal distances [50], WPCN seems to have the potential to meet the energy requirements of wireless devices with stringent QoS demands.

The WPCN has received attention in different setups [41, 42, 43, 44, 45, 46, 51, 52, 53, 54, 55, 56, 57]. In [41, 52, 54], the proposed harvest-and-transmit policy maximizes the sum-throughput in WPCN, where multiple users harvest energy from energy broadcast by HAP and use the harvested energy to transmit information to HAP in a time division multiple access (TDMA) manner. The works in [45] and [51] study WPCN in a random-access-network and cellular network, respectively. Reference [53] examines a new type of WPCN, where wireless charging vehicles furnish wireless power to mobile nodes. The works in [55] and [56] manifest the user cooperation in WPCN, where the user nearer to HAP relays the data of the distant user to maximize the weighted sum-rate. Authors in [57] calculate the achievable throughput of a relay-assisted communication, where a power beacon wirelessly powers the source and the relay.

Given the dramatic increase in different wireless applications in the limited spectrum, WPCN will have to coexist and share the spectrum with other established communication networks. Thus, WPCN, if made *cognitive* [5], can efficiently share the spectrum with an existing network without degrading the latter's QoS.

1.3.3.2 Simultaneous Wireless Information and Energy Transfer

Since RF signals can carry both information and energy simultaneously, it seems natural to use the same incoming RF signals to harvest the energy. This is important in the case where the relay have a battery with limited capacity, replacing or recharging which frequently may be inconvenient. But it is difficult for a receiver, in practice, to simultaneously decode information and harvest energy from the received RF signals. Thus two practical policies

are proposed to harvest energy and decode information separately [58, 59]. One is the time switching (TS) policy, where the time is switched between the energy harvesting and the information decoding; while the second policy is based on the power splitting (PS), where a part of the received power is used to harvest energy and the rest for information decoding. For example, in underlay mode, if the secondary relay is energy constrained, it can use a part of the incoming RF signal from ST to harvest energy. Using this harvested energy, the relay then forwards the information to SD. Also, if both PU and SU are transmitting simultaneously (e.g., in overlay and underlay), SU can use PU signals, being RF signals, to harvest energy.

1.4 Thesis Outline and Contributions

This thesis has four parts.

In Part I, we focus on the overlay mode of cognitive radio, where we investigate *inter-network cooperation*, i.e., the cooperation between primary and secondary networks, along with energy harvesting.

Chapter 2 [60]: We propose the optimal resource allocation policy which maximizes the sum-throughput of secondary users in a wireless powered cooperative cognitive radio networks. We prove an interesting result that the SU selection to relay primary data is independent of the energy harvested by SUs though the secondary network is a fully energy harvesting network. We also show that the optimal policy is flexible in the sense that it can be easily modified to induce three different fairness constraints.

Chapter 3 [61]: We introduce a two-level cooperation—information and energy cooperation—between energy harvesting primary and secondary networks. We also introduce a new performance metric termed *probability of cooperation* that captures the possibility of cooperation between primary and secondary networks.

Part II of the thesis investigates *intra-network cooperation*, where an intermediate node facilitates the communication between an ST and an SD under the primary's interference constraint.

Chapter 4 [62]: For EH cognitive intra-network relaying, we reveal a trade-off between

the primary's interference constraint and the energy constraint at EH cognitive relays. We derive a closed-form expression for the secondary outage probability for Nakagami-m fading channels. We show that there exist regions of dominance where the primary's interference constraint and the energy constraint dominate each other.

Chapter 5 [63, 64]: We exhibit the usefulness of the primary's interference as an energy source for the secondary network. We provide analytical expressions for the secondary outage probability when the cognitive intra-network relays harvest RF energy from multiple primary transmitters.

Chapter 6 [65]: We analyze secure communication between an ST and an SD via an EH untrusted relay node. We derive analytical expressions for the secrecy outage probability and the ergodic secrecy rate under primary's interference constraint. We show that having relay located away from ST is beneficial to keep the information confidential from the untrusted relay. This is in contrast with the case of trusted EH relay, where the relay is preferred to be placed closer to ST.

Chapter 7 [66]: In a non-EH relaying scenario, we provide a closed-form expression of the secondary outage probability when the best relay among multiple amplify-and-forward relays assists the direct link between an ST and an SD.

Part III of the thesis studies *intra-network cooperation* through cooperative spectrum sensing and multiple antenna spectrum sensing. First, for conventional energy detector, we aim to defend the attack of malicious users in cooperative spectrum sensing. Then we focus on the improved energy detector (IED), where the squaring operation of the conventional energy detector is replaced by an arbitrary positive operation p. For IED, we investigate the performance of multiple-antenna assisted spectrum sensing.

Chapter 8 [67]: We propose an outlier detection technique based on Dixon's method to detect the presence of malicious users in cooperative spectrum sensing.

Chapter 9 [68]: We provide closed-form expressions for the probabilities of detection and false alarm for an IED when an SU is equipped with spatially correlated multiple antennas to sense the presence of PU. We find the optimum value of power operation p for a given number of antennas and the correlation coefficient among them.

Finally, Part IV provides the conclusion to the thesis and includes appendices.

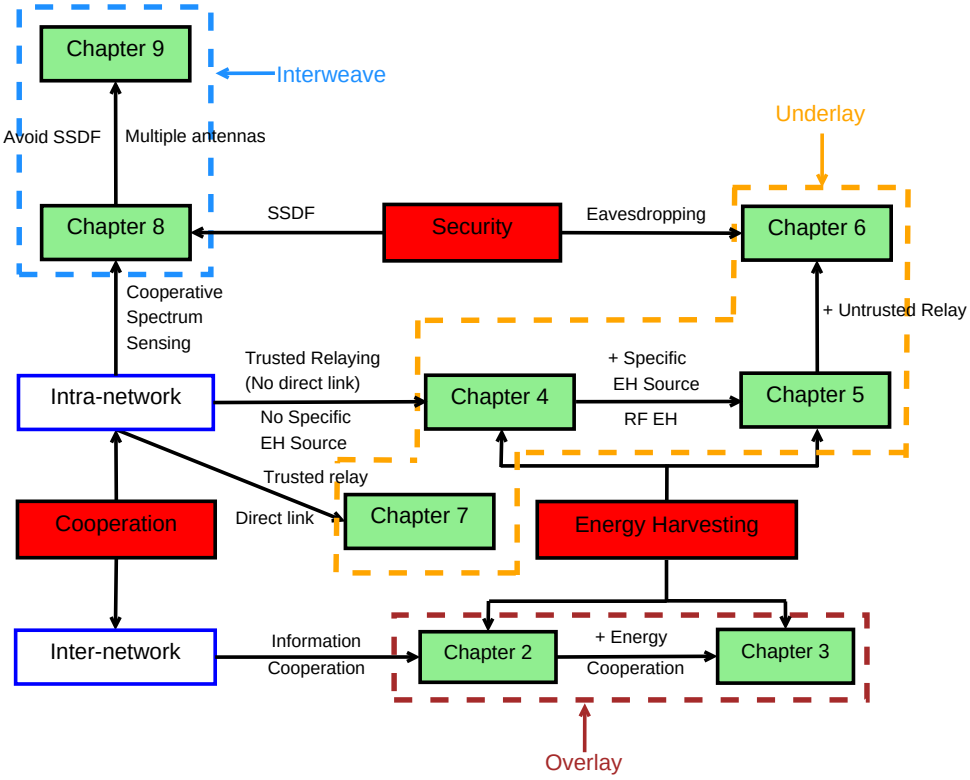

Figure 1.2: Flow of the thesis and interplay between chapters

The flow of the thesis and the interplay between chapters are depicted in Fig. 1.2.

Part I

Overlay Mode

Chapter 2

Resource Allocation and Fairness in Wireless Powered Cognitive Radio

2.1 Introduction

In this chapter, we focus on the inter-network cooperation between primary and secondary networks, where the secondary network helps maintain or improve QoS of the primary network and gets the spectrum access as a reward for the cooperation. Such scenario is termed cooperative cognitive radio networks (CCRN). In particular, we integrate a WPCN with a CCRN to develop a wireless powered CCRN (WP-CCRN), where multiple SUs powered wirelessly by an HAP help a PU relay the data. Thus we seize the benefits of WPCN and CCRN together. As a reward for the cooperation, the secondary network gains the spectrum access where SUs transmit to HAP using TDMA. The goal is to maximize the SU sum-throughput while optimally choosing SUs to relay PU data.

2.1.1 Related Work

A number of works have studied CCRN in a non-energy harvesting setup [10, 11, 12, 13, 69, 70, 71, 72, 73, 74]. For multiuser CCRN, the work in [74] proposes the best SU selection for relaying to maximize the SU sum-throughput. But in an energy harvesting scenario, the energy factor becomes crucial, and even the best SU to relay PU data may fail to meet the

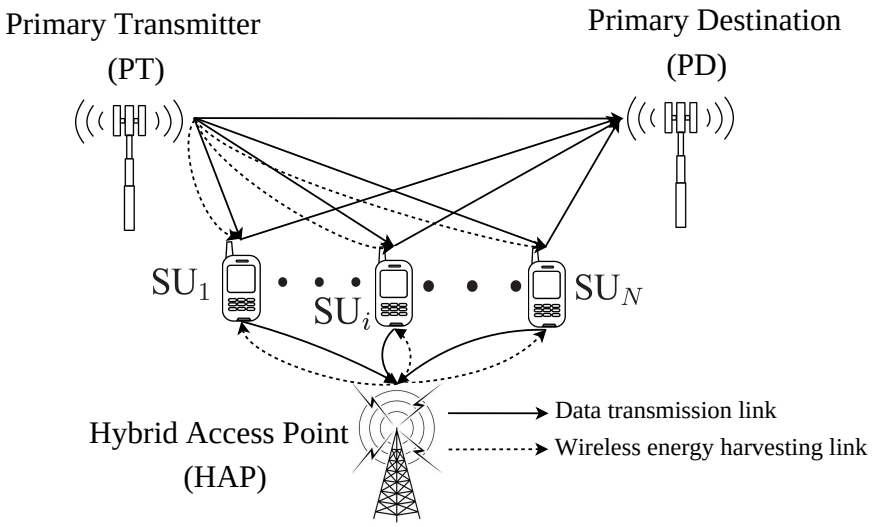

Figure 2.1: Wireless powered cooperative cognitive radio network.

primary rate constraint due to insufficient energy. This energy constraint may often lead to the selection of multiple SUs for relaying. As to wireless energy harvesting in CCRN, in [75, 76, 77, 78], an SU harvests RF energy from a PU's transmission which it uses to relay PU data and transmit its own data. In [79], under the save-then-transmit protocol, authors develop the optimal cooperation strategy for an SU that harvests energy from ambient radio signals. In [61], PU supplies energy to an SU to facilitate the data cooperation between PU and SU. But the works in [61, 75, 76, 77, 78, 79] consider a single-SU CCRN and assume that an SU harvests energy from either PU transmissions or ambient radio signals.

A recent work [80] investigates a cognitive wireless powered network, where it assumes non-causal knowledge of PU data. Contrary, we consider that SUs have to spend some time to receive and decode PU data before relaying. Also, [80] considers that a conventionally powered HAP from the secondary network (not energy harvesting SUs) transmits PU data; while in our proposed protocol, since multiple *energy harvesting* SUs may relay PU data, we provide the optimal SU selection strategy to decide which SUs will relay PU data. Moreover, we address the fairness issue for our proposed WP-CCRN.

Notation: Unless otherwise stated, the transmit power of a user, the energy, the noise power, and the throughput are given in Watts, Joules, Watts/Hz, and Nat/s/Hz, respectively.

2.2 System Model

We focus on a scenario where PU fails to meet its target rate via direct link and thus seeks cooperation from the secondary network. Fig. 2.1 shows the system model, where a primary pair consisting of a PT and a PD coexists with N SUs that communicate with an HAP. All nodes have a single antenna. The HAP has a stable and conventional energy supply, while SUs harvest energy from RF energy broadcast by HAP. At a time, an SU can receive either data or energy, but not both. Also, HAP cannot broadcast energy and receive data from SUs simultaneously. An ith SU is denoted by SU_i, $i \in \{1, \ldots, N\}$. Let g_{pp}, $g_{\mathrm{p}i}$, $g_{i\mathrm{p}}$, $g_{\mathrm{h}i}$, $g_{i\mathrm{h}}$, and g_{hp} denote channel power gains of PT-PD, PT-SU_i, SU_i-PD, HAP-SU_i, SU_i-HAP, and HAP-PD links, respectively.

Before we describe the cooperation protocol, we list the assumptions considered in the protocol below.

A1. The PD can coherently combine the data received from the primary direct link and the relaying links from SUs using maximal ratio combining (MRC).

A2. An SU relays PU data to PD in a decode-and-forward manner.

A3. In the rewarded period, SUs transmit to HAP using TDMA.

A4. All channels are independent and experience quasi-static Rayleigh fading, where the channel gains remain constant during one block of the transmission and change independently from one block to another. We assume the perfect knowledge of all channel power gains.

A5. HAP can act as a central controller to facilitate the cooperation between primary and secondary networks. It also coordinates among users, selects SUs to relay PU data, and maintains synchronization among secondary nodes for relaying primary data and transmitting their own data.

Considering that the SUs harvest energy, receive PU data, relay PU data, and access the channel, we propose a cooperation protocol that divides a fading block of duration T into four phases as depicted in Fig. 2.2. The final phase of SUs' spectrum access is subdivided into

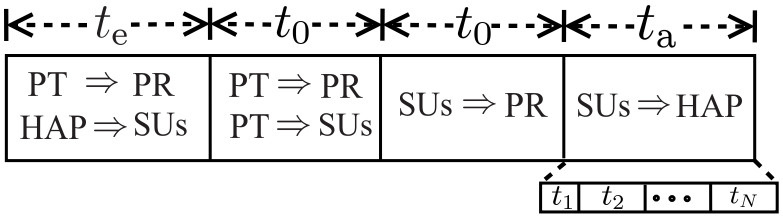

Figure 2.2: Cooperation protocol between primary and secondary users.

multiple slots where SUs transmit to HAP using TDMA. The following subsection discusses this four-phase cooperation protocol between PU and SUs.

2.2.1 Cooperation Protocol

2.2.1.1 Phase One

The HAP broadcasts *deterministic* RF signals with maximum power P_{e} Watts allowed by the peak power constraint from which SUs harvest energy. Simultaneously, PT broadcasts data with power P_{p} Watts. The SUs can use PT's transmission as a source of extra energy. Note that, since HAP's energy signal does not carry any information, it can be made deterministic, and thus PD can be made aware of it before the start of the transmission. In this way, PD can remove the interference caused by concurrent HAP's broadcast. Thus, in phase one, we can write PU's achievable throughput as

$$R_{\mathrm{p},1} = \frac{t_{\mathrm{e}}}{T} \ln\left(1 + \frac{g_{\mathrm{pp}} P_{\mathrm{p}}}{\mathcal{G} N_0}\right), \tag{2.1}$$

where N_0 is the additive white Gaussian noise (AWGN) power (in Nats/s/Hz) at PD. Also, $\mathcal{G}$ denotes the SNR gap from the AWGN channel capacity due to the practical modulation and coding schemes used [81]. Meanwhile, SU_i harvests energy

$$E_i = \eta\big(P_{\mathrm{e}} g_{\mathrm{h}i} + P_{\mathrm{p}} g_{\mathrm{p}i}\big) t_{\mathrm{e}}, \tag{2.2}$$

where η is the energy conversion efficiency factor with $0 < \eta \leq 1$. The term $P_{\mathrm{e}} g_{\mathrm{h}i}$ in (2.2) corresponds to the energy harvested from HAP's broadcast, while the term $P_{\mathrm{p}} g_{\mathrm{p}i}$ corresponds to the energy harvested from PT's transmission. The SUs use the energy harvested in this phase to relay PU data and transmit their own data in phases three and four, respectively.

2.2.1.2 Phases Two and Three

The relaying of PU data from SUs happens over two phases of equal duration, i.e., over phases two and three. In phase two of duration t_0, PU broadcasts its residual data after the phase one transmission, which SUs attempt to decode. The SUs that could decode PU data successfully form the decoding set $\mathcal{S}_\mathcal{D}$. An SU_i decodes the data successfully if no outage happens in phase two, i.e., the rate on PT-SU_i link is able to support the incoming data from PT. In this phase, the received SNR due to primary direct link transmission is given by $\frac{g_{\mathrm{pp}}P_{\mathrm{p}}}{\mathcal{G}N_0}$.

In phase three, if the decoding set $\mathcal{S}_\mathcal{D}$ is non-empty, then SUs chosen from it relay PU data. Before decoding the received signal, PD employs MRC. Thus, the resultant SNR at PD becomes the sum of SNRs over two channel uses, one on the primary direct link in phase two and the other on the secondary relaying link in phase three. Consequently, the achievable primary throughput with secondary cooperation becomes

$$R_{\mathrm{p},2} = \frac{t_0}{T}\ln\left(1+\frac{g_{\mathrm{pp}}P_{\mathrm{p}}}{\mathcal{G}N_0}+\frac{\sum_{\mathrm{SU}_i\in\mathcal{S}_\mathcal{D}} g_{i\mathrm{p}}P_{i\mathrm{p}}}{\mathcal{G}N_0}\right), \tag{2.3}$$

where $P_{i\mathrm{p}}$ is the power spent by SU_i on its relaying link. The term $\frac{\sum_{\mathrm{SU}_i\in\mathcal{S}_\mathcal{D}} g_{i\mathrm{p}}P_{i\mathrm{p}}}{\mathcal{G}N_0}$ in (2.3) corresponds to the SNR contribution from the relaying links of SUs that could decode PU data successfully. The power $P_{i\mathrm{p}} = 0$ for $\mathrm{SU}_i \in \mathcal{S}_\mathcal{D}$ that does not relay PU data as well as for SUs that could not decode PU data.

Given the transmissions on the primary direct link in phases one and two, and on the cooperative secondary relaying link in phase three, we can now write the overall primary throughput achieved under primary-secondary cooperation as

$$\begin{aligned} R_{\mathrm{p,c}} &= R_{\mathrm{p},1} + R_{\mathrm{p},2} \\ &= \frac{t_{\mathrm{e}}}{T}\ln\left(1+\frac{g_{\mathrm{pp}}P_{\mathrm{p}}}{\mathcal{G}N_0}\right) + \frac{t_0}{T}\ln\left(1+\frac{g_{\mathrm{pp}}P_{\mathrm{p}}}{\mathcal{G}N_0}+\frac{\sum_{\mathrm{SU}_i\in\mathcal{S}_\mathcal{D}} g_{i\mathrm{p}}P_{i\mathrm{p}}}{\mathcal{G}N_0}\right). \end{aligned} \tag{2.4}$$

2.2.1.3 Phase Four

The final phase is the rewarded period to SUs of duration t_a, where SUs may access the channel and transmit their own information to HAP in a TDMA fashion. Let t_i denote the

time allocated to SU_i and $t_a = \sum_{i=1}^{N} t_i$. Then, the rate achieved by SU_i is given by

$$R_i = \frac{t_i}{T} \ln\left(1 + \frac{g_{i\mathrm{h}} P_{i\mathrm{h}}}{\mathcal{G} N_0}\right), \tag{2.5}$$

where $P_{i\mathrm{h}}$ is the power used by SU_i to transmit its data.

2.2.2 System Constraints

We now define the system constraints that are common to four resource allocation schemes.

2.2.2.1 Primary Rate Constraint

The PU's achievable rate $R_{\mathrm{p,c}}$ under cooperation must meet the target primary rate $\bar{R}_{\mathrm{p}}$. That is,

$$R_{\mathrm{p,c}} \geq \bar{R}_{\mathrm{p}}. \tag{2.6}$$

In other words, the cooperation benefits PU if $\bar{R}_{\mathrm{p}} T$ amount of its data is delivered to PD successfully through it. Using (2.4), we can write the primary rate constraint as

$$\left[t_{\mathrm{e}} \ln\left(1 + \frac{g_{\mathrm{pp}} P_{\mathrm{p}}}{\mathcal{G} N_0}\right) + t_0 \ln\left(1 + \frac{g_{\mathrm{pp}} P_{\mathrm{p}}}{\mathcal{G} N_0} + \frac{\sum_{\mathrm{SU}_i \in \mathcal{S}_{\mathcal{D}}} g_{i\mathrm{p}} P_{i\mathrm{p}}}{\mathcal{G} N_0}\right)\right] \geq \bar{R}_{\mathrm{p}} T. \tag{2.7}$$

2.2.2.2 Decoding Constraint at SUs

In phase three, SUs that have decoded PU data in phase two can only participate in relaying. An SU_i can decode PU data successfully, i.e., $\mathrm{SU}_i \in \mathcal{S}_{\mathcal{D}}$ if

$$t_0 \ln\left(1 + \frac{g_{\mathrm{p}i} P_{\mathrm{p}}}{\mathcal{G} N_0}\right) \geq \bar{R}_{\mathrm{p}} T - t_{\mathrm{e}} \ln\left(1 + \frac{g_{\mathrm{pp}} P_{\mathrm{p}}}{\mathcal{G} N_0}\right), \tag{2.8}$$

where the term $t_0 \ln\left(1 + \frac{g_{\mathrm{p}i} P_{\mathrm{p}}}{\mathcal{G} N_0}\right)$ is the amount of data from PT that PT-SU_i link can support, $\bar{R}_{\mathrm{p}} T$ is the total amount of data PU wishes to send to PD, and $R_{\mathrm{p},1} T = t_{\mathrm{e}} \ln\left(1 + \frac{g_{\mathrm{pp}} P_{\mathrm{p}}}{\mathcal{G} N_0}\right)$ denotes the amount of data that PU could send successfully to PD in phase one (see (2.1)). Thus, the right hand side term of (2.8) represents the residual data after PT's direct link transmission in phase one. Therefore, the decoding constraint (2.8) implies that, to satisfy the primary rate constraint given in (2.7), an SU should be able to decode the residual PU data after phase one successfully.

2.2.2.3 Energy Neutrality Constraint at SUs

The amount of energy spent by SU_i on the relaying and access links cannot exceed the amount of its harvested energy from HAP's energy broadcast and PT's transmission in phase one. That is,

$$P_{i\mathrm{p}}t_0 + P_{i\mathrm{h}}t_i \leq \eta\big(P_{\mathrm{e}}g_{\mathrm{h}i} + P_{\mathrm{p}}g_{\mathrm{p}i}\big)t_{\mathrm{e}}, \quad i = 1, 2, \ldots, N, \tag{2.9}$$

where the terms $P_{i\mathrm{p}}t_0$ and $P_{i\mathrm{h}}t_i$ denote the energy spent by SU_i on its relaying and access links, respectively.

2.2.2.4 Total Time Constraint

The total time spent by SUs on energy harvesting in phase one of duration t_{e}, PU data reception and decoding in phase two of duration t_0, relaying PU data in phase three of duration t_0, and accessing the channel for their own transmission in final phase of duration $T - t_{\mathrm{e}} - 2t_0 = \sum_{i=1}^{N} t_i$, cannot exceed the slot duration T. That is,

$$t_{\mathrm{e}} + 2t_0 + \sum_{i=1}^{N} t_i \leq T. \tag{2.10}$$

Given the constraints in (2.7)-(2.10), our goal is to optimally allocate the time for each phase of the cooperation protocol, choose SUs for relaying, and divide the harvested energy at the relaying SUs between PU data relaying and own data transmission to HAP. Hereafter, we assume $T = 1$ without loss of generality.

2.3 Sum-Throughput Optimal Resource Allocation

In this section, our objective is to choose the optimal set of relaying SUs and find the optimal time and energy allocation for SUs that maximize the SU sum-throughput given by

$$R_{\mathrm{s,sum}} = \sum_{i=1}^{N} R_i = \sum_{i=1}^{N} t_i \ln\left(1 + \frac{g_{i\mathrm{h}}P_{i\mathrm{h}}}{\mathcal{G}N_0}\right). \tag{2.11}$$

Given the constraints discussed in Section 2.2.2, we formulate the SU sum-throughput maximization problem as follows:

$$\begin{aligned} \underset{\mathcal{S}_\mathcal{D}, \boldsymbol{P_{\mathrm{sh}}}, \boldsymbol{P_{\mathrm{sp}}}, \boldsymbol{t}}{\text{maximize}} \quad & R_{\mathrm{s,sum}} \\ \text{subject to} \quad & (2.7), (2.8), (2.9), (2.10), \\ & t_i, t_0, t_{\mathrm{e}} \geq 0, \quad \forall i, \\ & P_{i\mathrm{p}}, P_{i\mathrm{h}} \geq 0, \quad \forall i, \end{aligned} \tag{2.12}$$

where $\boldsymbol{P_{\mathrm{sh}}} = [P_{1\mathrm{h}}, \ldots, P_{N\mathrm{h}}]$, $\boldsymbol{P_{\mathrm{sp}}} = [P_{1\mathrm{p}}, \ldots, P_{N\mathrm{p}}]$, and $\boldsymbol{t} = [t_{\mathrm{e}}, t_0, \boldsymbol{t_a}]$ with $\boldsymbol{t_a} = [t_1, t_2, \ldots, t_N]$.
Claim 1: The optimization problem (2.12) is non-convex.

Proof. The energy neutrality constraint (2.9) is non-convex due to the product terms of optimization variables $P_{\mathrm{s}_i\mathrm{p}} t_0$ and $P_{\mathrm{s}_i\mathrm{h}} t_i$. Also, only SUs that belong to the decoding set $\mathcal{S}_\mathcal{D}$ can relay PU data. But, the decoding constraint (2.8) shows that the optimization variables t_0 and t_{e} decide which SUs can decode PU data successfully; thus, we do not know $\mathcal{S}_\mathcal{D}$ beforehand. Unknown $\mathcal{S}_\mathcal{D}$ and non-convexity of (2.9) make the problem (2.12) non-convex. □

Claim 2: With the change of variables and for a fixed decoding set $\mathcal{S}_\mathcal{D}$, the problem (2.12) reduces to a convex one.

Proof. The product of optimization variables—power and time—makes the constraint (2.9) non-convex. Thus, we rewrite the power-time product as energy and normalize it by their respective $\eta g_{\mathrm{h}i}$.[1] Regarding this, we denote $\frac{P_{i\mathrm{h}} t_i}{\eta g_{\mathrm{h}i}} = E_{i\mathrm{h}}$, $\frac{P_{i\mathrm{p}} t_0}{\eta g_{\mathrm{h}i}} = E_{i\mathrm{p}}$, and $\frac{P_{\mathrm{p}} g_{\mathrm{p}i}}{g_{\mathrm{h}i}} = \theta_i$, and rewrite (2.9) as

$$E_{i\mathrm{p}} + E_{i\mathrm{h}} \leq (P_{\mathrm{e}} + \theta_i) t_{\mathrm{e}}, \quad \forall i, \tag{2.13}$$

which is now an affine constraint. Still, the unknown $\mathcal{S}_\mathcal{D}$ makes problem (2.12) non-convex. But, after fixing $\mathcal{S}_\mathcal{D}$, we can reformulate (2.12) as an energy and time allocation problem as

[1] Normalization is for notational simplicity.

follows:

$$\underset{\boldsymbol{E_{\mathbf{sh}}},\boldsymbol{E_{\mathbf{sp}}},\boldsymbol{t}}{\text{maximize}} \sum_{i=1}^{N} t_i \ln\left(1+\frac{\gamma_{i\mathrm{h}}E_{i\mathrm{h}}}{t_i}\right) \tag{2.14a}$$

$$\text{subject to } \left[Q_1 t_{\mathrm{e}} + t_0 \ln\left(1+\gamma_{\mathrm{pp}}+\frac{\sum_{\mathrm{SU}_i\in\mathcal{S}_{\mathcal{D}}}\gamma_{i\mathrm{p}}E_{i\mathrm{p}}}{t_0}\right)\right] \geq \bar{R}_{\mathrm{p}}, \tag{2.14b}$$

$$t_0 \ln\left(1+\frac{g_{\mathrm{p}i}P_{\mathrm{p}}}{\mathcal{G}N_0}\right) \geq \bar{R}_{\mathrm{p}} - Q_1 t_{\mathrm{e}}, \forall\ \mathrm{SU}_i \in \mathcal{S}_{\mathcal{D}}, \tag{2.14c}$$

$$E_{i\mathrm{p}} + E_{i\mathrm{h}} \leq (P_{\mathrm{e}}+\theta_i)t_{\mathrm{e}}, \quad \forall i, \tag{2.14d}$$

$$t_{\mathrm{e}} + 2t_0 + \sum_{i=1}^{N} t_i \leq 1, \tag{2.14e}$$

$$t_i, t_0, t_{\mathrm{e}} \geq 0, \quad \forall i, \tag{2.14f}$$

$$E_{i\mathrm{p}}, E_{i\mathrm{h}} \geq 0, \quad \forall i, \tag{2.14g}$$

where $\boldsymbol{E_{\mathbf{sh}}} = [E_{1\mathrm{h}}, \ldots, E_{N\mathrm{h}}]$, $\boldsymbol{E_{\mathbf{sp}}} = [E_{1\mathrm{p}}, \ldots, E_{N\mathrm{p}}]$, $\gamma_{\mathrm{pp}} = \frac{g_{\mathrm{pp}}P_{\mathrm{p}}}{\mathcal{G}N_0}$, $\gamma_{i\mathrm{p}} = \eta g_{\mathrm{h}i}\frac{g_{i\mathrm{p}}}{\mathcal{G}N_0}$, $\gamma_{i\mathrm{h}} = \eta g_{\mathrm{h}i}\frac{g_{i\mathrm{h}}}{\mathcal{G}N_0}$, and

$$Q_1 = \ln\left(1+\frac{g_{\mathrm{pp}}P_{\mathrm{p}}}{\mathcal{G}N_0}\right). \tag{2.15}$$

As function $f(x) = \ln(1+x)$ is concave, its perspective function $f(x,y) = y\ln(1+\frac{x}{y})$ is also concave in terms of both x and y, for all $x, y > 0$. Since the sum of concave functions is concave, we can see that the objective is concave in nature. Also, the constraint (2.14b) is concave and the constraints (2.14c)-(2.14e) are affine. Thus, the problem (2.14) is convex. □

Although the joint optimization in (2.12) is non-convex, the problem structure is utilized to obtain a globally optimal solution. The following subsection describes the algorithm to achieve the globally optimal solution of (2.12).

2.3.1 Global Optimal Solution of (2.12)

Let us first sort $\boldsymbol{g_{\mathbf{ps}}} = [g_{\mathrm{p}1}, \ldots, g_{\mathrm{p}N}]$ in the decreasing order. Observe that, if SU_i with the channel power gain $g_{\mathrm{p}i}$ satisfies the decoding constraint (2.14c), SU_j with $g_{\mathrm{p}j} > g_{\mathrm{p}i}$ also satisfies (2.14c). Let $\boldsymbol{g}^j_{\mathbf{ps}}$ denote the jth element of the sorted $\boldsymbol{g_{\mathbf{ps}}}$. Now, we first assume that all SUs can successfully decode PU data, i.e., $|\mathcal{S}_{\mathcal{D}}| = N$, where $|\mathcal{S}_{\mathcal{D}}|$ is the cardinality of set

$\mathcal{S}_\mathcal{D}$. Then, we can rewrite the decoding constraint in (2.14c) as

$$t_0 \ln\left(1 + \frac{\boldsymbol{g}_{\mathbf{ps}}^{|\mathcal{S}_\mathcal{D}|} P_\mathrm{p}}{\mathcal{G} N_0}\right) \geq \bar{R}_\mathrm{p} - Q_1 t_\mathrm{e}, \tag{2.16}$$

where Q_1 is given by (2.15). We then solve the optimization problem (2.14) and obtain the corresponding objective value $R_{\mathrm{s,sum}}^{|\mathcal{S}_\mathcal{D}|}$ for $|\mathcal{S}_\mathcal{D}| = N$ using the iterative algorithm discussed in Section 2.3.2. Then, we exclude $|\mathcal{S}_\mathcal{D}|$-th element of the sorted $\boldsymbol{g}_{\mathbf{ps}}$ and solve the optimization problem (2.14) taking the decoding constraint (2.16) into account. We obtain the corresponding objective value $R_{\mathrm{s,sum}}^{|\mathcal{S}_\mathcal{D}|}$ with $|\mathcal{S}_\mathcal{D}| = N - 1$. This process is repeated until $|\mathcal{S}_\mathcal{D}| = 1$. Finally, the optimal SU sum-throughput is given by

$$R_{\mathrm{s,sum}}^* = \max\left(R_{\mathrm{s,sum}}^1, R_{\mathrm{s,sum}}^2, \ldots, R_{\mathrm{s,sum}}^N\right), \tag{2.17}$$

and the corresponding $\mathcal{S}_\mathcal{D}$ is the optimal decoding set. The sorting of $\boldsymbol{g}_{\mathbf{ps}}$ has reduced the search for the optimal decoding set from $2^N - 1$ (excluding null set) possibilities to N. This is because, we can ignore those choices of the decoding sets of SUs that contain an SU_j with $g_{\mathrm{p}j} > g_{\mathrm{p}i}$ that could not decode PU data, but SU_i with $g_{\mathrm{p}i}$ could decode PU data. Algorithm 1 summarizes the process of finding the global optimal solution of (2.12).

Algorithm 1 Finding the global optimal solution of (2.12)

1. Set $k = N$. Fix $|\mathcal{S}_\mathcal{D}| = k$.
2. Replace (2.14c) with (2.16).
3. Solve (2.14) using Algorithm 2 and compute the value of its objective $R_{\mathrm{s,sum}}^{|\mathcal{S}_\mathcal{D}|}$. If (2.14) is infeasible, set $R_{\mathrm{s,sum}}^{|\mathcal{S}_\mathcal{D}|} = 0$.
4. Set $k = k - 1$. If $k < 1$, stop; else, go to step 2.
5. $R_{\mathrm{s,sum}}^* = \max\left(R_{\mathrm{s,sum}}^1, R_{\mathrm{s,sum}}^2, \ldots, R_{\mathrm{s,sum}}^N\right)$.

In terms of complexity, the bottleneck of Algorithm 1 is N times application of Algorithm 2 having complexity $\mathcal{O}(N)$ (See complexity calculation for Algorithm 2 in Section 2.3.2.). Thus, Algorithm 1 has complexity $\mathcal{O}(N^2)$.

The following subsection 2.3.2 presents an algorithm to find the optimal solution of (2.14) for a given $\mathcal{S}_{\mathcal{D}}$. The constraint (2.14b) shows that the energy spent on the relaying link of SU_i depends on the energy spent by other users SU_j, $j \neq i$, on their relaying links. Also, the optimization variables $(\boldsymbol{E}_{\mathbf{sh}}, \boldsymbol{E}_{\mathbf{sp}})$ depend on the optimization variables $(\boldsymbol{t_a}, t_0)$ as seen from (2.14a) and (2.14b). Thus, the problem (2.14) is a convex problem with coupled variables and coupled constraints. This emphasizes the need for an iterative algorithm to compute the optimal solution. Though there are many standard algorithms to find the optimal solution of a convex optimization problem, given the coupled nature of problem (2.14) we use the following hierarchical decomposition based on block coordinate descent method [82, Chapter 1]. It allows us to break the problem (2.14) into two convex subproblems of decoupled nature.

2.3.2 Optimal Solution of (2.14) for a given $\mathcal{S}_{\mathcal{D}}$

For notational simplicity, let us denote the rate of SU_i as $R_i(E_{i\mathrm{h}}, t_i)$, i.e., R_i as a function of $E_{i\mathrm{h}}$ and t_i, and the rate of primary user as $R_{\mathrm{p,c}}(\boldsymbol{E}_{\mathbf{sp}}, t_{\mathrm{e}}, t_0)$, i.e., $R_{\mathrm{p,c}}$ as a function of $\boldsymbol{E}_{\mathbf{sp}}$, t_{e}, and t_0.

First, by fixing t_{e}, we decompose the problem (2.14) into two subproblems: `SP1`$-$for solving energy allocation $(\boldsymbol{E}_{\mathbf{sh}}, \boldsymbol{E}_{\mathbf{sp}})$ for a fixed $(\boldsymbol{t}_a, t_0)$ and `SP2`$-$for solving time allocation $(\boldsymbol{t}_a, t_0)$ for a fixed $(\boldsymbol{E}_{\mathbf{sh}}, \boldsymbol{E}_{\mathbf{sp}})$. The subproblems are given as

$$\begin{aligned} \texttt{SP1}: \underset{\boldsymbol{E}_{\mathbf{sh}}, \boldsymbol{E}_{\mathbf{sp}}}{\text{maximize}} \quad & \sum_{i=1}^{N} t_i \ln\left(1 + \frac{\gamma_{i\mathrm{h}} E_{i\mathrm{h}}}{t_i}\right) \\ \text{subject to} \quad & \text{(2.14b)}, \ \text{(2.14d)}, \ \text{(2.14g)}, \end{aligned} \tag{2.18}$$

$$\begin{aligned} \texttt{SP2}: \underset{t_0, \boldsymbol{t_a}}{\text{maximize}} \quad & \sum_{i=1}^{N} t_i \ln\left(1 + \frac{\gamma_{i\mathrm{h}} E_{i\mathrm{h}}}{t_i}\right) \\ \text{subject to} \quad & \text{(2.14b)}, \ \text{(2.14c)}, \ \text{(2.14e)}, \ \text{(2.14f)}. \end{aligned} \tag{2.19}$$

The subproblems are convex and they satisfy Slater's constraint qualification [82, Chapter 3]. Hence, the Karush-Kuhn-Tucker (KKT) conditions are necessary and sufficient to find the optimal solution.

The subproblems `SP1` and `SP2` form Level 1 of the iterative algorithm, and at Level 2, we solve the master problem to compute t_{e}, which is also convex. The levels 1 and 2 are executed

recursively until the optimization variables $(\boldsymbol{E}_{\mathbf{sh}}, \boldsymbol{E}_{\mathbf{sp}}, t_0, \boldsymbol{t_a})$ converge to a predetermined accuracy [83], resulting in the optimal solution.

Level 1: The Lagrangian $\mathcal{L}_1$ of `SP1` is

$$\begin{aligned}\mathcal{L}_1 = &\sum_{i=1}^{N} R_i(E_{i\mathrm{h}}, t_i) - \lambda\left(\bar{R}_{\mathrm{p}} - R_{\mathrm{p,c}}\left(\boldsymbol{E}_{\mathbf{sp}}, t_{\mathrm{e}}, t_0\right)\right) \\ &- \sum_{i=1}^{N} \mu_i(E_{i\mathrm{p}} + E_{i\mathrm{h}} - (P_{\mathrm{e}} + \theta_i)t_{\mathrm{e}}),\end{aligned} \tag{2.20}$$

where λ and $\boldsymbol{\mu} = [\mu_1, \ldots, \mu_N]$ denote the dual variables associated with the constraints (2.14b) and (2.14d), respectively. The dual problem of `SP1` is given by

$$\min_{\boldsymbol{\mu}} \max_{\boldsymbol{E}_{\mathbf{sh}}, \boldsymbol{E}_{\mathbf{sp}}} \mathcal{L}_1, \tag{2.21}$$

which is solved as follows. First, using KKT stationarity conditions, we solve the primal variable $E_{i\mathrm{p}}$ along with $E_{i\mathrm{h}}$ keeping $(E_{j\mathrm{p}}, t_0, \boldsymbol{t_a})$ and $(\lambda, \boldsymbol{\mu})$ fixed. Second, we compute the dual variable μ_i using bisection method.[2] We then repeat this two step process until $(E_{i\mathrm{h}}, E_{i\mathrm{p}})$ converge. In this manner, the dual problem (2.21) is solved for every SU_i $(i \in \{1, \ldots, N\})$, for every $j \neq i$. Now, by associating dual variables κ and ν with constraints (2.14c) and (2.14e), respectively, we write the Lagrangian $\mathcal{L}_2$ of time allocation problem `SP2` as

$$\begin{aligned}\mathcal{L}_2 = &\sum_{i=1}^{N} R_i(E_{i\mathrm{h}}, t_i) - \lambda\left(\bar{R}_{\mathrm{p}} - R_{\mathrm{p,c}}\left(\boldsymbol{E}_{\mathbf{sp}}, t_{\mathrm{e}}, t_0\right)\right) \\ &- \kappa\left(\bar{R}_{\mathrm{p}} - Q_1 t_{\mathrm{e}} - Q_2 t_0\right) - \nu\left(t_{\mathrm{e}} + 2t_0 + \sum_{i=1}^{N} t_i - 1\right),\end{aligned} \tag{2.22}$$

where Q_1 is given by (2.15) and $Q_2 = \ln\left(1 + \frac{\boldsymbol{h}_{\mathbf{ps}}^{|\mathcal{S}_{\mathcal{D}}|} P_{\mathrm{p}}}{\mathcal{G} N_0}\right)$. The corresponding dual problem is given by

$$\min_{\lambda, \kappa, \nu} \max_{t_0, \boldsymbol{t_a}} \mathcal{L}_2. \tag{2.23}$$

For fixed $(\boldsymbol{E}_{\mathbf{sh}}, \boldsymbol{E}_{\mathbf{sp}})$ and (λ, κ, ν), the primal variables $(t_0, \boldsymbol{t_a})$ can be found using KKT stationarity conditions. The dual variables that minimize $\max_{t_0, \boldsymbol{t_a}} \mathcal{L}_2$ are found using their

[2]Since the constraint (2.14b) is present in both `SP1` and `SP2`, the associated dual variable λ is solved in Level 2.

gradients given by

$$g_\lambda = R_{\mathrm{p,c}}(\boldsymbol{E}_{\mathbf{sp}}, t_\mathrm{e}, t_0) - \bar{R}_\mathrm{p}, \tag{2.24}$$

$$g_\kappa = Q_1 t_\mathrm{e} + Q_2 t_0 - \bar{R}_\mathrm{p}, \tag{2.25}$$

$$g_\nu = 1 - t_\mathrm{e} - 2t_0 - \sum_{i=1}^{N} t_i. \tag{2.26}$$

Level 2: Let l denote the iteration index of the algorithm. Having found $(\boldsymbol{E}^l_{\mathbf{sh}}, \boldsymbol{E}^l_{\mathbf{sp}}, t^l_0, \boldsymbol{t}^{\boldsymbol{l}}_{\boldsymbol{a}})$ and $(\lambda^l, \kappa^l, \boldsymbol{\mu}^l, \nu^l)$ for given t^{l-1}_e in Level 1, we solve the master primal problem for t^l_e given as

$$t^l_\mathrm{e} = \arg\max_{t_\mathrm{e}} \mathcal{G}(t_\mathrm{e}), \tag{2.27}$$

where $\mathcal{G}(t_\mathrm{e}) = \mathcal{L}_2|_{(t^l_0, \boldsymbol{t}^{\boldsymbol{l}}_{\boldsymbol{a}}, \lambda^l, \kappa^l, \nu^l)} + \sum_{i=1}^{N} \mu^l_i (E^l_{i\mathrm{p}} + E^l_{i\mathrm{h}} - (P_\mathrm{e} + \theta_i) t_\mathrm{e})$, which is the Lagrangian of the problem (2.14) for given t_e and $\mathcal{S}_\mathcal{D}$. Since $\mathcal{G}(t_\mathrm{e})$ is non-differentiable at t^l_e, we compute t^l_e using its subgradient given by

$$g_{t_e} = (\lambda^l + \kappa^l) Q_1 + \sum_{i=1}^{N} \mu^l_i (P_\mathrm{e} + \theta_i) - \nu^l. \tag{2.28}$$

The analytical expressions of optimization variables obtained through KKT conditions are presented in Proposition 2.1 as follows.

Proposition 2.1. *The optimal solution for the optimization problem* (2.14) *is given by*

$$E^*_{i\mathrm{h}} = t^*_i \left[\frac{1}{\mu^*_i} - \frac{1}{\gamma_{i\mathrm{h}}} \right]^+, \tag{2.29}$$

$$E^*_{i\mathrm{p}} = t^*_0 \left[\frac{\lambda^*}{\mu^*_i} - \frac{1 + \gamma_{\mathrm{pp}}}{\gamma_{i\mathrm{p}}} - \frac{\sum_{\mathrm{SU}_j \in \mathcal{S}_\mathcal{D}, j \neq i} \gamma_{j\mathrm{p}} E^*_{j\mathrm{p}}}{\gamma_{i\mathrm{p}}} \right]^+, \tag{2.30}$$

$$t^*_\mathrm{e} = 1 - 2t^*_0 - \sum_{i=1}^{N} t^*_i, \tag{2.31}$$

$$t^*_0 = \frac{\sum_{\mathrm{SU}_i \in \mathcal{S}_\mathcal{D}} \gamma_{i\mathrm{p}} E^*_{i\mathrm{p}}}{\exp\left(\mathcal{W}\left(\frac{-1}{\frac{2\nu^* - \kappa^* Q_2}{\lambda^*} + 1} \right) + \frac{2\nu^* - \kappa^* Q_2}{\lambda^*} + 1 \right) - 1 - \gamma_{\mathrm{pp}}}, \tag{2.32}$$

$$t^*_i = \frac{\gamma_{i\mathrm{h}} E^*_{i\mathrm{h}}}{\exp\left(\mathcal{W}\left(\frac{-1}{\nu^* + 1} \right) + \nu^* + 1 \right) - 1}, \tag{2.33}$$

where $[x]^+ \triangleq \max(x, 0)$ *and* $\mathcal{W}(\cdot)$ *is the Lambert W function [84].*

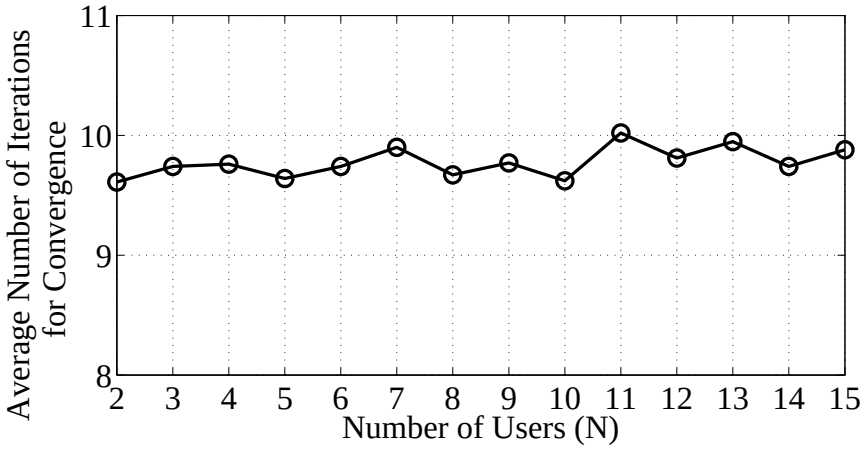

Figure 2.3: Average number of iterations till convergence for $\bar{R}_{\mathrm{p}} = 1.5$ nats/s/Hz and $P_{\mathrm{e}} = 20$ dBm.

Proof. See Appendix A.1. □

Algorithm 2 summarizes the above iterative procedure.

We now calculate the complexity of Algorithm 2. The "**While**" loop that uses bisection method runs for N times, thus having complexity $\mathcal{O}(N)$ as $\mu_{\min}$, $\mu_{\max}$, and ϵ are constant. The other bottleneck in the loop corresponding to l is the computation of t_i and t_0 having complexity $\mathcal{O}(N)$ (step 4.d.). Since steps $4-7$ are repeated for l times, the overall complexity of steps $4-7$ is $\mathcal{O}(lN)$. Fig. 2.3 shows the impact of average number of iterations l till convergence on the algorithm for the given simulation parameters considered in Section 2.5, where the number of iterations used till convergence remains almost the same with increase in N, and thus has complexity $\mathcal{O}(1)$. Finally, $\mathcal{O}(N)$ operations are done at step 8. Thus, Algorithm 2 has complexity $\mathcal{O}(N)$.

Convergence speed of Algorithm 2: Algorithm 2 is of iterative nature. Fig. 2.4 shows the number of iterations required for Algorithm 2 to converge for a specific randomly chosen channel realization. One iteration corresponds to one iteration l in Algorithm 2, steps $3-7$. As Fig. 2.4 shows, Algorithm 2 needs 11 iterations to converge. The primary rate converges to 1.5 nats/s/Hz which is the target primary rate. This is in accordance with Proposition 2.2, which says that, under the optimal condition, the target primary rate should be exactly met.

The following proposition states the properties of the optimal solution.

Algorithm 2 Finding the optimal solution of (2.14) for a given $\mathcal{S}_{\mathcal{D}}$

1. Initialize primal variables $\boldsymbol{E_{\mathbf{sp}}}, \boldsymbol{t}_a, t_0, t_{\mathrm{e}} > 0$, and dual variables $\lambda, \kappa, \nu > 0$

2. Set $\mu_{\min}, \mu_{\max} > 0$, $\epsilon = 10^{-5}$, step size $\alpha > 0$, and iteration index $l = 0$

3. **Repeat**: $l \leftarrow l + 1$, $\alpha \leftarrow \alpha/\sqrt{l}^*$

4. *Level 1*: **Repeat**

   - `To solve for (SP1)` -

   a. **For** $i = 1 : N$

      While $|\mu_{\max} - \mu_{\min}| > \epsilon$

      $\mu_i \leftarrow (\mu_{\min} + \mu_{\max})/2$

      Compute $(E_{i\mathrm{h}}, E_{i\mathrm{p}})$ using $(\boldsymbol{t_a}, t_0)$ in (2.29)-(2.30)

      If $(E_{i\mathrm{h}} + E_{i\mathrm{p}}) < (P_{\mathrm{e}} + \theta_i) t_{\mathrm{e}}^{l-1}$, $\mu_{\max} \leftarrow \mu_i$; Else, $\mu_{\min} \leftarrow \mu_i$

      End

   c. **End**

   - `To solve for (SP2)` -

   d. Compute (t_i, t_0) $\forall i$ using $(\boldsymbol{E_{\mathbf{sh}}}, \boldsymbol{E_{\mathbf{sp}}})$ in (2.32)-(2.33)

   e. Update the dual variables λ, κ, ν with their gradients given in (2.24) $-$ (2.26)

5. **Until** convergence

6. *Level 2*: Update the primal variable: $t_{\mathrm{e}}^l = \left[t_{\mathrm{e}}^{l-1} + \alpha \nabla t_{\mathrm{e}}\right]^+$

7. **Until** all the optimization parameters converge

8. Compute the optimal powers $P_{i\mathrm{h}}^* = \eta g_{\mathrm{h}i} \frac{E_{i\mathrm{h}}^*}{t_i^*}$, $P_{i\mathrm{p}}^* = \eta g_{\mathrm{h}i} \frac{E_{i\mathrm{p}}^*}{t_0^*}$ $\forall i$

* The step-size α is chosen such that it satisfies the diminishing step-size rule [82, Chapter 1].

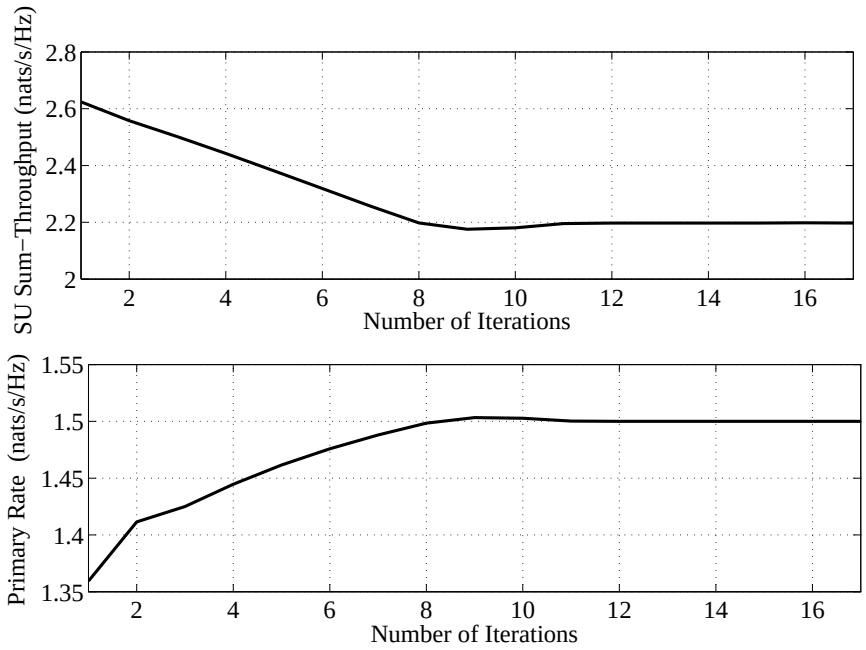

Figure 2.4: Algorithm 2 convergence speed for the simulation parameters considered in Section 2.5, $\bar{R}_{\mathrm{p}} = 1.5$ nats/s/Hz.

Proposition 2.2. *The optimal solution* $(\boldsymbol{E}^*_{\mathbf{sh}}, \boldsymbol{E}^*_{\mathbf{sp}}, \boldsymbol{t}^*)$ *satisfies the constraints* (2.14b), (2.14d), *and* (2.14e) *with equality.*

Proof. Assume that the constraints (2.14b) and (2.14d) are satisfied with strict inequality. For (2.14b), we can decrease $E_{i\mathrm{p}}$ on the relaying link without violating the primary rate constraint and increase $E_{i\mathrm{h}}$ on the secondary access link to HAP. This increases SU sum-throughput, which contradicts with our assumption of optimality. Similarly, for (2.14d), we can always increase $E_{i\mathrm{h}}$ without violating the constraint, resulting in higher sum-throughput, contradicting our assumption. Now, let us assume (2.14e) is satisfied with inequality. Then, we can increase t_i improving SU sum-throughput, contradicting with our assumption. □

2.3.3 SU Selection for Relaying

We now use the structural properties of the optimal solution to find the underlying SU selection to relay PU data. We proceed in this direction by first proving the following lemma, which will be used in the proof of Proposition 2.3.

Lemma 2.1. *For SU_i and SU_j transmitting in the rewarded period, we have $\frac{\gamma_{i\mathrm{h}}E^*_{i\mathrm{h}}}{t^*_i} = \frac{\gamma_{j\mathrm{h}}E^*_{j\mathrm{h}}}{t^*_j}$ with $i \neq j$.*

Proof. Rearranging terms of (2.33), we obtain

$$\exp\left(\mathcal{W}\left(\frac{-1}{\nu^*+1}\right)+\nu^*+1\right)-1 = \frac{\gamma_{i\mathrm{h}}E^*_{i\mathrm{h}}}{t^*_i}, \quad \forall i, \tag{2.34}$$

Since the term $\exp\left(\mathcal{W}\left(\frac{-1}{\nu^*+1}\right)+\nu^*+1\right)-1$ is same for all SUs who access the spectrum, we have $\frac{\gamma_{i\mathrm{h}}E^*_{i\mathrm{h}}}{t^*_i} = \frac{\gamma_{j\mathrm{h}}E^*_{j\mathrm{h}}}{t^*_j} = \frac{1}{C}$, where C is a constant. □

For STORA scheme, the following proposition states the underlying SU selection to relay PU data and the energy allocation at the relaying SUs.

Proposition 2.3. *1) The SUs are prioritized to relay primary data in the increasing order of ratio $\frac{\gamma_{i\mathrm{h}}}{\gamma_{i\mathrm{p}}}$. 2) The optimal energy allocated on the relaying link $E^*_{i\mathrm{p}}$ is fractional for at most one SU.*

Proof. 1) SUs that relay PU data have to allocate their harvested energy between relaying and transmitting their own data. The energy allocation subproblem `SP1` of the problem (2.14) given by (2.18) aims to maximize the objective (2.14a) under the primary rate constraint (2.14b) and the energy neutrality constraint (2.14d). Under the optimal condition, since the constraints (2.14b) and (2.14d) are met with equality (see Proposition 2.2), we can write them as

$$\sum_{\mathrm{SU}_i\in\mathcal{S}_\mathcal{D}} \gamma_{i\mathrm{p}}E_{i\mathrm{p}} = t_0\left(\exp\left(\frac{\bar{R}_\mathrm{p}-Q_1t_\mathrm{e}}{t_0}\right)-(1+\gamma_{\mathrm{pp}})\right), \tag{2.35}$$

$$E_{i\mathrm{p}} + E_{i\mathrm{h}} = (P_\mathrm{e}+\theta_i)t_\mathrm{e}, \quad \forall i, \tag{2.36}$$

respectively. Without altering the solution, we can make each $\gamma_{i\mathrm{p}}$ equal to a constant K and scale corresponding $\gamma_{i\mathrm{h}}$, $E_{i\mathrm{h}}$, and $E_{i\mathrm{p}}$ accordingly. Then, the energy allocation subproblem

SP1 can be reformulated as

$$\underset{\bar{\boldsymbol{E}}_{\mathbf{sh}},\bar{\boldsymbol{E}}_{\mathbf{sp}}}{\text{maximize}} \quad \sum_{i=1}^{N} t_i \ln\left(1+\frac{\bar{\gamma}_{i\mathrm{h}}\bar{E}_{i\mathrm{h}}}{t_i}\right) \tag{2.37a}$$

$$\text{subject to} \quad K\sum_{\mathrm{SU}_i\in\mathcal{S}_{\mathcal{D}}}\bar{E}_{i\mathrm{p}} = t_0\left(\exp\left(\frac{\bar{R}_{\mathrm{p}}-Q_1 t_{\mathrm{e}}}{t_0}\right)-(1+\gamma_{\mathrm{pp}})\right), \tag{2.37b}$$

$$\frac{K}{\gamma_{i\mathrm{p}}}(\bar{E}_{i\mathrm{p}}+\bar{E}_{i\mathrm{h}}) = (P_{\mathrm{e}}+\theta_i)t_{\mathrm{e}}, \quad \forall i, \tag{2.37c}$$

$$\bar{E}_{i\mathrm{p}},\bar{E}_{i\mathrm{h}} \geq 0, \quad \forall i, \tag{2.37d}$$

where $\bar{\gamma}_{i\mathrm{h}} = \gamma_{i\mathrm{h}}\frac{K}{\gamma_{i\mathrm{p}}}$, $\bar{E}_{i\mathrm{p}} = E_{i\mathrm{p}}\frac{\gamma_{i\mathrm{p}}}{K}$, $\bar{E}_{i\mathrm{h}} = E_{i\mathrm{h}}\frac{\gamma_{i\mathrm{p}}}{K}$, $\bar{\boldsymbol{E}}_{\mathbf{sh}} = [\bar{E}_{1\mathrm{h}},\ldots,\bar{E}_{N\mathrm{h}}]$, and $\bar{\boldsymbol{E}}_{\mathbf{sp}} = [\bar{E}_{1\mathrm{p}},\ldots,\bar{E}_{N\mathrm{p}}]$. Using (2.37a), the SU sum-throughput can be rewritten as

$$R_{\mathrm{s,sum}} = \sum_{i=1}^{N} t_i \ln\left(1+\frac{K\frac{\gamma_{i\mathrm{h}}}{\gamma_{i\mathrm{p}}}\bar{E}_{i\mathrm{h}}}{t_i}\right). \tag{2.38}$$

From Lemma 2.1, we have $\frac{\gamma_{i\mathrm{h}}E_{i\mathrm{h}}}{t_i} = \frac{1}{C}$, where C is a constant. Thus, we can write (2.38) as

$$R_{\mathrm{s,sum}} = \sum_{i=1}^{N} CK\frac{\gamma_{i\mathrm{h}}}{\gamma_{i\mathrm{p}}}\bar{E}_{i\mathrm{h}} \ln\left(1+\frac{1}{C}\right). \tag{2.39}$$

To exploit the structural properties of the optimization problem (2.37) with its objective (2.37a) replaced by (2.39), we write it in the generic resource allocation problem given as follows:

$$\underset{\boldsymbol{p},\boldsymbol{q}}{\text{maximize}} \quad \sum_{i=1}^{N} w_i p_i \tag{2.40a}$$

$$\text{subject to} \quad p_i + q_i = r + \delta_i, \tag{2.40b}$$

$$\sum_{i=1}^{N} q_i = s, \tag{2.40c}$$

$$\boldsymbol{p},\boldsymbol{q} \geq 0, \tag{2.40d}$$

where $w_i = CK\frac{\gamma_{i\mathrm{h}}}{\gamma_{i\mathrm{p}}}\ln\left(1+\frac{1}{C}\right)$, $p_i = \frac{K}{\gamma_{i\mathrm{p}}}\bar{E}_{i\mathrm{h}} = E_{i\mathrm{h}}$, $q_i = \frac{K}{\gamma_{i\mathrm{p}}}\bar{E}_{i\mathrm{p}} = E_{i\mathrm{p}}$, $r = P_{\mathrm{e}}t_{\mathrm{e}}$, $\delta_i = \theta_i t_{\mathrm{e}}$, $s = \frac{t_0}{K}\left(\exp\left(\frac{\bar{R}_{\mathrm{p}}-Q_1 t_{\mathrm{e}}}{t_0}\right)-(1+\gamma_{\mathrm{pp}})\right)$, $\boldsymbol{p} = [p_1,\ldots,p_N]$, and $\boldsymbol{q} = [q_1,\ldots,q_N]$. For simplicity of notation, let us denote SU_i-HAP link as $\mathbb{P}$ on which SU_i allocates the resource $p_i = E_{i\mathrm{h}}$.

Similarly, let us denote SU_i-PD link as $\mathbb{Q}$ on which SU_i allocates the resource $q_i = E_{i\mathrm{p}}$. Now, we solve (2.40) and exploit its structural properties to find the selection criterion to select SUs for relaying PU data.

We split the resource allocation problem in (2.40) into three cases to obtain its optimal solution. Without loss of generality, let us assume that $w_1 > w_2 > \ldots > w_N$. We denote $\delta' = \min(\delta_1, \delta_2, \ldots, \delta_N)$.

Case 1: Let $s < r + \delta'$. Consider following two possible strategies:

1. Strategy 1: $q_i = s$, $q_j = 0$ with $j \neq i$.
2. Strategy 2: $q_i = a_i s$. Here, each $0 \leq a_i < 1$ can be chosen arbitrarily such that $\sum_{i=1}^{N} a_i = 1$.

Under strategy 1, if SU_1 allocates s on $\mathbb{Q}$ link, the objective of problem (2.40) can be rewritten as

$$\begin{aligned}\sum_{i=1}^{N} w_i p_i &= w_1(r + \delta_1 - s) + \sum_{j=2}^{N} w_j(r + \delta_j) \\ &= \sum_{i=1}^{N} w_i(r + \delta_i) - w_1 s \\ &< \sum_{i=1}^{N} w_i(r + \delta_i) - w_2 s \\ &\;\;\vdots \qquad\quad \vdots \qquad\quad \vdots \\ &< \sum_{i=1}^{N} w_i(r + \delta_i) - w_N s. \end{aligned} \tag{2.41}$$

Thus, allocating the resource s fully on $\mathbb{Q}$ link of SU_N with the lowest weight w_N, i.e., when $q_N = s$, maximizes the objective. Now, under strategy 2, we can write the objective as

$$\begin{aligned}\sum_{i=1}^{N} w_i p_i &= \sum_{i=1}^{N} w_i(r + \delta_i - a_i s) \\ &= \sum_{i=1}^{N} w_i(r + \delta_i) - \sum_{i=1}^{N} a_i w_i s. \end{aligned} \tag{2.42}$$

Since $\sum_{i=1}^{N} a_i w_i s > \sum_{i=1}^{N} a_i w_N s = w_N s$, we have (2.41) $>$ (2.42). Thus, strategy 1 outperforms strategy 2 and allocating complete resource s to SU with the lowest weight yields the

optimal solution, i.e., $q_N^* = s$ and $q_i^* = 0$ if $i \neq N$. From (2.40b), we then have $p_N^* = r+\delta_N - s$ and $p_i^* = r + \delta_i$ if $i \neq N$.[3]

Case 2: Let $r + \delta' \leq s \leq r + \delta_N$. Under strategy 1, for SU_i with $r + \delta_i < s$, we cannot allocate complete resource s as it makes $p_i < 0$. Similar argument applies for strategy 2 and when $r + \delta_i < a_i s$. Then, excluding such users and following the same proof for *Case 1*, we can show that the objective is maximized if user N with the lowest weight is allocated the resource s fully. Therefore, p_i^* and q_i^* are the same as those for *Case 1*.

Case 3: Let $s > r + \delta_N$. In this case, the $\mathbb{Q}$ link of user N can accommodate at the most $r + \delta_N$ out of the resource s. This implies that we have to allocate the resource s over $\mathbb{Q}$ links of more than one user. Following the proof given for *Case 1*, we can show that $q_N^* = r + \delta_N$ and $p_N^* = 0$. Now, the problem (2.40) reduces to finding $\boldsymbol{p}$ and $\boldsymbol{q}$ of dimension $N - 1$, i.e., with $N - 1$ users. In this modified optimization problem, s in (2.40c) is replaced by $s - (r + \delta_N)$. Here, we have to investigate two cases depending on whether $(s - (r + \delta_N)) \leq r + \delta_{N-1}$ or $(s - (r + \delta_N)) > r + \delta_{N-1}$, to obtain the optimal solution of the modified optimization problem. Based on the aforementioned discussion in this proof, we get $q_{N-1}^* = \min(r + \delta_{N-1}, s - (r + \delta_N))$ and $p_{N-1}^* = r + \delta_{N-1} - q_{N-1}^*$. The problem (2.40) then can be further reduced to dimension $(N - 2)$ and later upto $(N - (N - 1))$ recursively. Combining the solution of each recursive step together, we can finally write the optimal solution to the problem (2.40) as

$$q_i^* = \begin{cases} \min(r + \delta_i, s), & \text{if } w_i = \min(\boldsymbol{w}), \\ \min\left(r + \delta_i, \left[s - \sum\limits_{\{j:j\neq i, w_j \leq w_i\}} q_j^*\right]^+\right), & \text{otherwise}, \end{cases} \tag{2.43}$$

and

$$p_i^* = r + \delta_i - q_i^*, \ \ \forall i, \tag{2.44}$$

which also comprises the optimal solutions for cases 1 and 2.

The optimal solution of (2.40a)-(2.40d) given in (2.43) and (2.44) along with its derivation shows that the objective (2.40a) is maximized when the resources q_i on $\mathbb{Q}$ links of SUs are

[3]If $w_i = w_j = \min \boldsymbol{w}$ with $i \neq j$, then we can randomly allocate resource s completely to either SU_i or SU_j.

allocated in the increasing order of the weights w_i on their corresponding $\mathbb{P}$ links. Since the subproblem (2.37) is identical to (2.40), the SU sum-throughput given by (2.39) under the constraints (2.37b)-(2.37d) is maximized when the SU with the lowest $w_i = CK\frac{\gamma_{i\mathrm{h}}}{\gamma_{i\mathrm{p}}}\ln\left(1+\frac{1}{C}\right)$, i.e., $\frac{\gamma_{i\mathrm{h}}}{\gamma_{i\mathrm{p}}}$ (since $CK\ln\left(1+\frac{1}{C}\right)$ is same for all SUs), is prioritized to relay PU data and then the SU with the next lowest $\frac{\gamma_{i\mathrm{h}}}{\gamma_{i\mathrm{p}}}$. This completes the proof of the first part of Proposition 2.3.

2) If the cooperation from SU with the lowest $\frac{\gamma_{i\mathrm{h}}}{\gamma_{i\mathrm{p}}}$ to relay PU data cannot meet the primary rate constraint even after it has spent its complete harvested energy on the relaying link, then only the SU with the next lowest $\frac{\gamma_{i\mathrm{h}}}{\gamma_{i\mathrm{p}}}$ is considered to relay PU data, and so on. Thus, at most one SU will spend a fraction of its harvested energy on the relaying link, while other relaying SUs spend their complete harvested energy to relay PU data. □

The following remark highlights the unfairness created among SUs by the STORA scheme.

Remark 2.2. *Relaying SUs that spend their complete harvested energy in relaying achieve zero throughput. Contrary, SUs that do not relay PU data gain spectrum access and use their complete harvested energy to achieve non-zero individual throughput. Thus, the STORA scheme creates unfairness among SUs in terms of individual throughput.*

2.4 Resource Allocation with Fairness Constraints

In this section, we examine three fairness enhancing schemes.

2.4.1 Equal Time Allocation

The goal is to maximize the SU sum-throughput under the condition of allocating all SUs equal time to access the channel, i.e., $t_1 = t_2 = \ldots = t_N = t_{\mathrm{eq}}$. The condition of equal time to each SU ensures that all SUs get an opportunity to access the channel unlike STORA scheme. For a fixed decoding set $\mathcal{S}_{\mathcal{D}}$, the problem of SU sum-throughput maximization with

equal time allocation is formulated as follows:

$$\begin{aligned} \underset{\boldsymbol{E_{\mathbf{sh}}},\boldsymbol{E_{\mathbf{sp}}},t_{\mathrm{e}},t_0,t_{\mathrm{eq}}}{\text{maximize}} \quad & \sum_{i=1}^{N} t_{\mathrm{eq}} \ln\left(1+\frac{\gamma_{i\mathrm{h}}E_{i\mathrm{h}}}{t_{\mathrm{eq}}}\right) \\ \text{subject to} \quad & (2.14\mathrm{b})-(2.14\mathrm{d}) \\ & t_{\mathrm{e}}+2t_0+Nt_{\mathrm{eq}}\leq 1, \\ & \boldsymbol{E_{\mathbf{sh}}},\boldsymbol{E_{\mathbf{sp}}},t_{\mathrm{e}},t_0,t_{\mathrm{eq}}\geq 0. \end{aligned} \tag{2.45}$$

The problem in (2.45) is a convex optimization problem and Proposition 2.2 also holds true for (2.45). The STORA and ETA problems differ only in their allocation of the access time. Thus, we can use the same approach as that of STORA scheme to solve (2.45) with the optimal t_{eq} given in the following proposition.

Proposition 2.4. *The optimal spectrum time t^*_{eq} of an SU is the solution of the equation*

$$\sum_{i=1}^{N} \ln\left(1+\frac{\gamma_{i\mathrm{h}}E^*_{i\mathrm{h}}}{t^*_{\mathrm{eq}}}\right)-\frac{\frac{\gamma_{i\mathrm{h}}E^*_{i\mathrm{h}}}{t^*_{\mathrm{eq}}}}{1+\frac{\gamma_{i\mathrm{h}}E^*_{i\mathrm{h}}}{t^*_{\mathrm{eq}}}}=N\nu^*. \tag{2.46}$$

Proof. See Appendix A.2. □

As (2.46) shows, we cannot obtain the closed-form expression for t^*_{eq}. But, we can find t^*_{eq} numerically using bisection method. Interestingly, an asymptotic solution in closed-form exists when HAP experiences high received SNR conditions, i.e., when $\frac{\gamma_{i\mathrm{h}}E^*_{i\mathrm{h}}}{t^*_{\mathrm{eq}}} \gg 1$. In this case, (2.46) can be written

$$\sum_{i=1}^{N} \ln\left(\frac{\gamma_{i\mathrm{h}}E^*_{i\mathrm{h}}}{t^*_{\mathrm{eq}}}\right)=N\nu^*, \tag{2.47}$$

which yields $\sum_{i=1}^{N}\ln\left(\gamma_{i\mathrm{h}}E^*_{i\mathrm{h}}\right)=N\nu^*+N\ln(t^*_{\mathrm{eq}})$. Rearranging terms, we get

$$t^*_{\mathrm{eq}}=\frac{1}{\exp(\nu^*)}\left(\prod_{i=1}^{N}\gamma_{i\mathrm{h}}E^*_{i\mathrm{h}}\right)^{\frac{1}{N}}. \tag{2.48}$$

Thus, (2.48) shows that, under high SNR conditions, the time allocated for spectrum access to an SU is proportional to the geometric mean of the received energies at HAP. Substituting (2.48) in (2.47), the objective of (2.45), i.e., SU sum-throughout, can be written as

$$C_2\left(\prod_{i=1}^{N}\gamma_{i\mathrm{h}}E^*_{i\mathrm{h}}\right)^{\frac{1}{N}}\ln\left(\frac{1}{C_2}\left(\prod_{i=1}^{N}\gamma_{i\mathrm{h}}E^*_{i\mathrm{h}}\right)^{\frac{N-1}{N}}\right), \tag{2.49}$$

where $C_2 = \frac{1}{\exp(\nu^*)}$. Thus, even if a single SU is allocated zero energy on the link to HAP, the objective (2.49) becomes zero. Therefore, each SU attains non-zero throughput. This implies that no SU spends full amount of harvested energy relaying PU data.

Let us now consider the case where SUs experience poor channel conditions to HAP, i.e., a low SNR scenario. Using the approximation $\ln(1+x) \approx x$ for $x \ll 1$, the objective in (2.45) becomes $\sum_{i=1}^{N} \gamma_{i\mathrm{h}} E_{i\mathrm{h}}$. Then, using optimality conditions given in Proposition 2.2, the energy allocation subproblem is written as

$$\begin{aligned} \underset{\boldsymbol{E_{\mathrm{sh}}}, \boldsymbol{E_{\mathrm{sp}}}}{\text{maximize}} \quad & \sum_{i=1}^{N} \gamma_{i\mathrm{h}} E_{i\mathrm{h}} \\ \text{subject to} \quad & (2.35), (2.36), \boldsymbol{E_{\mathrm{sh}}}, \boldsymbol{E_{\mathrm{sp}}} \geq 0, \end{aligned} \tag{2.50}$$

which is equivalent to the problem in (2.40). Then, the energy allocation in ETA scheme in low SNR regime is same as the energy allocation in STORA scheme, i.e., SUs are prioritized to relay PU data in the increasing order of the ratio $\frac{\gamma_{i\mathrm{h}}}{\gamma_{i\mathrm{p}}}$, and at most one SU spends fractional energy on the relaying link. This implies that an SU might not have residual energy for spectrum access, despite being allocated time to access. Thus, in low SNR regime, even though the relay and energy allocation is same as that of STORA scheme, the unused time due to the lack of energy causes lower sum-throughput in ETA scheme compared to STORA scheme. Since the problem in (2.45) has the same structure as the problem (2.14) for STORA scheme, we can use Algorithms 1 and 2 to compute the optimal solution of (2.45), which has the same complexity as STORA scheme, i.e., $\mathcal{O}(N^2)$.

2.4.2 Minimum Throughput Maximization

The aim is to guarantee minimum throughput to each SU and yet maximize the SU sum-throughput. For a fixed $\mathcal{S}_{\mathcal{D}}$, the throughput maximization problem for MTM scheme is given by

$$\begin{aligned} \underset{\boldsymbol{E_{\mathrm{sh}}}, \boldsymbol{E_{\mathrm{sp}}}, \boldsymbol{t}, R_{\min}}{\text{maximize}} \quad & R_{\min} \\ \text{subject to} \quad & t_i \ln\left(1 + \frac{\gamma_{i\mathrm{h}} E_{i\mathrm{h}}}{t_i}\right) \geq R_{\min}, && \text{(2.51a)} \\ & (2.14\mathrm{b}) - (2.14\mathrm{g}), R_{\min} \geq 0. && \text{(2.51b)} \end{aligned}$$

Since the term $t_i \ln\left(1+\frac{\gamma_{i\mathrm{h}}E_{i\mathrm{h}}}{t_i}\right)$ in (2.51a) monotonically increases with t_i and $E_{i\mathrm{h}}$, (2.51a) implies that the maximum $R_{\min}$ is obtained when rates of all SUs are equal [41]. Thus, unless $R_{\min}=0$, all SUs get a chance to transmit on the direct link to HAP and no SU spends full amount of harvested energy on the relaying link. The SUs that have not decoded PU data successfully can access the spectrum, and thus Proposition 2.2 holds true.

The problem (2.51) is convex and Slater's condition [82, Chapter 3] holds true. Thus, the analytical expressions of the optimization variables can be obtained using KKT conditions. Similar to the STORA problem, for a fixed $\mathcal{S}_{\mathcal{D}}$, this problem can be divided into two levels, one for solving the energy allocation and time allocation on secondary links and other for solving t_{e} and $R_{\min}$ as a master primal problem. The Lagrangian dual of the energy allocation subproblem for a fixed $(R_{\min}, t_{\mathrm{e}})$ is given by

$$\begin{aligned}\max_{\boldsymbol{E_{\mathrm{sh}}},\boldsymbol{E_{\mathrm{sp}}}}\ & R_{\min}-\sum_{i=1}^{N}\rho_i\left(R_{\min}-R_i(E_{i\mathrm{h}},t_i)\right)-\lambda\left(\bar{R}_{\mathrm{p}}-R_{\mathrm{p,c}}(\boldsymbol{E_{\mathrm{sp}}},t_0)\right)\\ &-\sum_{i=1}^{N}\mu_i(E_{i\mathrm{p}}+E_{i\mathrm{h}}-(P_{\mathrm{e}}+\theta_i)t_{\mathrm{e}}),\end{aligned} \tag{2.52}$$

where ρ_i is the dual variable associated with the secondary rate constraint (2.51a) and dual of the time allocation subproblem is

$$\begin{aligned}\max_{t_0,\boldsymbol{t_a}}\ & R_{\min}-\sum_{i=1}^{N}\rho_i\left(R_{\min}-R_i(E_{i\mathrm{h}},t_i)\right)-\lambda\bar{R}_{\mathrm{p}}+\lambda R_{\mathrm{p,c}}(\boldsymbol{E_{\mathrm{sp}}},t_{\mathrm{e}},t_0)-\kappa\left(\bar{R}_{\mathrm{p}}-Q_1t_{\mathrm{e}}-Q_2t_0\right)\\ &-\nu(t_{\mathrm{e}}+2t_0+\sum_{i=1}^{N}t_i-1).\end{aligned} \tag{2.53}$$

The dual variables (λ,κ,ν) can be computed using their gradients given by (2.24)-(2.26), while the dual variable $\boldsymbol{\mu}$ is obtained using bisection method. The dual variable $\boldsymbol{\rho}$ minimizing the dual function (2.53) can be found using its gradient given by $g_{\rho_i}=R_i(E_{i\mathrm{h}},t_i)-R_{\min}$. The master primal problem in charge of updating t_{e} and $R_{\min}$ can be solved using subgradient based methods like ellipsoid method [82, Chapter 1] with their subgradients given by (2.28) and $g_{R_{\min}}=1-\sum_{i=1}^{N}\rho_i$, respectively. The Levels 1 and 2 are executed in a similar fashion as that of Algorithm 2 with additional dual update using $g_{\boldsymbol{\rho}}$ in Level 1 and primal update using $g_{R_{\min}}$ in Level 2. The decoding set that maximizes the sum-throughput can be found using the strategy presented in section 2.3.1 and Algorithm 1.

The following proposition provides the analytical expressions corresponding to the optimal solution.

Proposition 2.5. *The optimal energy and time allocation for the MTM scheme is given by*

$$[E^*_{\mathrm{s}_i\mathrm{h}},\ E^*_{i\mathrm{p}}] = \left[t_i^* \left[\frac{\rho_i^*}{\mu_i^*} - \frac{1}{\gamma_{i\mathrm{h}}} \right]^+, (2.30) \right],$$

$$[t^*_{\mathrm{e}},\ t^*_0,\ t^*_i] = \left[(2.31),\ (2.32),\ \frac{\gamma_{i\mathrm{h}} E^*_{i\mathrm{h}}}{\exp\left(\mathcal{W}\left(\frac{-1}{\frac{\nu^*}{\rho_i^*}+1} \right) + \frac{\nu^*}{\rho_i^*} + 1 \right) - 1} \right].$$

Proof. See Appendix A.3. □

Complexity of MTM scheme: Algorithm 2 for MTM scheme needs to update $N + 3$ dual variables. Updating these variables using the interior point method has complexity $\mathcal{O}(N^3)$ [82, Chapter 4], which dominates the complexity of Algorithm 2 for MTM scheme. Including the complexity of Algorithm 1, the complexity to calculate the optimal solution for MTM scheme is $\mathcal{O}(N^4)$.

2.4.3 Proportional Time Allocation

To divide the reward-generated access time among SUs, one of the plausible criteria is to allocate the access time to an SU proportional to its contribution in the received primary SNR. Then, in this case, to obtain an opportunity to access the spectrum, an SU has to relay PU data. Now, to relay PU data, the SU should decode PU data successfully. Based on this *decode-relay-then-access* condition, the optimization problem for the PTA scheme is formulated for a fixed $\mathcal{S}_{\mathcal{D}}$ as

$$\underset{\boldsymbol{E_{\mathrm{sh}}}, \boldsymbol{E_{\mathrm{sp}}}, \boldsymbol{t}}{\text{maximize}} \quad \sum_{i=1}^{N} t_i \ln\left(1 + \frac{\gamma_{i\mathrm{h}} E_{i\mathrm{h}}}{t_i}\right) \tag{2.54a}$$

$$\text{subject to} \quad t_i = \sum_{j=1}^{N} t_j \frac{\gamma_{i\mathrm{p}} E_{i\mathrm{p}}}{\sum_{j=1}^{N} \gamma_{j\mathrm{p}} E_{j\mathrm{p}}}, \tag{2.54b}$$

$$(2.14\mathrm{b}) - (2.14\mathrm{g}), \tag{2.54c}$$

where (2.54b) is the proportional time allocation constraint. Let us define the ratio

$$\frac{\sum_{j=1}^{N} t_j}{\sum_{j=1}^{N} \gamma_{j\mathrm{p}} E_{j\mathrm{p}}} = \frac{t_i}{\gamma_{i\mathrm{p}} E_{i\mathrm{p}}} = \zeta, \tag{2.55}$$

where ζ is a positive constant whose optimal value is unknown. Equation (2.55) implies $t_i = \zeta \gamma_{i\mathrm{p}} E_{i\mathrm{p}}$ and $\sum_{j=1}^{N} t_j = \zeta \sum_{j=1}^{N} \gamma_{j\mathrm{p}} E_{j\mathrm{p}}$; nevertheless, the former includes the latter. Therefore, the constraint (2.54b) can be replaced by

$$t_i = \zeta \gamma_{i\mathrm{p}} E_{i\mathrm{p}}. \tag{2.56}$$

Observe that the product of the optimization variables ζ and $E_{i\mathrm{p}}$, for all i, in (2.56) makes the problem (2.54) non-convex. However, for a given ζ, the constraint (2.56) is affine. The other constraints which are independent of ζ are either concave or affine as shown for STORA, ETA, and MTM schemes. Therefore, for a given ζ, the problem (2.54) is a convex optimization problem. The optimal decoding set $\mathcal{S}_{\mathcal{D}}$ can be obtained using the strategy proposed in section 2.3.1 and Algorithm 1. Using (2.56), for a fixed $(\mathcal{S}_{\mathcal{D}}, \zeta, t_{\mathrm{e}})$, the energy allocation and time allocation subproblems are given by

$$\begin{aligned} \texttt{SP3}: \quad \underset{\boldsymbol{E}_{\mathbf{sh}}, \boldsymbol{E}_{\mathbf{sp}}}{\text{maximize}} \quad & \sum_{i=1}^{N} R_i(E_{i\mathrm{h}}, \zeta \gamma_{i\mathrm{p}} E_{i\mathrm{p}}) \\ \text{subject to} \quad & (2.14\mathrm{b}), (2.14\mathrm{d}), (2.14\mathrm{g}) \end{aligned} \tag{2.57}$$

and

$$\begin{aligned} \texttt{SP4}: \quad \underset{t_0}{\text{maximize}} \quad & \sum_{i=1}^{N} R_i(E_{i\mathrm{h}}, \zeta \gamma_{i\mathrm{p}} E_{i\mathrm{p}}) \\ \text{subject to} \quad & (2.14\mathrm{b}), (2.14\mathrm{c}), \\ & t_{\mathrm{e}} + 2t_0 + \sum_{i=1}^{N} \zeta \gamma_{i\mathrm{p}} E_{i\mathrm{p}} \leq 1, \\ & t_0 \geq 0, \end{aligned} \tag{2.58}$$

respectively. The time allocation subproblem `SP4` reduces to a feasibility problem to solve for t_0 than solving both $(\boldsymbol{t_a}, t_0)$, and the master problem is responsible for updating t_{e} as that of the STORA scheme. For a given ζ, the subproblems `SP3` and `SP4`, and the master

problem are solved iteratively in a similar manner as that of in Algorithm 2. Since strong duality holds for a fixed ζ, the optimization variables can be found using KKT conditions as presented in Proposition 2.6. To gain insights on the effect of ζ on the SU sum-throughput, we obtain the Lagrangian of the problem (2.54) as

$$\begin{aligned}\mathcal{L}_4 = &\sum_{i=1}^{N} R_i(E_{i\mathrm{h}}, \zeta\gamma_{i\mathrm{p}}E_{i\mathrm{p}}) - \lambda\left(\bar{R}_{\mathrm{p}} - R_{\mathrm{p,c}}\left(\boldsymbol{E}_{\mathbf{sp}}, t_{\mathrm{e}}, t_0\right)\right)\\ &- \sum_{i=1}^{N}\mu_i(E_{i\mathrm{p}} + E_{i\mathrm{h}} - (P_{\mathrm{e}} + \theta_i)t_{\mathrm{e}})\\ &- \kappa\left(\bar{R}_{\mathrm{p}} - Q_1 t_{\mathrm{e}} - Q_2 t_0\right) - \nu(t_{\mathrm{e}} + 2t_0 + \sum_{i=1}^{N}\zeta\gamma_{i\mathrm{p}}E_{i\mathrm{p}} - 1). \end{aligned} \tag{2.59}$$

The Hessian of $\mathcal{L}_4$ with respect to ζ is

$$\frac{\partial^2\mathcal{L}_4}{\partial\zeta^2} = -\sum_{i=1}^{N}\frac{\gamma_{i\mathrm{h}}^2E_{i\mathrm{h}}^2}{\zeta^3\left(1+\frac{\gamma_{i\mathrm{h}}E_{i\mathrm{h}}}{\gamma_{i\mathrm{p}}E_{i\mathrm{p}}}\right)^2\gamma_{i\mathrm{p}}E_{i\mathrm{p}}} \leq 0. \tag{2.60}$$

This implies that $\mathcal{L}_4$ is a concave function of ζ. Then, the optimal value of ζ can be found using one dimensional search methods like golden section search [82, Appendix C] over $\zeta \geq 0$.

We give the analytical expressions corresponding to the optimal solution in the following proposition.

Proposition 2.6. *The optimal solution of the proportional time allocation (PTA) scheme is*

$$\begin{aligned}\left[E_{i\mathrm{h}}^*,\ E_{i\mathrm{p}}^*\right] &= \left[\zeta^*\gamma_{i\mathrm{p}}E_{i\mathrm{p}}^*\left[\frac{1}{\mu_i} - \frac{1}{\gamma_{i\mathrm{h}}^*}\right]^+,\ \mathcal{E}_i^*\right],\\ [t_{\mathrm{e}}^*,\ t_0^*,\ t_i^*] &= \left[1 - 2t_0^* - \sum_{i=1}^{N}\zeta^*\gamma_{i\mathrm{p}}E_{i\mathrm{p}}^*,\ (2.32),\ \zeta^*\gamma_{i\mathrm{p}}E_{i\mathrm{p}}^*\right],\end{aligned}$$

where $\mathcal{E}_i^*$ is the solution of

$$\ln(1+z_i^*) - \frac{z_i^*}{1+z_i^*} = \frac{\lambda^*/\zeta^*}{1+\gamma_{\mathrm{pp}} + \frac{\sum_{i=1}^{N}\gamma_{i\mathrm{p}}E_{i\mathrm{p}}^*}{t_0^*}} + \frac{\mu_i^*}{\zeta^*\gamma_{i\mathrm{p}}} + \frac{\nu^*}{\gamma_{i\mathrm{p}}},$$

with $z_i^* = \frac{\gamma_{i\mathrm{h}}E_{i\mathrm{h}}^*}{\zeta^*\gamma_{i\mathrm{p}}E_{i\mathrm{p}}^*}$ for all $\mathrm{SU}_i \in \mathcal{S}_{\mathcal{D}}$.

Proof. See Appendix A.4. □

Complexity of PTA scheme: In PTA scheme, we have additional golden section search for the variable ζ, which has complexity $\mathcal{O}(\frac{1}{\epsilon})$ for the ϵ-accurate solution. Since ϵ is constant (10^{-5} in our case), the complexity of PTA scheme is same as that of STORA scheme, i.e, $\mathcal{O}(N^2)$.

2.5 Results and Discussions

The instantaneous channel power gain of the link between user i and j is denoted as $g_{ij}d_{ij}^{-\beta}$, where g_{ij} is the instantaneous Rayleigh channel power gain with unit mean, d_{ij} is the distance between users i and j, and β is the path-loss exponent which is assumed to be 3. We use $P_{\mathrm{p}} = 20$ dBm, $\eta = 0.5$, $N_0 = -70$ dBm/Hz, and $\mathcal{G} = 8.8$ dB (for uncoded quadrature amplitude modulation) [81]. The PT and PD are situated at 50m from each other. The locations of PT, PD, and HAP are collinear, with HAP at equal distances from PT and PD. Unless otherwise stated, SUs are randomly located around HAP within a circle of radius 10m.[4] The results are averaged over 2000 channel realizations.

2.5.1 Performance Comparison of SU Selection Schemes

Fig. 2.5 compares the performance of the STORA scheme with that of the best SU selection (BSS) [74], the random single SU selection (RSS-S), and the random multiple SUs selection (RSS-M). The BSS allocates resources such that the SU sum-throughput is maximized with one SU relaying PU data; while in RSS-S, a random SU is chosen to relay PU data. In RSS-M, first a single SU is chosen randomly to relay PU data; if the cooperation from that chosen SU fails to meet the target primary rate, the second SU is chosen randomly for relaying, and so on.

Fig. 2.5(a) shows the effect of the target primary rate $\bar{R}_{\mathrm{p}}$ on the SU sum-throughput. In BSS scheme, a single SU may not be able to support $\bar{R}_{\mathrm{p}}$ due to insufficient harvested energy, failing to forge the cooperation (see Fig. 2.5(b)). This reduces the probability of cooperation and decreases the SU sum-throughput. The probability of cooperation is obtained as the ratio of number of channel realizations that result in successful cooperation between PU

[4]We take care that the distance between any two nodes is at least one metre.

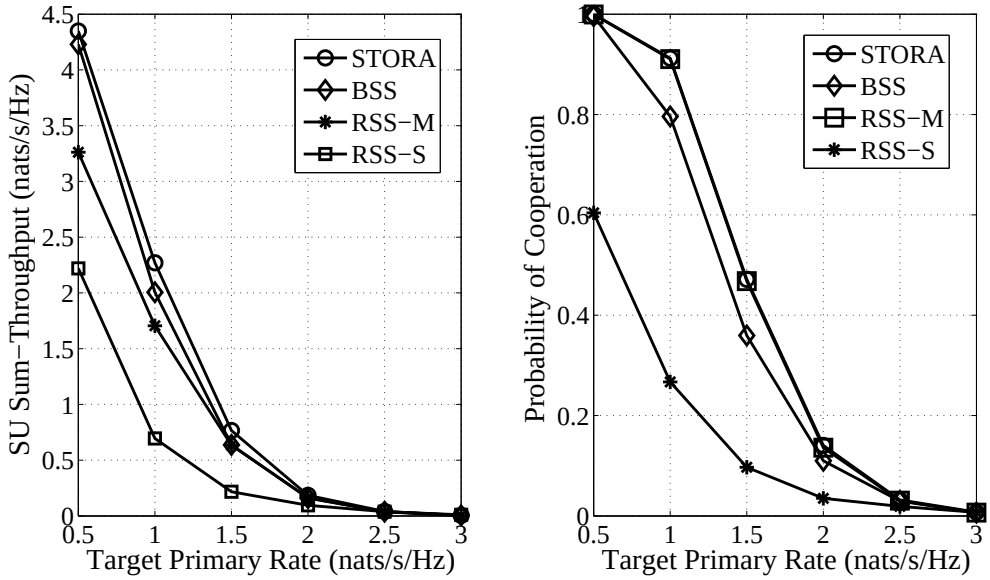

(a) (b)

Figure 2.5: Effect of target primary rate ($\bar{R}_{\mathrm{p}}$) on the (a) SU sum-throughput, (b) probability of cooperation. $N = 4$ and $P_{\mathrm{e}} = 20$ dBm.

and SUs to the total number of channel realizations considered in simulations. In RSS-S scheme, the random selection of a single SU may not be able to meet $\bar{R}_{\mathrm{p}}$, which reduces the chances of cooperation. As Fig. 2.5(b) shows, RSS-M achieves the same probability of cooperation as that of STORA due to the selection of multiple SUs for relaying. But, since RSS-M chooses relaying SUs randomly, it fails to exploit the resources efficiently, resulting in the reduced SU sum-throughput. Also, Fig. 2.5(b) shows that, with the increase in $\bar{R}_{\mathrm{p}}$, it becomes more difficult for SUs to satisfy $\bar{R}_{\mathrm{p}}$, reducing the probability of cooperation as expected. In Fig. 2.5(b), the probability of cooperation less than one indicates that the primary rate constraint given by (2.6) may not be satisfied through secondary cooperation in each fading state. The following subsection discusses the effect of the constraint of meeting target primary rate on the SU sum-throughput in detail.

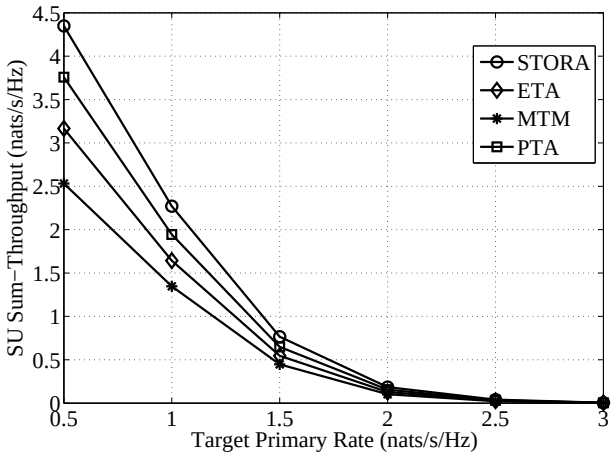

(a) SU sum-throughput $R_{\mathrm{s,sum}}$

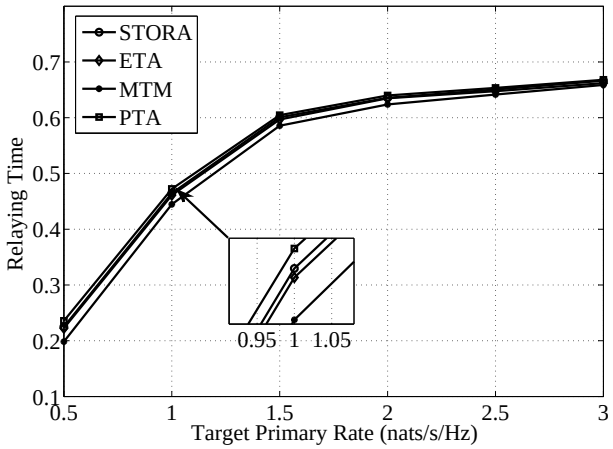

(b) Time spent by SUs on relaying t_0

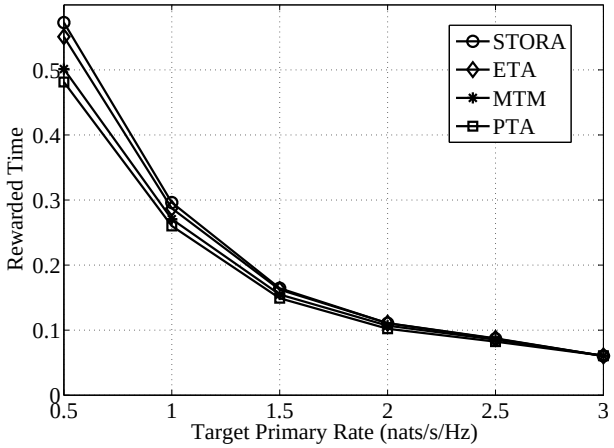

(c) Rewarded time for SUs to access the spectrum t_a

Figure 2.6: Effect of target primary rate ($\bar{R}_{\mathrm{p}}$) for different resource allocation schemes for $N = 4$ and $P_{\mathrm{e}} = 20$dBm.

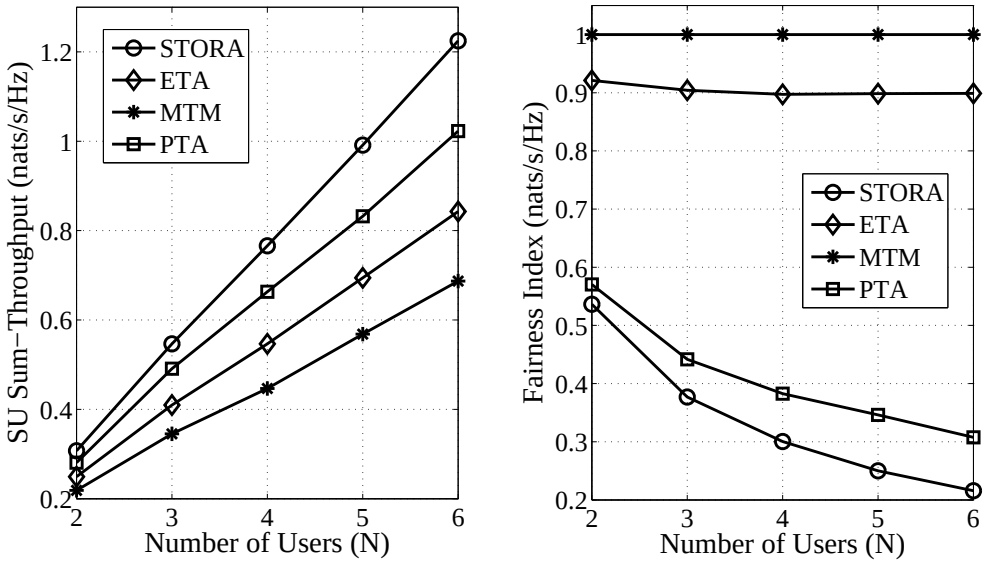

(a) (b)

Figure 2.7: Effect of number of SUs on the (a) SU sum-throughput, (b) fairness. $\bar{R}_{\mathrm{p}} = 2$ nats/s/Hz and $P_{\mathrm{e}} = 20$ dBm.

2.5.2 Effect of Primary Rate Constraint

As the target primary rate $\bar{R}_{\mathrm{p}}$ increases, the relaying SUs spend more time to relay PU data (see Fig. 2.6(b)) which reduces SUs' spectrum access time (see Fig. 2.6(c)), deteriorating the SU sum-throughput. As shown in Fig. 2.6(a), the STORA scheme achieves the highest SU sum-throughput as it allocates resources efficiently. The ETA scheme allocates all SUs equal time for the spectrum access irrespective of their harvested energy, the residual energy left with them after relaying, and the channel gains. As Fig. 2.6(a) shows, MTM scheme's efforts to uplift SUs with unfavourable conditions to the level of SUs with favourable conditions expend the resources the least efficiently, achieving the lowest SU sum-throughput. In PTA scheme, the *decode-relay-then-access* constraint, as Fig. 2.6(b) shows, forces PTA scheme to spend the highest time in decoding and relaying as SUs with poor links to PT consume additional time to decode PU data successfully, reducing the SU sum-throughput compared to the STORA scheme.

2.5.3 Effect of Number of Secondary Users

The increase in number of SUs N increases the user diversity as well as the possibility of having more users with higher harvested energy and good channel gains to HAP. This increases the number of SUs available to relay PU data, and time and energy available for the spectrum access. This improves the SU sum-throughput. Fig. 2.7(b) shows the fairness achieved by each of the resource allocation schemes through Jain's fairness index $\mathcal{FI}$ [85] given by $\mathcal{FI} = \frac{\left(\sum_{i=1}^{N} x_i\right)^2}{N\sum_{i=1}^{N} x_i^2}$, where x_i is the throughput of ith SU. Higher the fairness index, fairer is the scheme. Figs. 2.7(a) and 2.7(b) together highlight the tradeoff between the SU sum-throughput and fairness. That is, the STORA scheme achieves the highest sum-throughput, but is the least fairness inducing scheme; while MTM scheme is the fairest scheme as all SUs achieve the same throughput, but achieves the lowest sum-throughput as the resource allocation becomes inefficient from network's point of view. In ETA, though assigning equal time to each SU results in some fairness, it does not maximize the SU sum-throughput. In PTA, the contribution of an SU on the relaying link decides its time-share in the spectrum access. Though this provides better fairness compared to STORA, the PTA scheme loses to the STORA scheme in terms of the SU sum-throughput due to the *decode-relay-then-access* constraint.

2.5.4 Effect of HAP's Transmit Power

Fig. 2.8(a) depicts the effect of HAP's transmit power P_{e} on the SU sum-throughput. As P_{e} increases, SUs harvest more energy from HAP's energy broadcast, which in turn increases the energy available for SUs' own transmissions for a given $\bar{R}_{\mathrm{p}}$. This improves SU sum-throughput. Fig. 2.8(b) shows that the trend of fairness achieved by each of the four resource allocation schemes remains the same as that shown in Fig. 2.7(b).

2.5.5 Effect of SUs' Location Radius Around HAP

We consider that SUs are located randomly within a circle of radius R meters around HAP, where the channels suffer from only path-loss attenuation. Fig. 2.9 shows that the increase in R is unfavourable to the SU sum-throughput. The increase in R increases the possibility

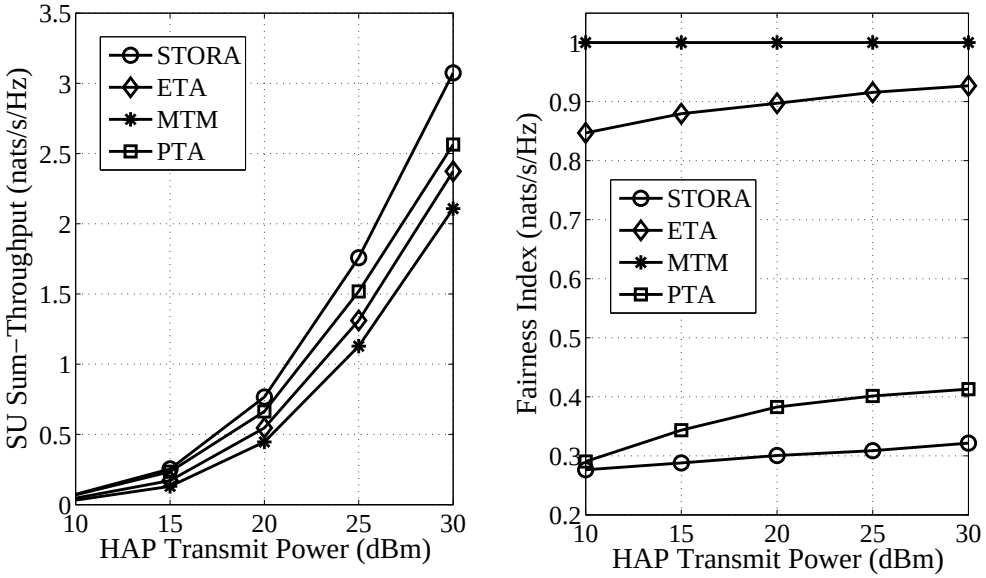

(a) (b)

Figure 2.8: Effect of HAP's transmit power on (a) SU sum-throughput, (b) fairness. $\bar{R}_{\mathrm{p}} = 1.5$ nats/s/Hz and $P_{\mathrm{e}} = 20$ dBm.

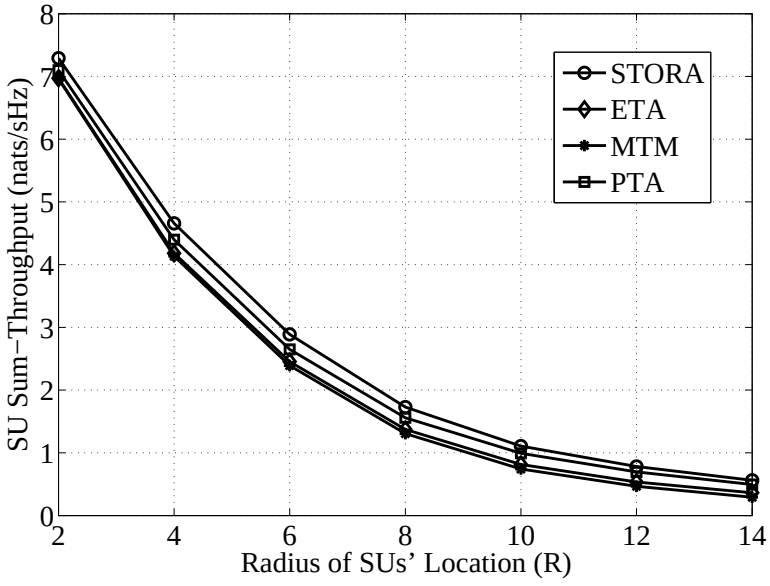

Figure 2.9: Effect of SUs' distribution around HAP on SU sum-throughput for $N = 4$ and $\bar{R}_{\mathrm{p}} = 1.5$ nats/s/Hz.

that SUs are located farther from the HAP, which has doubly negative effect on SU sum-throughput. First, the harvested energy by SUs reduces due to path-loss, which ultimately reduces the energy available for relaying and SUs' own transmissions. As a result, the SU sum-throughput deteriorates. Second, in the rewarded time, SUs have to transmit data to HAP over longer distances, which causes the fall in the received SNR at HAP. This further decreases SU sum-throughput.

2.6 Chapter Summary

The main contribution of this chapter is the integration of a wireless powered communication network with a cooperative cognitive radio network to reap the advantages of the both together. Given the primary rate constraint, the STORA scheme jointly performs the relay selection and energy and time allocation for SUs. But the STORA scheme creates unfairness among SUs as some SUs may get zero individual throughput. Other investigated resource allocation schemes like ETA, MTM, and PTA enhance fairness, but achieve lower secondary sum-throughput compared to the STORA scheme due to the throughput-fairness tradeoff. By allowing SUs to obtain equal throughput under all conditions, MTM scheme becomes the fairest scheme among the four schemes, but sacrifices the most on sum-throughput. Though the *decode-relay-then-access* constraint puts PTA scheme behind the STORA scheme in terms of the SU sum-throughput, PTA still seems to be a good compromise between the sum-throughput and fairness. The STORA scheme provides a mechanism to trade-off fairness with overall throughput. In fact, STORA scheme generalizes the existing algorithms, because the optimal algorithm proposed for STORA can be modified to accommodate different fairness constraints considered in this chapter.

Chapter 3

Information and Energy Cooperation

3.1 Introduction

Given the advancements in wireless energy transfer, it is natural to ask the question whether the information cooperation can be supplemented by the energy cooperation between two nodes. Energy cooperation is useful in a scenario where there is no dedicated energy source, such as HAP, available to power users. In this regard, this chapter focuses on energy cooperation along with information cooperation between primary and secondary users.

Consider the case of low energy availability with SU. In this case, if PT-PD channel is in deep fade and ST-PD channel is of good quality, neither PT can transmit its information nor ST can relay. Therefore, the information cooperation is not guaranteed if the relaying ST is energy-constrained. But, using the energy provided by PU, an ST can help relay PU message and in turn gain the spectrum access as a reward. Thus, expanding the cooperation to the energy level between PU and SU in addition to the information increases the probability of cooperation, improving the system's overall spectral efficiency. This motivates us to study the information and energy cooperation together in CR. Also, we aim to forge the cooperation between primary and secondary networks over multiple slots, i.e., over a finite horizon, and under the finite battery constraint at ST.

3.1.1 Related Work

In cooperative cognitive radio framework, most existing works (e.g., see [7, 8, 9, 10, 13, 69, 70, 72, 74, 86, 87]) have focused only on information cooperation between PU and SU. In [72, 87], an interference-free information cooperation is proposed using quadrature signaling. Authors in [37, 88] consider non-CR scenarios where a transmitter furnishes the relay with energy for information cooperation, while authors in [89] propose the joint information and energy cooperation in EH cellular networks. In CR with infinite battery, a recent work in [75] studies the joint information and energy cooperation between PU and SU in a single slot with an objective to provide best-effort QoS (does not assure minimum QoS) for SU while guaranteeing minimum QoS to PU (as considered in Chapter 2). However, when SU is required to provide real-time service requiring the minimum rate guarantee, provisioning the best-effort QoS may not be useful.

Notation: A bold-faced symbol (e.g., $\boldsymbol{P}$) denotes the vector of length N. The term $\sum_{i=a}^{b}(\cdot) = 0$ if $b < a$. The notation $[x]^+$ means $\max(x, 0)$. The symbol P^* denotes the optimal value, while $\boldsymbol{P}^*$ corresponds to the sequence of P_i^*s for $i = 1, \ldots, N$. Throughout the chapter, we assume $k = 1, \ldots, N$.

3.2 System Model

We consider that PT and ST are energy harvesting nodes, and have no other conventional energy source. The ST has a battery of finite capacity $B_{\max}$ to store the incoming energy, whereas PT harvests energy at a higher rate than that of ST and has a large battery of sufficient capacity. This is generally the case when PT is a primary base-station, equipped with sophisticated energy harvesting devices. As shown in Fig. 3.1, to realize the cooperation, ST relays PT's traffic to PD and receives an opportunity to transmit its own data to SD. Without loss of generality, we consider each slot duration to be unity. Thus, the terms energy and power can be used interchangeably. We focus on the case where PT and ST are located in close proximity to each other, and thus, the time required by ST to learn PT's message can be neglected [7, 8, 9]. We assume that PT and ST always have data to transmit. To allow concurrent transmissions by PT and ST without mutual interference,

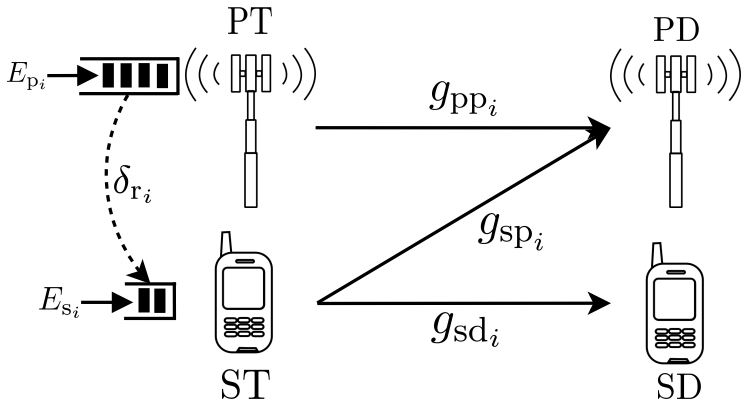

Figure 3.1: Information and energy cooperation in slot i.

we employ the following cooperation framework as in [72, 87]. The PT and ST transmit on orthogonal channels by exploiting quadrature components of quadrature phase shift keying (QPSK). That is, PT transmits data to PD using binary phase shift keying, which is in-phase component of QPSK; ST uses QPSK for transmission, where it relays PT's traffic using in-phase component of QPSK (I-channel) and transmits its own data using quadrature-phase component (Q-channel). The PD can coherently combine the received signals from PT and ST.

In slot i, let f_{pp_i}, f_{sp_i}, and f_{sd_i} denote Rayleigh channel power gains of PT-PD, ST-PD, and ST-SD links, respectively. The channel remains static in a slot, but changes independently over slots. The energy harvesting process at both PU and SU is assumed to be stationary and ergodic. We use the Bernoulli model for illustration, which is as follows: At the beginning of slot i, PU harvests energy E_{p_i}, which is equal to E_{p} with probability θ_{p} and zero otherwise; while SU harvests energy E_{s_i} which is equal to E_{s} with probability θ_{s} and zero otherwise. The PT transmits with power P_{p_i} on PT-PD link and transfers energy δ_{r_i} to ST. Note that PT transmits data and energy over orthogonal channels to ST. The ST receives an energy $\eta\delta_{\mathrm{r}_i}$, where η $(0 < \eta \leq 1)$ is the energy transfer efficiency. We assume that PT and ST have the perfect global channel state information.

The PD employs MRC to combine the signals from PT and ST. Let $R_{\mathrm{p,c}_i}$ and $R_{\mathrm{p,nc}_i}$ denote the rates achieved by PU with and without cooperation in ith slot, respectively, which are

as follows:

$$R_{\mathrm{p,c}_i} = \ln\left(1 + g_{\mathrm{pp}_i} P_{\mathrm{p}_i} + g_{\mathrm{sp}_i} P_{\mathrm{sp}_i}\right), \tag{3.1}$$

$$R_{\mathrm{p,nc}_i} = \ln\left(1 + g_{\mathrm{pp}_i} P'_{\mathrm{p}_i}\right), \tag{3.2}$$

where P_{sp_i} denotes the power with which ST performs relaying, $g_{\mathrm{pp}_i} = f_{\mathrm{pp}_i}/N_0$ and $g_{\mathrm{sp}_i} = f_{\mathrm{sp}_i}/N_0$ are the normalized channel power gains on PT-PD and ST-PD links, respectively, and N_0 is AWGN power. The power P'_{p_i} on PT-PD link under no cooperation is obtained by maximizing the objective $\sum_{i=1}^{N} R_{\mathrm{p,nc}_i}$ subject to the constraint $\sum_{i=1}^{k} P'_{\mathrm{p}_i} \leq \sum_{i=1}^{k} E_{\mathrm{p}_i}$ for $\forall k$. The secondary rate R_{s_i} in slot i is

$$R_{\mathrm{s}_i} = \ln\left(1 + g_{\mathrm{sd}_i} P_{\mathrm{sd}_i}\right), \tag{3.3}$$

where P_{sd_i} is the power with which ST transmits to SD and $g_{\mathrm{sd}_i} = f_{\mathrm{sd}_i}/N_0$. We now define the constraints in our problem before formulating it.

Cooperation rate constraint: The PU's average rate with cooperation over N slots must be at least its average rate without cooperation, i.e.,

$$\frac{1}{N}\sum_{i=1}^{N} R_{\mathrm{p,c}_i} \geq \frac{1}{N}\sum_{i=1}^{N} R_{\mathrm{p,nc}_i} = \bar{R}_{\mathrm{p}}. \tag{3.4}$$

Secondary rate constraint: The SU should achieve minimum average rate $\bar{R}_{\mathrm{s}}$ over N slots during cooperation. That is,

$$\frac{1}{N}\sum_{i=1}^{N} \ln\left(1 + g_{\mathrm{sd}_i} P_{\mathrm{sd}_i}\right) \geq \bar{R}_{\mathrm{s}}. \tag{3.5}$$

Energy neutrality constraints: The energy spent by PT till any slot k cannot exceed the total harvested energy till that slot. Thus, over a finite horizon of N slots, we have

$$\sum_{i=1}^{k} \left(P_{\mathrm{p}_i} + \delta_{\mathrm{r}_i}\right) \leq \sum_{i=1}^{k} E_{\mathrm{p}_i}, \quad \forall k. \tag{3.6}$$

Similarly, for ST, we write the energy neutrality constraint as

$$\sum_{i=1}^{k} \left(P_{\mathrm{sp}_i} + P_{\mathrm{sd}_i}\right) \leq \sum_{i=1}^{k} \left(E_{\mathrm{s}_i} + \eta\delta_{\mathrm{r}_i}\right), \quad \forall k. \tag{3.7}$$

Finite battery constraint: The ST cannot store more energy than the finite capacity $B_{\max}$ of the battery. That is,

$$\sum_{i=1}^{k} \left(E_{\mathrm{s}_i} + \eta\delta_{\mathrm{r}_i}\right) - \sum_{i=1}^{k-1} \left(P_{\mathrm{sp}_i} + P_{\mathrm{sd}_i}\right) \leq B_{\max}, \quad \forall k. \tag{3.8}$$

3.3 Problem Formulation and Optimal Solution

The objective is to maximize PU's rate with cooperation over a finite horizon of N slots, i.e., $\sum_{i=1}^{N} R_{\mathrm{p,c}_i}$. The entire problem is now formulated as follows:

$$\begin{aligned}
\underset{\substack{\boldsymbol{P_p},\boldsymbol{\delta_r},\\ \boldsymbol{P_{sp}},\boldsymbol{P_{sd}}}}{\text{maximize}} \quad & \sum_{i=1}^{N} R_{\mathrm{p,c}_i}, && \text{(3.9a)}\\
\text{subject to} \quad & \frac{1}{N}\sum_{i=1}^{N} R_{\mathrm{p,c}_i} \geq \bar{R}_{\mathrm{p}}, && \text{(3.9b)}\\
& \frac{1}{N}\sum_{i=1}^{N} \ln\left(1+g_{\mathrm{sd}_i}P_{\mathrm{sd}_i}\right) \geq \bar{R}_{\mathrm{s}}, && \text{(3.9c)}\\
& \sum_{i=1}^{k}\left(P_{\mathrm{p}_i}+\delta_{\mathrm{r}_i}\right) \leq \sum_{i=1}^{k} E_{\mathrm{p}_i} \quad \forall k, && \text{(3.9d)}\\
& \sum_{i=1}^{k}\left(P_{\mathrm{sp}_i}+P_{\mathrm{sd}_i}\right) \leq \sum_{i=1}^{k}\left(E_{\mathrm{s}_i}+\eta\delta_{\mathrm{r}_i}\right) \quad \forall k, && \text{(3.9e)}\\
& \sum_{i=1}^{k}\left(E_{\mathrm{s}_i}+\eta\delta_{\mathrm{r}_i}\right) - \sum_{i=1}^{k-1}\left(P_{\mathrm{sp}_i}+P_{\mathrm{sd}_i}\right) \leq B_{\max} \quad \forall k, && \text{(3.9f)}\\
& P_{\mathrm{p}_i}, \delta_{\mathrm{r}_i}, P_{\mathrm{sp}_i}, P_{\mathrm{sd}_i} \geq 0, \quad \forall i. && \text{(3.9g)}
\end{aligned}$$

Since the objective and constraints (3.9b), (3.9c) are concave, and the constraints (3.9d)-(3.9f) are affine, the problem (3.9) is convex. The feasible region $\mathcal{F}$ of problem (3.9) is defined by the constraints (3.9b) - (3.9g). Firstly, we propose the necessary conditions that our optimal solution must satisfy and then proceed to find the optimal solution.

3.3.1 Optimality Conditions

Proposition 3.1. *The optimal power policy $P^*_{\mathrm{sd}_i}$ $(1 \leq i \leq N)$ must meet* $\bar{R}_{\mathrm{s}} = \frac{1}{N}\sum_{i=1}^{N} \ln\left(1+g_{\mathrm{sd}_i}P^*_{\mathrm{sd}_i}\right)$.

Proof. Assume the constraint (3.9c) is satisfied with strict inequality. We can then reduce some $P^*_{\mathrm{sd}_i}$ without violating the constraint and increase the power to relay PU's data; say, increasing some $P^*_{\mathrm{sp}_i}$, which improves PU's rate. This contradicts the assumption that $P^*_{\mathrm{sd}_i}$ is optimal. □

Proposition 3.2. *The optimal power policy* $P^*_{\mathrm{p}_i}$ *and* $\delta^*_{\mathrm{r}_i}$ *must meet* $\sum_{i=1}^{N}\left(P^*_{\mathrm{p}_i}+\delta^*_{\mathrm{r}_i}\right) = \sum_{i=1}^{N} E_{\mathrm{p}_i}$.

Proof. Suppose the constraint (3.9d) is satisfied with strict inequality. That is, PT is left with some unused energy at the end of N slots. Then, we can increase either some $P^*_{\mathrm{p}_i}$, or some $\delta^*_{\mathrm{r}_i}$ which contributes to $P^*_{\mathrm{sp}_i}$ without violating the constraint, achieving a higher PU rate. This contradicts the assumption that $P^*_{\mathrm{p}_i}$ and $\delta^*_{\mathrm{r}_i}$ are optimal. □

Proposition 3.3. *The optimal power policy* $P^*_{\mathrm{sd}_i}$, $P^*_{\mathrm{sp}_i}$, *and* $\delta^*_{\mathrm{r}_i}$ *must meet* $\sum_{i=1}^{N}\left(P^*_{\mathrm{sp}_i}+P^*_{\mathrm{sd}_i}\right) = \sum_{i=1}^{N}\left(E_{\mathrm{s}_i}+\eta\delta^*_{\mathrm{r}_i}\right)$.

Proof. We omit this proof as it can be obtained based on the similar argument given in the proof for Proposition 3.2. □

3.3.2 Optimal Solution

We rewrite the objective in (3.9) by incorporating (3.9b) in the objective as $\sum_{i=1}^{N} R_{\mathrm{p,c}_i} - N\bar{R}_{\mathrm{p}}$, which is non-negative in the feasible region $\mathcal{F}$. Then, the Lagrangian of the problem (3.9) is

$$\begin{aligned}
\mathcal{L} = &\Big(\sum_{i=1}^{N}\ln\left(1+g_{\mathrm{pp}_i}P_{\mathrm{p}_i}+g_{\mathrm{sp}_i}P_{\mathrm{sp}_i}\right)-N\bar{R}_{\mathrm{p}}\Big)-\lambda\left(N\bar{R}_{\mathrm{s}}-\sum_{i=1}^{N}\ln\left(1+g_{\mathrm{sd}_i}P_{\mathrm{sd}_i}\right)\right)\\
&-\sum_{k=1}^{N}\mu_k\left(\sum_{i=1}^{k}\left(P_{\mathrm{p}_i}+\delta_{\mathrm{r}_i}-E_{\mathrm{p}_i}\right)\right)-\sum_{k=1}^{N}\gamma_k\left(\sum_{i=1}^{k}\left(P_{\mathrm{sp}_i}+P_{\mathrm{sd}_i}-E_{\mathrm{s}_i}-\eta\delta_{\mathrm{r}_i}\right)\right)\\
&-\sum_{k=1}^{N}\gamma'_k\left(\sum_{i=1}^{k}\left(E_{\mathrm{s}_i}+\eta\delta_{\mathrm{r}_i}\right)-\sum_{i=1}^{k-1}\left(P_{\mathrm{sp}_i}+P_{\mathrm{sd}_i}\right)-B_{\max}\right)\\
&+\sum_{k=1}^{N}\tau_{1,k}P_{\mathrm{p}_k}+\sum_{k=1}^{N}\tau_{2,k}\delta_{\mathrm{r}_k}+\sum_{k=1}^{N}\tau_{3,k}P_{\mathrm{sp}_k}+\sum_{k=1}^{N}\tau_{4,k}P_{\mathrm{sd}_k},
\end{aligned}\tag{3.10}$$

where λ, $\boldsymbol{\mu}$, $\boldsymbol{\gamma}$, $\boldsymbol{\gamma'}$, $\boldsymbol{\tau_1}$, $\boldsymbol{\tau_2}$, $\boldsymbol{\tau_3}$, and $\boldsymbol{\tau_4}$ are dual variables. The Karush-Kuhn-Tucker (KKT) stationarity conditions are

$$\frac{g_{\mathrm{pp}_i}}{1+g_{\mathrm{pp}_i}P^*_{\mathrm{p}_i}+g_{\mathrm{sp}_i}P^*_{\mathrm{sp}_i}}-\sum_{k=i}^{N}\mu^*_k+\tau^*_{1,i}=0, \tag{3.11}$$

$$-\sum_{k=i}^{N}\mu^*_k+\eta\sum_{k=i}^{N}\gamma^*_k-\eta\sum_{k=i}^{N}\gamma'^*_k+\tau^*_{2,i}=0, \tag{3.12}$$

$$\frac{g_{\mathrm{sp}_i}}{1+g_{\mathrm{pp}_i}P^*_{\mathrm{p}_i}+g_{\mathrm{sp}_i}P^*_{\mathrm{sp}_i}}-\sum_{k=i}^{N}\gamma^*_k+\sum_{k=i+1}^{N}\gamma'^*_k+\tau^*_{3,i}=0, \tag{3.13}$$

$$\frac{\lambda^* g_{\mathrm{sd}_i}}{1+g_{\mathrm{sd}_i}P^*_{\mathrm{sd}_i}}-\sum_{k=i}^{N}\gamma^*_k+\sum_{k=i+1}^{N}\gamma'^*_k+\tau^*_{4,i}=0, \tag{3.14}$$

and the complementary slackness conditions are as follows:

$$\lambda^*\left(N\bar{R}_{\mathrm{s}}-\sum_{i=1}^{N}\ln\left(1+g_{\mathrm{sd}_i}P^*_{\mathrm{sd}_i}\right)\right)=0, \tag{3.15}$$

$$\mu^*_k\sum_{i=1}^{k}\left(P^*_{\mathrm{p}_i}+\delta^*_{\mathrm{r}_i}-E_{\mathrm{p}_i}\right)=0, \tag{3.16}$$

$$\gamma^*_k\sum_{i=1}^{k}\left(P^*_{\mathrm{sp}_i}+P^*_{\mathrm{sd}i}-E_{\mathrm{s}i}-\eta\delta^*_{\mathrm{r}_i}\right)=0, \tag{3.17}$$

$$\gamma'^*_k\left(\sum_{i=1}^{k}\left(E_{\mathrm{s}_i}+\eta\delta^*_{\mathrm{r}_i}\right)-\sum_{i=1}^{k-1}\left(P^*_{\mathrm{sp}_i}+P^*_{\mathrm{sd}_i}\right)-B_{\max}\right)=0, \tag{3.18}$$

$$\tau^*_{1,k}P^*_{\mathrm{p}_k}=\tau^*_{2,k}\delta^*_{\mathrm{r}_k}=\tau^*_{3,k}P^*_{\mathrm{sp}_k}=\tau^*_{4,k}P^*_{\mathrm{sd}_k}=0 \tag{3.19}$$

for all k. For the ease of computation, we neglect the dual variables $\boldsymbol{\tau}_1, \boldsymbol{\tau}_2, \boldsymbol{\tau}_3$, and $\boldsymbol{\tau}_4$ associated with the non-negativity of power vectors. Rather, we incorporate the non-negativity by projecting the powers onto the positive orthant and use them wherever necessary. From (3.11)-(3.14), we obtain

$$P^*_{\mathrm{p}_i}=\left[\frac{1}{\sum_{k=i}^{N}\mu^*_k}-\frac{1}{g_{\mathrm{pp}_i}}-\frac{g_{\mathrm{sp}_i}}{g_{\mathrm{pp}_i}}P^*_{\mathrm{sp}_i}\right]^+, \tag{3.20}$$

$$P^*_{\mathrm{sp}_i}=\left[\frac{1}{\sum_{k=i}^{N}\gamma^*_k-\sum_{k=i+1}^{N}\gamma'^*_k}-\frac{1}{g_{\mathrm{sp}_i}}-\frac{g_{\mathrm{pp}_i}}{g_{\mathrm{sp}_i}}P^*_{\mathrm{p}_i}\right]^+, \tag{3.21}$$

$$P^*_{\mathrm{sd}_i}=\left[\frac{\lambda}{\sum_{k=i}^{N}\gamma^*_k-\sum_{k=i+1}^{N}\gamma'^*_k}-\frac{1}{g_{\mathrm{sd}_i}}\right]^+, \tag{3.22}$$

$$\frac{\eta g_{\mathrm{sp}_i} - g_{\mathrm{pp}_i}}{1 + g_{\mathrm{pp}_i} P^*_{\mathrm{p}_i} + g_{\mathrm{sp}_i} P^*_{\mathrm{sp}_i}} = \tau^*_{1,i} + \eta \gamma'^*_i - \tau^*_{2,i} - \eta \tau^*_{3,i}. \tag{3.23}$$

Note that, given the strict concave nature of rate constraints at PT and ST, the associated optimal power vectors $(\boldsymbol{P}^*_{\mathrm{p}}, \boldsymbol{P}^*_{\mathrm{sp}}, \boldsymbol{P}^*_{\mathrm{sd}})$ are unique; whereas, $\boldsymbol{\delta}^*_{\mathrm{r}}$ can have multiple possible values. Due to the affine nature of constraints (3.9d)-(3.9f) associated with $\boldsymbol{\delta}^*_{\mathrm{r}}$, the expression to evaluate $\boldsymbol{\delta}^*_{\mathrm{r}}$ cannot be found. Also, $\boldsymbol{P}^*_{\mathrm{p}}$ and $\boldsymbol{P}^*_{\mathrm{sp}}$ are dependent on each other as seen from (3.20) and (3.21). Thus, to compute the optimal power vectors based on (3.20)-(3.22), we employ an iterative algorithm, which is explained below.

3.3.3 Iterative Algorithm to Compute Optimal Solution

From (3.9), we observe that the power transfer variable $\boldsymbol{\delta}_{\mathrm{r}}$ couples the energy neutrality constraints at PT and ST given by (3.9d), (3.9e) and the finite battery constraint at ST in (3.9f). Also, the constraint (3.9b) couples the powers $\boldsymbol{P}_{\mathrm{p}}$ and $\boldsymbol{P}_{\mathrm{sp}}$. Now, to decouple the variables and find the optimal solution, we propose the following approach. First, to decouple (3.9d) and (3.9e)-(3.9f), we perform the primal decomposition [90] by fixing the coupling variable $\boldsymbol{\delta}_{\mathrm{r}}$. Then, we divide the problem (3.9) into three layers. In each iteration, Layer 1 solves the power allocation for $\boldsymbol{P}_{\mathrm{p}}$, while Layer 2 solves the power allocation for $(\boldsymbol{P}_{\mathrm{sp}}, \boldsymbol{P}_{\mathrm{sd}})$, and finally, Layer 3 updates $\boldsymbol{\delta}_{\mathrm{r}}$. Note that Layers 1 and 2 decouple the powers $\boldsymbol{P}_{\mathrm{p}}$ and $\boldsymbol{P}_{\mathrm{sp}}$. This three-layer problem is solved in an iterative manner until all optimization variables converge. To begin with, we initialize the primal variables $\boldsymbol{\delta}_{\mathrm{r}}, \boldsymbol{P}_{\mathrm{sp}}, \boldsymbol{P}_{\mathrm{sd}}$, and dual variables $\lambda, \boldsymbol{\mu}, \boldsymbol{\gamma}, \boldsymbol{\gamma}'$. Below, we explain the sub-problems in each layer.

Layer 1: The sub-problem to solve for the power vector $\boldsymbol{P}_{\mathrm{p}}$ on the direct link of PT is

$$\begin{aligned} \underset{\boldsymbol{P}_{\mathrm{p}}}{\text{maximize}} \quad & \sum_{i=1}^{N} R_{\mathrm{p,c}_i} - N \bar{R}_{\mathrm{p}} \\ \text{subject to} \quad & (3.9\mathrm{d}), P_{\mathrm{p}_i} \geq 0 \ \ \forall i. \end{aligned} \tag{3.24}$$

For a given $\boldsymbol{\delta}_{\mathrm{r}}$, $\boldsymbol{P}_{\mathrm{sp}}$, and $\boldsymbol{\mu}$, $\boldsymbol{P}_{\mathrm{p}}$ is evaluated using (3.20). The dual problem of (3.24) is given by $\min\limits_{\boldsymbol{\mu} \geq 0} \ \max\limits_{\boldsymbol{P}_{\mathrm{p}} \in \mathcal{F}} \ \mathcal{L}_1$, where $\mathcal{L}_1$ is the corresponding Lagrangian function. Since the dual function $\max\limits_{\boldsymbol{P}_{\mathrm{p}} \in \mathcal{F}} \ \mathcal{L}_1$ is differentiable, the dual variable $\boldsymbol{\mu}$ that minimizes the dual problem in

(3.24) is found using gradient method as

$$\mu_k = \left[\mu_k + s\sum_{i=1}^{k}\left(P_{\mathrm{p}_i} + \delta_{\mathrm{r}_i} - E_{\mathrm{p}_i}\right)\right]^+, \forall k,$$

where s denotes the positive step size chosen to satisfy the diminishing step size rule [82].

Layer 2: The sub-problem for jointly solving the power allocation $(\boldsymbol{P}_{\mathrm{sp}}, \boldsymbol{P}_{\mathrm{sd}})$ is

$$\begin{aligned} \underset{\boldsymbol{P}_{\mathrm{sp}},\boldsymbol{P}_{\mathrm{sd}}}{\text{maximize}} \quad & \sum_{i=1}^{N} R_{\mathrm{p,c}_i} - N\bar{R}_{\mathrm{p}} \\ \text{subject to} \quad & (3.9\mathrm{c}), (3.9\mathrm{e}), (3.9\mathrm{f}), P_{\mathrm{sp}_i}, P_{\mathrm{sd}_i} \geq 0 \ \ \forall i. \end{aligned} \tag{3.25}$$

Using the results obtained in (3.21) and (3.22), we compute $(\boldsymbol{P}_{\mathrm{sp}}, \boldsymbol{P}_{\mathrm{sd}})$ for given $\boldsymbol{P}_{\mathrm{p}}$, $\boldsymbol{\delta}_{\mathrm{r}}$, and $\lambda, \boldsymbol{\gamma}, \boldsymbol{\gamma'}$. As in Layer 1, the dual variables minimizing the dual problem of (3.25) given by $\min\limits_{\lambda,\boldsymbol{\gamma},\boldsymbol{\gamma'},\geq 0} \ \max\limits_{\boldsymbol{P}_{\mathrm{sp}},\boldsymbol{P}_{\mathrm{sd}}\in\mathcal{F}} \ \mathcal{L}_2$, are updated using their gradients as

$$\begin{aligned} \lambda &= \left[\lambda + s\left(N\bar{R}_{\mathrm{s}} - \sum_{i=1}^{N}\ln\left(1 + g_{\mathrm{sd}_i}P_{\mathrm{sd}_i}\right)\right)\right]^+, \\ \gamma_k &= \left[\gamma_k + s\left(\sum_{i=1}^{k}\left(P_{\mathrm{sp}i} + P_{\mathrm{sd}i} - E_{\mathrm{s}i} - \eta\delta_{\mathrm{r}_i}\right)\right)\right]^+, \\ \gamma'_k &= \left[\gamma'_k + s\left(\sum_{i=1}^{k}(E_{\mathrm{s}_i} + \eta\delta_{\mathrm{r}_i}) - \sum_{i=1}^{k-1}\left(P_{\mathrm{sp}_i} + P_{\mathrm{sd}_i}\right) - B_{\max}\right)\right]^+ \end{aligned}$$

for all k, and $\mathcal{L}_2$ is the Lagrangian of (3.25). The computation of the set of primal, dual variables $(\boldsymbol{P}_{\mathrm{p}}, \boldsymbol{\mu})$, and $(\boldsymbol{P}_{\mathrm{sp}}, \boldsymbol{P}_{\mathrm{sd}}, \lambda, \boldsymbol{\mu}, \boldsymbol{\gamma}, \boldsymbol{\gamma'})$ is done recursively in their corresponding layers 1 and 2 until they converge to a predetermined accuracy.

Layer 3: In Layer 3, the primal variable $\boldsymbol{\delta}_{\mathrm{r}}$ is updated using sub-gradient method as

$$\delta_{\mathrm{r}_i} = \left[\delta_{\mathrm{r}_i} - s\left(\sum_{j=i}^{N}\left(\mu_j - \eta\gamma_j + \eta\gamma'_j\right)\right)\right]^+ \forall i.$$

Since each layer involves solving a convex problem, this three-layer iterative approach is guaranteed to converge to the optimal solution [82].

3.4 Specific Scenarios

In this section, we provide specific scenarios to gain insights about the joint information and energy cooperation protocol. The primary rate mainly depends on PT-PD and ST-PD links, characterized by channel power gains g_{pp_i} and g_{sp_i}, respectively. Unlike the only direct link transmission, i.e., via PT-PD link, PT can achieve user diversity with the help of ST and through ST-PD link. Hence, it is important to investigate the effects of both links on the optimal solution.

3.4.1 The case when $g_{\mathrm{pp}_i} > g_{\mathrm{sp}_i}$

Given ST has the knowledge about the primary message, it looks natural for PT to allocate the power for its transmission on the link chosen from PT-PD and ST-PD links with the better channel power gain. That is, when $g_{\mathrm{pp}_i} > g_{\mathrm{sp}_i}$, it may appear that P_{sp_i} is zero. However, this is not always true, which we show through the following proposition.

Proposition 3.4. *When $g_{\mathrm{pp}_i} > g_{\mathrm{sp}_i}$, $\delta^*_{\mathrm{r}_i}$ and $P^*_{\mathrm{sp}_i}$ cannot be non-zero simultaneously.*

Proof. When $g_{\mathrm{pp}_i} > g_{\mathrm{sp}_i}$, from (3.23), we observe that the left side term of the equation is negative since $0 < \eta \leq 1$, and $\left(1 + g_{\mathrm{pp}_i} P^*_{\mathrm{p}i} + g_{\mathrm{sp}_i} P^*_{\mathrm{sp}_i}\right) > 0$. Thus, the right side term of (3.23) is also negative, making $(\tau^*_{2,i} + \eta\tau^*_{3,i}) > (\tau^*_{1,i} + \eta\gamma'^*_i)$.

Suppose $\delta^*_{\mathrm{r}_i}$ and $P^*_{\mathrm{sp}_i}$ are non-zero in slot i. Then, from the complementary slackness condition in (3.19), we have $\tau^*_{2,i} = \tau^*_{3,i} = 0$. This leads to $0 > (\tau^*_{1,i} + \eta\gamma'^*_i)$, which is impossible as $\tau^*_{1,i} \geq 0$ and $\gamma'^*_i \geq 0$, arriving at a contradiction. □

Note that Proposition 3.4 holds for both finite and infinite battery cases. We further elaborate Proposition 3.4 intuitively as follows. In some slot i with $g_{\mathrm{pp}_i} > g_{\mathrm{sp}_i}$, PT is unwilling to spend power on ST-PD link, which is weaker than PT-PD link. Given this, PT has no incentive to transfer energy to ST, making $\delta^*_{\mathrm{r}_i} = 0$. Then, $P^*_{\mathrm{sp}_i} > 0$ means that ST relays PT's message with the energy left with it after satisfying its rate constraint $\bar{R}_{\mathrm{s}}$. On the other hand, the case $\delta^*_{\mathrm{r}_i} > 0$ and $P^*_{\mathrm{sp}_i} = 0$ occurs if ST is *energy-depleted*. That is, PT feeds ST $\delta^*_{\mathrm{r}_i}$ amount of energy in that slot which either contributes towards satisfying SU's rate constraint or is to be utilized in future slots.

3.4.2 The case when $g_{\mathrm{pp}_i} < \eta g_{\mathrm{sp}_i}$

Proposition 3.5. *When* $g_{\mathrm{pp}_i} < \eta g_{\mathrm{sp}_i}$,

$$P^*_{\mathrm{p}_i} \begin{cases} = 0, & E_i < B_{\max} \\ \geq 0, & E_i = B_{\max}, \end{cases} \tag{3.26}$$

where $E_i = \sum_{j=1}^{i} \left(E_{\mathrm{s}_j} + \eta \delta^*_{\mathrm{r}_j} \right) - \sum_{j=1}^{i-1} \left(P^*_{\mathrm{sp}_j} + P^*_{\mathrm{sd}_j} \right)$ *is the energy available with ST at the start of slot* i.

Proof. When $g_{\mathrm{pp}_i} < \eta g_{\mathrm{sp}_i}$, from (3.23), we see that the left side term of the equation is positive, implying the right side term of (3.23) is also positive, making $(\tau^*_{1,i} + \eta \gamma'^*_i) > (\tau^*_{2,i} + \eta \tau^*_{3,i})$.

For $E_i < B_{\max}$, from (3.18), we have $\gamma'^*_i = 0$. Thus, if $P^*_{\mathrm{p}_i} > 0$, $\tau^*_{1,i} = 0$ leading to $(\tau^*_{2,i} + \eta \tau^*_{3,i}) < 0$, which is impossible since $\tau^*_{2,i} \geq 0$ and $\tau^*_{3,i} \geq 0$. For $E_i = B_{\max}$, $\gamma'^*_i > 0$ from (3.18). Thus, $P^*_{\mathrm{p}_i}$ can be either non-zero with $\eta \gamma'^*_i > \tau^*_{2,i} + \eta \tau^*_{3,i}$ or zero with $\tau^*_{1,i} + \eta \gamma'^*_i > \tau^*_{2,i} + \eta \tau^*_{3,i}$. □

In some slot i, let us first consider $E_i < B_{\max}$. Here, PT is willing to spend its transmission power only on ST-PD link as $g_{\mathrm{pp}_i} < \eta g_{\mathrm{sp}_i}$. Thus, PT will transfer energy $\delta^*_{\mathrm{r}_i}$ to ST as long as $E_i < B_{\max}$, keeping $P^*_{\mathrm{p}_i} = 0$. However, with $E_i = B_{\max}$, ST cannot accommodate additional energy from PT, which forces PT to either transmit on PT-PD link or store the energy for the transmission in future slots, depending on future channels gains on PT-PD and ST-PD links.

Numerical Example:

We provide a numerical example to illustrate Propositions 3.4 and 3.5. Let $N = 5$, $\boldsymbol{g_p} = [0.0191\ 0.0080\ 0.0036\ 0.0024\ 0.0119]$, $\boldsymbol{g_{sp}} = [0.0065\ 0.0074\ 0.0194\ 0.0256\ 0.0067]$, $\boldsymbol{g_{sd}} = [0.0027\ 0.0140\ 0.0164\ 0.0201\ 0.0010]$, $\boldsymbol{E_s} = [0\ 0\ 1\ 0\ 1]$, $\boldsymbol{E_p} = [7\ 0\ 0\ 7\ 0]$, $B_{\max} = 3.5$ J, $\eta = 1$, $N_0 = 0$ dBm, $\bar{R}_{\mathrm{s}} = 0.5$ nats/slot/Hz. PU's sum-rate in cooperation scheme $R_{\mathrm{p,c}} = 3.6914$ nats/slot/Hz, and $R_{\mathrm{p,nc}} = 3.0073$ nats/slot/Hz without cooperation. The optimal power allocation is given in Table 3.1.

We observe that PT-PD link is better than ST-PD link in the first, second, and last slots, where we have $\delta^*_{\mathrm{r}_1}, \delta^*_{\mathrm{r}_2} > 0, \delta^*_{\mathrm{r}_5} = 0$ and $P^*_{\mathrm{sp}_1}, P^*_{\mathrm{sp}_2} = 0, P^*_{\mathrm{sp}_5} > 0$ which is in agreement with

Table 3.1: Optimal Solution to Numerical Example

Slot	1	2	3	4	5
$P^*_{\mathrm{sd}_i}$	0.0000	0.2249	0.2354	0.3165	0.0000
$P^*_{\mathrm{sp}_i}$	0.0000	0.0000	2.5014	3.1835	1.0000
$P^*_{\mathrm{p}_i}$	2.5555	2.4828	0.0000	0.0000	3.5000
$\delta^*_{\mathrm{r}_i}$	0.7216	0.4908	0.7493	3.5000	0.0000
E_i	0.7216	1.2124	2.7368	3.5000	1.0000

Proposition 3.4. Also, we note that, energy transfers in the first two slots contribute towards $P^*_{\mathrm{sd}_2}$, i.e., it helps SU to achieve its rate constraint as ST has not harvested enough energy and is energy-depleted. In the last slot, we have $\delta^*_{\mathrm{r}_5} = 0$ and $P^*_{\mathrm{sp}_5} = 1$, implying ST has spent its harvested energy on the relaying link since its rate constraint is satisfied. This is also in agreement with Proposition 3.3, which says that no energy should be left with ST at the end of the horizon under the optimal solution. This could also be seen as a virtual two-way energy cooperation between PU and SU to maximize the primary rate given the rate constraints of both PU and SU are satisfied. Thus, the energy spent by PT satisfying SU's rate constraint in earlier slots is a wise investment by PU to improve its maximum achieved rate. Similarly, we can also validate the Proposition 3.5 from Table 3.1.

3.5 Results and Discussions

We consider a scenario where the distances between PT-PD, ST-PD, and ST-SD are each 5m. The mean channel power gain of the channel between nodes i and j is given by $d_{ij}^{-\rho}$, where d_{ij} is the distance between nodes i and j and ρ is the path-loss exponent, which is assumed to be 2.7. ST is located close to PT at a distance of 0.5m. Thus, PT prefers the help from ST to relay the data and gains user diversity. Due to the close-proximity of PT and ST, ST can learn PT's message in negligible time [86]. The noise power is 0 dBm. The probability of harvesting energy in a slot at PT and ST is $\theta_{\mathrm{p}} = \theta_{\mathrm{s}} = 0.5$. Unless otherwise stated, we obtain the results over 1000 channel and energy realizations.

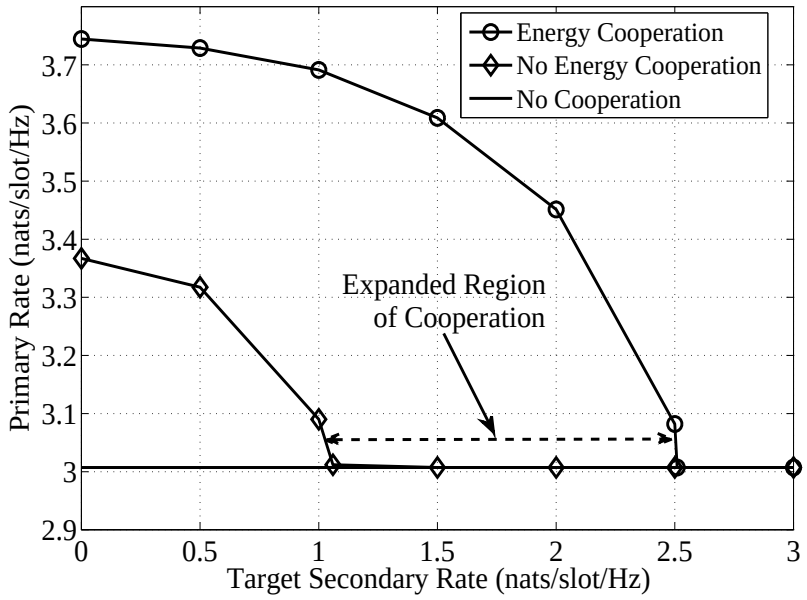

Figure 3.2: Rate regions with and without energy cooperation.

3.5.1 Effect of Energy Cooperation

Fig. 3.2 compares the rate regions for joint information and energy cooperation scheme to that of only information cooperation for a specific randomly chosen channel realization and system parameters given in the numerical example in Section 3.4. We observe that the joint information and energy cooperation expands the achievable rate region compared to that with only information cooperation. As seen from Fig. 3.2, in the case of only information cooperation, SU can impose the rate constraint ($\bar{R}_{\mathrm{s}}$) at the most 1.06 nats/slot/Hz, beyond which increasing $\bar{R}_{\mathrm{s}}$ reduces the primary rate below the no cooperation rate, in turn, entering the infeasible region. Thus, the cooperation is not beneficial to PU any more and it pulls out of it achieving no cooperation rate. On the other hand, enlarging the cooperation to energy level pushes the cooperation region to a higher $\bar{R}_{\mathrm{s}}$ (2.51 nats/slot/Hz from 1.06 nats/slot/Hz). Note that when there is no cooperation between PU and SU, PU transmits solely in the channel, and its rate is unaffected by $\bar{R}_{\mathrm{s}}$.

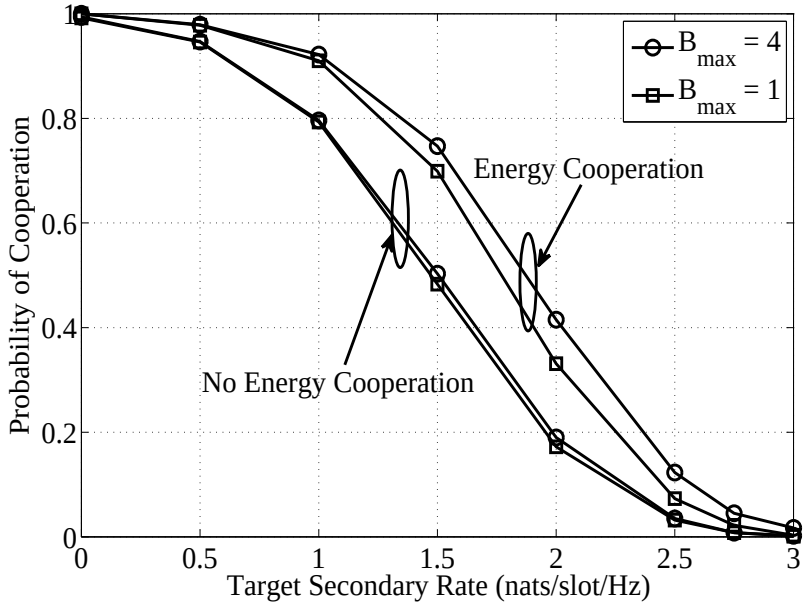

Figure 3.3: Probability of cooperation with and without energy cooperation, $N = 5$, $\eta = 0.3$, $E_{\mathrm{p}} = 7$, $E_{\mathrm{s}} = 1$.

3.5.2 Effect of Secondary Rate Constraint

Fig. 3.3 shows that the joint information and energy cooperation scheme between PU and SU increases the probability of cooperation compared to only information cooperation scheme, where the probability of cooperation is the ratio of number of channel and energy realizations that result in successful cooperation between PU and SU to the total number of channel and energy realizations considered in simulations. This is because, the energy cooperated by PU to the energy-constrained SU increases its lifetime and keeps the latter active in the network. Also, as SU imposes higher rate constraint $\bar{R}_{\mathrm{s}}$, the probability of cooperation in both cases reduces. This is due to the fact that, with higher $\bar{R}_{\mathrm{s}}$, it becomes more difficult to satisfy both primary and secondary rate constraints together given the energies harvested by PU and SU, making one of them to fall out of the cooperation. Another important observation is that the smaller ST's battery size ($B_{\max}$) reduces the probability of cooperation as less energy can be accommodated in SU's battery lowering the powers for relaying as well as its own transmission.

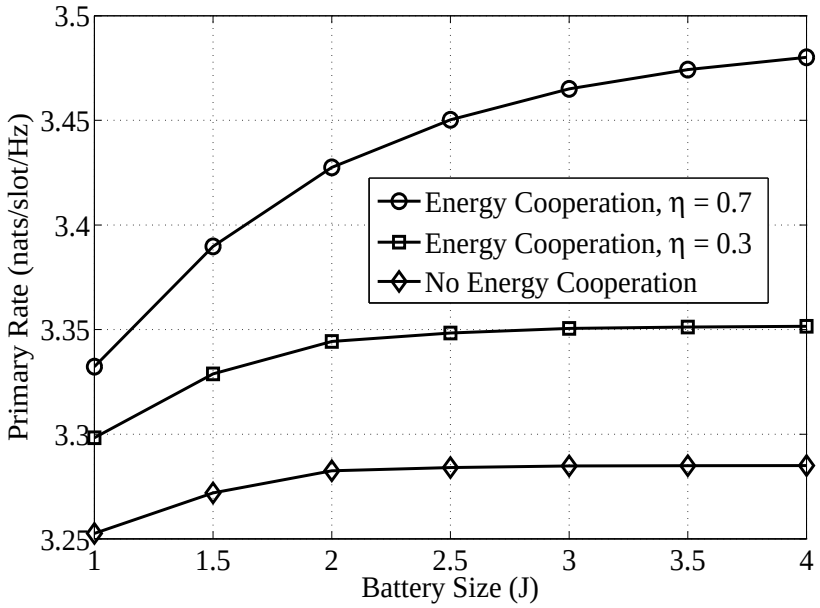

Figure 3.4: Effect of ST's finite battery size ($B_{\max}$), $N = 5$, $\bar{R}_{\rm s} = 0.5$ nats/slot/Hz, $E_{\rm p} = 7$, $E_{\rm s} = 1$.

3.5.3 Effect of Battery Size

Fig. 3.4 shows the effect of ST's battery size ($B_{\max}$), where the proposed joint information and energy cooperation scheme outperforms the only information cooperation scheme. We note that the increase in $B_{\max}$ improves the primary rate in both cases with and without energy cooperation as expected. In a slot, the lower $B_{\max}$ limits the energy transferred by PT to ST even if the latter has a better channel to PD. Thus, the gain achieved with energy cooperation over without energy cooperation scheme is low. But, with increase in $B_{\max}$, PT can cooperate more energy to the energy-constrained ST keeping the latter active for the cooperation and obtain significant rate gain over no energy cooperation scheme. If the battery size is sufficiently large to accommodate the harvested and transferred energy, there is a very limited additional advantage in making the battery size even bigger. Also, the higher energy transfer efficiency η makes more energy available to SU, increasing the probability of cooperation and thus the primary rate.

3.6 Chapter Summary

This chapter proposes the energy cooperation between energy harvesting primary and secondary users in addition to the information cooperation over a finite horizon with finite capacity battery. The joint information and energy cooperation expands the region of cooperation between primary and secondary users improving the chances of cooperation. This, in turn, increases the user diversity, through which the primary user achieves significant rate gains compared to only information cooperation while assuring the rate-guaranteed service to both users. We observe that the finite battery size at the secondary transmitter restricts the secondary rate and the gain of the energy cooperation.

Part II

Underlay Mode

Chapter 4

Energy Harvesting Cognitive Relays in Nakagami-m Channels

4.1 Introduction

In underlay mode, the interference constraint at PU limits the transmit power of SU, which restricts its transmission range. One solution to improve the coverage and the reliability of SU's transmission is the use of an intermediate secondary user as a relay [91, 92, 93]. This is a type of *intra-network cooperation*. But the relays may have limited battery reserves, and recharging or replacing the battery frequently may be inconvenient. This invokes the need for an external power source to keep relays active in the network. The EH relays can overcome such energy shortage while exploiting the spatial diversity [94, 95].

For EH relays, the optimal use of available energy is crucial. Low transmission power to conserve energy may prolong the lifetime of a relay, however, at the cost of increased outage; whereas higher transmission power improves the transmission quality, but at the expense of higher energy consumption rate reducing the future chances of transmission. Due to this EH nature of relays, the best relay selection becomes tricky as only relays having sufficient energy to forward the data to the destination, called *active relays*, can be considered for the selection, making energy a crucial factor in the relay selection. In addition, in spectrum sharing, EH relay's transmit power depends not only on the energy availability with it, but also on the

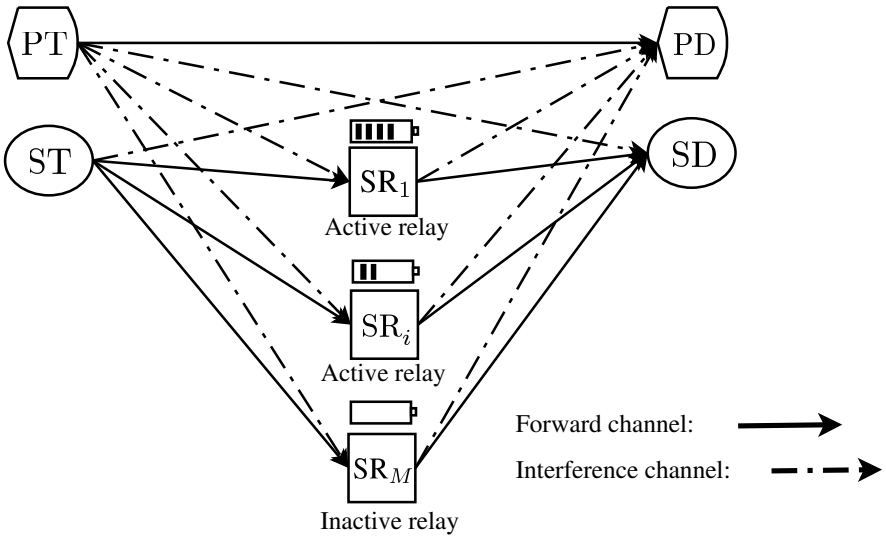

Figure 4.1: Secondary transmissions via EH relays with underlay spectrum sharing.

maximum power allowed by PU's outage constraint. For example, in a case where a relay has harvested less energy, it may not transmit with the maximum power allowed by PU's outage constraint. On the contrary, even if the relay has harvested large amount of energy, a tight PU's outage constraint may not allow relay to transmit with higher power. Thus there exists an interesting tussle between these two constraints putting a stronger restriction on relay's transmit power.

4.1.1 Related Work

The works in [21, 91, 92, 93, 96, 97, 98, 99, 100, 101, 102] have considered the use non-EH secondary relays to facilitate spectrum sharing. The works in [59, 88, 94, 95, 103] have analyzed the effect of energy harvesting nature of relays on the system performance in non-cognitive radio scenarios. As to the EH relays in cognitive radio, [63, 104, 105] consider an EH secondary relay which helps relay the secondary data, and perform the secondary outage analysis for Rayleigh fading channels under the interference constraint at the primary receiver; while the work in [106] studies cooperative communication via multiple EH relays.

4.2 System Model

As shown in Fig. 4.1, the network consists of a PT, a PD, an ST, an SD, and M energy harvesting DF secondary relays (SRs). The PT, PD, ST, and SD are conventional nodes with constant energy supply (e.g., battery). The ST-SD direct link is unavailable. The ST communicates with SD over ith half-duplex EH relay (SR_i), $i \in \{1, 2, \ldots, M\}$. The channel between a transmitter p and a receiver q is a Nakagami-m fading channel; h_{pq} denotes the channel coefficient. That, we denote channel coefficients of links PT-PD, PT-SR_i, PT-SD, ST-PD, ST-SR_i, SR_i-SD, and SR_i-PD by h_{pp}, $h_{\mathrm{p}i}$, h_{pd}, h_{sp}, $h_{\mathrm{s}i}$, $h_{i\mathrm{d}}$, and $h_{i\mathrm{p}}$, respectively. The channel power gain is denoted by $g_{pq} = |h_{pq}|^2$ and is Gamma-distributed with mean Ω_{pq} and fading severity parameter m_{pq}. We can write the probability density function (PDF) and cumulative distribution function (CDF) of a random variable $U = g_{pq}$ as

$$f_U(u) = \frac{\alpha_{pq}^{m_{pq}}}{\Gamma(m_{pq})} u^{m_{pq}-1} \exp(-\alpha_{pq} u), \tag{4.1}$$

$$F_U(u) = \frac{\Upsilon(m_{pq}, \alpha_{pq} u)}{\Gamma(m_{pq})} = 1 - \frac{\Gamma(m_{pq}, \alpha_{pq} u)}{\Gamma(m_{pq})}, \tag{4.2}$$

respectively, where $\Gamma(\cdot)$, $\Gamma(\cdot, \cdot)$, and $\Upsilon(\cdot, \cdot)$ are the complete, upper incomplete, and lower incomplete Gamma functions [107], respectively; $\alpha_{pq} = m_{pq}/\Omega_{pq}$. The channels are independent of each other. For PT-PD, ST-PD, and SR_i-PD links, we assume the mean channel power gain knowledge due to limited feedback; while SR_i and SD have the instantaneous channel gain knowledge for respective receiving links, i.e., ST-SR_i and PT-SR_i links at SR_i, and SR_i-SD and PT-SD links at SD. The secondary communication happens over two phases, each of T-second duration. All channels experience block-fading and remain constant for $2T$-second, i.e., two phases of secondary communication. In phase 1, ST transmits to EH secondary relays, while in phase 2, the received signal from ST is forwarded by one of the relays to SD after decoding.

4.2.1 Energy Harvesting Model

The energy harvesting process of a relay i is stationary and ergodic [94], with mean $H_{\mathrm{av},i}$ Joules per second (J/s). This model encompasses different energy harvesting sources like

solar, vibrations, RF signals in the surroundings [36], and different energy harvesting profiles [108]. The EH relay stores the harvested energy in a battery with negligible leakage. For analytical tractability, we assume the capacity of the energy storage to be large. In addition, the energy consumption occurs only in data transmission; any other energy expenditure, e.g., energy consumption in signal reception and processing, is not considered for the purpose of exposition.

4.2.2 Maximum Secondary Transmit Powers in Spectrum Sharing

In this work, we characterize QoS of PU by its outage probability. For constant transmit power of PT (P_{PT}), the PU outage probability should be below a certain threshold Θ_{p} given the interference from the secondary transmitter and the relay. This constraint limits the transmit powers of ST and SR to P_{s} and P_{r}, respectively. In phase 1, the outage probability of PU $\mathrm{P}_{\mathrm{p,out,ST}}$ when ST is transmitting, is given as

$$\mathrm{P}_{\mathrm{p,out,ST}} = \mathbb{P}\left(\log_2\left(1+\gamma_{\mathrm{PD}}\right) \leq \bar{R}_{\mathrm{p}}\right) \leq \Theta_{\mathrm{p}}, \tag{4.3}$$

where $\mathbb{P}$ denotes the probability, $\gamma_{\mathrm{PD}} = \frac{P_{\mathrm{p}} g_{\mathrm{pp}}}{P_{\mathrm{s}} g_{\mathrm{sp}} + N_0}$ is SINR at PD, N_0 being the noise power of AWGN at all receivers, and $\bar{R}_{\mathrm{p}}$ is the desired data rate on the primary link.

Proposition 4.1. *We write* $\mathrm{P}_{\mathrm{p,out,ST}}$ *as follows:*

$$\mathrm{P}_{\mathrm{p,out,ST}} = 1 - \left[\frac{\alpha_{\mathrm{sp}}^{m_{\mathrm{sp}}} \exp\left(\frac{-\alpha_{\mathrm{pp}}\theta_{\mathrm{p}}N_0}{P_{\mathrm{p}}}\right)}{\Gamma(m_{\mathrm{sp}})} \sum_{k=0}^{m_{\mathrm{pp}}-1} \left(\frac{\alpha_{\mathrm{pp}}\theta_{\mathrm{p}}N_0}{P_{\mathrm{p}}}\right)^k \frac{1}{k!} \sum_{t=0}^{k} \binom{k}{t} \left(\frac{P_{\mathrm{s}}}{N_0}\right)^t \times \frac{\Gamma(m_{\mathrm{sp}}+t)}{\left(\frac{\alpha_{\mathrm{pp}}\theta_{\mathrm{p}}P_{\mathrm{s}}}{P_{\mathrm{p}}} + \alpha_{\mathrm{sp}}\right)^{m_{\mathrm{sp}}+t}}\right]. \tag{4.4}$$

Proof. The proof is given in Appendix B.1. □

Using (4.4), the value of maximum ST power P_{s} allowed by PU's outage constraint Θ_{p} can be numerically found. Similarly, in phase 2, the maximum allowable transmit power P_{r} for a relay can be numerically found from (4.5), replacing the role of secondary transmitter

in (4.4) by the secondary relay and replacing corresponding channel parameters.

$$\mathrm{P}_{\mathrm{p,out,SR}} = 1 - \left[\frac{\alpha_{\mathrm{rp}}^{m_{\mathrm{rp}}} \exp\left(\frac{-\alpha_{\mathrm{pp}}\theta_{\mathrm{p}}N_0}{P_{\mathrm{p}}}\right)}{\Gamma(m_{\mathrm{rp}})} \sum_{k=0}^{m_{\mathrm{pp}}-1} \left(\frac{\alpha_{\mathrm{pp}}\theta_{\mathrm{p}}N_0}{P_{\mathrm{p}}}\right)^k \frac{1}{k!} \sum_{t=0}^{k} \binom{k}{t} \left(\frac{P_{\mathrm{r}}}{N_0}\right)^t \times \frac{\Gamma(m_{\mathrm{rp}}+t)}{\left(\frac{\alpha_{\mathrm{pp}}\theta_{\mathrm{p}}P_{\mathrm{r}}}{P_{\mathrm{p}}} + \alpha_{\mathrm{rp}}\right)^{m_{\mathrm{rp}}+t}} \right]. \tag{4.5}$$

4.2.3 Active Relays and Best Relay Selection

Assume that out of the total M relays, N relays are active ($N \in \{0, 1, \ldots, M\}$) due to energy availability, and a relay has to be selected from active N relays. An *active* relay is the relay having sufficient energy to forward the received data from ST.

For an opportunistic DF relaying, the relay with the largest end-to-end SINR at SD, called *the best relay*, is selected to forward the signal. When N relays are available for selection, the largest end-to-end SINR at SD is given by

$$\gamma_{\mathrm{tot}}^{N} = \max_{\mathrm{SR}_i \in \mathbb{R}} (\min(\gamma_i, \gamma_{i\mathrm{d}})), \tag{4.6}$$

where $\mathbb{R}$ is the set of active relays. Note that $\mathbb{R}$ is an empty set when no relay is active. γ_i and $\gamma_{i\mathrm{d}}$ are SINRs at ith relay and at SD over $\mathrm{R}_i - \mathrm{D}$ channel, respectively, and are given as

$$\gamma_i = \frac{P_{\mathrm{s}} g_{\mathrm{s}i}}{P_{\mathrm{p}} g_{\mathrm{p}i} + N_0}, \tag{4.7}$$

$$\gamma_{i\mathrm{d}} = \frac{P_i g_{i\mathrm{d}}}{P_{\mathrm{p}} g_{\mathrm{pd}} + N_0}, \tag{4.8}$$

where we obtain P_{s} and $P_i = P_{\mathrm{r}}$ from (4.4) and (4.5), respectively.

4.3 Secondary Outage Analysis

Now, when we select the best relay out of N active relays, the secondary outage probability $\mathrm{P}_{\mathrm{s,out}}^{N}$ can be given as

$$\mathrm{P}_{\mathrm{s,out}}^{N}(\gamma) = \mathbb{P}(\gamma_{\mathrm{tot}}^{N} \leq \gamma) = \mathbb{P}\left(\max_{\mathrm{SR}_i \in \mathbb{R}} (\min(\gamma_i, \gamma_{i\mathrm{d}})) \leq \gamma \right), \tag{4.9}$$

where secondary's desired secondary rate is $\bar{R}_{\mathrm{s}} = \frac{1}{2}\log_2(1+\gamma)$. For the ease of representation and without compromising the insight into analysis, we consider $m_{\mathrm{s}i} = m_{\mathrm{sr}}$, $m_{i\mathrm{d}} = m_{\mathrm{rd}}$,

$m_{\mathrm{p}i} = m_{\mathrm{pr}}$, $m_{i\mathrm{p}} = m_{\mathrm{rp}}$, $\Omega_{\mathrm{s}i} = \Omega_{\mathrm{sr}}$, $\Omega_{i\mathrm{d}} = \Omega_{\mathrm{rd}}$, $\Omega_{\mathrm{p}i} = \Omega_{\mathrm{pr}}$, and $\Omega_{i\mathrm{p}} = \Omega_{\mathrm{rp}}$. Then, we have $P_i = P_{\mathrm{r}}$. Below we give the closed-form expression for $\mathrm{P}^N_{\mathrm{s,out}}$.

Proposition 4.2. *We write* $\mathrm{P}^N_{\mathrm{s,out}}(\gamma)$ *as follows:*

$$\begin{aligned}\mathrm{P}^N_{\mathrm{s,out}}(\gamma) = &\sum_{r_0=0}^{N}\sum_{r_1=0}^{r_0}\cdots\sum_{r_{m_{\mathrm{rd}}-1}=0}^{r_{m_{\mathrm{rd}}-2}}\binom{N}{r_0}\binom{r_0}{r_1}\cdots\binom{r_{m_{\mathrm{rd}}-2}}{r_{m_{\mathrm{rd}}-1}}\mathcal{A}^{N-r_{m_{\mathrm{rd}}-1}}(-1)^{N+r_{m_{\mathrm{rd}}-1}}\\ &\times\left[\exp\left(-\frac{\alpha_{\mathrm{rd}}\gamma N_0(N-r_{m_{\mathrm{rd}}-1})}{P_{\mathrm{r}}}\right)\left(\frac{\alpha_{\mathrm{rd}}\gamma N_0}{P_{\mathrm{r}}}\right)^{R_{m_{\mathrm{rd}}}}\prod_{k=1}^{m_{\mathrm{rd}}-1}\left(\frac{1}{k!}\right)^{r_{k-1}-r_k}\right]\\ &\times\left[\sum_{p=0}^{R}\binom{R}{p}\left(\frac{P_{\mathrm{p}}}{N_0}\right)^p\frac{1}{(m_{\mathrm{pd}}-1)!}\frac{\alpha_{\mathrm{pd}}^{m_{\mathrm{pd}}}(m_{\mathrm{pd}}+p-1)!}{\left(\alpha_{\mathrm{pd}}+\frac{\alpha_{\mathrm{rd}}\gamma P_{\mathrm{p}}(N-r_{m_{\mathrm{rd}}-1})}{P_{\mathrm{r}}}\right)^{m_{\mathrm{pd}}+p}}\right],\end{aligned}\tag{4.10}$$

where $\mathcal{A}$ *is given by* (B.13).

Proof. See Appendix B.2. A key idea in the proof is to consider the dependency between $\gamma_{i\mathrm{d}}$ and $\gamma_{j\mathrm{s}}$ ($i \neq j, j \in \{1, 2, \ldots, M\}$), originating due to the common term g_{pd}. □

For an EH relay, its operation is subject to the energy neutrality constraint, which states that a relay cannot spend more energy than it has harvested. Thus, it is possible that the relay might remain inactive for some time due to the lack of energy.

Let us denote the probability of a relay i being active by $\delta_i \geq 0$. In a non-spectrum sharing scenario, δ_i depends on the relay's energy harvesting and consumption rates. Based on these two factors, the relay i operates in two regions as follows:

- *Energy constrained region* ($\delta_i < 1$)
- *Energy unconstrained region* ($\delta_i = 1$).

A relay operates in the energy unconstrained region if its average energy consumption rate is less than the average energy harvesting rate, i.e., the relay is always active.

We assume $H_{\mathrm{av},i} = H_{\mathrm{av}}$ without loss of generality. Then, we have $\delta_i = \delta$. The energy available with the relay depends on the factors that, how frequently the relay is selected; its harvested energy till now; and when was the energy harvested. As we will show later, in the case of spectrum sharing with PU, the probability of a relay being active, i.e., δ, depends not only on the energy harvesting rate, the total number of relays in the system, the energy

consumed by a relay in its each transmission, but also on PU's outage constraint. Using the following proposition given in [94], we show the dependency of δ on PU's outage constraint.

Proposition 4.3. *Let the probability of selecting a relay be ω. Then, $\omega = \frac{2H_{\text{av}}}{P_{\text{r}}}$. The relays remain active with the probability*

$$\delta = 1 - \left[(1 - M\omega)^{+}\right]^{\frac{1}{M}}. \tag{4.11}$$

All the relays become energy unconstrained, i.e., $\delta = 1$, when $\omega \geq 1/M$. We denote $(x)^{+} = \max(0, x)$.

The expression for ω in Proposition 4.3 is obtained from the energy neutrality constraint and stationarity and ergodicity of the energy harvesting process. From Proposition 4.3, one can notice that the probability of a relay being active depends on the power P_{r} with which the relay performs a transmission. Equations (4.5) and (4.11) together show that P_{r}, in turn, the probability of a relay being active, depends on the primary outage constraint.

Given N out of M relays are active, each with the probability δ, we obtain the final expression for the secondary outage probability with EH relays by unconditioning over the number of active relays as

$$\mathrm{P}_{\text{s,out}} = \sum_{N=1}^{M} \binom{M}{N} \delta^{N} (1-\delta)^{M-N} \mathrm{P}^{N}_{\text{s,out}} + (1-\delta)^{M} \mathrm{P}^{0}_{\text{s,out}}, \tag{4.12}$$

where $\mathrm{P}^{N}_{\text{s,out}}$ given by (4.10) is the secondary outage probability when we select the best relay among active N relays to forward the signal from ST; $\mathrm{P}^{0}_{\text{s,out}}$ is the secondary outage probability when no relay is active, and is equal to 1.

4.4 Results and Discussions

In spectrum sharing, PU's outage constraint governs the maximum transmit power of relays. In addition, if relays are energy harvesting, due to the limited available harvested energy, the probability of a relay being active plays an important role in the performance of the secondary system. In this section, we will first discuss the effect of PU's outage constraint on SU's outage performance for the case when an EH relay on selection, uses the maximum power

allowed by the primary, aiming to reduce the secondary outage probability; even though, it might also reduce the relay's probability of being active. Then, we shall consider the case when, along with PU's outage constraint, EH relays aim to keep their probability of being active to one ($\delta = 1$)−which we call the *energy constraint*. In this case, we shall show that the transmit power of the relay is regulated by the dominant of the two constraints−PU's outage constraint and energy constraint−and we will find the region of dominance for each constraint. Finally, we will see from results that in both the above cases, relaxing PU's outage constraint beyond a level does not offer any benefit to the secondary system with EH relays.

4.4.1 System Parameters and Simulation Setup

We consider following parameter values: PU transmit power, $P_{\mathrm{p}} = 15\,\mathrm{dB}$; the desired primary rate, $\bar{R}_{\mathrm{p}} = 0.4\,\mathrm{bits/s/Hz}$; the desired secondary rate, $\bar{R}_{\mathrm{s}} = 0.2\,\mathrm{bits/s/Hz}$; noise power, $N_0 = -60$ dBm. Denote fading severity parameters on forward and interference channels by m_{f} and m_{int}, respectively. We consider a 2-D topology, where $(x_i,\, y_i)$ defines the coordinate of ith user. The mean channel gain between ith user with coordinate $(x_i,\, y_i)$ and jth user with coordinate $(x_j,\, y_j)$ is $d_{ij}^{-\Delta}$, where d_{ij} is the distance between users i and j in meters and Δ is the path-loss coefficient which is assumed to be 4. Without any loss of generality, ST is placed at (0, 0), M relays are clustered and collocated closely around (50, 0), and SD is placed at (100, 0). Also, PT and PD are located at (50, 50) and (100, 50), respectively. The number of iterations for simulations is up to 10^6.

4.4.2 Effect of PU's Outage Constraint

Figs. 4.2 and 4.3 show the effect of PU's outage constraint on the outage probability of the secondary system with EH relays. The selected EH relay transmits with the maximum power allowed by PU's outage constraint. We notice that the increase in the primary outage threshold Θ_{p} increases the maximum transmit power P_{r} allowed for the relay, which initially reduces the secondary outage probability $P_{\mathrm{s,out}}$. However, with the increase in the threshold Θ_{p} beyond a level, a *tipping point* will be reached after which $P_{\mathrm{s,out}}$ will increase even with the increase in P_{r} as relays will consume energy at a higher rate than they will harvest, i.e., relays will become *energy constrained* (see plots for $H_{\mathrm{av}} = 1, 2$ in Fig. 4.2). This will reduce

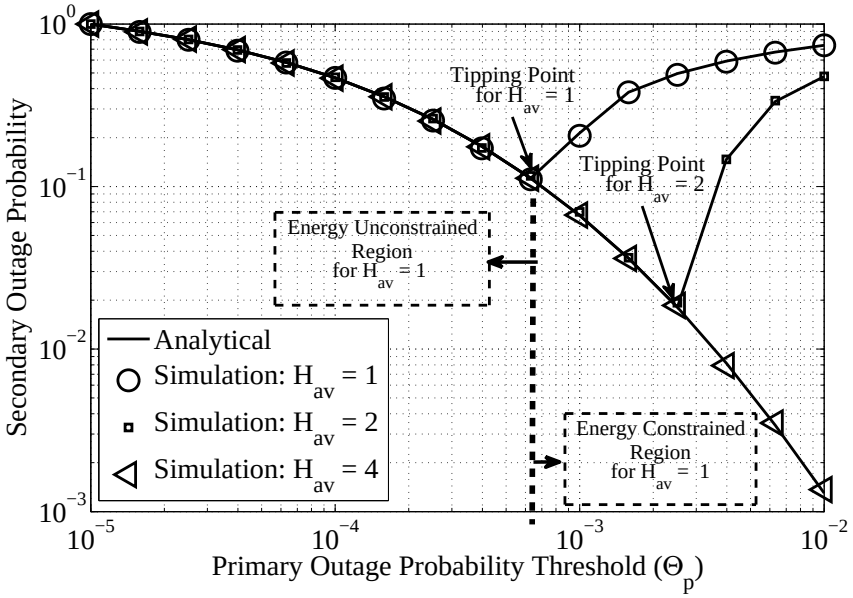

Figure 4.2: Secondary outage probability ($P_{\mathrm{s,out}}$) vs. primary outage probability threshold (Θ_{p}), $M = 3$, $m_{\mathrm{f}} = 2$, $m_{\mathrm{int}} = 1$.

the probability of a relay being active, thereby reducing the number of relays available to forward the data to SD. As long as P_{r} is below a certain level so that $\omega = \frac{2H_{\mathrm{av}}}{P_{\mathrm{r}}} \geq 1/M$ as shown in Proposition 3, the relays operate in the *energy unconstrained region*, i.e., the harvested power is more than the transmit power P_{r}. But, with relaxation of PU's outage constraint, eventually the value of P_{r} increases such that $\omega < 1/M$, making relays energy constrained and increasing $P_{\mathrm{s,out}}$. Also, increase in the harvesting rate H_{av} delays the occurrence of the *tipping point* as expected, and at high harvesting rates, the relays might operate completely in the energy unconstrained region due to availability of abundant energy (see the plot for $H_{\mathrm{av}} = 4$ in Fig. 4.2).

Remark 4.1. *Relaxing PU's outage constraint may not always improve the performance of EH secondary relays in spectrum sharing. That is, unlike conventional non-EH case, due to lack of energy, the relays with EH capability may not transmit with the maximum allowed power even though they are allowed to do so.*

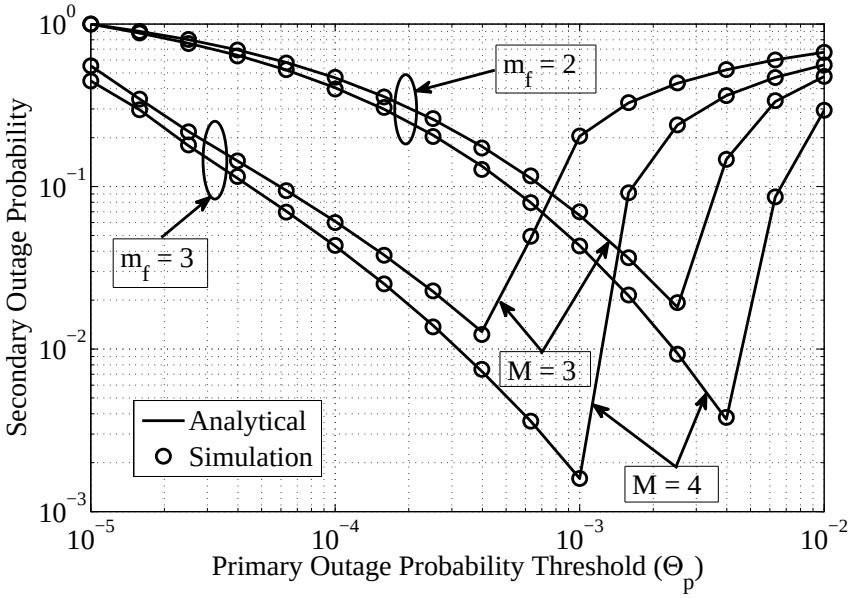

Figure 4.3: Secondary outage probability ($P_{\text{s,out}}$) vs. primary outage probability threshold (Θ_{p}), effect of fading severity parameter and number of relays M, $m_{\text{int}} = 1$, $H_{\text{av}} = 2\,\text{J/s}$.

4.4.3 Effect of Fading Severity Parameter

Fig. 4.3 shows the effect of fading severity parameter on $P_{\text{s,out}}$. We notice that, before the *tipping point*, i.e, in the energy unconstrained region, $P_{\text{s,out}}$ is lower for higher fading severity parameter m_{f} on forward channels. However, the trend reverses after the *tipping point*. This is because, with the increase in m_{f}, the fading effect subsides over the primary link between PT and PD, providing an extra margin for maximum secondary relay transmit power P_{r} for a given Θ_{p}. This helps in achieving lower $P_{\text{s,out}}$ for higher m_{f} in the energy unconstrained region, where the energy harvesting rate is higher than the energy consumption rate. As shown in Fig. 4.3, for a given harvesting rate, due to higher allowed P_{r} (higher energy consumption rate) for higher m_{f}, the *tipping point* arrives earlier than that for lower m_{f}. After the *tipping point*, since relays enter the energy constrained region, higher m_{f}, in turn, higher energy consumption rate, reduces the probability of a relay being active. This often leads to non-availability of relays for transmission, increasing $P_{\text{s,out}}$ for higher m_{f}. Also, increase in the number of relays M increases the probability of being active (see (4.11)) as the candidate relays for cooperation increases (increased diversity) due to which a certain relay is chosen

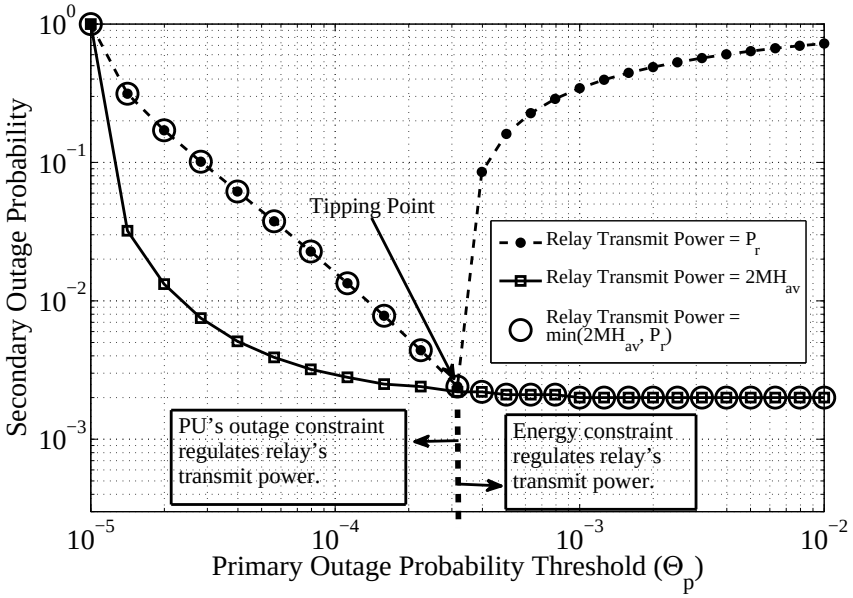

Figure 4.4: Secondary outage probability ($P_{\mathrm{s,out}}$) vs. primary outage probability threshold (Θ_{p}), $M = 3$, $m_{\mathrm{f}} = 3$, $m_{\mathrm{int}} = 2$, $H_{\mathrm{av}} = 2\,\mathrm{J/s}$.

less frequently. This reduces $P_{\mathrm{s,out}}$.

4.4.4 Joint Effect of PU's Outage Constraint and Energy Constraint

From discussions of Figs. 4.2 and 4.3, we note that EH relays being inconsiderate towards their probability of being active, leads to SU's inferior outage performance beyond the tipping point. Now, for instance, assume that EH relays try to remain always active ($\delta = 1$), i.e., try to satisfy the energy constraint, irrespective of PU's outage constraint, and transmit with power $P_{\mathrm{s,a}}$. From Proposition 3, we can see that satisfying the energy constraint corresponds to $\omega \geq 1/M$, i.e., $P_{\mathrm{s,a}} \leq 2MH_{\mathrm{av}}$. That is, as long as EH relays transmit with power no greater than $2MH_{\mathrm{av}}$, they always remain active. Now, if we combine the energy constraint with PU's outage constraint, Fig. 4.4 shows that in the *energy unconstrained region*, though an EH relay may transmit with maximum power $2MH_{\mathrm{av}}$ maintaining $\delta = 1$, the power $2MH_{\mathrm{av}}$ does not satisfy PU's outage constraint, i.e., $2MH_{\mathrm{av}} > P_{\mathrm{r}}$. This leads to higher $P_{\mathrm{s,out}}$ in EH relay spectrum sharing scenario governed by both the energy constraint and PU's constraint than it would have been in EH non-spectrum sharing scenario governed by the

energy constraint alone. In the *energy constrained region*, the energy constraint becomes dominant, i.e., $2MH_{\text{av}} < P_{\text{r}}$. Thus, even though PU's outage constraint is satisfied, and allows EH relays to transmit with the maximum power P_{r}, the energy constraint is violated, causing $\delta < 1$ and increasing in $P_{\text{s,out}}$ as discussed for Figs. 4.2 and 4.3. Therefore, we can see from the above discussion that, to satisfy both constraints, the maximum power with which EH relays may transmit is $\min(2MH_{\text{av}}, P_{\text{r}})$. As shown in Fig. 4.4, in the energy constrained region (after the tipping point), though transmitting with power $\min(2MH_{\text{av}}, P_{\text{r}})$ avoids the increase in $P_{\text{s,out}}$, relaxing PU's outage constraint does not improve SU's outage performance.

4.5 Chapter Summary

Under the primary outage constraint, this chapter has analyzed the outage performance of the secondary communication via energy harvesting relays in Nakagami-m channel. In a spectrum sharing scenario, the results show that, besides energy harvesting nature of relays, the primary outage constraint also strongly influences the probability of a relay being active. We note that relays should keep their probability of being active to one; otherwise, obeying only the primary outage constraint may lead to the inferior secondary outage performance. That is, in energy harvesting spectrum sharing, due to the energy constraint, relaxing the primary outage constraint may not always improve secondary outage performance unlike in non-energy harvesting case. Further, we have found the region of dominance for each of the constraints and proposed the optimal transmit power for relays to subside their inferior performance in the energy constrained region. We observe that increase in the number relays and lower fading severity parameter delays the entry of relays into the energy constrained region, boosting the secondary outage performance.

Chapter 5

Interference-Assisted Energy Harvesting in Cognitive Relaying

In the previous chapter, we considered the stationary and the ergodic energy harvesting process, which assumed no specific energy harvesting source. In underlay mode, the PU interference constraint limits the transmit powers of secondary transmitter and relay. But, PU, being a legacy user, has no such restriction on its transmit power. Due to this, SU may experience heavy interference from PU, which deteriorates QoS of SU. Nevertheless, since the interference is an RF signal, it can be leveraged as a potential source of energy [58, 103, 109]. In this regard, this chapter focuses on the RF energy harvesting at the secondary relay from primary's interference.

5.1 System and Channel Models

As shown in Fig. 5.1, consider a primary network consisting of L pairs of PTs and PDs, where each PU pair communicates over a channel of bandwidth B Hz. The secondary network consists of an ST which communicates with an SD through an energy harvesting decode-and-forward SR. The secondary network shares the spectrum of bandwidth BL Hz with PUs, provided that QoS of each primary link is maintained above a given threshold.

Let h_i, h_{sr}, h_{rd}, $h_{\mathrm{s}i}$, $h_{\mathrm{r}i}$, $h_{i\mathrm{r}}$, and $h_{i\mathrm{d}}$ denote the channel coefficients of ith primary link PT_i-PD_i ($i = 1, 2, \ldots, L$), ST-SR, SR-SD, ST-PD_i, SR-PD_i, PT_i-SR, and PT_i-SD,

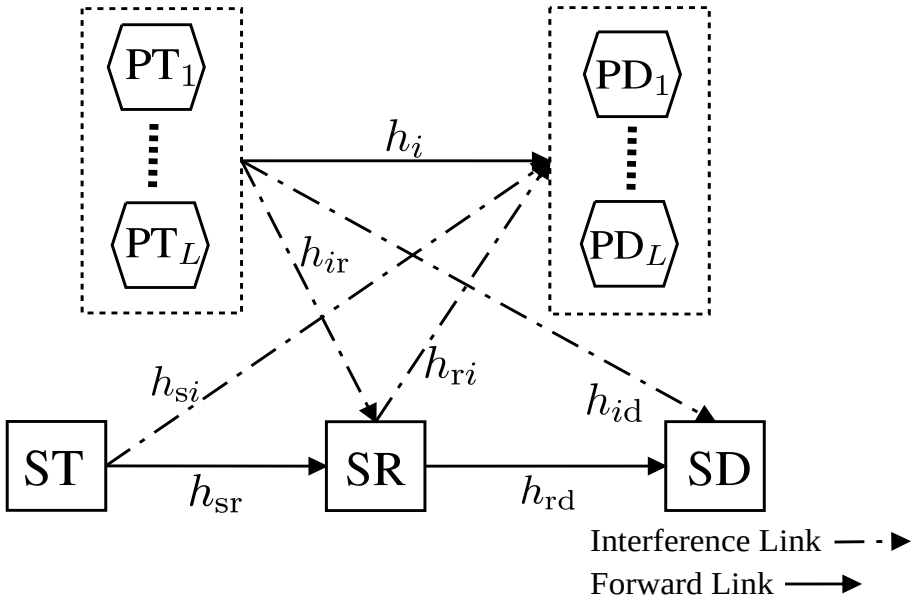

Figure 5.1: Secondary communication via an EH relay in spectrum sharing.

respectively. All channels are independent of each other and experience quasi-static Rayleigh fading,[1] i.e., the channels remain constant for one slot of secondary communication and change independently from one slot to another. The instantaneous channel power gains are exponentially distributed random variables. Let us denote the mean channel power gain of $g_{\mathrm{k}} = |h_{\mathrm{k}}|^2$ by Ω_{k}, where $\mathrm{k} \in \{i, \mathrm{sr}, \mathrm{rd}, \mathrm{s}i, \mathrm{r}i, i\mathrm{r}, i\mathrm{d}\}$. For simplicity, we consider PT-PR links are identically distributed, i.e., $\Omega_i = \Omega_{\mathrm{pp}}$; interference channels from PTs to a node and vice-versa are also identically distributed, i.e., $\Omega_{i\mathrm{r}} = \Omega_{\mathrm{pr}}$, $\Omega_{i\mathrm{d}} = \Omega_{\mathrm{ps}}$, $\Omega_{\mathrm{s}i} = \Omega_{\mathrm{sp}}$, and $\Omega_{\mathrm{r}i} = \Omega_{\mathrm{rp}}$. We assume the knowledge of mean channel power gains for PT$_i$-PD$_i$, ST-PD$_i$, and SR-PD$_i$ links, while SR and SD have the knowledge of instantaneous channels gains for the respective receiving links, i.e., for ST-SR and PT$_i$-SR links at SR and for SR-SD and PT$_i$-SD links at SD.

Assuming no direct link between transmitter and destination due to high attenuation, the secondary communication happens over two-hops. In the first hop, ST transmits data to SR, while in the second hop, SR forwards the received data to SD after decoding. The SR is an EH node, that is capable of harvesting energy from the received RF signals. Energy

[1]This assumption is purely for analytical tractability.

harvesting is considered to be the only power source for SR. The SR may use some part of the received information signal to gather the energy required to forward the information to SD. In addition, as in spectrum sharing, the primary and secondary network transmit simultaneously, SR experiences the interference from L PTs, which is also an RF signal. Thus, SR can also harvest additional energy from the primary interference in the energy harvesting phase, converting it into a useful energy source. The ST and PTs are the conventional nodes with constant power supply (e.g. battery).

5.2 Maximum Allowed Secondary Transmit Powers

In the spectrum sharing scenario, the interference constraints at PDs govern the maximum transmit powers of ST and SR. We model the interference constraint at a PD as its outage probability, i.e., ST and SR should limit their transmit powers so that the outage probability of each primary link remains below a given threshold. Let us denote the maximum allowed transmit powers of ST and SR due to the primary outage constraint as P_{s} and P_{sr}, respectively. Then, in the first hop of the secondary communication when ST transmits to SR, given the constant transmit power of PT (P_{p}), the outage probability for ith primary link can be written as follows:

$$\mathrm{P}^{i}_{\mathrm{p,out,ST}} = \mathbb{P}\left(B\log_2\left(1+\gamma_{\mathrm{PD}_i}\right) \leq \bar{R}_{\mathrm{p}}\right) \leq \Theta_{\mathrm{p}}, \tag{5.1}$$

where $\gamma_{\mathrm{PD}_i} = \frac{P_{\mathrm{p}} g_i}{P_{\mathrm{s}} g_{si}}$ is the signal-to-interference ratio (SIR)[2] at PD_i, $\bar{R}_{\mathrm{p}}$ is the desired primary rate for each primary link, and Θ_{p} is the primary outage threshold for each PU. Ensuring that the outage probability of the primary link having the worst SIR stays below Θ_{p}, we can write the primary outage constraint with interference from ST as

$$\mathrm{P}_{\mathrm{p,out,ST}} = \mathbb{P}\left(\max_{i=1,2,\ldots,L} \mathrm{P}^{i}_{\mathrm{p,out,ST}}\right) \leq \Theta_{\mathrm{p}}. \tag{5.2}$$

Then, from (5.1), and using the independence between g_i and g_{si}, we can write (5.2) as

$$\mathrm{P}_{\mathrm{p,out,ST}} = 1 - \prod_{i=1}^{L}\left(1 - \mathbb{P}\left(\frac{P_{\mathrm{p}} g_i}{P_{\mathrm{s}} g_{si}} \leq \zeta_{\mathrm{p}}\right)\right), \tag{5.3}$$

where $\zeta_{\mathrm{p}} = 2^{\bar{R}_{\mathrm{p}}/B} - 1$.

[2]Since our focus is interference-limited spectrum sharing environment where the interference power dominates the noise power, the latter can be neglected.

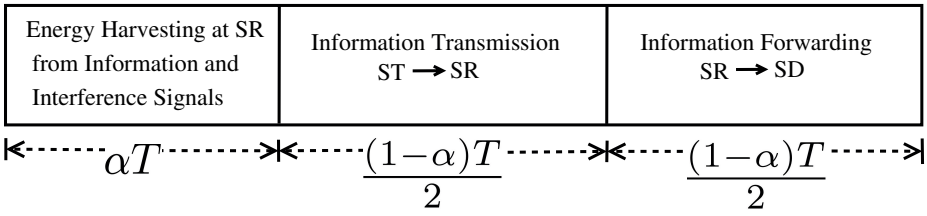

Figure 5.2: Time switching protocol for the interference-assisted energy harvesting and information processing at SR.

Proposition 5.1. *The maximum allowed transmit power for ST under the primary outage constraint is*

$$P_{\mathrm{s}} = \frac{P_{\mathrm{p}}\Omega_{\mathrm{pp}}}{\zeta_{\mathrm{p}}\Omega_{\mathrm{sp}}}\left[\left(\frac{1}{1-\Theta_{\mathrm{p}}}\right)^{\frac{1}{L}} - 1\right]^{+}. \tag{5.4}$$

Proof. The proof is given in Appendix C.1. □

Similarly, in the second hop of the secondary communication when SR transmits to SD, following the same procedure to derive P_{s}, the maximum transmit power for SR is given as

$$P_{\mathrm{sr}} = \frac{P_{\mathrm{p}}\Omega_{\mathrm{pp}}}{\zeta_{\mathrm{p}}\Omega_{\mathrm{rp}}}\left[\left(\frac{1}{1-\Theta_{\mathrm{p}}}\right)^{\frac{1}{L}} - 1\right]^{+}. \tag{5.5}$$

Besides the primary outage constraint, at both ST and SR, we also impose the peak power constraint P_{pk}. Then, the maximum transmit powers for ST and SR respectively become

$$P_{\mathrm{sm}} = \min\left(P_{\mathrm{s}}, P_{\mathrm{pk}}\right), \tag{5.6}$$

$$P_{\mathrm{r}} = \min\left(P_{\mathrm{sr}}, P_{\mathrm{pk}}\right). \tag{5.7}$$

5.3 Relaying Protocol at Secondary Relay

At SR, we adopt a time switching protocol to harvest energy from received RF signals as shown in Fig. 5.2. In this protocol, at the start of a slot, for αT duration ($0 < \alpha < 1$), SR harvests energy from ST's signal and interference from L PTs, where T is the duration of one slot of the secondary communication. The remaining time slot of duration $(1-\alpha)T$ is divided into two sub-slots, each of duration $\frac{(1-\alpha)T}{2}$. In the first sub-slot, ST transmits information to SR; while SR forwards the information to SD in the next sub-slot. Thus, when ST transmits

with $P_{\rm sm}$ and each PT transmits with $P_{\rm p}$, the energy harvested by SR in αT duration is given as

$$E_{\rm SR,H} = (\alpha T)\eta \left(P_{\rm sm} g_{\rm sr} + \sum_{i=1}^{L} P_{\rm p} g_{ir} \right), \tag{5.8}$$

where η, with $0 < \eta \leq 1$, is the energy conversion efficiency factor. The SR uses harvested energy to forward the information to SD. Then, given the amount of harvested energy, the transmit power of SR in the absence of peak power constraint and primary outage constraint can be given by[3]

$$P_{\rm SR,H} = \frac{2E_{\rm SR,H}}{(1-\alpha)T} = \frac{2\eta\alpha}{1-\alpha} \left(P_{\rm sm} g_{\rm sr} + \sum_{i=1}^{L} P_{\rm p} g_{ir} \right). \tag{5.9}$$

Now, by incorporating the primary outage constraint and the peak power constraint, the maximum transmit power for the energy harvesting SR can be given as follows:

$$P_{\rm rm} = \min\left(P_{\rm SR,H}, P_{\rm r}\right), \tag{5.10}$$

where $P_{\rm r}$ is given by (5.7). Hereafter, without loss of generality, we assume that the duration of a time-slot is $T = 1$.

5.4 Secondary Outage Analysis

The secondary communication between ST and SD via SR experiences an outage if the rate on one of the ST-SR and SR-SD links falls below the target rate $\bar{R}_{\rm s}$. Then, we can write the secondary outage probability $P_{\rm s,out}$ as follows:

$$P_{\rm s,out} = \mathbb{P}\left(\min\left(R_{\rm sr}, R_{\rm rd}\right) < \bar{R}_{\rm s}\right), \tag{5.11}$$

where $R_{\rm sr}$ and $R_{\rm rd}$ are the rates on ST-SR and SR-SD links, respectively, and can be given as

$$\begin{aligned} R_{\rm sr} &= \frac{1-\alpha}{2} BL \log_2\left(1+\gamma_{\rm r}\right), \\ R_{\rm rd} &= \frac{1-\alpha}{2} BL \log_2\left(1+\gamma_{\rm d}\right). \end{aligned} \tag{5.12}$$

[3]Usually, the energy consumption by the circuitry of SR in the information processing is negligible compared to that in the transmission [59, 110]. Thus, we assume that SR uses all the harvested energy for the transmission.

Here, γ_{r} and γ_{d} are SIRs at SR and SD, respectively, and are given as

$$\gamma_{\mathrm{r}} = \frac{P_{\mathrm{sm}} g_{\mathrm{sr}}}{\sum_{i=1}^{L} P_{\mathrm{p}} g_{i\mathrm{r}}}, \tag{5.13}$$

$$\begin{aligned}\gamma_{\mathrm{d}} &= \frac{P_{\mathrm{rm}} g_{\mathrm{rd}}}{\sum_{i=1}^{L} P_{\mathrm{p}} g_{i\mathrm{d}}} \\ &= \frac{\min\left(\frac{2\eta\alpha}{1-\alpha}\left(P_{\mathrm{sm}} g_{\mathrm{sr}} + \sum_{i=1}^{L} P_{\mathrm{p}} g_{i\mathrm{r}}\right), P_{\mathrm{r}}\right) g_{\mathrm{rd}}}{\sum_{i=1}^{L} P_{\mathrm{p}} g_{i\mathrm{d}}}.\end{aligned} \tag{5.14}$$

Note that γ_{r} given by (5.13) and γ_{d} given by (5.14) are dependent random variables due to the presence of common random variable $\sum_{i=1}^{L} P_{\mathrm{p}} g_{i\mathrm{r}}$. Then, we can rewrite the secondary outage probability from (5.11) as follows:

$$\begin{aligned}P_{\mathrm{s,out}}(\xi_{\mathrm{s}}) &= \mathbb{P}\left(\min\left(\gamma_{\mathrm{r}}, \gamma_{\mathrm{d}}\right) < \xi_{\mathrm{s}}\right), \\ &= 1 - \mathbb{P}\left(\gamma_{\mathrm{r}} \geq \zeta_{\mathrm{s}}, \gamma_{\mathrm{d}} \geq \zeta_{\mathrm{s}}\right),\end{aligned} \tag{5.15}$$

where $\min\left(\gamma_{\mathrm{r}}, \gamma_{\mathrm{d}}\right)$ is the instantaneous end-to-end SIR between ST and SD and $\xi_{\mathrm{s}} = 2^{\frac{2\bar{R}_{\mathrm{s}}}{(1-\alpha)BL}} - 1$.

Proposition 5.2. *For ST's fixed transmission rate $\bar{R}_{\mathrm{s}}$, we write the secondary outage probability $P_{\mathrm{s,out}}$ as a function of ζ_{s} as*

$$P_{\mathrm{s,out}}(\zeta_{\mathrm{s}}) = 1 - \frac{1}{(P_{\mathrm{p}}\Omega_{\mathrm{pd}})^{L}}(I_1 + I_2 + I_3), \tag{5.16}$$

where

$$I_1 = \int_{u=0}^{\delta_1} \int_{x=\frac{\zeta_{\mathrm{s}} u}{P_{\mathrm{sm}}}}^{\frac{P_{\mathrm{r}} - \theta u}{\theta P_{\mathrm{sm}}}} f_X(x) f_U(u) \left(\frac{1}{P_{\mathrm{p}}\Omega_{\mathrm{pd}}} + \frac{\zeta_{\mathrm{s}}}{\theta(P_{\mathrm{sm}} x + u)\Omega_{\mathrm{rd}}}\right)^{-L} \mathrm{d}x\, \mathrm{d}u, \tag{5.17a}$$

$$I_2 = \frac{\Upsilon(L, \omega\delta_1) \exp\left(-\frac{P_{\mathrm{r}}}{\theta P_{\mathrm{sm}}\Omega_{\mathrm{sr}}}\right)}{\Gamma(L)(P_{\mathrm{p}}\Omega_{\mathrm{pr}})^{L}\omega^{L}\left(\frac{1}{P_{\mathrm{p}}\Omega_{\mathrm{pd}}} + \frac{\zeta_{\mathrm{s}}}{P_{\mathrm{r}}\Omega_{\mathrm{rd}}}\right)^{L}}, \tag{5.17b}$$

$$I_3 = \frac{\Gamma(L, \varphi\delta_1)}{\Gamma(L)(P_{\mathrm{p}}\Omega_{\mathrm{pr}})^L \varphi^L \left(\frac{1}{P_{\mathrm{p}}\Omega_{\mathrm{pd}}} + \frac{\zeta_{\mathrm{s}}}{P_{\mathrm{r}}\Omega_{\mathrm{rd}}}\right)^L}, \tag{5.17c}$$

with

$$\delta_1 = \frac{P_{\mathrm{r}}}{(1+\zeta_{\mathrm{s}})\theta}, \tag{5.17d}$$

$$\theta = \frac{2\eta\alpha}{1-\alpha}, \tag{5.17e}$$

$$\omega = \frac{1}{P_{\mathrm{p}\Omega_{\mathrm{pr}}}} - \frac{1}{P_{\mathrm{sm}}\Omega_{\mathrm{sr}}}, \tag{5.17f}$$

and

$$\varphi = \frac{1}{P_{\mathrm{p}\Omega_{\mathrm{pr}}}} + \frac{\zeta_{\mathrm{s}}}{P_{\mathrm{sm}}\Omega_{\mathrm{sr}}}. \tag{5.17g}$$

Also, $f_X(x)$ and $f_U(u)$ denote the probability density functions of random variables X and U and are given as

$$f_X(x) = \frac{1}{\Omega_{\mathrm{sr}}} \exp\left(-\frac{x}{\Omega_{\mathrm{sr}}}\right) \tag{5.17h}$$

and

$$f_U(u) = \frac{u^{L-1}\exp(-\frac{u}{P_{\mathrm{p}}\Omega_{\mathrm{pr}}})}{\Gamma(L)(P_{\mathrm{p}}\Omega_{\mathrm{pr}})^L}, \tag{5.17i}$$

respectively.

Proof. The proof is given in Appendix C.2. □

5.5 Results and Discussions

5.5.1 System Parameters and Simulation Setup

We assume the following system parameters: The desired primary rate, $\bar{R}_{\mathrm{p}} = 0.4\,\mathrm{bits/s/Hz}$, the desired secondary rate, $\bar{R}_{\mathrm{s}} = 0.2\,\mathrm{bits/s/Hz}$, the energy conversion efficiency factor, $\eta = 0.5$, the primary transmit power, $P_{\mathrm{p}} = 20\,\mathrm{dB}$. We consider a 2-D simulation setup, where (x_i, y_i) is the coordinate of ith user. The mean channel gain between ith and jth users is $d_{ij}^{-\rho}$, where d_{ij} is the distance between users i and j, and ρ is the path-loss coefficient which is assumed to be 4. The ST, SR, and SD are placed at (0, 0), (0.5, 0), and (1, 0), respectively. The PTs are collocated at (0.5, 1), while PDs are collocated at (1, 1).

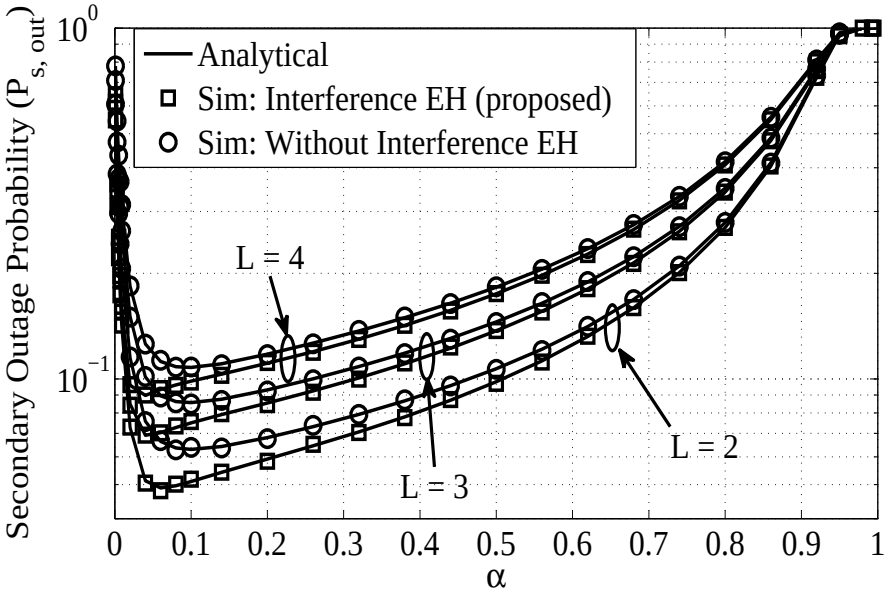

Figure 5.3: With interference EH versus without interference EH for different number of primary transceivers (L), $\Theta_{\mathrm{p}} = 10^{-2}$, $P_{\mathrm{pk}} = 20\,\mathrm{dB}$.

5.5.2 Effect of the Interference-Assisted Energy Harvesting

Fig. 5.3 shows SU's outage probability $P_{\mathrm{s,out}}$ against the energy harvesting ratio α. We observe that the proposed method of SR harvesting energy from the primary interference in addition to that from the received information signal, achieves lower $P_{\mathrm{s,out}}$ than the conventional method where SR treats the interference as an unwanted signal in EH phase. This improvement comes from the extraction of an additional energy from the interference, which helps increase the relay's transmit power on SR-SD link, enhancing SIR at SD. For a given number of primary transceivers L, as α increases from 0 to 1, $P_{\mathrm{s,out}}$ reduces first, and then increases beyond the optimal value of α that minimizes $P_{\mathrm{s,out}}$. This trade-off can be attributed to two conflicting effects that are dependent on α. The increase in α allows SR to harvest more energy from the information signal and the primary interference, improving SIR of SR-SD link, which in turn, reduces $P_{\mathrm{s,out}}$. On the contrary, the time for data transmission reduces with increasing α, which reduces SU's throughput. This pushes SU into the outage more often, increasing its outage probability. Also, we can see that the extra energy gained from the primary interference reduces the optimal value of α as expected.

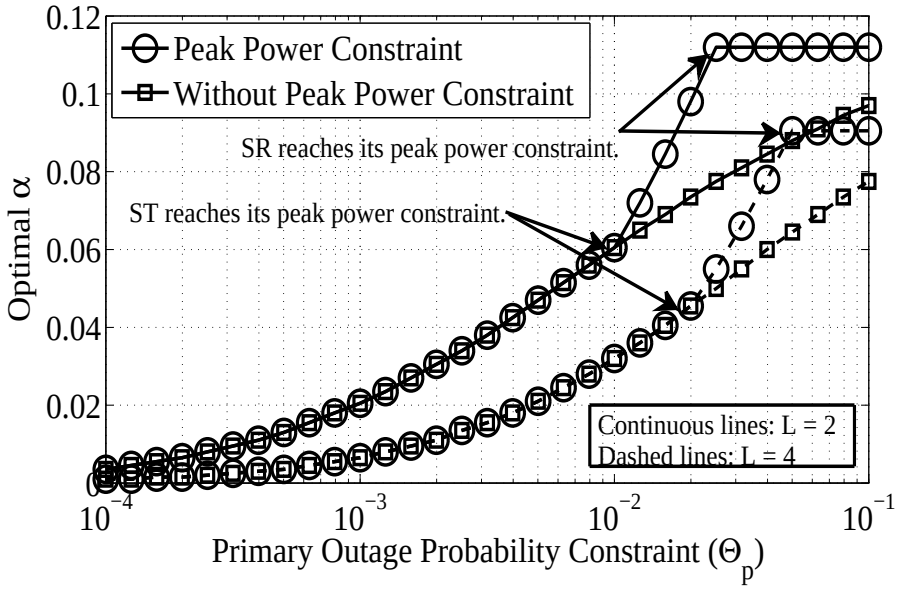

Figure 5.4: Optimal α versus the primary outage constraint for different number of primary transceivers (L), $P_{\text{pk}} = 20\,\text{dB}$.

Similarly, the increase in the number of primary transceivers L furnishes SR with the more harvested energy through the interference, which further reduces the optimal α. But, as shown in Fig. 5.3, the deteriorating effect of the interference−decrease in SIR at both SR and SD−is more dominant, which increases $P_{\text{s,out}}$. An another negative consequence of the increase in L is the stricter primary outage constraint. Since SU should satisfy the outage constraint of each PU, the increase in the number of PUs makes the constraint more difficult to satisfy, reducing the maximum allowed transmit powers for both ST and SD.

5.5.3 Effect of the Primary Outage Constraint

Figs. 5.4 and 5.5 show the effect of the primary outage constraint (Θ_{p}) on the optimal α and its corresponding minimum $P_{\text{s,out}}$, respectively, for different L and peak power constraint of P_{pk}. From (5.16), (5.17a), (5.17b), and (5.17c), we can see that, deriving the analytical expression for the optimal α is difficult due to their intricate nature; however, the optimal α can be easily obtained numerically. We note from Fig. 5.4 that, relaxing the primary outage constraint Θ_{p} increases the optimal α. This is because, relaxing Θ_{p} allows ST and SR to

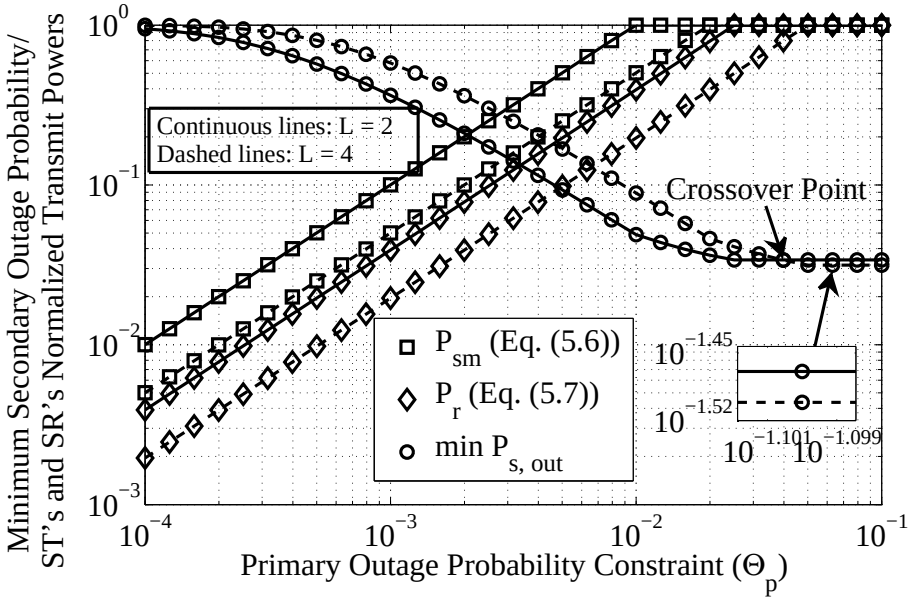

Figure 5.5: Minimum $P_{\mathrm{s,out}}$ versus the primary outage constraint with peak power constraint for different number of primary transceivers (L), $P_{\mathrm{pk}} = 20\,\mathrm{dB}$.

transmit with higher powers. Thus, α increases to cater relay's higher transmit power. Also, higher transmit powers of ST and SR increases SIR on both ST-SR and SR-SD links, which provides an extra margin to increase α improving SU's outage performance.

The peak power constraint becomes active due to the increased maximum allowed powers for ST (P_{s}, (5.4)) and SR (P_{sr}, (5.5)) with the relaxation of Θ_{p} beyond a threshold. This is seen in Fig. 5.4, where ST reaches its peak power constraint first[4] which forces ST to transmit with peak power P_{pk} even though the further relaxation of Θ_{p} allows it to transmit with higher power. After this point, to serve the increasing SR's transmit power for a fixed ST's power P_{pk}, the optimal α increases at a faster rate than that without the peak power constraint till the peak power constraint of SR is reached. Once SR's peak power constraint is reached, SR is also forced to transmit with the fixed power P_{pk} for any further increase in Θ_{p}, and the optimal α remains the same thereafter.

[4]In simulation setup, ST is located farther from the primary destinations than SR. This allows ST to transmit with higher power than that of SR for the same Θ_{p}, causing ST to reach the peak power constraint before SR. For the purpose of exposition, the effect of distances among nodes is not addressed in this work.

As aforementioned, the increase in L reduces the maximum allowed power for both ST and SR, which delays the arrival of the peak power constraint as shown in Fig. 5.4. This has an interesting consequence on the minimum $P_{\text{s,out}}$ as shown in Fig. 5.5. At the stringent Θ_{p}, for lower L ($L = 2$), the minimum $P_{\text{s,out}}$ is lower than that for higher L ($L = 4$). However, there exists a crossover point, after which the trend reverses; because, for $L = 2$, the peak power constraint is reached for both ST and SR earlier, forcing them to transmit with fixed power P_{pk} even with the further relaxation of Θ_{p}. Meanwhile, for $L = 4$, more energy is harvested from the interference than for $L = 2$, and ST and SR may keep increasing their transmit powers even at Θ_{p} for which the peak power constraint for $L = 2$ is reached, allowing the former to achieve a better minimum $P_{\text{s,out}}$ at higher Θ_{p}. Note that we do not observe such behavior in Fig. 5.3, as for $\Theta_{\text{p}} = 10^{-2}$ as assumed in it, the peak power constraint is not reached for $L = 2, 3$, and 4. Combining both the primary outage constraint and the peak power constraint, Fig. 5.5 has plotted the maximum allowed transmit powers for ST and SR normalized by their peak power constraint power P_{pk}.

5.6 Chapter Summary

For the proposed scenario, we have derived a closed-form expression for the secondary outage probability. We have shown that harvesting energy from the primary interference achieves a better secondary outage performance and reduces the optimal value of the energy harvesting ratio α. Though the increase in the number of primary transceivers reduces the optimal value of α further, it increases the minimum secondary outage probability when the peak power constraint is inactive. Interestingly, the trend reverses for the minimum secondary outage probability, once the peak power constraint becomes active with the relaxation of the primary outage constraint.

Chapter 6

Cognitive Energy Harvesting Untrusted Relaying

6.1 Introduction

In previous chapters, we observed that the broadcast nature of the wireless medium facilitated the cooperative relaying. But, at the same time, the open nature of wireless medium also allows eavesdroppers an opportunity to decode the confidential information. In fact, the cooperation from a relay raises security concerns if the relay itself is an eavesdropper. In this chapter, we investigate such possibility where the energy harvesting relay is *untrusted*.

Traditional approaches to achieve secure communication include upper-layer cryptographic techniques which require intensive key distribution and management. Unlike this paradigm, the physical-layer security achieves the secure communication by exploiting the nature of the channel. In this regard, Wyner introduced the wiretap channel and showed that the perfect secure communication was possible without relying on private keys [111].

The eavesdropper could be an internal node belonging to the same network. To discourage eavesdropping, jamming signals can be used, where the goal is to deteriorate the reception of the eavesdropper. In an energy harvesting scenario, the jamming signal provides an additional advantage. Since the jamming signal is an RF signal, it can be used an RF energy source to increase the harvested energy. In this regard, we address the problem of secure communication

via an energy harvesting untrusted relay under the primary's interference constraint.

6.1.1 Related Work

As to the cooperative relaying, the works in [112, 113, 114, 115, 116, 117] have studied the physical-layer security in the presence of external eavesdroppers that are different from the relay and try to intercept the transmitter-relay and/or relay-destination communications. In [118], the authors show that even the communication via an untrusted relay can be beneficial for the relay channel with orthogonal components. The work in [119] shows that the positive secrecy rate is achievable with the destination-assisted jamming, where the destination sends jamming signals during the transmitter-relay communication.

Recently, with wireless energy harvesting, a few works have studied the physical-layer security in the presence of external eavesdroppers for different scenarios like point-to-point communication with a single antenna [120, 121] and multiple antennas [122, 123, 124, 125], and the cooperative communication via a relay [126, 127, 128, 129]. However, the works in [126, 127, 128, 129] assume the relay to be trusted, and external eavesdroppers attempt to intercept the relay-assisted communication between the transmitter and the destination. Also, the works on untrusted relay till now have assumed that the conventional energy source, such as battery, powers the relay in a non-cognitive radio scenario (see, e.g., [22, 118, 119, 130, 131, 132, 133, 134, 135, 136, 137, 138, 139]).

6.2 System Model

6.2.1 Destination-Assisted Jamming and Channel Model

As shown in Fig. 6.1, an ST communicates with an SD via an AF energy harvesting SR, provided the interference caused to PD stays below an acceptable limit.[1] Despite relay's information cooperation, ST and SD wish to keep the information secret from the relay. To maintain the confidentiality of the ST's information, SD transmits a jamming signal to the relay when ST sends the information to the relay. Each node operates in a half-duplex mode.

[1]For analytical tractability, we do not consider the primary's interference.

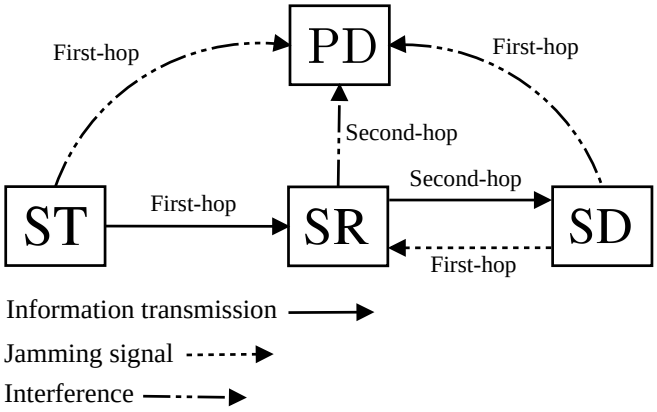

Figure 6.1: System Model for the secure communication between a secondary transmitter and a secondary destination via an energy harvesting untrusted secondary relay with destination-assisted jamming under the primary's interference constraint.

The direct link between ST and SD is unavailable.[2] Let $h_{\rm sr}$, $h_{\rm rd}$, $h_{\rm dr}$, $h_{\rm sp}$, $h_{\rm rp}$, and $h_{\rm dp}$ denote the channel coefficients on links ST-SR, SR-SD, SD-SR, ST-PD, SR-PD, and SD-PD, respectively. We consider a quasi-static block-fading Rayleigh channel between two nodes. That is, the channel remains constant over a slot-duration of T during which ST transmits to SD via SR. The channel power gain is given by $g_{ij} = |h_{ij}|^2$, which has exponential distribution with mean Ω_{ij}, i.e.,

$$f_{g_{ij}}(x) = \frac{1}{\Omega_{ij}} \exp\left(-\frac{x}{\Omega_{ij}}\right), \quad x \geq 0, \tag{6.1}$$

where $f_{g_{ij}}(x)$ is the probability density function of random variable g_{ij}. We assume the channel between SR and SD reciprocal, i.e., $h_{\rm rd} = h_{\rm dr}$. In this work, the ST is assumed to have no CSI, while the CSI of ST-SR and SR-SD channels are available at SR and SD, respectively. Also, we assume the statistical channel information of links corresponding to PD. That is, the mean channel power gains of links ST-PD, SD-PD, and SR-PD are known.

6.2.2 Energy Harvesting and Information Processing Model

The untrusted relay harvests energy from the received RF signals which it uses to forward the ST's information to SD. To activate the energy harvesting circuitry at the relay, the

[2]Since SD operates in a half-duplex mode and sends the jamming signal to SR during its reception of information from ST, it cannot receive the information from ST.

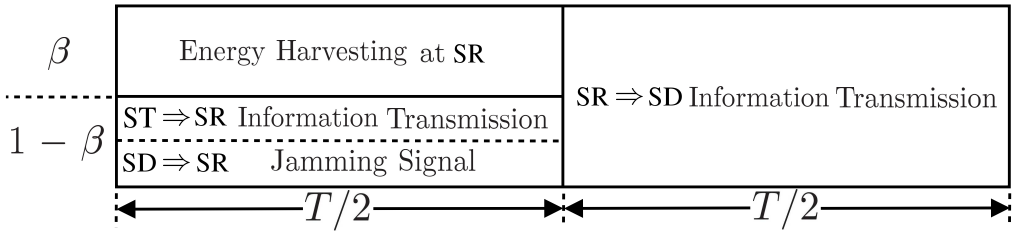

Figure 6.2: Power splitting policy for the secure communication via an energy harvesting untrusted relay.

received power must exceed the minimum threshold power θ_H.[3] We assume that the relay has no other energy source and uses the harvested energy completely for the transmission as the power consumed by the relay's transmit/receive circuitry is negligible compared to the power required for the transmission.

We adopt power splitting ploicy and time switching policy at the relay to separately harvest energy from the received RF signals and process the information [140]. Note that the relay may attempt to decode the confidential information with the power used for the information processing.

6.3 Power Splitting Policy Based Relaying

Fig. 6.2 shows the PS policy based relaying protocol, where ST-SD communication happens in a slot of duration T. Two phases of equal duration $T/2$ divide the slot. In the first phase, ST transmits information to the relay with power $P_{\rm s}$. At the same time, the destination sends a jamming signal with power $P_{\rm d}$ to the relay to maintain the confidentiality of the information from the relay. The relay uses a fraction β of the received power for energy harvesting and the remaining $(1-\beta)$ portion for information processing, where $0 \leq \beta \leq 1$. Using the harvested energy, in the second phase, the relay forwards the received information to SD after amplification. Note that the transmit powers of ST, SR, and SD should meet the primary's interference constraint.

[3]The threshold θ_H is usually between -30 dBm to -10 dBm, depending on various factors like channel conditions, frequency of the received RF signals, and energy harvesting circuitry type (linear, non-linear, tunable, etc.) [36].

6.3.1 Primary's Interference Constraint

In this work, we characterize the interference constraint at the primary destination by the *interference outage constraint*. This constraint requires that the probability that the instantaneous received interference power at the primary destination exceeds the predefined interference threshold $\mathcal{I}_{\mathrm{p}}$ should be less than or equal to a target outage probability Θ_{p}.

Since ST and SD transmit at the same time in the first phase, the interference outage constraint can be defined as

$$\mathbb{P}\left((P_{\mathrm{s}}g_{\mathrm{sp}} + P_{\mathrm{d}}g_{\mathrm{dp}}) > \mathcal{I}_{\mathrm{p}}\right) \leq \Theta_{\mathrm{p}}, \tag{6.2}$$

where $\mathbb{P}(\cdot)$ denotes the probability. Also, in the second phase, the relay's transmit power is restricted by the primary's interference outage constraint. Let $P_{\mathcal{I}}$ denote relay's transmit power limited by the primary's interference outage constraint. Then, we have

$$\mathbb{P}\left(P_{\mathcal{I}}g_{\mathrm{rp}} > \mathcal{I}_{\mathrm{p}}\right) \leq \Theta_{\mathrm{p}}. \tag{6.3}$$

Then, we can write the maximum allowed $P_{\mathcal{I}}$ as

$$P_{\mathcal{I}} = -\frac{\mathcal{I}_{\mathrm{p}}}{\Omega_{\mathrm{rp}}\ln(\Theta_{\mathrm{p}})}. \tag{6.4}$$

The derivation of (6.4) is given in Appendix D.1.

6.3.2 Energy Harvesting at Relay

In the aforementioned PS policy, the relay harvests energy E_H given as

$$E_H = \eta\beta\left(P_{\mathrm{s}}g_{\mathrm{sr}} + P_{\mathrm{d}}g_{\mathrm{dr}}\right)(T/2), \tag{6.5}$$

where η is the energy conversion efficiency factor with $0 < \eta \leq 1$, which is dependent on the energy harvesting circuitry of the relay. The terms $P_{\mathrm{s}}g_{\mathrm{sr}}$ and $P_{\mathrm{d}}g_{\mathrm{dr}}$ in (6.5) denote the power received at the relay due to the information signal from ST and the jamming signal from SD, respectively. In the second phase of duration $T/2$, the relay's transmit power to forward the information to destination is given as

$$P_{H1} = \frac{E_H}{T/2} = \eta\beta\left(P_{\mathrm{s}}g_{\mathrm{sr}} + P_{\mathrm{d}}g_{\mathrm{dr}}\right). \tag{6.6}$$

Including the primary's interference outage constraint, we can write the relay's transmit power as

$$P_H = \min(P_{H1}, P_{\mathcal{I}}). \tag{6.7}$$

6.3.3 Information Processing and Relaying Protocol

In phase one, the received signal $y_{\rm r}$ for the information processing at the relay is given by

$$y_{\rm r} = \sqrt{(1-\beta)P_{\rm s}}h_{\rm sr}x_{\rm s} + \sqrt{(1-\beta)P_{\rm d}}h_{\rm dr}x_{\rm d} + n_{\rm r}, \tag{6.8}$$

where $x_{\rm s}$ is ST's message with unit power, $x_{\rm d}$ is the unit power jamming signal sent by the destination, and $n_{\rm r}$ is AWGN at the relay. We assume that the power splitting does not affect the noise power. Based on the received signal $y_{\rm r}$ in (6.8), the relay may attempt to decode ST's message $x_{\rm s}$. We can write the SNR at the relay as

$$\gamma_{\rm r} = \frac{(1-\beta)P_{\rm s}g_{\rm sr}}{(1-\beta)P_{\rm d}g_{\rm dr} + N_0}, \tag{6.9}$$

where N_0 is the noise power of AWGN $n_{\rm r}$.

In phase two, the relay amplifies the received signal $y_{\rm r}$ by a factor ξ based on its power constraint and forwards the resultant signal $x_{\rm r}$ to the destination, which is given as

$$x_{\rm r} = \xi y_{\rm r} \tag{6.10}$$

$$= \sqrt{\frac{P_H}{(1-\beta)P_{\rm s}g_{\rm sr} + (1-\beta)P_{\rm d}g_{\rm dr} + N_0}}y_{\rm r}. \tag{6.11}$$

Then, we substitute (6.8) in (6.10) and then use (6.10) to write the received signal $y'_{\rm d}$ at the destination as

$$\begin{aligned} y'_{\rm d} &= h_{\rm rd}x_{\rm r} + n_{\rm d} \\ &= \xi\sqrt{(1-\beta)P_{\rm s}}h_{\rm sr}h_{\rm rd}x_{\rm s} + \xi\sqrt{(1-\beta)P_{\rm d}}h_{\rm rd}h_{\rm dr}x_{\rm d} + \xi h_{\rm rd}n_{\rm r} + n_{\rm d}, \end{aligned} \tag{6.12}$$

where $n_{\rm d}$ is the AWGN at the destination with power N_0. Since $x_{\rm d}$ is the jamming signal sent by SD itself to the relay in phase one, the SD can remove the term $\xi\sqrt{(1-\beta)P_{\rm d}}h_{\rm rd}h_{\rm dr}x_{\rm d}$ from (6.12) and decode the information from the rest of the received signal. Thus, the resultant received signal $y_{\rm d}$ at SD becomes

$$y_{\rm d} = \xi\sqrt{(1-\beta)P_{\rm s}}h_{\rm sr}h_{\rm rd}x_{\rm s} + \xi h_{\rm rd}n_{\rm r} + n_{\rm d}. \tag{6.13}$$

When $P_{H1} \leq P_{\mathcal{I}}$, we have $P_H = P_{H1}$. Then, substituting P_{H1} from (6.6) in (6.11), and then using ξ from (6.11) in (6.13), we get

$$y_{\mathrm{d}} = \frac{\sqrt{\eta\beta(1-\beta)P_{\mathrm{s}}\left(P_{\mathrm{s}}g_{\mathrm{sr}} + P_{\mathrm{d}}g_{\mathrm{dr}}\right)}h_{\mathrm{sr}}h_{\mathrm{rd}}x_{\mathrm{s}}}{\sqrt{(1-\beta)P_{\mathrm{s}}g_{\mathrm{sr}} + (1-\beta)P_{\mathrm{d}}g_{\mathrm{dr}} + N_0}} + \frac{\sqrt{\eta\beta\left(P_{\mathrm{s}}g_{\mathrm{sr}} + P_{\mathrm{d}}g_{\mathrm{dr}}\right)}h_{\mathrm{rd}}n_{\mathrm{r}}}{\sqrt{(1-\beta)P_{\mathrm{s}}g_{\mathrm{sr}} + (1-\beta)P_{\mathrm{d}}g_{\mathrm{dr}} + N_0}} + n_{\mathrm{d}}. \tag{6.14}$$

The first term on the right hand side of (6.14) represents the signal part, while the second and third terms correspond to the total received noise at the destination. Then, the SNR at the destination can be written as

$$\gamma_{\mathrm{d}} = \frac{\eta\beta(1-\beta)P_{\mathrm{s}}g_{\mathrm{sr}}g_{\mathrm{rd}}}{\eta\beta g_{\mathrm{rd}}N_0 + N_0(1-\beta) + \frac{N_0^2}{(P_{\mathrm{s}}g_{\mathrm{sr}}+P_{\mathrm{d}}g_{\mathrm{dr}})}}. \tag{6.15}$$

When $P_{H1} \geq P_{\mathcal{I}}$, i.e., $P_H = P_{\mathcal{I}}$, we can write γ_{d} in the similar way.

6.3.4 Secure Communication via an Untrusted Relay

When the relay is considered untrusted, we can write the instantaneous secrecy rate R_{sec} of the relay-assisted communication as [141]

$$\begin{aligned} R_{\mathrm{sec}} &= \frac{1}{2}\left[\log_2\left(1+\gamma_{\mathrm{d}}\right) - \log_2\left(1+\gamma_{\mathrm{r}}\right)\right]^+ \\ &= \frac{1}{2}\left[\log_2\left(\frac{1+\gamma_{\mathrm{d}}}{1+\gamma_{\mathrm{r}}}\right)\right]^+, \end{aligned} \tag{6.16}$$

where $[x]^+ = \max(x, 0)$. The factor $\frac{1}{2}$ characterizes the two-hop communication between ST and SD.

For the rest of the Section 6.3, we assume $P_{\mathrm{s}} = P_{\mathrm{d}} = P$ for analytical tractability. In this case, the power P is limited by the primary's interference constraint given in (6.2). The following proposition provides the upper limit on P.

Proposition 6.1. *The maximum allowed power P satisfies the following equality:*

$$\Theta_{\mathrm{p}} = \begin{cases} \frac{\Omega_{\mathrm{sp}}}{\Omega_{\mathrm{sp}}-\Omega_{\mathrm{dp}}}\exp\left(-\frac{\mathcal{I}_{\mathrm{p}}}{P\Omega_{\mathrm{sp}}}\right) + \frac{\Omega_{\mathrm{dp}}}{\Omega_{\mathrm{dp}}-\Omega_{\mathrm{sr}}}\exp\left(-\frac{\mathcal{I}_{\mathrm{p}}}{P\Omega_{\mathrm{dp}}}\right), & \text{if } \Omega_{\mathrm{sp}} \neq \Omega_{\mathrm{dp}} \\ 1 - \Upsilon\left(2, \frac{\mathcal{I}_{\mathrm{p}}}{P\Omega_{\mathrm{sp}}}\right), & \text{if } \Omega_{\mathrm{sp}} = \Omega_{\mathrm{dp}}, \end{cases} \tag{6.17}$$

where $\Upsilon(a,t) = \int_0^t x^{a-1}\exp(-x)\mathrm{d}x$ is the lower incomplete Gamma function.

Proof. The proof is given in Appendix D.2. □

6.3.4.1 Secrecy Outage Probability

The secrecy outage probability is an important measure of the secrecy performance. It allows us to determine the probability of attaining a target secrecy rate. Given the energy harvesting circuitry of the relay is active, we can express the secrecy outage probability as [141]

$$P_{\text{out}} = \mathbb{P}\left(R_{\text{sec}} < R_{\text{th}}\right), \tag{6.18}$$

where R_{sec} is the instantaneous secrecy rate given by (6.16) and R_{th} is the target secrecy rate. Then, substituting γ_{r} from (6.9) and γ_{d} from (6.15), we can rewrite (6.18) as

$$P_{\text{out}} = \mathbb{P}\left(\frac{1+\frac{\eta\beta(1-\beta)Pg_{\text{sr}}g_{\text{rd}}}{(N_0\eta\beta g_{\text{rd}}+N_0(1-\beta))+\frac{N_0^2}{P(g_{\text{sr}}+g_{\text{rd}})}}}{1+\frac{(1-\beta)Pg_{\text{sr}}}{(1-\beta)Pg_{\text{rd}}+N_0}} < 2^{2R_{\text{th}}}\right). \tag{6.19}$$

We can further express the secrecy outage probability in (6.19) analytically as given in Proposition 6.2.

Proposition 6.2. *The secrecy outage probability for PS policy can be approximately expressed as*

$$P_{\text{out}} \approx 1 - \frac{1}{\Omega_{\text{rd}}}\int_{\theta_1}^{\infty} \exp\left(-\frac{\delta-1}{\nu(x)\Omega_{\text{sr}}} - \frac{x}{\Omega_{\text{rd}}}\right) \mathrm{d}x, \tag{6.20}$$

where $\delta = 2^{2R_{\text{th}}}$ *with*

$$\theta_1 = \frac{\frac{\delta-1}{1-\beta} + \sqrt{\left(\frac{\delta-1}{1-\beta}\right)^2 + \frac{4\delta P}{\eta\beta N_0}}}{2(P/N_0)}, \tag{6.21a}$$

and

$$\nu(x) = (1-\beta)\left(\frac{\eta\beta Px}{N_0\left(\eta\beta x + (1-\beta)\right)} - \frac{P\delta}{P(1-\beta)x + N_0}\right). \tag{6.21b}$$

Proof. See Appendix D.3. □

Equation (6.20) is obtained using the high SNR approximation of the received SNR at the destination given as

$$\gamma_{\text{d}} \approx \frac{\eta\beta(1-\beta)Pg_{\text{sr}}g_{\text{rd}}}{N_0\left(\eta\beta g_{\text{rd}} + (1-\beta)\right)}. \tag{6.22}$$

Equation (6.22) can be obtained from the exact expression given in (6.15) of $\gamma_{\rm d}$ by neglecting the term $\frac{N_0^2}{(P_{\rm s}g_{\rm sr}+P_{\rm d}g_{\rm dr})}$ (due to negligible N_0^2 at high SNR) from the denominator of (6.15). The approximation in (6.22) is analytically more tractable than the exact expression in (6.19).[4] Although the integral in (6.20) cannot be expressed in a closed form, it can be easily evaluated numerically as the integrand consists of elementary functions.

As aforementioned in Section 6.2.2, the received power at the relay must be greater than the minimum power threshold θ_H to activate the energy harvesting circuitry. Using channel reciprocity on the relay-destination link, we can write the received power P_R at the relay as

$$P_R = (Pg_{\rm sr} + Pg_{\rm rd})\,. \tag{6.23}$$

If the received power P_R is less than the power threshold θ_H, the energy harvesting circuitry at the relay stays inactive, leading to the power outage. The following proposition gives the expression for the power outage probability $\mathbb{P}\left(P_R < \theta_H\right)$.

Proposition 6.3. *We write the power outage probability* $P_{\rm p,out}$ *as follows:*

$$P_{\rm p,out} = \begin{cases} 1 - \frac{\Omega_{\rm sr}}{\Omega_{\rm sr}-\Omega_{\rm rd}} \exp\left(-\frac{\theta_H}{P\Omega_{\rm sr}}\right) & \\ -\frac{\Omega_{\rm rd}}{\Omega_{\rm rd}-\Omega_{\rm sr}} \exp\left(-\frac{\theta_H}{P\Omega_{\rm rd}}\right), & \text{if } \Omega_{\rm sr} \neq \Omega_{\rm rd} \\ \Upsilon\left(2, \frac{\theta_H}{P\Omega_{\rm sr}}\right), & \text{if } \Omega_{\rm sr} = \Omega_{\rm rd}, \end{cases} \tag{6.24}$$

where $\Upsilon(a,t) = \int_0^t x^{a-1}\exp(-x){\rm d}x$ *is the lower incomplete Gamma function.*

Proof. The proof is given in Appendix D.4. □

For an energy constrained untrusted relay, a secrecy outage can also occur if the power received by the relay is insufficient to activate the energy harvesting circuitry [142]. Thus, combining with (6.20), we can write the overall secrecy outage probability $P_{\rm out}^{\rm s}$ as [142]

$$P_{\rm out}^{\rm s} = P_{\rm p,out} + (1 - P_{\rm p,out})P_{\rm out}, \tag{6.25}$$

where $P_{\rm out}$ is given by (6.20).

[4] In fact, the complex structure of (6.19) does not allow us to get an exact analytical expression for the secrecy outage probability. This is because, the term $(g_{\rm sr} + g_{\rm dr})$ in the denominator of (6.19) prevents the separation of two random variables $g_{\rm sr}$ and $g_{\rm rd}$, which in turn, impedes the simplification of (6.19) to get an exact analytical expression.

6.3.4.2 Probability of Positive Secrecy Rate

The destination-assisted jamming helps to keep ST's information confidential from the relay and achieve the secure communication. In this regard, the probability P_{pos} of achieving strictly positive secrecy rate is an important measure of the secrecy performance. We provide the exact and approximate analytical expression for P_{pos} in the following proposition.

Proposition 6.4. *We write the exact and high SNR approximation analytical expressions for the probability of achieving strictly positive secrecy rate P_{pos} as follows:*

$$P_{\text{pos}} = (1 - P_{\text{p,out}}) \left[\exp\left(-\frac{\theta_3}{\Omega_{\text{rd}}}\right) + \frac{1}{\Omega_{\text{rd}}} \int_{\theta_2}^{\theta_3} \exp\left(-\left(\frac{\psi(x)}{\Omega_{\text{sr}}} + \frac{x}{\Omega_{\text{rd}}}\right)\right) \mathrm{d}x \right] \tag{6.26a}$$

$$\approx (1 - P_{\text{p,out}}) \exp\left(-\sqrt{\frac{\theta_2}{\Omega_{\text{rd}}^2}}\right), \text{ (\textit{high SNR approximation})}, \tag{6.26b}$$

where

$$\theta_2 = \mathcal{A}, \tag{6.27a}$$

$$\theta_3 = \left(\frac{\mathcal{B}}{2} + \sqrt{\left(\frac{\mathcal{B}}{2}\right)^2 + \left(-\frac{\mathcal{A}}{3}\right)^3}\right)^{\frac{1}{3}} + \left(\frac{\mathcal{B}}{2} - \sqrt{\left(\frac{\mathcal{B}}{2}\right)^2 + \left(-\frac{\mathcal{A}}{3}\right)^3}\right)^{\frac{1}{3}}, \tag{6.27b}$$

with $\mathcal{A} = \frac{N_0}{\eta\beta P}$ *and* $\mathcal{B} = \frac{N_0^2}{\eta\beta(1-\beta)P^2}$, *and*

$$\psi(x) = \frac{N_0^2}{P(1-\beta)(\eta\beta P x^2 - N_0)} - x. \tag{6.27c}$$

with

$$\psi(x) \begin{cases} < 0, & 0 \le x < \theta_2 \\ \ge 0, & \theta_2 \le x \le \theta_3, \\ < 0, & \theta_3 < x < \infty. \end{cases} \tag{6.28}$$

θ_2 is the positive root of the equation $g(x) = \eta\beta P x^2 - N_0 = 0$, while θ_3 is the real root of $\psi(x) = 0$ that is equivalent to a cubic equation given as $x^3 - \mathcal{A}x - \mathcal{B} = 0$.

Proof. The proof is given in Appendix D.5. □

6.3.4.3 Ergodic Secrecy Rate

Another important secrecy metric is the ergodic secrecy rate, which is the maximum transmission rate at which the eavesdropper fails to decode the secret information that is being transmitted. We can obtain the ergodic secrecy rate by averaging out the instantaneous secrecy rate R_{sec} over all possible channel realizations. Therefore, in the case of untrusted relaying, the ergodic secrecy rate, with the inclusion of power outage probability $P_{\text{p,out}}$ given by (6.24), can be given as

$$\begin{aligned}\bar{R}_{\text{sec}} &= (1-P_{\text{p,out}})\mathbb{E}\left[R_{\text{sec}}\right] \\ &= (1-P_{\text{p,out}})\mathbb{E}\left[\frac{1}{2}\left[\log_2\left(\frac{1+\gamma_{\text{d}}}{1+\gamma_{\text{r}}}\right)\right]^+\right],\end{aligned} \tag{6.29}$$

where $\mathbb{E}[\cdot]$ is the expectation operator. Using (6.9) and (6.15) in (6.29), we can write the analytical expression for $\bar{R}_{\text{sec}}$ as

$$\begin{aligned}\bar{R}_{\text{sec}} = (1-P_{\text{p,out}})\int_{x=0}^{\infty}\int_{y=0}^{\infty}\left[\frac{1}{2}\log_2\left(\frac{1+\frac{\eta\beta(1-\beta)Pxy}{\eta\beta N_0 y+N_0(1-\beta)+\frac{N_0^2}{P(x+y)}}}{1+\frac{(1-\beta)Px}{(1-\beta)Py+N_0}}\right)\right]^+ \\ \times f_{g_{\text{sr}}}(x)f_{g_{\text{rd}}}(y)\,\mathrm{d}x\,\mathrm{d}y.\end{aligned} \tag{6.30}$$

Using high SNR approximation for γ_{d} as given in (6.22), we can write $\bar{R}_{\text{sec}}$ as

$$\begin{aligned}\bar{R}_{\text{sec}} \approx (1-P_{\text{p,out}})\int_{x=0}^{\infty}\int_{y=0}^{\infty}\left[\frac{1}{2}\log_2\left(\frac{1+\frac{\eta\beta(1-\beta)Pg_{\text{sr}}g_{\text{rd}}}{N_0(\eta\beta g_{\text{rd}}+(1-\beta))}}{1+\frac{(1-\beta)Pg_{\text{sr}}}{(1-\beta)Pg_{\text{rd}}+N_0}}\right)\right]^+ \\ \times f_{g_{\text{sr}}}(x)f_{g_{\text{rd}}}(y)\,\mathrm{d}x\,\mathrm{d}y.\end{aligned} \tag{6.31}$$

The expressions in (6.30) and (6.31) do not admit a closed form and are intractable. Alternatively, we provide a closed-form lower bound on (6.31) as given in the following Proposition. The lower bound on the ergodic secrecy rate ensures the minimum ergodic secrecy rate under all possible channel conditions for a given set of parameters.

Proposition 6.5. *The ergodic secrecy rate* $\bar{R}_{\text{sec}}$ *in* (6.31) *is lower bounded as*

$$\bar{R}_{\text{sec}} \geq (1-P_{\text{p,out}})\max\left(\frac{1}{2\ln(2)}(T_1-T_2),0\right), \tag{6.32}$$

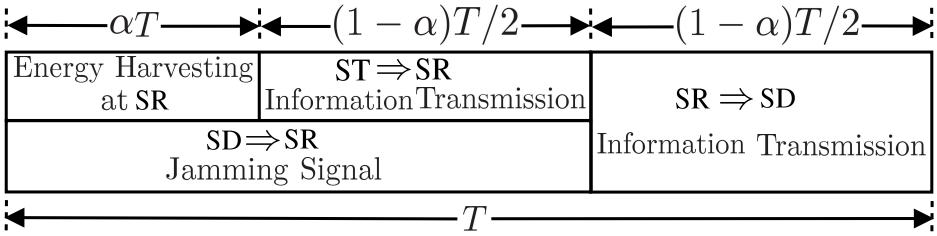

Figure 6.3: Time switching policy for the secure communication via an energy harvesting untrusted relay.

where

$$T_1 \geq \ln\left(1+\exp\left(-2\phi-\ln\left(\frac{1}{m_x m_z}\right)\right)+\exp\left(\frac{1}{m_z}\right)+\mathrm{Ei}\left(-\frac{1}{m_z}\right)\right) \tag{6.33a}$$

and

$$T_2=\begin{cases} 1+\frac{1}{m_x}\exp\left(\frac{1}{m_x}\right)\mathrm{Ei}\left(-\frac{1}{m_x}\right), & \frac{m_y}{m_x}=1 \\ \frac{m_x}{m_x-m_y}\left[\exp\left(\frac{1}{m_y}\right)\mathrm{Ei}\left(-\frac{1}{m_y}\right)\right. & \\ \left.-\exp\left(\frac{1}{m_x}\right)\mathrm{Ei}\left(-\frac{1}{m_x}\right)\right], & \frac{m_y}{m_x}\neq 1, \end{cases} \tag{6.33b}$$

with $m_x=\frac{(1-\beta)P\Omega_{\mathrm{sr}}}{N_0}$, $m_y=\frac{(1-\beta)P\Omega_{\mathrm{rd}}}{N_0}$, $m_z=\frac{\eta\beta\Omega_{\mathrm{rd}}}{1-\beta}$, $\phi\approx 0.577215$, *is the Euler's constant [107, 9.73], and* $\mathrm{Ei}(x)=-\int_{-x}^{\infty}(\exp(-t)/t)\,\mathrm{d}t$, *is the exponential integral [107, 8.21].*

Proof. The proof is given in Appendix D.6. □

The lower bound given in (6.32) is tight in high SNR regime, which is depicted in Fig. 6.8 of Section 6.5. Proposition 6.5 shows that the ergodic secrecy rate depends on the power splitting factor β, energy conversion efficiency factor η, and mean channel gains of ST-SR and SR-SD links.

6.4 Time Switching Policy Based Relaying

Fig. 6.3 shows TS policy based relaying protocol for the secure communication via untrusted relay. The communication between ST and SD happens over two hops and in a duration of T. The SR harvests energy for αT duration ($0\leq\alpha\leq 1$) from the received RF signals. The relay spends its harvested energy to forward the received information from ST to SD.

The remaining $(1-\alpha)T$ duration is further split in two sub-slots of equal duration of $\frac{(1-\alpha)T}{2}$. In the first sub-slot, ST transmits the information to SR, which is forwarded to SD in the second sub-slot after the amplification. The SD sends a jamming signal during the ST-SR transmission.

6.4.1 Energy Harvesting at Relay

For the aforementioned TS policy, the energy E_H harvested during αT duration is given by

$$E_H = \eta\alpha T \left(P_{\rm s} g_{\rm sr} + P_{\rm d} g_{\rm dr}\right). \tag{6.34}$$

The relay uses this harvested energy to forward ST's information to SD with power given by

$$P_{H1} = \frac{E_H}{(1-\alpha)T/2} = \frac{2\eta\alpha \left(P_{\rm s} g_{\rm sr} + P_{\rm d} g_{\rm dr}\right)}{1-\alpha}. \tag{6.35}$$

Similar to PS policy, under the primary's interference outage constraint, the relay's transmit power can be given by

$$P_H = \min(P_{H1}, P_{\mathcal{I}}), \tag{6.36}$$

where $P_{\mathcal{I}}$ is given by (6.4).

6.4.2 Information Processing and Relaying Protocol

After the energy harvesting phase, the relay switches to information processing phase, where the received signal is given by

$$y_{\rm r} = \sqrt{P_{\rm s}} h_{\rm sr} x_{\rm s} + \sqrt{P_{\rm d}} h_{\rm dr} x_{\rm d} + n_{\rm r}. \tag{6.37}$$

Note that, unless otherwise stated, all notations in this section have the same meanings as they have in Section 6.3 on the power splitting policy based relaying. Using the received signal $y_{\rm r}$ given in (6.37), the relay may attempt to decode the signal from ST. The received SNR at the relay is given by

$$\gamma_{\rm r} = \frac{P_{\rm s} g_{\rm sr}}{P_{\rm d} g_{\rm dr} + N_0}. \tag{6.38}$$

The relay forwards the amplified version of the received signal to SD, which is given by

$$x_{\rm r} = \xi y_{\rm r} = \sqrt{\frac{P_H}{P_{\rm s} g_{\rm sr} + P_{\rm d} g_{\rm dr} + N_0}}\, y_{\rm r}. \tag{6.39}$$

Then the received signal $y'_{\rm d}$ at SD is given by

$$y'_{\rm d} = h_{\rm rd}x_{\rm r} + n_{\rm d}. \tag{6.40}$$

After subtracting the term corresponding to the known jamming signal $x_{\rm d}$, the resultant received signal $y_{\rm d}$ at SD becomes

$$y_{\rm d} = \xi\sqrt{P_{\rm s}}h_{\rm sr}h_{\rm rd}x_{\rm s} + \xi h_{\rm rd}n_{\rm r} + n_{\rm d}. \tag{6.41}$$

When $P_{H1} \leq P_{\mathcal{I}}$, we have $P_H = P_{H1}$. Substituting P_{H1} from (6.35) in (6.39), and then ξ from (6.39) in (6.41), we can write the received signal $y_{\rm d}$ as

$$y_{\rm d} = \frac{\sqrt{2\eta\alpha P_{\rm s}\left(P_{\rm s}g_{\rm sr} + P_{\rm d}g_{\rm dr}\right)}h_{\rm sr}h_{\rm rd}x_{\rm s}}{\sqrt{(1-\alpha)(P_{\rm s}g_{\rm sr} + P_{\rm d}g_{\rm dr} + N_0)}} + \frac{\sqrt{2\eta\alpha\left(P_{\rm s}g_{\rm sr} + P_{\rm d}g_{\rm dr}\right)}h_{\rm rd}n_{\rm r}}{\sqrt{(1-\alpha)(P_{\rm s}g_{\rm sr} + P_{\rm d}g_{\rm dr} + N_0)}} + n_{\rm d}. \tag{6.42}$$

The first term on the right hand side of (6.42) represents the received signal part at SD, while the last two terms represent the overall noise at SD. Thus, we can write the received SNR at SD as

$$\gamma_{\rm d} = \frac{2\eta\alpha P_{\rm s}g_{\rm sr}g_{\rm rd}}{2\eta\alpha g_{\rm rd}N_0 + N_0(1-\alpha) + \frac{N_0^2(1-\alpha)}{(P_{\rm s}g_{\rm sr}+P_{\rm d}g_{\rm dr})}}. \tag{6.43}$$

When $P_{H1} \geq P_{\mathcal{I}}$, i.e., $P_H = P_{\mathcal{I}}$, we can write $\gamma_{\rm d}$ in the similar way. For the rest of the Section 6.4, we assume $P_{\rm s} = P_{\rm d} = P$ for analytical tractability. Similar to PS policy, we can obtain the maximum allowed P for TS policy from Proposition 6.1.

6.4.3 Secure Communication Via an Untrusted Relay

For the proposed TS policy, the instantaneous secrecy rate can be given by

$$\begin{aligned} R_{\rm sec} &= \frac{(1-\alpha)}{2}\left[\log_2\left(1+\gamma_{\rm d}\right) - \log_2\left(1+\gamma_{\rm r}\right)\right]^+ \\ &= \frac{(1-\alpha)}{2}\left[\log_2\left(\frac{1+\gamma_{\rm d}}{1+\gamma_{\rm r}}\right)\right]^+, \end{aligned} \tag{6.44}$$

where $\gamma_{\rm r}$ and $\gamma_{\rm d}$ are given by (6.38) and (6.43), respectively. The factor $(1-\alpha)/2$ denotes the effective time of information transmission between ST and SD.

6.4.3.1 Secrecy Outage Probability

We can express the secrecy outage probability as given in the Proposition 6.6.

Proposition 6.6. *For TS policy, given the energy harvesting circuitry of the relay is active, the secrecy outage probability is analytically given by* (6.20)*, where* $\delta = 2^{\frac{2R_{\rm th}}{1-\alpha}}$ *with*

$$\theta_1 = \frac{(\delta-1) + \sqrt{(\delta-1)^2 + 4\delta\frac{P(1-\alpha)}{2\eta\alpha N_0}}}{2(P/N_0)}, \tag{6.45}$$

and

$$\nu(x) = \left(\frac{2\eta\alpha P x}{N_0\left(2\eta\alpha x + (1-\alpha)\right)} - \frac{P\delta}{Px + N_0}\right). \tag{6.46}$$

Proof. The proof follows the same steps used in Appendix D.3 to derive the secrecy outage probability for PS policy in Proposition 6.2. □

Note that, for TS policy, the secrecy outage probability under high SNR approximation as given by (6.20) is obtained by approximating the exact expression of $\gamma_{\rm d}$ in (6.43) as

$$\gamma_{\rm d} \approx \frac{2\eta\alpha P g_{\rm sr} g_{\rm rd}}{N_0\left(2\eta\alpha g_{\rm rd} + (1-\alpha)\right)}, \tag{6.47}$$

where we have used the channel reciprocity, i.e., $h_{\rm rd} = h_{\rm dr}$. We have obtained (6.47) from the exact expression of received SNR at SD given in (6.43) by neglecting the term $\frac{N_0^2(1-\alpha)}{(P_{\rm s}g_{\rm sr}+P_{\rm d}g_{\rm dr})}$ in the denominator of (6.43) due to negligible value of N_0^2 at high SNR. Now, considering the power outage probability, we can finally write the total secrecy outage probability as (6.25). Note that the power outage probability for PS and TS policies is the same.

6.4.3.2 Probability of Positive Secrecy Rate

The following proposition gives the analytical expression for $P_{\rm pos}$.

Proposition 6.7. *We can write* $P_{\rm pos}$ *as* (6.26)*, where* $\theta_2 = \mathcal{A}$*,* θ_3 *is given by* (6.27b) *with* $\mathcal{A} = \frac{N_0(1-\alpha)}{2\eta\alpha P}$ *and* $\mathcal{B} = \frac{N_0^2(1-\alpha)}{2\eta\alpha P^2}$*, and*

$$\psi(x) = \frac{N_0^2}{P\left(\frac{2\eta\alpha}{1-\alpha}Px^2 - N_0\right)} - x.$$

Proof. The proof follows the same steps used in Appendix D.5 for PS policy. □

6.4.3.3 Ergodic Secrecy Rate

With the inclusion of the power outage probability $P_{\mathrm{p,out}}$ given in (6.24), the ergodic secrecy rate is calculated by averaging the instantaneous secrecy rate over all possible channel realizations and is given as

$$\begin{aligned}\bar{R}_{\mathrm{sec}} &= (1-P_{\mathrm{p,out}})\mathbb{E}[R_{\mathrm{sec}}] \\ &= (1-P_{\mathrm{p,out}})\mathbb{E}\left[\frac{(1-\alpha)}{2}\left[\log_2\left(\frac{1+\gamma_{\mathrm{d}}}{1+\gamma_{\mathrm{r}}}\right)\right]^+\right]. \end{aligned} \tag{6.48}$$

Using (6.38) and (6.43) in (6.48), we can write the analytical expression for $\bar{R}_{\mathrm{sec}}$ as

$$\begin{aligned}\bar{R}_{\mathrm{sec}} &= (1-P_{\mathrm{p,out}}) \\ &\times \int_{x=0}^{\infty}\int_{y=0}^{\infty}\left[\frac{(1-\alpha)}{2}\log_2\left(\frac{1+\frac{2\eta\alpha Pxy}{2\eta\alpha N_0 y+N_0(1-\alpha)+\frac{N_0^2(1-\alpha)}{P(x+y)}}}{1+\frac{Px}{Py+N_0}}\right)\right]^+ \\ &\times f_{g_{\mathrm{sr}}}(x)f_{g_{\mathrm{rd}}}(y)\,\mathrm{d}x\,\mathrm{d}y. \end{aligned} \tag{6.49}$$

Using high SNR approximation for γ_{d} as given in (6.47), we can write $\bar{R}_{\mathrm{sec}}$ as

$$\begin{aligned}\bar{R}_{\mathrm{sec}} &\approx (1-P_{\mathrm{p,out}}) \\ &\times \int_{x=0}^{\infty}\int_{y=0}^{\infty}\left[\frac{(1-\alpha)}{2}\log_2\left(\frac{1+\frac{2\eta\alpha Pxy}{2\eta\alpha N_0 y+N_0(1-\alpha)}}{1+\frac{Px}{Py+N_0}}\right)\right]^+ \\ &\times f_{g_{\mathrm{sr}}}(x)f_{g_{\mathrm{rd}}}(y)\,\mathrm{d}x\,\mathrm{d}y. \end{aligned} \tag{6.50}$$

Both (6.49) and (6.50) do not admit a closed form. Alternatively, we present a closed-form lower bound on (6.50) as given in the following Proposition.

Proposition 6.8. *We lower bound the ergodic secrecy rate* $\bar{R}_{\mathrm{sec}}$ *in* (6.50) *by*

$$\bar{R}_{\mathrm{sec}} \geq (1-P_{\mathrm{p,out}})\max\left(\frac{1-\alpha}{2\ln(2)}(T_1-T_2),0\right), \tag{6.51}$$

where T_1 *and* T_2 *are given by* (6.33a) *and* (6.33b)*, respectively, with* $m_x=\frac{P\Omega_{\mathrm{sr}}}{N_0}$, $m_y=\frac{P\Omega_{\mathrm{rd}}}{N_0}$, *and* $m_z=\frac{2\eta\alpha\Omega_{\mathrm{rd}}}{1-\alpha}$.

Proof. The proof follows the same steps used in Appendix D.6 to derive the lower bound on ergodic secrecy capacity for PS policy in Proposition 6.5. □

The lower bound given in (6.51) is tight in high SNR regime, which is depicted in Fig. 6.8 of Section 6.5.

6.5 Results and Discussions

In this section, we numerically investigate the secrecy performance of the communication between ST and SD via an untrusted wireless energy harvesting relay SR. For different system parameters like the power splitting ratio, energy harvesting time, primary's outage threshold, transmit SNR, ST-SR and SR-SD distances, target secrecy rate, path-loss exponent, and the energy conversion efficiency factor, we discuss how they impact the secrecy outage probability and ergodic secrecy rate under both PS and TS policies.

6.5.1 System Parameters and Simulation Setup

Unless otherwise stated, we consider following system parameters. Energy conversion efficiency, $\eta = 0.7$; energy harvesting circuitry activation threshold, $\theta_H = -30$ dBm [36, 143]; and noise power, $N_0 = 10^{-4}$. The ST, SD, and PD are located at (0,0), (10,0), and (5,5), respectively. Unless otherwise stated, SR is located at (5,0). The mean channel power gains $\Omega_{\rm sr}$ and $\Omega_{\rm rd}$ of the exponential random variables $g_{\rm sr}$ and $g_{\rm rd}$ are $d_{\rm sr}^{-\rho}$ and $d_{\rm rd}^{-\rho}$, respectively, where ρ is the path-loss exponent. Unless otherwise stated, $\rho = 2.7$, $\mathcal{I}_{\rm p} = -4.7$ dB, and $\Theta_{\rm p} = -20$ dB.

6.5.2 Effect of power splitting ratio β and energy harvesting time α

6.5.2.1 Effect of β

As Fig. 6.4 shows, for PS policy, with the increase in β, the secrecy outage probability initially decreases to a minimum value. The value of β corresponding to the minimum secrecy outage probability is the optimal value of β. If we increase β further beyond the optimal value, the secrecy outage probability also increases. This is because, as β increases, the relay harvests more energy, which in turn, increases the relay's transmit power (provided it satisfies primary's interference constraint) improving the information reception at SD. Also, the increased β reduces the received signal strength at the relay which degrades the received

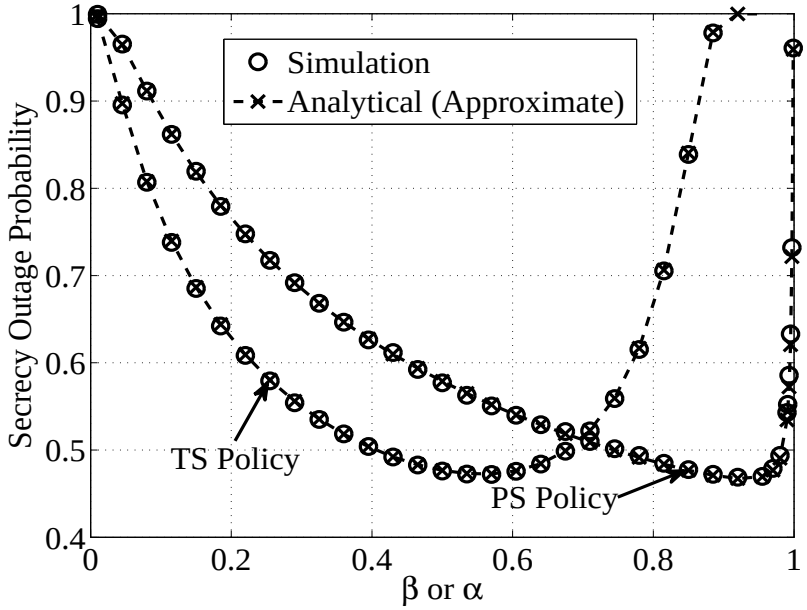

Figure 6.4: Effect of the power splitting ratio β and the energy harvesting time α for PS and TS policies, respectively, on the secrecy outage probability, $R_{\text{th}} = 0.5$ bits/s/Hz.

SNR γ_{r} at the relay. This enhances the secrecy rate of the communication which reduces the secrecy outage probability. But, once β crosses the optimal value, the poor signal strength at the relay delivers a negative effect on the secrecy outage probability. Due to the amplification of the poor received signal, the relay forwards a noisy signal to SD which reduces the received SNR γ_{d} at SD. The increased harvested energy due to the increased β, in turn, the higher transmit power of the relay, cannot compensate the loss in γ_{d} because of the reduced signal strength. This pushes the secret ST-SD communication into the outage more often, increasing the secrecy outage probability. On the similar line, for Fig. 6.5, we can explain the initial increase of the ergodic secrecy rate with β and then its fall after the optimal β. Figs. 6.4 and 6.5 also show that the simulation results are in excellent agreement with analytical results.

6.5.2.2 Effect of α

Fig. 6.4 shows that, for TS policy, as the energy harvesting time α increases, the secrecy outage probability reduces initially and reaches the minimum value for the optimal value of α.

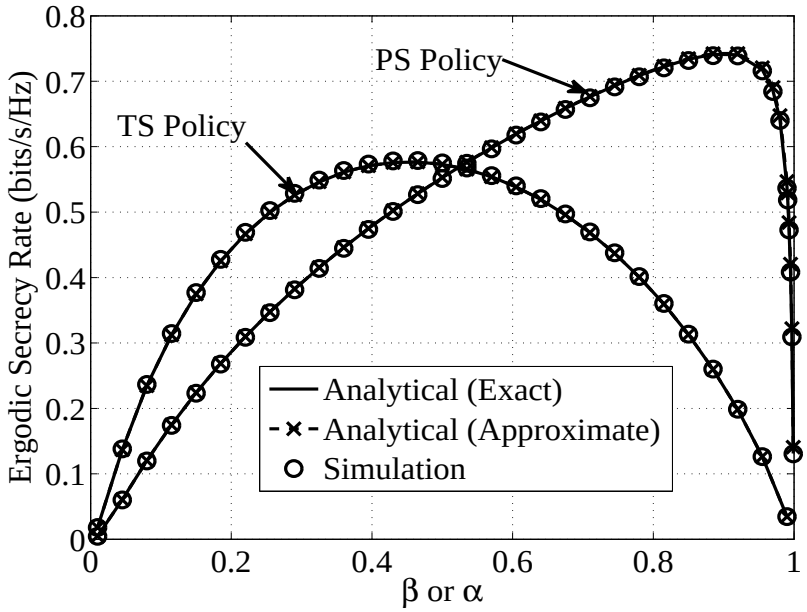

Figure 6.5: Effect of the power splitting ratio β and the energy harvesting time α for PS and TS policies, respectively, on the ergodic secrecy rate.

However, the secrecy outage probability begins to increase as α increases beyond its optimal value. This is because, as α increases, the relay spends more time on the energy harvesting, which in turn, increases its transmit power improving the received SNR at SD. Meanwhile, the increase in α reduces the time available for information processing at both SR and SD. Now, at the relay, the reduced time for information processing has two opposite effects on the secrecy outage probability. Firstly, it degrades the reception of the signal at the relay and thus deteriorates the eavesdropping channel of the relay improving the secrecy outage probability. On the contrary, since the relay amplifies and forwards the received signal to SD, the reception at SD also degrades. Now, when α is less than its optimal value and increasing, the positive effects due to the increased harvested energy at the relay and deterioration of the eavesdropping channel are dominant, and the secrecy outage probability reduces. Once α crosses the optimal value, the effect of the reduced time for information processing becomes dominant, increasing the secrecy outage probability. Similarly, for Fig. 6.5, we can explain the initial increase of the ergodic secrecy rate with α and then its fall after the optimal α.

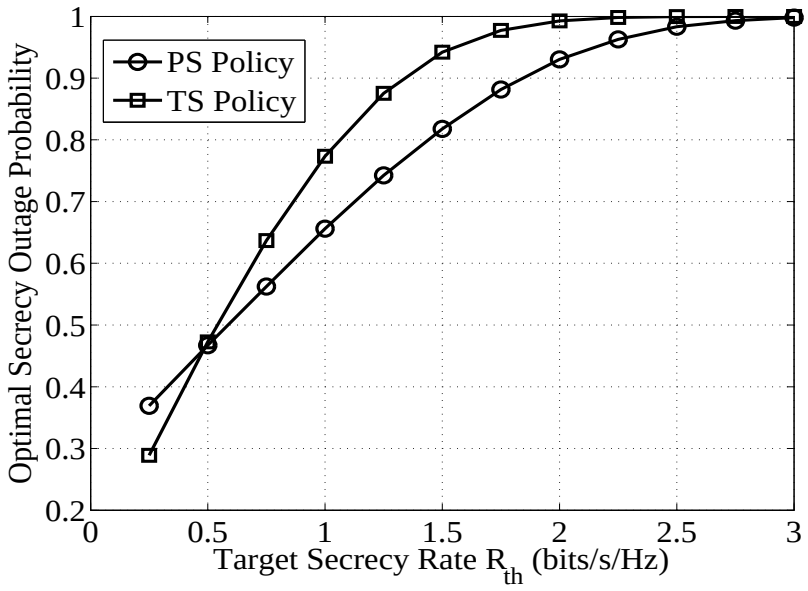

Figure 6.6: Effect of target secrecy rate on the optimal secrecy outage probability for PS and TS policies.

6.5.3 Effect of Target Secrecy Rate R_{th}

Fig. 6.6 plots the optimal secrecy outage probability versus the target secrecy rate R_{th}. As the required secrecy rate constraint becomes tighter, the optimal secrecy outage probability increases. This is because, the higher R_{th} is set, the more it becomes difficult to satisfy, and the likelihood of the secure communication between ST and SD running into the outage increases. Fig. 6.6 also shows that TS policy achieves lower secrecy outage probability at low R_{th} (till 0.5 bits/s/Hz) than that of PS policy. On the contrary, at higher secrecy rate constraint, PS policy outperforms TS policy.

6.5.4 Effect of Transmit SNR

To gain insights about how the transmit powers of ST and SD affect the secrecy performance, let us assume that there is no primary interference constraint. In this case, Fig. 6.7 illustrates the effect of the transmit SNR, i.e., P/N_0, on the optimal secrecy outage probability for both PS and TS policies. For a fixed noise power N_0, the variation in transmit SNR is equivalent to the variation of ST's and SD's power P. The increase in transmit SNR has its constructive

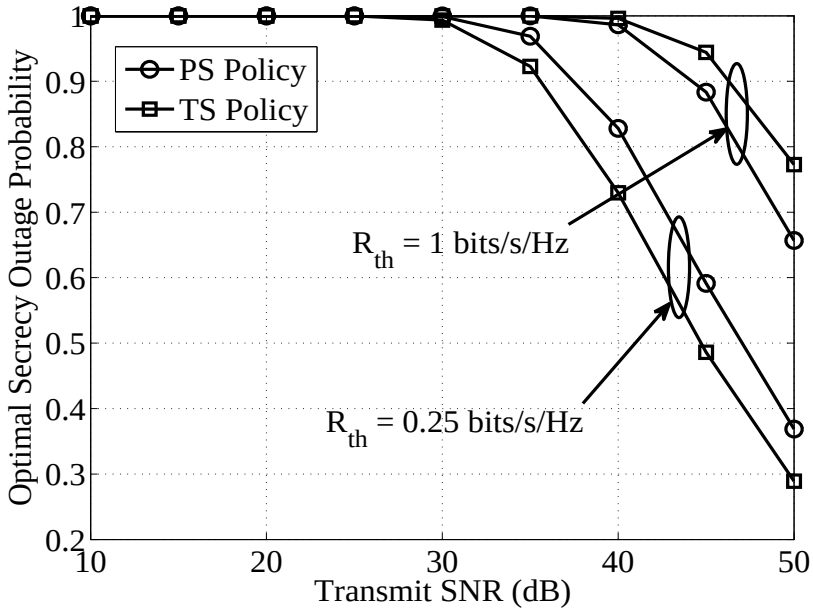

Figure 6.7: Optimal secrecy outage probability versus transmit SNR (P/N_0) for PS and TS policies, $N_0 = -10$ dBm.

as well as destructive effects on the secure communication. The increase in transmit SNR increases the signal strengths of both information signal from ST and jamming signal from SD From the expressions of received SNR γ_r at the relay given by (6.9) and (6.38) for PS and TS policies, respectively, we can note that γ_r increases with the increase in transmit SNR. This increases the chances of the untrusted relay decoding the information, which leads to the increase in the secrecy outage probability. On the other hand, the increase in transmit SNR increases the energy harvested by the relay due to higher received powers from information and jamming signals. This causes an increase in the relay's transmit power, which improves SNR at SD. Also, when relay amplifies and forwards its received signal to SD, the signal strength is further improved due to the increased signal strength at the relay as a result of the increased transmit SNR. As Fig. 6.7 shows, the increase in transmit SNR has an overall positive impact on the secrecy performance of the system.

Now, if we bring the primary's interference outage constraint back, then the increase in the transmit powers of ST and SD is same as the increase in the interference outage threshold Θ_p. We can see this from Fig. 6.9, where the trend of optimal secrecy outage probability

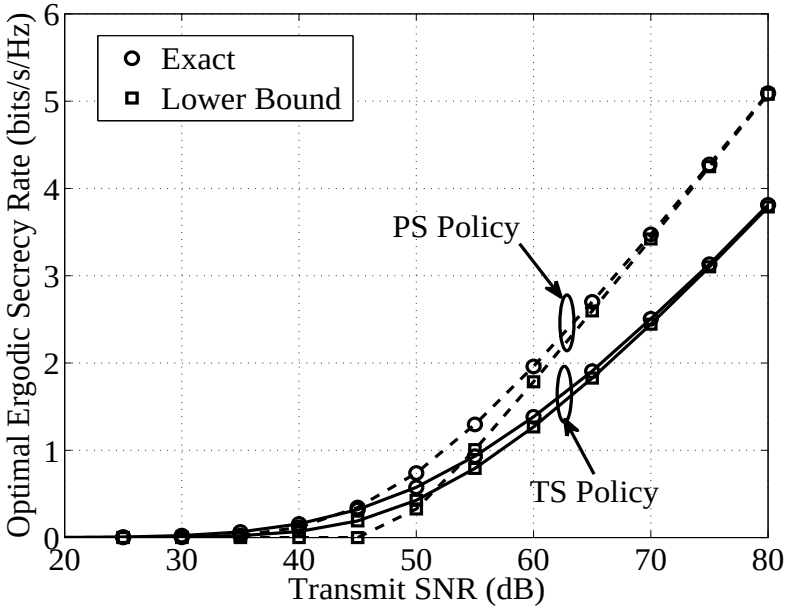

Figure 6.8: Optimal ergodic secrecy rate versus transmit SNR (P/N_0) for PS and TS policies, $N_0 = -10$ dBm.

against the interference outage threshold remains the same as that of against the increase in transmit SNR in Fig. 6.7.

Similarly, Fig. 6.8 shows that the optimal ergodic secrecy rate improves with the increase in transmit SNR. One interesting observation is that, at lower transmit SNR values, TS policy achieves better optimal ergodic secrecy rate than that of PS policy. On the other hand, at higher transmit SNR, PS policy attains higher ergodic secrecy rate compared to TS policy. From Fig. 6.8, we can note that, with the increase in transmit SNR, the performance with the closed-form lower bound on the ergodic secrecy rate approaches the performance with the exact analytical expression. Thus, the closed-form lower bound is tight at high transmit SNR for both PS and TS policies.

6.5.5 Effect of Relay Placement

Fig. 6.10 depicts the effect of the relay placement on the optimal secrecy outage probability for different target secrecy rates and path-loss exponents ρ under both PS and TS policies.

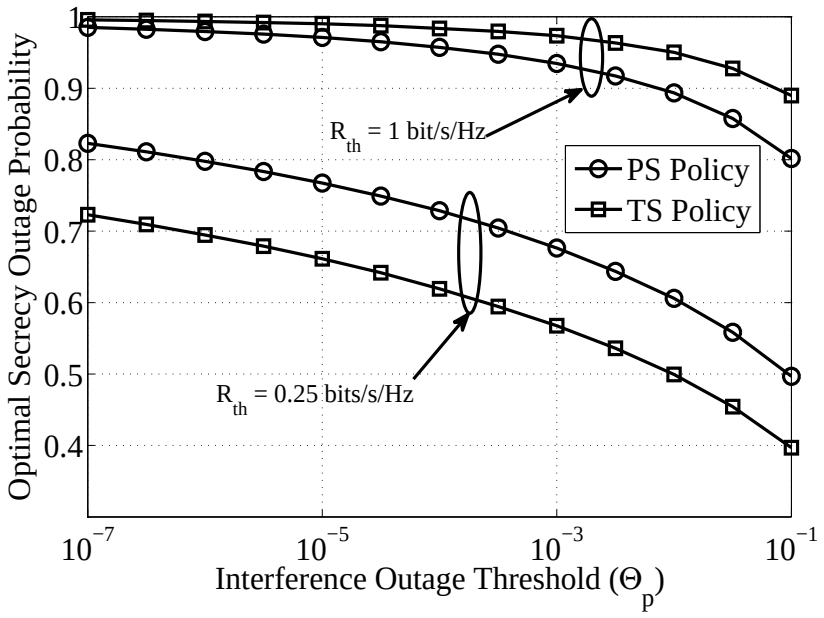

Figure 6.9: Optimal ergodic secrecy rate versus interference outage threshold (Θ_{p}) for PS and TS policies, $\mathcal{I}_{\mathrm{p}} = -4.7$ dB.

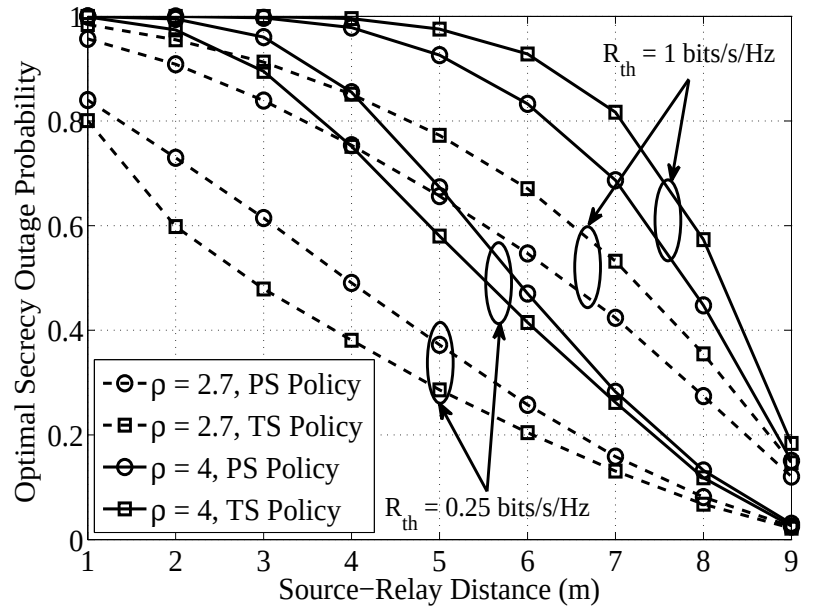

Figure 6.10: Effect of relay placement on the optimal secrecy outage probability for PS and TS policies with different path-loss exponents $\rho = 2.7, 4$, $\mathcal{I}_{\mathrm{p}} = -4.7$ dB, $\Theta_{\mathrm{p}} = 0.01$.

We vary the ST-SR distance d_{sr}, while the SR-SD distance d_{rd} is $10 - d_{\mathrm{sr}}$. The values of path-loss exponent ρ considered are $\rho = 2.7$ and 4. Before discussing Fig. 6.10, it is important to understand how d_{sr} affects the secrecy performance in both constructive and destructive ways. Under both PS and TS policies, as d_{sr} increases, the received information signal strength at the relay decreases due to the higher path-loss $d_{\mathrm{sr}}^{-\rho}$. This discourages the eavesdropping intention of the untrusted relay, improving the secrecy performance. Also, as d_{sr} increases, the SR-SD distance d_{rd} reduces, which makes the received jamming signal at the relay stronger. This further enhances the secrecy performance. The decrease in d_{rd} brings the relay closer to SD due to which the lesser amount of harvested energy is sufficient to perform the reliable communication between SR and SD because of the reduced path-loss $d_{\mathrm{rd}}^{-\rho}$. This saving in the energy is important as, the energy harvested by the relay decreases with the increase in d_{sr}. Another negative effect of the increased d_{sr} on the secrecy performance is that, due to the amplify-and-forward nature of the relay, as the received signal strength at the relay reduces with the increase in d_{sr}, the information signal strength at SD also deteriorates. This reduces the secrecy rate and thus increases the secrecy outage probability.

Fig. 6.10 shows that the constructive effects of the increase in d_{sr} overtake its destructive effects irrespective of the secrecy rate threshold R_{th} under both PS and TS policies and the optimal secrecy outage probability decreases monotonically with the increase in d_{sr}. Thus, the optimum placement of the relay is closer to SD. Note that, in the case of wireless energy harvesting communication via a relay without secrecy constraints, the optimum relay placement is close to the transmitter [59]. But, as shown in Figs. 6.10 and 6.11, to have secure communication, the relay placement close to the transmitter is not preferred.

Fig. 6.11 shows that, for the optimal ergodic secrecy rate, the relay placement has similar effects on the secrecy performance as that on the optimal secrecy outage probability. One interesting observation is that, with the variation in d_{sr}, there exists a crossover point between PS and TS policies, and the location of the crossover point depends on the path-loss exponent. For example, for the path-loss exponent $\rho = 2.7$, TS policy achieves higher optimal ergodic secrecy rate than that of PS policy below $d_{\mathrm{sr}} = 2$m, i.e., the crossover occurs at $d_{\mathrm{sr}} = 2$m; while for $\rho = 4$, TS policy achieves higher optimal ergodic secrecy rate than that of PS policy below $d_{\mathrm{sr}} = 5$m, i.e., the crossover occurs at $d_{\mathrm{sr}} = 5$m. This is because, at a given

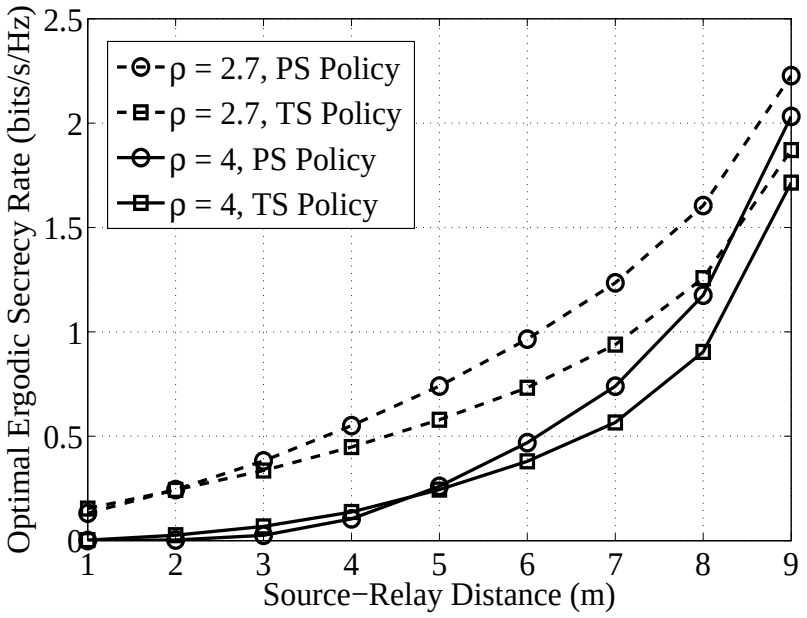

Figure 6.11: Effect of relay placement on the optimal ergodic secrecy rate for PS and TS policies with different path-loss exponents $\rho = 2.7, 4$, $\mathcal{I}_{\mathrm{p}} = -4.7$ dB, $\Theta_{\mathrm{p}} = 0.01$.

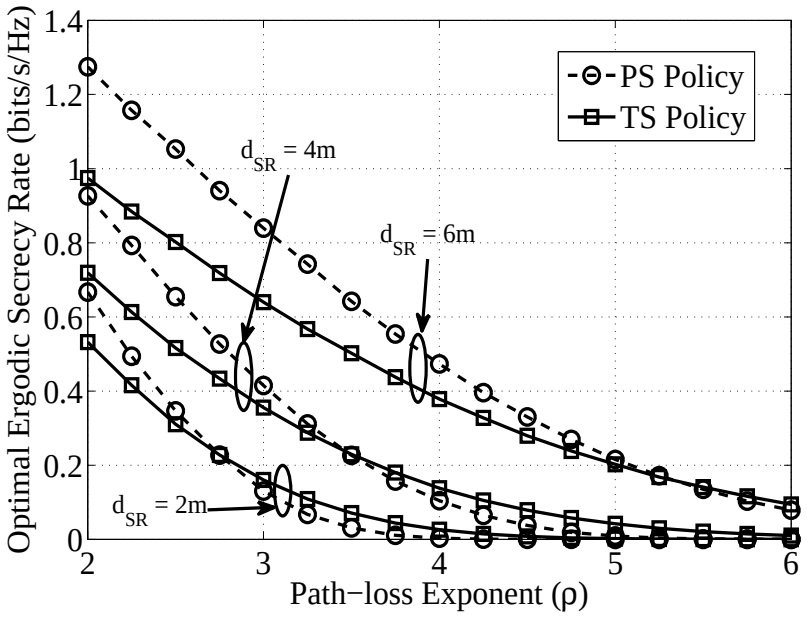

Figure 6.12: Effect of path-loss exponent on the optimal ergodic secrecy rate for PS and TS policies with different ST-SR distances $d_{\mathrm{sr}} = 2\mathrm{m}, 4\mathrm{m}, 6\mathrm{m}$, $\mathcal{I}_{\mathrm{p}} = -4.7$ dB, $\Theta_{\mathrm{p}} = 0.01$.

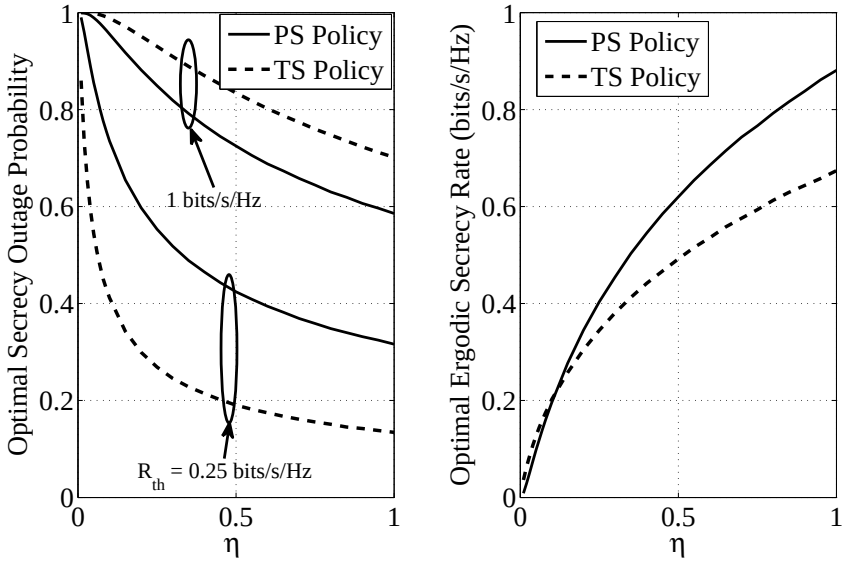

(a) (b)

Figure 6.13: Effect of the energy conversion efficiency factor η (a) on the optimal secrecy outage probability, (b) on the optimal ergodic secrecy rate, $\mathcal{I}_{\mathrm{p}} = -4.7$ dB, $\Theta_{\mathrm{p}} = 0.01$.

path-loss exponent, below the crossover point, the loss in information processing time due to the energy harvesting time in TS policy is lesser than the loss incurred in the relay's transmit power due to power splitting in PS policy. As the distance between SR and SD decreases (with the increase in d_{sr}), the relay may transmit with lower power due to lower path-loss. This subsides the loss incurred in power splitting in PS policy compared to the loss in time for TS policy, and PS policy outperforms TS policy at higher d_{sr}. The increase in path-loss exponent delays the arrival of the crossover point, because, for higher path-loss exponent, the distance between SR and SD should be lower than that in the case of lower path-loss exponent to subside the loss incurred in power splitting. This effect of path-loss exponent on the optimal ergodic secrecy rate can also be seen in Fig. 6.12 for different ST-SR distances. In addition to the effect of the path-loss exponent on the crossover point, Fig. 6.12 shows that the increase in path-loss exponent is detrimental for the secure communication.

6.5.6 Effect of Energy Conversion Efficiency Factor η

The energy conversion efficiency factor η determines what fraction of the received power the relay can actually harvest. Thus, higher η allows relay to harvest more energy, which in turn, boosts relay's transmit power. This results in the enhanced received SNR at SD, reducing the secrecy outage probability and improving the ergodic secrecy rate, as shown in Figs. 6.13(a) and 6.13(b), respectively. At lower η, TS policy achieves better optimal ergodic secrecy rate than that of PS policy and the trend reverses at higher η.

6.6 Chapter Summary

We have investigated the secrecy performance of ST-SD communication via an energy harvesting amplify-and-forward untrusted relay under the primary's interference outage constraint. The energy-starved relay harvests energy from the received radio-frequency signals. In this case, besides keeping the information confidential from the untrusted relay, the destination-assisted jamming signal supplies energy to relay. This energy augments the energy harvested from the received information signal. The PS and TS policies at the relay enable it to harvest energy and process the received information. For this proposed scenario, we have derived analytical expressions for two secrecy metrics, viz., the secrecy outage probability and the ergodic secrecy rate.

The numerical study of the aforementioned secrecy metrics against different system parameters provides useful design insights. For instance, the variation of power splitting ratio in PS policy and energy harvesting time in TS policy affect the secrecy performance in both constructive and destructive ways. Thus, the optimal power splitting ratio and the optimal energy harvesting time exist, that maximize the secrecy performance in terms of both secrecy metrics. The optimal values of secrecy metrics depend on the system parameters. For example, the higher target secrecy rate we set, the more it becomes difficult to achieve, increasing the optimal secrecy outage probability. Also, at higher target secrecy rate, PS policy outperforms TS policy by achieving the lower optimal secrecy outage probability. Though the increase in transmit SNR increases the possibility of relay decoding the confidential information, the resulting higher harvested energy and the jamming power dominate the negative

effect. Thus, the increase in transmit SNR is beneficial to the secure communication. We also observe that, for high transmit SNR, PS policy achieves better ergodic secrecy rate than that of TS policy. The relay location is important in the secure communication. In general, having relay located away from ST is beneficial to keep the information confidential from the relay. This is in contrast with the case of trusted energy harvesting relay, where the relay is preferred to be placed closer to ST. Finally, higher energy conversion efficiency factor increases the harvested energy by the relay, which in turn, improves secrecy performance. In particular, at higher energy conversion efficiency factor, PS policy achieves better optimal ergodic secrecy rate than that of TS policy.

Chapter 7

Direct Link-Assisted Secondary Relays Under Primary Interference

7.1 Introduction

For the underlay mode, till now (Chapters 3-6), we assumed that the direct link between ST and SD is unavailable. In this chapter, we relax this assumption for non-EH scenario and study the outage performance of the secondary network. The relays are often helpful when a transmitter cannot reliably communicate with the destination on its direct link. Even if the direct link is available, the relay can still be useful as it improves the reliability of communication by exploiting the spatial diversity. For example, the destination can select the best link from the direct link and the relaying link, which in turn improves the chances of satisfactory reception of information at the destination [144]. Alternatively, the destination can combine the signals received on the direct link and the relaying link and achieve improved SNR.

7.1.1 Related Work

In [93, 145], authors have derived a closed-form expression of the secondary outage probability with the direct link and primary interference under PU's outage probability constraint. In [144], authors consider a spectrum sharing scenario, where a single AF relay assists sec-

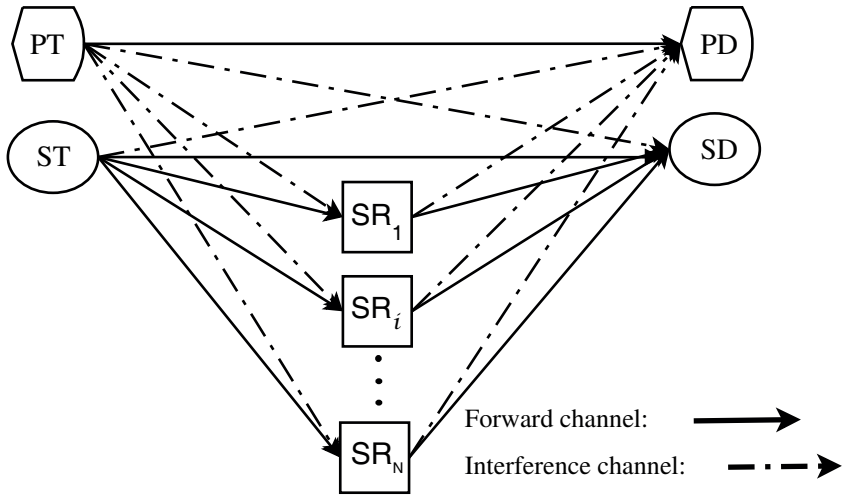

Figure 7.1: Secondary transmissions via AF relays in spectrum sharing.

ondary direct link communication, and the signals at SD are combined by selection combining; but the PU interference is ignored. In [146], authors study the effect of PU's interference on secondary outage probability for AF relays in the absence of direct link, while [102] uses similar setup like [146] for DF relays. Authors in [147, 148] study a secondary system with DF relays under direct link and primary interference with the interference power constraint at PU. The references [21, 149] consider the direct secondary link along with DF relays and calculate the secondary outage probability. But, they ignore the effect of PU's interference on the secondary transmission.

7.2 System Model

Consider a cognitive radio network consisting of a PT, a PD, an ST, an SD, and N AF secondary relays, as shown in Fig. 7.1. The ST communicates with SD via the direct link as well as ith AF relay ($i = 1, 2, \ldots, N$). The relays operate in a half-duplex mode. The communication between ST and SD happens over two time slots, each of T-second duration. In the first time slot, ST transmits the signal with power P_{s} to SD over the direct link, and to secondary relays; while in the second time slot, the best relay amplifies the received signal and forwards it to SD with power $P_{\mathrm{s}i}$. At SD, two received signal copies−first via direct link and second via the best relay−are combined by MRC. We consider the peak power constraint

$P_{\rm pk}$ on transmit powers of ST and ith SR. In addition, the constraint that the primary outage probability should be below a predefined value regulates the transmit powers of ST and ith secondary relay. Denote the powers of ST and ith secondary relay, when they are regulated by the primary outage constraint alone, by $P_{\rm u,ST}$ and $P_{\rm u,SR_i}$, respectively. Then, combining both above constraints, the maximum allowable powers for ST and ith SR become

$$P_{\rm s} = \min\left(P_{\rm pk}, P_{\rm u,ST}\right) \tag{7.1}$$

and

$$P_{{\rm s}i} = \min\left(P_{\rm pk}, P_{\rm u,SR_i}\right), \tag{7.2}$$

respectively. Let $h_{\rm pp}$, $h_{{\rm p}i}$, $h_{\rm pd}$, $h_{{\rm s}i}$, $h_{\rm sd}$, $h_{\rm sp}$, $h_{i{\rm d}}$, and $h_{i{\rm p}}$ denote Rayleigh channel coefficients of links PT-PD, PT-SR$_i$, PT-SD, ST-SR$_i$, ST-SD, ST-PD, SR$_i$-SD, and SR$_i$-PD, respectively. Therefore, the channel power gain $g_{ij} = |h_{ij}|^2$ is exponentially distributed with the mean channel power gain Ω_{ij}. Thus, we can write PDF and CDF of $X = |h_{ij}|^2$ as

$$f_X(x) = \frac{1}{\Omega_{ij}} \exp\left(-\frac{x}{\Omega_{ij}}\right), x \geq 0, \tag{7.3}$$

$$F_X(x) = 1 - \exp\left(-\frac{x}{\Omega_{ij}}\right), x \geq 0, \tag{7.4}$$

respectively. We consider that the channels are independent of each other, experience block-fading, and remain constant for two slots of the secondary communication, i.e., for $2T-$second..

7.3 Maximum Average Allowable Transmit Power for Secondary Transmitter and Relays

We use the primary outage probability to characterize QoS of primary transmissions. The outage probability of the primary user should be below a certain value $\Theta_{\rm p}$, given the interference from the secondary transmitter and relay. For a constant primary transmit power $P_{\rm p}$, we can calculate the primary outage probability as

$$\mathrm{P}_{\mathrm{out_p}} = \mathbb{P}\left(\log_2\left(1 + \frac{P_{\rm p} g_{\rm pp}}{P_{\rm t,ST} g_{\rm sp} + N_0}\right) < \bar{R}_{\rm p}\right) \leq \Theta_{\rm p}, \tag{7.5}$$

where $\bar{R}_{\mathrm{p}}$ is the primary user's desired data rate, N_0 is AWGN power at all receivers, and $P_{\mathrm{t,ST}}$ is the transmit power of ST. The term $\frac{P_{\mathrm{p}} g_{\mathrm{pp}}}{P_{\mathrm{t,ST}} g_{\mathrm{sp}} + N_0}$ represents the received SINR at PD. In (7.5), at the maximum allowed average power $P_{\mathrm{u,ST}}$ for ST, i.e., when $P_{\mathrm{t,ST}} = P_{\mathrm{u,ST}}$, the weak inequality becomes equality. Thus, from (7.5), conditioned on $g_{\mathrm{sp}} = x$, we can write

$$\mathrm{P}_{\mathrm{out_p}}\Big|_{g_{\mathrm{sp}}=x} = \mathbb{P}\bigg(g_{\mathrm{pp}} < \frac{\theta_{\mathrm{p}}(P_{\mathrm{u,ST}} x + N_0)}{P_{\mathrm{p}}}\bigg) = \Theta_{\mathrm{p}}, \tag{7.6}$$

where $\theta_{\mathrm{p}} = 2^{\bar{R}_{\mathrm{p}}} - 1$. Thus, we can write (7.6) as

$$\mathrm{P}_{\mathrm{out_p}}\Big|_{g_{\mathrm{sp}}=x} = 1 - \exp\left(-\frac{\theta_{\mathrm{p}}(P_{\mathrm{u,ST}} x + N_0)}{\Omega_{\mathrm{pp}} P_{\mathrm{p}}}\right). \tag{7.7}$$

Taking expectation with respect to g_{sp}, we obtain

$$\mathrm{P}_{\mathrm{out_p}} = 1 - \frac{\exp\left(-\frac{\theta_{\mathrm{p}} N_0}{\Omega_{\mathrm{pp}} P_{\mathrm{p}}}\right)}{1 + \frac{\theta_{\mathrm{p}} P_{\mathrm{u,ST}} \Omega_{\mathrm{sp}}}{\Omega_{\mathrm{pp}} P_{\mathrm{p}}}}. \tag{7.8}$$

Rearranging the terms and using (7.6), we find the maximum secondary transmit power $P_{\mathrm{u,ST}}$ under alone primary outage constraint as

$$P_{\mathrm{u,ST}} = \frac{P_{\mathrm{p}} \Omega_{\mathrm{pp}}}{\theta_{\mathrm{p}} \Omega_{\mathrm{sp}}} \left[\frac{\exp\left(\frac{\theta_{\mathrm{p}} N_0}{\Omega_{\mathrm{pp}} P_{\mathrm{p}}}\right)}{1 - \Theta_{\mathrm{p}}} - 1\right]^+, \tag{7.9}$$

where $[x]^+ = \max(x, 0)$. After combining with the peak power constraint, the maximum average allowable transmit power P_{s} for the secondary transmitter can be given by (7.1). Similar to (7.9), the transmit power of ith secondary relay regulated alone by the primary outage constraint can be readily found as

$$P_{\mathrm{u,SR}_i} = \frac{P_{\mathrm{p}} \Omega_{\mathrm{pp}}}{\theta_{\mathrm{p}} \Omega_{i\mathrm{p}}} \left[\frac{\exp\left(\frac{\theta_{\mathrm{p}} N_0}{\Omega_{\mathrm{pp}} P_{\mathrm{p}}}\right)}{1 - \Theta_{\mathrm{p}}} - 1\right]^+. \tag{7.10}$$

After combining with the peak power constraint, the maximum average allowable transmit power $P_{\mathrm{s}i}$ for relay i can be given by (7.2).

7.4 Derivation of Secondary Outage Probability

The AF relays cooperate opportunistically, where the relay with the largest end-to-end SINR at the secondary destination is selected to forward the received signal in the second time

slot. Thus, after receiving the signal from both time slots, SD combines them using MRC technique. The end-to-end SINR is given by [150, 151]

$$\begin{aligned}\gamma_{\text{eq}} &= \gamma_{\text{sd}} + \max_{\text{SR}_i \in \mathbb{R}} \left(\frac{\gamma_{\text{s}i}\gamma_{i\text{d}}}{1 + \gamma_{\text{s}i} + \gamma_{i\text{d}}} \right) \\ &\leq \gamma_{\text{sd}} + \max_{\text{SR}_i \in \mathbb{R}} (\min(\gamma_{\text{s}i}, \gamma_{i\text{d}})) = \gamma_{\text{tot}}, \end{aligned} \tag{7.11}$$

where $\mathbb{R}$ is the set of relays given as $\mathbb{R} = \{\text{SR}_1, \ldots, \text{SR}_i, \ldots, \text{SR}_N\}$, $\gamma_{\text{s}i}$, γ_{sd}, and $\gamma_{i\text{d}}$ denote SINR at the ith relay, and SINR at SD due to direct transmission and relaying respectively, which are given by

$$\gamma_{\text{s}i} = \frac{P_{\text{s}} g_{\text{s}i}}{P_{\text{p}} g_{\text{p}i} + N_0}, \tag{7.12}$$

$$\gamma_{\text{sd}} = \frac{P_{\text{s}} g_{\text{sd}}}{P_{\text{p}} g_{\text{pd}} + N_0}, \tag{7.13}$$

$$\gamma_{i\text{d}} = \frac{P_{\text{s}i} g_{i\text{d}}}{P_{\text{p}} g_{\text{pd}} + N_0}. \tag{7.14}$$

For analytical tractability, we use the upper bound given in (7.11), which is tight in medium to high SINR range [150, 151]. We can obtain P_{s} and $P_{\text{s}i}$ from (7.1) and (7.2). The secondary outage occurs when the instantaneous SINR of the secondary transmission falls below the designated threshold, θ_{s}. Thus, we can write the secondary outage probability as

$$\mathcal{P}_o \;=\; \mathbb{P}(\gamma_{\text{sd}} + \max_{\text{SR}_i \in \mathbb{R}} (\min(\gamma_{\text{s}i}, \gamma_{i\text{d}})) < \theta_{\text{s}}), \tag{7.15}$$

where $\theta_{\text{s}} = 2^{2\bar{R}_{\text{s}}} - 1$ with $\bar{R}_{\text{s}}$ is the desired secondary data rate. From (7.11), we can see that, γ_{sd}, $\gamma_{i\text{d}}$, and $\gamma_{\text{R}_j\text{D}}$ $(i \neq j)$ contain a common term g_{pd}, that makes them dependent. Thus, conditioning on $g_{\text{pd}} = y$ and denoting $Z = \max_{\text{SR}_i \in \mathbb{R}} (\min(\gamma_{\text{s}i}, \gamma_{i\text{d}}))$, we can write

$$\mathbb{P}(\gamma_{\text{tot}} < \theta_{\text{s}})\big|_{g_{\text{pd}}=y} = \mathbb{P}\left(\gamma_{\text{sd}} < \theta_{\text{s}} - Z\right) = \int_0^{\theta_{\text{s}}} F_{\gamma_{\text{sd}}}\left(\theta_{\text{s}} - z\right) f_Z(z) \mathrm{d}z. \tag{7.16}$$

Now, we have

$$F_{\gamma_{\text{sd}}}(z)\big|_{g_{\text{pd}}=y} = \mathbb{P}\left(g_{\text{sd}} < \frac{z(P_{\text{p}} y + N_0)}{P_{\text{s}}}\right) = 1 - \exp\left(-\frac{z(P_{\text{p}} y + N_0)}{\Omega_{\text{sd}} P_{\text{s}}}\right). \tag{7.17}$$

We also have

$$F_Z(z)\big|_{g_{\rm pd}=y} = \mathbb{P}\left(\max_{{\rm SR}_i\in\mathbb{R}}\left(\min\left(\gamma_{{\rm s}i},\gamma_{i{\rm d}}\right)\right)<z\right)$$
$$= \prod_{i=1}^{N}\mathbb{P}\left(\min\left(\gamma_{{\rm s}i},\gamma_{i{\rm d}}\right)<z\right) \tag{7.18}$$
$$= \prod_{i=1}^{N}\left[1-\mathbb{P}\left(\gamma_{{\rm s}i}>z\right)\mathbb{P}\left(\gamma_{i{\rm d}}>z\right)\right], \tag{7.19}$$

where (7.18) results from the independence of $\gamma_{{\rm s}i}$ and $\gamma_{i{\rm d}}$, given y. For ease of presentation and without compromising the insight into analysis, we assume that mean channel gains of ST-SR$_i$ are the same for all relays and so is for SR$_i$-SD, PT-SR$_i$, and SR$_i$-PD channels. Thus, we have $P_{{\rm s}i}=P_{\rm r}$. Next, given $g_{\rm pd}=y$, we compute $\mathbb{P}\left(\gamma_{{\rm s}i}>z\right)$ as

$$\mathbb{P}\left(\gamma_{{\rm s}i}>z\right) = \mathbb{P}\left(g_{{\rm s}i}>\frac{z\left(P_{\rm p}g_{{\rm p}i}+N_0\right)}{P_{\rm s}}\right)$$
$$= \int_0^\infty \mathbb{P}\left(g_{{\rm s}i}>\frac{z\left(P_{\rm p}w+N_0\right)}{P_{\rm s}}\right) f_{g_{{\rm p}i}}(w){\rm d}w$$
$$= \int_0^\infty \exp\left(-\frac{z\left(P_{\rm p}w+N_0\right)}{\Omega_{\rm sr}P_{\rm s}}\right)\frac{\exp\left(-\frac{w}{\Omega_{\rm pr}}\right)}{\Omega_{\rm pr}}{\rm d}w$$
$$= \frac{\exp\left(-\frac{zN_0}{\Omega_{\rm sr}P_{\rm s}}\right)}{1+\frac{z\Omega_{\rm pr}P_{\rm p}}{\Omega_{\rm sr}P_{\rm s}}}. \tag{7.20}$$

We also compute $\mathbb{P}\left(\gamma_{i{\rm d}}>z\right)$ as

$$\mathbb{P}\left(\gamma_{i{\rm d}}>z\right) = \mathbb{P}\left(g_{i{\rm d}}>\frac{z\left(P_{\rm p}g_{\rm pd}+N_0\right)}{P_{\rm s}}\right) = \exp\left(-\frac{z\left(P_{\rm p}y+N_0\right)}{\Omega_{\rm rd}P_{\rm r}}\right). \tag{7.21}$$

Thus, by substituting (7.20) and (7.21) in (7.19), we have

$$F_Z(z)\big|_{g_{\rm pd}=y} = \left(1-\frac{\exp\left(-zN_0\left(\frac{1}{\Omega_{\rm sr}P_{\rm s}}+\frac{1}{\Omega_{\rm rd}P_{\rm r}}\right)\right)}{1+\frac{z\Omega_{\rm pr}P_{\rm p}}{\Omega_{\rm sr}P_{\rm s}}}\exp\left(-\frac{zP_{\rm p}y}{\Omega_{\rm rd}P_{\rm r}}\right)\right)^N$$
$$= \left[\sum_{n=0}^{N}\binom{N}{n}(-1)^n\frac{\exp\left(-nzN_0\left(\frac{1}{\Omega_{\rm sr}P_{\rm s}}+\frac{1}{\Omega_{\rm rd}P_{\rm r}}\right)\right)}{\left(1+\frac{z\Omega_{\rm pr}P_{\rm p}}{\Omega_{\rm sr}P_{\rm s}}\right)^n}\exp\left(-\frac{nzP_{\rm p}y}{\Omega_{\rm rd}P_{\rm r}}\right)\right]. \tag{7.22}$$

Hence, PDF of Z is given by

$$f_Z(z)\big|_{g_{\rm pd}=y} = \sum_{n=1}^{N} \binom{N}{n} (-1)^{n+1} n \exp\left(-nzN_0\left(\frac{1}{\Omega_{\rm sr}P_{\rm s}} + \frac{1}{\Omega_{\rm rd}P_{\rm r}}\right)\right) \times \exp\left(-\frac{nzP_{\rm p}y}{\Omega_{\rm rd}P_{\rm r}}\right)\left[\frac{\left(\frac{N_0}{\Omega_{\rm sr}P_{\rm s}} + \frac{N_0}{\Omega_{\rm rd}P_{\rm r}} + \frac{P_{\rm p}y}{\Omega_{\rm rd}P_{\rm r}}\right)}{\left(1+\frac{z\Omega_{\rm pr}P_{\rm p}}{\Omega_{\rm sr}P_{\rm s}}\right)^{n}} + \frac{\frac{\Omega_{\rm pr}P_{\rm p}}{\Omega_{\rm sr}P_{\rm s}}}{\left(1+\frac{z\Omega_{\rm pr}P_{\rm p}}{\Omega_{\rm sr}P_{\rm s}}\right)^{n+1}}\right].$$

From (7.16), we have

$$\begin{aligned}\mathbb{P}(\gamma_{\rm tot} < \theta_{\rm s})\big|_{g_{\rm pd}=y} &= \int_0^{\theta_{\rm s}} \left(1 - \exp\left(-\frac{\theta_{\rm s}\left(P_{\rm p}y + N_0\right)}{\Omega_{\rm sd}P_{\rm s}}\right)\exp\left(\frac{z\left(P_{\rm p}y+N_0\right)}{\Omega_{\rm sd}P_{\rm s}}\right)\right) f_Z(z)\big|_{g_{\rm pd}=y}{\rm d}z \\ &= F_Z(\theta_{\rm s})\big|_{g_{\rm pd}=y} - \exp\left(-\frac{\theta_{\rm s}\left(P_{\rm p}y+N_0\right)}{\Omega_{\rm sd}P_{\rm s}}\right)\sum_{n=1}^{N}\binom{N}{n}(-1)^{n+1}n \\ &\times \int_0^{\theta_{\rm s}} \exp\left(-zN_0\left(\frac{n}{\Omega_{\rm sr}P_{\rm s}} + \frac{n}{\Omega_{\rm rd}P_{\rm r}} - \frac{1}{\Omega_{\rm sd}P_{\rm s}}\right)\right) \\ &\times \frac{\exp\left(-P_{\rm p}yz\left(\frac{n}{\Omega_{\rm rd}P_{\rm r}} - \frac{1}{\Omega_{\rm sd}P_{\rm s}}\right)\right)}{\left(1+\frac{z\Omega_{\rm pr}P_{\rm p}}{\Omega_{\rm sr}P_{\rm s}}\right)^{n}} \\ &\times \left(\frac{N_0}{\Omega_{\rm sr}P_{\rm s}} + \frac{N_0}{\Omega_{\rm rd}P_{\rm r}} + \frac{\frac{\Omega_{\rm pr}P_{\rm p}}{\Omega_{\rm sr}P_{\rm s}}}{\left(1+\frac{z\Omega_{\rm pr}P_{\rm p}}{\Omega_{\rm sr}P_{\rm s}}\right)}\frac{P_{\rm p}y}{\Omega_{\rm rd}P_{\rm r}}\right){\rm d}z. \end{aligned} \tag{7.23}$$

Hence, the outage probability can be expressed as

$$\mathcal{P}_o = E_Y\left[\mathbb{P}(\gamma_{\rm tot} < \theta_{\rm s})\big|_{Y=y}\right] = \mathcal{I}_1 - \mathcal{I}_2 - \mathcal{I}_3, \tag{7.24}$$

where $E_Y[\cdot]$ is the expectation operator on Y and

$$\begin{aligned}\mathcal{I}_1 = \sum_{n=0}^{N}\binom{N}{n}(-1)^n \frac{\exp\left(-n\theta_{\rm s}N_0\left(\frac{1}{\Omega_{\rm sr}P_{\rm s}} + \frac{1}{\Omega_{\rm rd}P_{\rm r}}\right)\right)}{\left(1+\frac{\theta_{\rm s}\Omega_{\rm pr}P_{\rm p}}{\Omega_{\rm sr}P_{\rm s}}\right)^{n}} \\ \times \int_0^{\infty} \exp\left(-\frac{n\theta_{\rm s}P_{\rm p}y}{\Omega_{\rm rd}P_{\rm r}}\right)\frac{\exp\left(-\frac{y}{\Omega_{\rm pd}}\right)}{\Omega_{\rm pd}}{\rm d}y, \end{aligned} \tag{7.25}$$

$$\mathcal{I}_2 = \exp\left(-\frac{\theta_{\rm s}N_0}{\Omega_{\rm sd}P_{\rm s}}\right)\sum_{n=1}^{N}\binom{N}{n}(-1)^{n+1}n$$
$$\times\int_0^{\theta_{\rm s}}\exp\left(-zN_0\left(\frac{n}{\Omega_{\rm sr}P_{\rm s}}+\frac{n}{\Omega_{\rm rd}P_{\rm r}}-\frac{1}{\Omega_{\rm sd}P_{\rm s}}\right)\right)$$
$$\times\frac{\left(\frac{N_0}{\Omega_{\rm sr}P_{\rm s}}+\frac{N_0}{\Omega_{\rm rd}P_{\rm r}}+\frac{\frac{\Omega_{\rm pr}P_{\rm p}}{\Omega_{\rm sr}P_{\rm s}}}{\left(1+\frac{z\Omega_{\rm pr}P_{\rm p}}{\Omega_{\rm sr}P_{\rm s}}\right)}\right)}{\left(1+\frac{z\Omega_{\rm pr}P_{\rm p}}{\Omega_{\rm sr}P_{\rm s}}\right)^n}$$
$$\times\int_{y=0}^{\infty}\exp\left(-P_{\rm p}y\left(\frac{nz}{\Omega_{\rm rd}P_{\rm r}}+\frac{\theta_{\rm s}}{\Omega_{\rm sd}P_{\rm s}}-\frac{z}{\Omega_{\rm sd}P_{\rm s}}\right)\right)\frac{\exp\left(-\frac{y}{\Omega_{\rm pd}}\right)}{\Omega_{\rm pd}}{\rm d}y\,{\rm d}z, \tag{7.26}$$

$$\mathcal{I}_3 = \exp\left(-\frac{\theta_{\rm s}N_0}{\Omega_{\rm sd}P_{\rm s}}\right)\sum_{n=1}^{N}\binom{N}{n}(-1)^{n+1}n$$
$$\times\int_0^{\theta_{\rm s}}\exp\left(-zN_0\left(\frac{n}{\Omega_{\rm sr}P_{\rm s}}+\frac{n}{\Omega_{\rm rd}P_{\rm r}}-\frac{1}{\Omega_{\rm sd}P_{\rm s}}\right)\right)\frac{\frac{P_{\rm p}}{\Omega_{\rm rd}P_{\rm r}}}{\left(1+\frac{z\Omega_{\rm pr}P_{\rm p}}{\Omega_{\rm sr}P_{\rm s}}\right)^n}$$
$$\times\int_0^{\infty}y\exp\left(-P_{\rm p}y\left(\frac{nz}{\Omega_{\rm rd}P_{\rm r}}+\frac{\theta_{\rm s}}{\Omega_{\rm sd}P_{\rm s}}-\frac{z}{\Omega_{\rm sd}P_{\rm s}}\right)\right)\frac{\exp\left(-\frac{y}{\Omega_{\rm pd}}\right)}{\Omega_{\rm pd}}{\rm d}y\,{\rm d}z. \tag{7.27}$$

We use the following results in (7.28) and (7.29) to derive the integrations $\mathcal{I}_i, i = 1, 2, 3$: When Y is an exponential random variable with mean Ω_Y, we have

$$E_Y\left[\exp\left(-RY\right)\right] = \frac{1}{\Omega_Y}\int_0^{\infty}\exp\left(-\left(R+\frac{1}{\Omega_Y}\right)\right){\rm d}y$$
$$= \frac{1}{1+\Omega_Y R}, \tag{7.28}$$

$$E_Y\left[Y\exp\left(-RY\right)\right] = \frac{1}{\Omega_Y}\int_0^{\infty}y\exp\left(-\left(R+\frac{1}{\Omega_Y}\right)\right){\rm d}y$$
$$= \frac{\Omega_Y}{\left(1+\Omega_Y R\right)^2}, \tag{7.29}$$

with $R \geq 0$. Using (7.28), we compute $\mathcal{I}_1$ as

$$\mathcal{I}_1 = \sum_{n=0}^{N}\binom{N}{n}(-1)^n\frac{\exp\left(-n\theta_{\rm s}N_0\left(\frac{1}{\Omega_{\rm sr}P_{\rm s}}+\frac{1}{\Omega_{\rm rd}P_{\rm r}}\right)\right)}{\left(1+\frac{\theta_{\rm s}\Omega_{\rm pr}P_{\rm p}}{\Omega_{\rm sr}P_{\rm s}}\right)^n\left(1+\frac{n\theta_{\rm s}\Omega_{\rm pd}P_{\rm p}}{\Omega_{\rm rd}P_{\rm r}}\right)}. \tag{7.30}$$

To compute $\mathcal{I}_2$, we write it as

$$\mathcal{I}_2 = \exp\left(-\frac{\theta_{\rm s}N_0}{\Omega_{\rm sd}P_{\rm s}}\right)\sum_{n=1}^{N}n\binom{N}{n}(-1)^{n+1}\left(\mathcal{I}_{2,1,n}+\mathcal{I}_{2,2,n}\right), \tag{7.31}$$

where

$$\mathcal{I}_{2,1,n} = \int_0^{\theta_s} \frac{\left(\frac{N_0}{\Omega_{sr}P_s} + \frac{N_0}{\Omega_{rd}P_r}\right)}{\left(1+\frac{z\Omega_{pr}P_p}{\Omega_{sr}P_s}\right)^n} \frac{\exp\left(-zN_0\left(\frac{n}{\Omega_{sr}P_s} + \frac{n}{\Omega_{rd}P_r} - \frac{1}{\Omega_{sd}P_s}\right)\right)\mathrm{d}z}{\left(1+\Omega_{pd}P_p\left(\frac{nz}{\Omega_{rd}P_r} + \frac{\theta_s}{\Omega_{sd}P_s} - \frac{z}{\Omega_{sd}P_s}\right)\right)} \tag{7.32}$$

and

$$\mathcal{I}_{2,2,n} = \int_0^{\theta_s} \frac{\frac{\Omega_{pr}P_p}{\Omega_{sr}P_s}}{\left(1+\frac{z\Omega_{pr}P_p}{\Omega_{sr}P_s}\right)^{n+1}} \frac{\exp\left(-zN_0\left(\frac{n}{\Omega_{sr}P_s} + \frac{n}{\Omega_{rd}P_r} - \frac{1}{\Omega_{sd}P_s}\right)\right)\mathrm{d}z}{\left(1+\Omega_{pd}P_p\left(\frac{nz}{\Omega_{rd}P_r} + \frac{\theta_s}{\Omega_{sd}P_s} - \frac{z}{\Omega_{sd}P_s}\right)\right)}. \tag{7.33}$$

To compute $\mathcal{I}_{2,1,n}$ and $\mathcal{I}_{2,2,n}$, we use the following notations for convenience of presentation:

$$\begin{aligned} S &= N_0\left(\frac{n}{\Omega_{sr}P_s} + \frac{n}{\Omega_{rd}P_r} - \frac{1}{\Omega_{sd}P_s}\right), \\ \mu &= \Omega_{pd}P_p\left(\frac{n}{\Omega_{rd}P_r} - \frac{1}{\Omega_{sd}P_s}\right), \\ \tau &= \frac{\frac{\Omega_{pd}P_p\theta_s}{\Omega_{sd}P_s}+1}{\mu}, \\ \pi_1 &= \left(\frac{\Omega_{sr}P_s}{\Omega_{pr}P_p}\right). \end{aligned} \tag{7.34}$$

Thus, we can write

$$\mathcal{I}_{2,1,n} = \frac{\pi_1^n}{\mu}\left(\frac{N_0}{\Omega_{sr}P_s} + \frac{N_0}{\Omega_{rd}P_r}\right) \underbrace{\int_0^{\theta_s} \frac{\exp(-Sz)}{(z+\pi_1)^n(z+\tau)}\mathrm{d}z}_{\mathcal{J}_{2,1,n}}. \tag{7.35}$$

For $\Omega_{sd} > \Omega_{sr}$ and $\Omega_{sd} > \Omega_{rd}$, we have $S > 0, \mu > 0, \tau > 0$ and we can write (7.35) in terms of the exponential integral as shown later in this section. Using the substitution, $r = z + \pi_1$ and denoting $\chi = \tau - \pi_1$, we write

$$\mathcal{J}_{2,1,n} = \exp(S\pi_1)\int_{\pi_1}^{\pi_1+\theta_s} \frac{\exp(-Sr)}{r^n(r+\chi)}\mathrm{d}r. \tag{7.36}$$

Using the partial fraction expansion, we have

$$\frac{1}{r^n(r+\chi)} = \sum_{m=0}^{n-1}\frac{(-1)^m}{\chi^{m+1}r^{n-m}} + \frac{1}{(-\chi)^n(r+\chi)}, \tag{7.37}$$

Thus, we can write

$$\begin{aligned}\mathcal{J}_{2,1,n} &= \exp(S\pi_1)\int_{\pi_1}^{\pi_1+\theta_\mathrm{s}} \exp(-Sr)\left(\sum_{m=0}^{n-1}\frac{(-1)^m}{\chi^{m+1}r^{n-m}}+\frac{1}{(-\chi)^n(r+\chi)}\right)\mathrm{d}r \\ &= \exp(S\pi_1)\sum_{m=0}^{n-1}\frac{(-1)^m}{\chi^{m+1}}\int_{\pi_1}^{\pi_1+\theta_\mathrm{s}}\frac{\exp(-Sr)}{r^{n-m}}\mathrm{d}r\frac{\exp(S\pi_1)}{(-\chi)^n}\int_{\pi_1+\chi}^{\pi_1+\chi+\theta_\mathrm{s}}\frac{\exp(-S(p-\chi))}{p}\mathrm{d}p.\end{aligned} \tag{7.38}$$

We substitute $p = r + \chi$ in (7.38). Then we get

$$\begin{aligned}\mathcal{J}_{2,1,n} = \exp(S\pi_1)\sum_{m=0}^{n-1}\frac{(-1)^m}{\chi^{m+1}}S^{n-m-1}\int_{S\pi_1}^{S(\pi_1+\theta_\mathrm{s})}\frac{\exp(-z)}{z^{n-m}}\mathrm{d}z \\ +\frac{\exp(S(\pi_1+\chi))}{(-\chi)^n}\int_{S\tau}^{S(\tau+\theta_\mathrm{s})}\frac{\exp(-y)}{y}\mathrm{d}y.\end{aligned} \tag{7.39}$$

In (7.39), we use substitution $z = Sr$ and $y = Sp$ and get

$$\begin{aligned}\mathcal{J}_{2,1,n} &= \exp(S\pi_1)\left(\sum_{m=0}^{n-2}\frac{(-1)^m}{\chi^{m+1}}S^{n-m-1}\left[\Gamma(m-n+1,S\pi_1)-\Gamma(m-n+1,S(\pi_1+\theta_\mathrm{s}))\right]\right) \\ &+\exp(S\pi_1)\frac{(-1)^{n-1}}{\chi^n}\left[\mathrm{E}_1(S\pi_1)-\mathrm{E}_1(S(\pi_1+\theta_\mathrm{s}))\right] \\ &+\exp(S\tau)\frac{(-1)^n}{\chi^n}\left[\mathrm{E}_1(S\tau)-\mathrm{E}_1(S(\tau+\theta_\mathrm{s}))\right],\end{aligned} \tag{7.40}$$

where $\Gamma(.,.)$ and $\mathrm{E}_1(\cdot)$ are upper incomplete gamma function and exponential integral [107], respectively with $\mathrm{E}_1(x) = \int_x^\infty \frac{\exp(-t)}{t}\mathrm{d}t$. Similarly, we compute $\mathcal{I}_{2,2,n}$ by representing it as

$$\mathcal{I}_{2,2,n} = \frac{\pi_1^n}{\mu}\underbrace{\int_0^{\theta_\mathrm{s}}\frac{\exp(-Sz)}{(z+\pi_1)^{n+1}(z+\tau)}\mathrm{d}z}_{\mathcal{J}_{2,2,n}}, \tag{7.41}$$

where $\mathcal{J}_{2,2,n}$ is computed as

$$\begin{aligned}\mathcal{J}_{2,2,n} &= \exp(S\pi_1)\left(\sum_{m=0}^{n-1}\frac{(-1)^m}{\chi^{m+1}}S^{n-m}\left[\Gamma(m-n,S\pi_1)-\Gamma(m-n,S(\pi_1+\theta_\mathrm{s}))\right]\right) \\ &+\exp(S\pi_1)\frac{(-1)^n}{\chi^{n+1}}\left[\mathrm{E}_1(S\pi_1)-\mathrm{E}_1(S(\pi_1+\theta_\mathrm{s}))\right] \\ &+\exp(S\tau)\frac{(-1)^{n+1}}{\chi^{n+1}}\left[\mathrm{E}_1(S\tau)-\mathrm{E}_1(S(\tau+\theta_\mathrm{s}))\right].\end{aligned} \tag{7.42}$$

We note that $\mathcal{J}_{2,2,n} = \mathcal{J}_{2,1,n}$ with n replaced by $n+1$. Thus, we can use the same procedure to compute both these expressions. Using (7.29), we write $\mathcal{I}_3$ as

$$\begin{aligned}\mathcal{I}_3 &= \exp\left(-\frac{\theta_{\rm s}N_0}{\Omega_{\rm sd}P_{\rm s}}\right)\sum_{n=1}^{N}\binom{N}{n}(-1)^{n+1}n \\ &\times \int_0^{\theta_{\rm s}} \exp\left(-zN_0\left(\frac{n}{\Omega_{\rm sr}P_{\rm s}}+\frac{n}{\Omega_{\rm rd}P_{\rm r}}-\frac{1}{\Omega_{\rm sd}P_{\rm s}}\right)\right) \\ &\times \frac{\frac{P_{\rm p}}{\Omega_{\rm rd}P_{\rm r}}}{\left(1+\frac{z\Omega_{\rm pr}P_{\rm p}}{\Omega_{\rm sr}P_{\rm s}}\right)^n}\frac{\Omega_{\rm pd}}{\left(1+\Omega_{\rm pd}P_{\rm p}\left(\frac{nz}{\Omega_{\rm rd}P_{\rm r}}+\frac{\theta_{\rm s}}{\Omega_{\rm sd}P_{\rm s}}-\frac{z}{\Omega_{\rm sd}P_{\rm s}}\right)\right)^2}\,{\rm d}z \\ &= \frac{\Omega_{\rm pd}P_{\rm p}}{\Omega_{\rm rd}P_{\rm r}}\exp\left(-\frac{\theta_{\rm s}N_0}{\Omega_{\rm sd}P_{\rm s}}\right)\sum_{n=1}^{N}\binom{N}{n}(-1)^{n+1}n\frac{\pi_1^n}{\mu^2}\int_0^{\theta_{\rm s}}\underbrace{\frac{\exp(-Sz)}{(z+\pi_1)^n(z+\tau)^2}}_{\mathcal{J}_{3,n}}{\rm d}z, \end{aligned} \tag{7.43}$$

where we use the same notations as for the case of $\mathcal{I}_2$. With the substitution of $t = z+\pi_1$, $\mathcal{J}_{3,n}$ can be written as

$$\mathcal{J}_{3,n} = \exp(S\pi_1)\int_{\pi_1}^{\pi_1+\theta_{\rm s}}\frac{\exp(-St)}{t^n(t+\chi)^2}{\rm d}t \tag{7.44}$$

For computation of $\mathcal{J}_{3,n}$, we use the following partial fraction expansion:

$$\frac{1}{r^n(r+\chi)^2} = \left(\sum_{m=0}^{n-1}\frac{(-1)^m(m+1)}{\chi^{m+2}r^{n-m}}\right)+\frac{1}{(-\chi)^n(r+\chi)^2}-\frac{n}{(-\chi)^{n+1}(r+\chi)}. \tag{7.45}$$

Using the steps similar to that of the derivation of $\mathcal{I}_{2,1,n}$ given in (7.35), we, hereby, can write the expression of $\mathcal{J}_{3,n}$ as

$$\begin{aligned}\mathcal{J}_{3,n} &= \exp(S\pi_1)\Bigg(\sum_{m=0}^{n-2}\frac{(-1)^m(m+1)}{\chi^{m+2}}S^{n-m-1} \\ &\quad\times\left[\Gamma(m-n+1,S\pi_1)-\Gamma(m-n+1,S(\pi_1+\theta_{\rm s}))\right]\Bigg) \\ &\quad+\exp(S\pi_1)\frac{(-1)^{n-1}}{\chi^{n+1}}\left[{\rm E}_1(S\pi_1)-{\rm E}_1(S(\pi_1+\theta_{\rm s}))\right] \\ &\quad+\exp(S\tau)\frac{(-1)^n}{\chi^n}\left[\Gamma(-1,S\tau)-\Gamma(-1,S(\tau+\theta_{\rm s}))\right] \\ &\quad+\exp(S\tau)\frac{(-1)^n n}{\chi^{n+1}}\left[{\rm E}_1(S\tau)-{\rm E}_1(S(\tau+\theta_{\rm s}))\right]. \end{aligned} \tag{7.46}$$

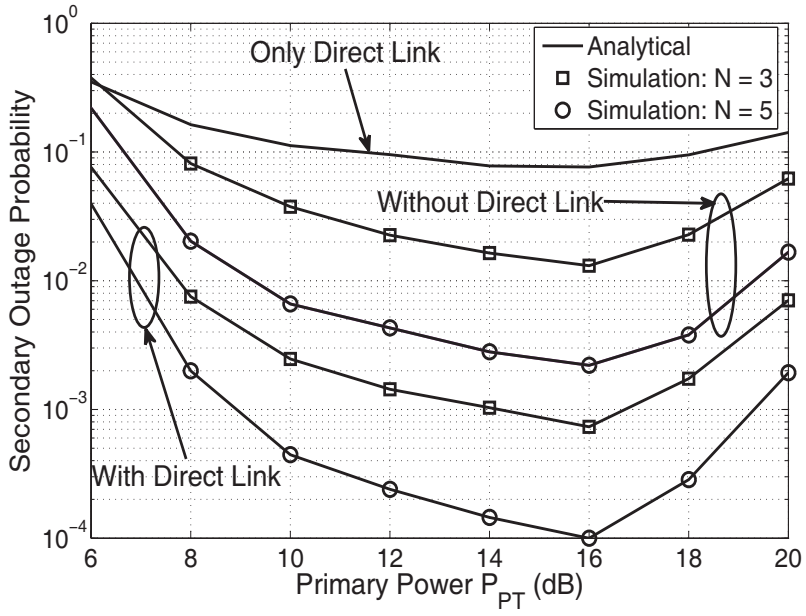

Figure 7.2: Secondary outage probability versus Primary power ($P_{\rm p}$) for different number of relays N, with and without direct link, $P_{\rm pk} = 15$dB, $\Theta_{\rm p} = 10^{-1}$.

7.5 Results and Discussions

Using the analysis performed in previous sections, we investigate the effects of direct link, primary interference, primary outage constraint, and the peak power constraint on the outage performance of the secondary system. We also validate the analysis by simulation results. The simulation parameters are as follow: $\Omega_{\rm sd} = 1.5$, $\Omega_{\rm pp} = \Omega_{\rm sr} = \Omega_{\rm rd} = 1$; $\Omega_{\rm pr} = \Omega_{\rm pd} = \Omega_{\rm sp} = \Omega_{\rm rp} = 0.5$, $N_0 = 1$, $\bar{R}_{\rm p} = 0.4$bits/s/Hz, $\bar{R}_{\rm s} = 0.1$bits/s/Hz.

Fig. 7.2 shows the effect of primary power $P_{\rm p}$ on the secondary outage probability $\mathcal{P}_o$. The increase in $P_{\rm p}$ has two opposite effects on $\mathcal{P}_o$: 1) It improves the quality of the primary link, in turn, increases SINR at the primary destination. This leads to decrease in the primary outage probability, providing an extra margin for transmit powers of secondary transmitter ST ($P_{\rm s}$) and the selected relay SR ($P_{\rm r}$), which further helps reduce the secondary outage probability; 2) it increases the interference to the secondary system, thereby increasing the secondary outage probability. From Fig. 7.2, we can observe that, initially, the secondary outage probability reduces as $P_{\rm p}$ increases. However, if $P_{\rm p}$ is increased beyond a level, the

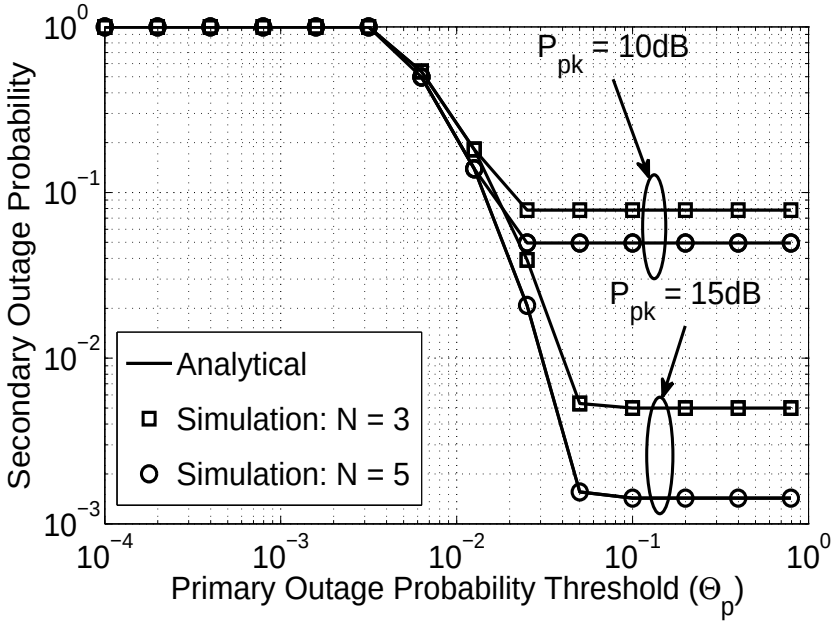

Figure 7.3: Secondary outage probability versus Primary outage probability threshold (Θ_{p}) for different values of peak power constraint P_{pk} and number of relays N, $P_{\mathrm{p}} = 20$dB.

peak power constraint is reached for SU, which does not allow further increase in P_{s} and P_{r}. Thus, with an additional increase in the primary power, SINR at the secondary destination reduces as P_{s} and P_{r} cannot be increased further, degrading SU's outage performance. We can also see from Fig. 7.2 that the presence of direct link effectively helps in improving SU's performance. Also, the increase in the number of relays improves secondary's outage performance due to the increase in the diversity gain.

Fig. 7.3 shows the effect of the primary outage probability threshold Θ_{p} on the secondary outage probability. We can see that increase in Θ_{p} relaxes the constraint on P_{s} and P_{r}. But, if we increase Θ_{p} beyond a level, the peak power constraint is reached, and ST and SR may transmit with the maximum power P_{pk} even though they are allowed, by the primary, to transmit with higher power than P_{pk}. In this case, unlike in Fig. 7.2, the primary power, in turn, the primary interference to SD remains constant. Thus, irrespective of the increase in Θ_{p}, the secondary outage probability remains constant−we call it as floor−once the peak power constraint is reached. We can also notice from Fig. 7.3 that relaxing the peak power

constraint delays the arrival of the floor as expected.

7.6 Chapter Summary

In this chapter, we have derived the closed-form expression of the secondary outage probability when the best relay among multiple AF relays assists the direct link between the secondary transmitter and the secondary destination. Through numerical results, we have shown that the increase in the primary's transmit power can be beneficial to the secondary network as it improves the primary link as well. The peak power constraint restricts the decrease in the secondary outage probability as the primary's outage probability threshold increases.

Part III

Interweave Mode

Chapter 8

Malicious User Suppression in Cooperative Spectrum Sensing

8.1 Introduction

Overlay and underlay modes are based on the possibility of concurrent transmissions by primary and secondary networks. When such simultaneous transmission is not permitted by the primary network, the secondary users have to access the spectrum opportunistically, which involves the detection of spectrum holes.

The performance of a detection scheme is usually measured in terms of two probabilities: the probability of detection and the probability of false alarm. The probability of detection is the probability of correctly detecting the presence of PU in the band; while, the probability of false alarm is the probability of falsely detecting the presence of PU in the band. For a good detection performance, the probability of detection should be as high as possible to avoid the harmful interference to PU and the probability of false alarm should be as low as possible to allow SU to exploit the spectrum usage opportunities efficiently.

Energy detection [152, 153] is a popular spectrum sensing method due to its easy implementation and low complexity. In conventional energy detection, the received signals by an SU are squared, integrated, and then compared with a predetermined threshold to take a decision on the presence or absence of PU. However, energy detection suffers from an inferior detection performance at low SNR. In addition, multi-path fading, shadowing, and hidden

terminal problem make PU detection more challenging [16].

In this chapter, we investigate the performance of the cooperative spectrum sensing (CSS) for the energy detection in the presence of malicious users using Dixon's outlier detection technique.

8.1.1 Related Work

In [23], authors have used Weighted Sequential Probability Ratio Test (WSPRT) to identify malicious users based on reputation rating assigned to every cooperating SU. In [24], authors compute the suspicious level of SUs based on their past sensing reports. Trust values as well as consistency values of cooperating SUs are calculated, which are then used to eliminate the influence of malicious users on the primary user detection. Outlier based malicious user detection is proposed in [25] where malicious users are detected by applying an outlier detection method and corresponding sensing reports are ignored while making a final decision on the availability of a spectrum band. In [154], authors have compared several outliers detection methods for low SNR scenario.

8.2 System Model

We have N SUs cooperating among each other to detect the presence of a single PU. Secondary users employ energy detection [152] to detect the presence or absence of PU locally. Then they send their energy values through an error-free control channels to the fusion center. Let H_0 and H_1 be the hypotheses representing absence and presence of PU, respectively. We denote energy received by nth SU in decibels during kth sensing iteration by $e_n[k]$. Under hypothesis H_0, this is given by

$$e_n[k] = 10\log_{10}\left(\int_{T_k}^{T_k+T-1} |v_n(t)|^2\,\mathrm{d}t\right). \tag{8.1}$$

Similarly, under hypothesis H_1,

$$e_n[k] = 10\log_{10}\left(\int_{T_k}^{T_k+T-1} |x(t)+v_n(t)|^2\,\mathrm{d}t\right), \tag{8.2}$$

where T denotes the length of sensing interval and T_k represents the time when kth time interval begins. $x(t)$ is primary signal and $v_n(t)$ is AWGN received by nth SU.

8.3 Attack Models for SSDF

Here, we consider three types of malicious user data falsification attacks, namely always YES attack, always NO attack and malicious user randomly sending true or false values of received energy to the fusion center. In always YES case, every time malicious user reports comparatively higher received energy than the other honest cooperating SUs to the fusion center. The intention of this kind of malicious user is to fool other SUs to believe that the spectrum is occupied. This type of malicious user is known as selfish user and this attack is known as selfish SSDF [155]. This attack results in increase in false alarm probability. In always NO case, the malicious user always reports very low received energy suggesting absence of primary user so that SUs start using corresponding channel. The intention of this kind of attack is to cause interference to the primary user and it is known as interference SSDF [155]. In the third type of attack which is known as confusing SSDF [155], malicious user sends randomly true or false value of received energy to fusion center with the purpose to confuse other SUs.

8.4 Dixon's Test

Outlier factor is a measure of deviation of a data point from the rest of the data. In outlier detection techniques, outlier factors are used to detect presence of malicious users in CSS system. Each SU in CSS is assigned a set of outlier factors based on its local energy detection based spectrum sensing. In this test for outliers, the data values are arranged in ascending order and outlier factor $o_n[k]$ for nth user for kth sensing iteration is calculated as follows [27]:

$$o_n[k] = \begin{cases} \dfrac{e_{sN}[k] - e_{s(N-1)}[k]}{e_{sN}[k] - e_{s1}[k]}, & 3 \leq N \leq 7 \\ \dfrac{e_{sN}[k] - e_{s(N-1)}[k]}{e_{sN}[k] - e_{s2}[k]}, & 8 \leq N \leq 10 \\ \dfrac{e_{sN}[k] - e_{s(N-2)}[k]}{e_{sN}[k] - e_{s2}[k]}, & 11 \leq N \leq 13 \\ \dfrac{e_{sN}[k] - e_{s(N-2)}[k]}{e_{sN}[k] - e_{s3}[k]}, & 14 \leq N \leq 20 \end{cases}, \tag{8.3}$$

$$o_n[k] = \begin{cases} \dfrac{e_{s2}[k] - e_{s1}[k]}{e_{sN}[k] - e_{s1}[k]}, & 3 \leq N \leq 7 \\ \dfrac{e_{s2}[k] - e_{s1}[k]}{e_{s(N-1)}[k] - e_{s1}[k]}, & 8 \leq N \leq 10 \\ \dfrac{e_{s3}[k] - e_{s1}[k]}{e_{s(N-1)}[k] - e_{s1}[k]}, & 11 \leq N \leq 13 \\ \dfrac{e_{s3}[k] - e_{s1}[k]}{e_{s(N-2)}[k] - e_{s1}[k]}, & 14 \leq N \leq 20 \end{cases}, \tag{8.4}$$

where N is the number of cooperating SUs, while $e_{sN}[k]$, $e_{s(N-1)}[k]$, $e_{s(N-2)}[k]$, $e_{s1}[k]$, $e_{s2}[k]$, and $e_{s3}[k]$ are the highest, the second highest, the third highest, the lowest, the second lowest, and the third lowest energy values received at FC, respectively.

The value of $o_n[k]$ is compared with a critical value Q. Critical values can be obtained from standard table [156] available for Dixon's test. If calculated $o_n[k]$ is less than the critical value for the given significance level, then the energy value under evaluation is assumed to belong the same normal population as the rest of values. It is also known as null hypothesis. On the other hand, if $o_n[k]$ is greater than that of the critical value, it is considered that the energy value under evaluation comes from an outlier. This is called as an alternate hypothesis. Equation (8.3) is used when there is a presence of suspicious high value of received energy, while equation (8.4) is used if there is an outlier representing very low energy value. Whether an outlier (if it exists) is of low energy or high energy value can be found out from (8.3) and

(8.4). Initially, the outlier factor $o_n[k]$ is calculated using (8.3), and if it exceeds critical value Q, then it favors the presence of outlier reporting high energy. Similar is the case for the detection of low energy outlier.

8.5 Results and Discussions

For the purpose of simulation, we have taken $N = 20$ cooperating SUs. Also, the primary signal is assumed to be binary phase shift keying (BPSK) modulated. At fusion center, the energy values received from all the sensors are combined by averaging and it is then compared with the threshold as follows:

$$\frac{1}{N}\sum_{n=1}^{N} e_n[k] \lessgtr_{H_0}^{H_1} e_T, \tag{8.5}$$

where e_T is the threshold used at fusion center. The threshold is calculated by fixing the probability of false alarm to a predefined value. We assume that the malicious user providing always NO decision reports energy corresponding to SNR that is 20 dB lower than the average received SNR for normal user. Similarly, the malicious user with always YES decision reports energy corresponding to SNR that is 20 dB higher than the average received SNR. For random YES-NO case, it is assumed that the SNR is either 20 dB higher or lower than the average received SNR for normal user. The significance level taken is 0.10. For simulation, we fixed the average received SNR for normal user to be 0 dB.

We have compared Dixon's test with test based on Grubb's test and boxplot method. We have simulated two methods based on Grubb's test which were presented in [25]. For sake of completeness, we state the equations governing the calculation of outlier factors for those two methods based on Grubb's test. Grubb's Test assigns outliers $o_n[k]$ for nth SU in kth iteration based on received energy values in decibels $e_n[k]$ as follows [25]:

$$o_n[k] = \frac{e_n[k] - \mu_n[k]}{\sigma_n[k]}, \tag{8.6}$$

where $\mu_n[k]$ denotes the sample mean of $e_n[k]$ and $\sigma_n[k]$ is the sample standard deviation of $e_n[k]$.

As addressed in [25], the mean and the standard deviation represent the estimation of location and scale, respectively, that are susceptible to malicious user attacks. A robust

estimate of location is the bi-weight scale (BWS), which can be used to replace mean to calculate the outlier factor [157]. It is given by:

$$\mu^*[k] = \frac{\sum w_n[k] e_n[k]}{\sum w_n[k]}, \tag{8.7}$$

where

$$w_n[k] = \begin{cases} \left\{ \left(1 - \left(\dfrac{e_n[k] - \mu^*[k]}{c_1 S} \right)^2 \right) \right\}, & \left(1 - \left(\dfrac{e_n[k] - \mu^*[k]}{c_1 S} \right)^2 \right) < 1 \\ 0, & \text{Otherwise} \end{cases} \tag{8.8}$$

and

$$S = \text{median} \left\{ |e_n[k] - \mu^*[k]| \right\}. \tag{8.9}$$

At first, all data points are allocated equal weights and then the bi-weight estimate is calculated recursively using (8.8) in (8.7) and then using (8.7) in (8.9). S is the median absolute deviation from the location estimate $\mu^*[k]$. The parameter c_1 is the tuning constant and has a value of 6 [158]. Observations at a distance of more than $c_1 S$ have been allocated zero weight.

A robust alternative to standard deviation can be given by BWS as follows:

$$\sigma^*[k] = \sqrt{\frac{N \sum_{u_n^2 < 1} \left(e_n[k] - \mu^*[k] \right)^2 (1 - u_n^2)^4,}{s(s-1)}} \tag{8.10}$$

where

$$s = \sum_{u_n^2 < 1} (1 - u_n^2)(1 - 5u_n^2) \tag{8.11}$$

and

$$u_n = \frac{e_n[k] - \mu^*[k]}{c_2 \text{median} \left\{ |e_n[k] - \mu^*[k]| \right\}}. \tag{8.12}$$

Here, c_2 is the tuning constant which is taken as 9 [158].

8.5.1 Grubb's Method 1

In this method, outlier factors are calculated using (8.6) with bi-weight as the location estimate and BWS as the scale estimate. These outlier factors are then compared with a threshold [25] for each iteration. If outlier factor lies above threshold, then the user is considered as malicious user.

8.5.2 Grubb's Method 2

In this method, Grubb's test was modified to assign penalty factors. Here we give basic background of the method. Detailed analysis can be obtained from [25]. Penalty factors are calculated as follows [25]:

$$P_n[k] = \sum_{k' \in S_+[k]} \left(o_n^+[k'-1] + o_n^-[k'] \right) + \sum_{k' \in S_-[k]} \left(o_n^-[k'-1] + o_n^+[k'] \right), \tag{8.13}$$

where

$$o_n^-[k'] = \begin{cases} \dfrac{-(e_n[k'] - \mu_a^*[k'])}{\sigma_a^*[k']}, & e_n[k'] < \mu_a^*[k'] \\ \\ 0, & \text{Otherwise} \end{cases} \tag{8.14}$$

$$o_n^+[k'] = \begin{cases} \dfrac{e_n[k'] - \mu_a^*[k']}{\sigma_a^*[k']}, & e_n[k'] > \mu_a^*[k'] \\ \\ 0, & \text{Otherwise,} \end{cases} \tag{8.15}$$

where $\mu_a^*[k']$ and $\sigma_a^*[k']$ are adjusted bi-weight estimates of mean and standard deviation calculated from (8.7) and (8.10), respectively. $S_+[k]$ and $S_-[k]$ are sets of iterations such that $\Delta\mu_a^*[k'] = \mu_a^*[k] - \mu_a^*[k-1]$ is positive and negative in those corresponding iterations, respectively.

New outlier factors are defined based on above penalty factors as follows:

$$\bar{o}_n[k] = \frac{P_n[k] - \mu_P^*[k]}{\sigma_P^*[k]} \tag{8.16}$$

where $\mu_P^*[k]$ is the bi-weight location for $P_n[k]$ and $\sigma_P^*[k]$ is the Bi-weight scale estimates for $P_n[k]$.

8.5.3 Boxplot Method

In boxplot method, data are arranged in ascending order. In our case, data are energy values in decibels. Then, lower and upper threshold are calculated as follows:

$$Q_{lower} = Q_1 - 1.5Q_{intqrt} \tag{8.17}$$

and

$$Q_{upper} = Q_3 + 1.5Q_{intqrt}, \tag{8.18}$$

where Q_{lower} and Q_{upper} represent lower and upper threshold respectively. Q_1 is the first quartile, Q_3 is the third quartile, and Q_{intqrt} is $Q_3 - Q_1$, i.e., interquartile range. We have taken multiplier as 1.5 [159].

8.5.4 Comparison of tests

Fig. 8.1 shows receiver operating characteristic (ROC) curve for always YES malicious user attack when reported energy of always YES malicious user is 20 dB higher than that of normal user. We can see that Dixon's test performs better than that of Grubb's modified tests and boxplot test. When the probability of false alarm fixed to 0.02, the values of probability of detection for Dixon's test, Grubb's Method 1, Grubb's method 2, and boxplot method are 0.9172, 0.8758, 0.9086, and 0.815, respectively. Between two methods of Grubb's test, the second method gives better performance than that of the first method because of more robust calculation by assigning penalty factors [25]. The worst performance of boxplot test can be explained as follows. Boxplot test detects multiple malicious users. In our case it detects 3-4 malicious users out of 20 users even though in simulation setup we assumed the presence of only one malicious user. This removes 3-4 normal users from cooperation which degrades the performance of cooperative spectrum sensing.

Fig. 8.2 shows ROC curve performance for the case of always NO attack, when always NO malicious user reports energy lower than 20 dB than that of normal user. It shows similar trend in the performance curve as in the always YES attack. Dixon's test again outperforms Grubb's tests and boxplot test.

Fig. 8.3 shows ROC curve performance for the case of confusing SSDF attacks. In this case, we have assumed that the malicious user randomly switches its reported energy between 20dB lower and 20 dB higher than that of the normal users. For this case also, Dixon's test gives better performance than Grubb's tests and boxplot test.

8.5.5 Limitations of Dixon's Test

Fig. 8.4 shows the performance of Dixon's test when there are two malicious users present and compares it with the case when there is only one malicious user. We have considered the case of always YES malicious users. Since Dixon's test is applicable for detecting single

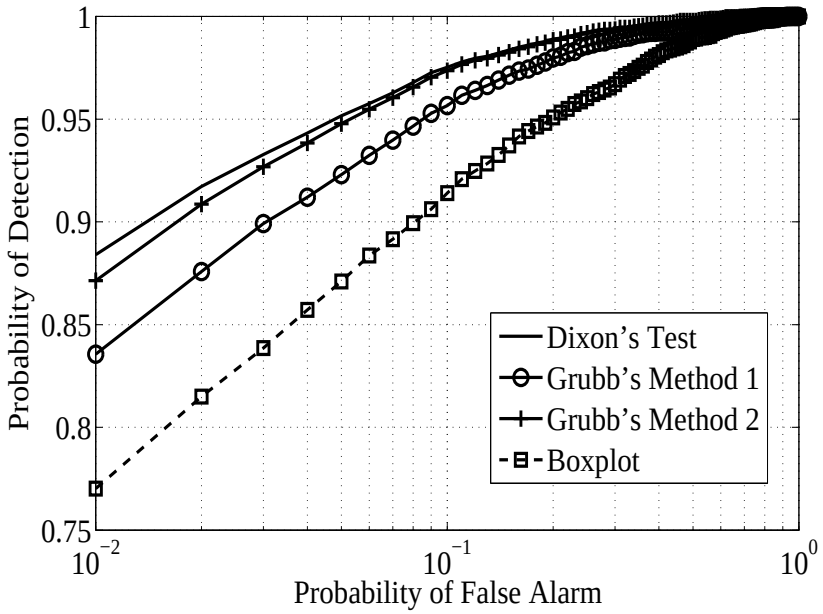

Figure 8.1: Probability of false alarm versus probability of detection for average normal SNR = 0 dB for always YES malicious user

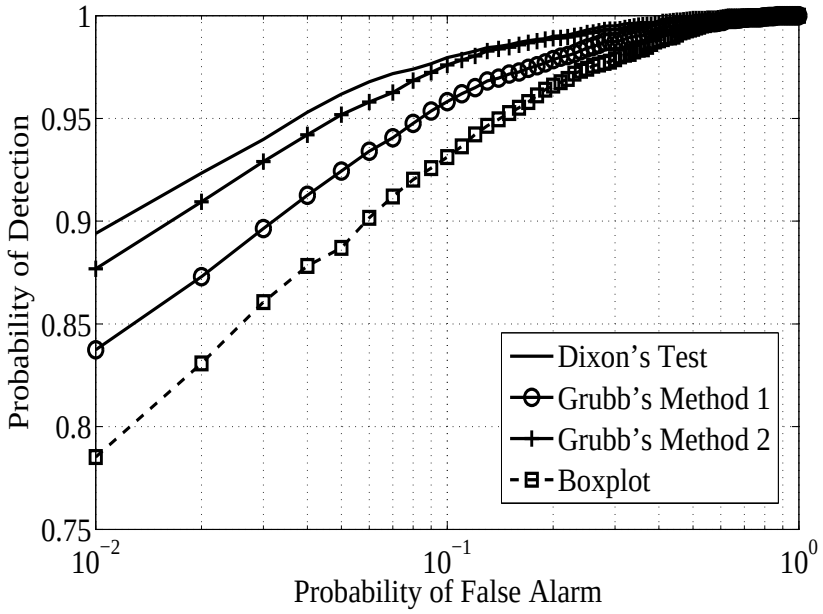

Figure 8.2: Probability of false alarm versus probability of detection for average normal SNR = 0 dB for always NO malicious user

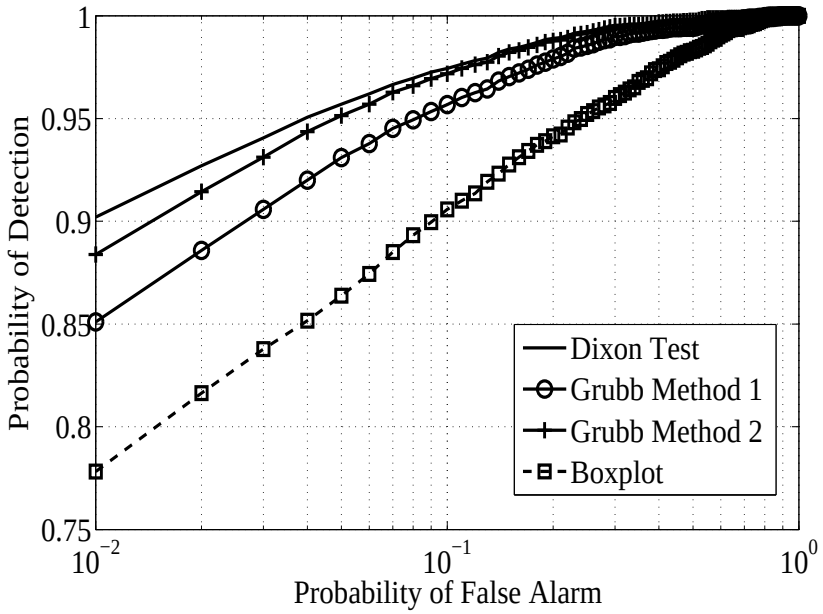

Figure 8.3: Probability of false alarm versus probability of detection for average normal SNR = 0 dB for malicious user with random reporting

malicious user, we can see that Dixon's test for detecting single malicious user performs better than detecting two malicious users. We also notice from the simulations that for the case of presence of one malicious user when we do not apply any malicious user detection technique, it is performing even better than the perfect removal of single malicious user case. This is because in this case, we have considered always YES attack where malicious user's energy is higher than normal user.

Dixon's test cannot be repetitively applied for detection of more than one malicious users. We explain this with the help of an example. If we consider the case of three malicious users all employing always YES attack, i.e., they are all reporting high primary user energy. Let us assume that these three energy values reported by malicious users are almost equal. Then we can see from (8.3) for the case where N lies between 14 and 20, numerator becomes very small and $o_n[k]$ will be smaller than critical value. So even though there are three malicious users present representing always high value of primary user energy, it will not be detected by Dixon's test.

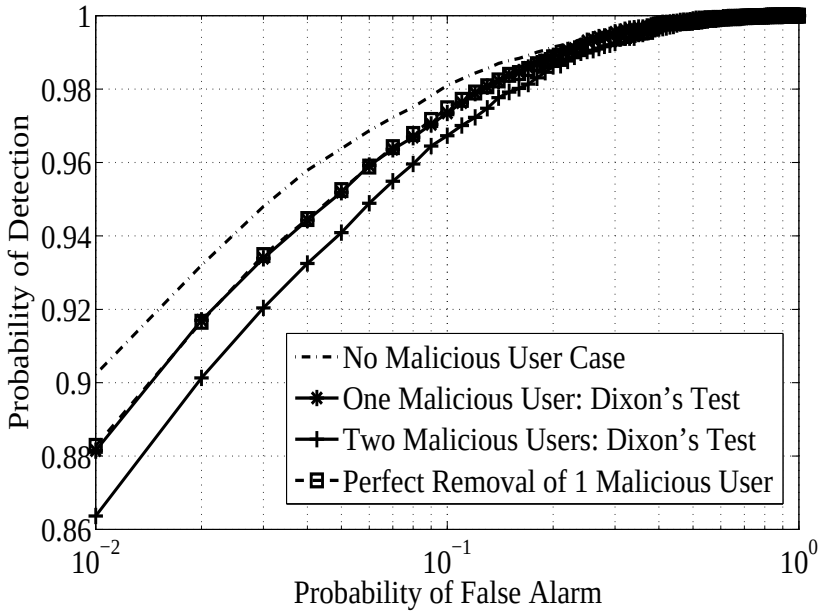

Figure 8.4: Probability of false alarm versus probability of detection for average normal SNR = 0 dB for no, one and two malicious users for Dixon's test

8.6 Chapter Summary

In this chapter, we investigated the use of Dixon's test based outlier detection technique in cooperative spectrum sensing to detect single malicious user. Monte-Carlo simulations are performed to compare Dixon's test with Grubb's based test and boxplot test. It is observed that Dixon's test performs better than Grubb's test and boxplot test. We also showed the limitation of Dixon's test for the case of multiple malicious users.

Chapter 9

Impact of Antenna Correlation on Improved Energy Detector

9.1 Introduction

As we observed in the previous chapter, the CSS improves the spectrum sensing performance, but may suffer from the malicious users' attack. An alternative to CSS is multiple antenna spectrum sensing which still exploits spatial diversity (called micro-diversity), and is the focus of this chapter. If separated by sufficient spacing, each multiple antenna can act as an individual terminal and can provide diversity gain. But the large distances between the primary transmitter and receiving antennas can lead to small received channel angular spread value, which makes receiving antennas correlated. This results in the degraded spectrum sensing performance [20].

In practice, three criteria are used to evaluate the detection performance, which are as follows: (i) Maximization of the probability of detection keeping the probability of false alarm constant, (ii) minimization of the probability of false alarm keeping the probability of detection constant, and (iii) minimization of the total error rate, that is, the sum of the probability of miss detection (1 − probability of detection) and the probability of false alarm. Minimizing the total error rate makes the detection scheme robust to sensing errors.

To further improve the detection performance of an energy detector, the author in [160]

replaced the squaring operation of the conventional energy detector (CED) by an arbitrary positive power operation p, and then found the optimum value of p. This new energy detector is called *improved energy detector* (IED). We can see that the improved energy detector with $p = 2$ is the conventional energy detector. In this chapter, we integrate IED with multiple correlated antennas and investigate the effect of exponential antenna correlation on the optimum value of p.

9.1.1 Related Work

The works in [160, 161, 162, 163, 164, 165] showed that IED can achieve a better detection performance than CED, i.e., the optimum power operation p may be different from the squaring operation. In [166, 167], authors observed that the value of $p \neq 2$ may provide more robustness against noise uncertainty in energy detection. For IED, in [160, 161, 162, 163, 166, 167], a single antenna was considered for spectrum sensing; whereas [17, 19, 168, 169, 170] use multiple antennas to improve the system performance of CED. In [171], authors have used uncorrelated multiple antennas for IED and an optimum power operation p is found.

9.2 System Model

A binary hypothesis problem models the detection of PU as follows:

$$y_j = \begin{cases} s_j + n_j, & H_1, \\ n_j, & H_0, \end{cases} \tag{9.1}$$

where y_j is jth received sample by an antenna of an SU, s_j is jth sample of the block faded primary signal with $j = 1, 2, \ldots, N$, n_j is i.i.d. AWGN with zero mean and variance σ_n^2, H_1 and H_0 represent the hypotheses corresponding to the presence and absence of PU, respectively. s_j follows Gaussian distribution with zero mean and variance σ_s^2. We assume that the primary signal samples s_j are independent. The primary signal samples and noise samples are considered independent of each other.

Let M be the number of receive antennas at SU. We use the improved energy detection [160] for spectrum sensing. We can write the test statistic W for the improved energy

detection as

$$W = \sum_{j=1}^{N} \sum_{i=1}^{M} \left(\left| \frac{y_{ij}}{\sigma_n} \right| \right)^p, \tag{9.2}$$

where y_{ij} is jth received sample by the ith antenna, $p > 0$ is an arbitrary constant. Using central limit theorem, for large N ($N > 10$), we may approximate W by Gaussian distribution [172]. We consider the exponential antenna correlation model:

9.2.1 Exponential Correlation Model

When antennas are equispaced in a linear fashion, the correlation among neighbouring antennas is higher than that of the distant antennas. In this case, the exponential antenna correlation model is more appropriate to describe the spatial correlation [20, 173, 174]. The exponential correlation model can be given in terms of antenna correlation matrix $\mathbf{R}^{\text{exp}}_{M\times M}$ with its components R^{exp}_{mn} as

$$R^{\text{exp}}_{mn} = \begin{cases} \rho^{n-m}, & m \leq n, \\ R^{\text{exp}}_{nm}, & m > n, \end{cases} \quad m, n = 1, \ldots, M. \tag{9.3}$$

9.3 Effect of Antenna Correlation on Detection Performance

Let

$$W_j = \sum_{i=1}^{M} \left(\left| \frac{y_{ij}}{\sigma_n} \right| \right)^p = \sum_{i=1}^{M} |Z_i|^p \tag{9.4}$$

for $j = 1, \ldots, N$, where $\dfrac{y_{ij}}{\sigma_n} = Z_i$. Here, the spatial correlation among antennas reflects in received samples y_{ij} on each antennas, which makes the test statistic W in (9.2) correlated. In the following subsections, we find the mean and variance of W under both hypotheses H_0 and H_1, and then derive the expressions for the probability of detection P_D and the probability of false alarm P_F.

9.3.1 Mean and Variance of W_j:

Let us define

$$G_p = \frac{2^{p/2}}{\sqrt{\pi}} \Gamma\left(\frac{p+1}{2} \right),$$

where $\Gamma(\cdot)$ is the Gamma function. The mean of W_j can be given using [107, 3.462.9] as $\mu_{W_j} = \mathbb{E}[W_j] = M\mathbb{E}\left[\left|\frac{y_{ij}}{\sigma_n}\right|^p\right] = Mr^pG_p$ with

$$r = \frac{\sigma_y}{\sigma_n} = \begin{cases} 1, & H_0, \\ \sqrt{\gamma+1}, & H_1, \end{cases} \tag{9.5}$$

where σ_y^2 is variance of the received signal y_{ij}, γ is average received signal-to-noise ratio (SNR) given by $\gamma = \frac{\sigma_s^2}{\sigma_n^2}$ and $\mathbb{E}[\cdot]$ is the expectation operator. Also, the variance of W_j can be given using [107, 3.462.9] as

$$\begin{aligned} \sigma_{W_j}^2 &= \mathbb{E}[W_j^2] - (\mathbb{E}[W_j])^2 \\ &= \mathbb{E}\left[\left(\sum_{i=1}^{M}|Z_i|^p\right)^2\right] - (Mr^pG_p)^2 \\ &= \mathbb{E}\left[\sum_{i=1}^{M}|Z_i|^{2p} + \sum_{m,n,m\neq n}|Z_m|^p|Z_n|^p\right] - (Mr^pG_p)^2 \\ &= r^{2p}(MG_{2p} - M^2G_p^2) + \sum_{m,n,m\neq n}\mathbb{E}\left[|Z_m|^p|Z_n|^p\right]. \end{aligned} \tag{9.6}$$

For exponential correlation model, we define c, related to the correlation between Z_m and Z_n, that is, the correlation between samples at mth and nth antenna, by (E.3) as derived in the Appendix,

$$c = \frac{\mathbb{E}[Z_mZ_n]}{1+\gamma} = \frac{\gamma\rho^{|m-n|}}{1+\gamma}. \tag{9.7}$$

9.3.2 Mean and Variance of W:

We assume that at a given time, the received signal samples at different antennas may be correlated. Also, we consider the samples at an antenna are independent. Therefore, we can write mean μ_W and variance σ_W^2 of W as $\mu_W = \mathbb{E}[W] = N\mathbb{E}[W_j]$ and $\sigma_W^2 = N\sigma_{W_j}^2$, respectively.

Under H_0

As the correlation coefficient ρ is zero, $\mathbf{R}$ becomes the identity matrix. So, Z_m and Z_n are independent. Also, from (9.5), $r = 1$. Then $\mathbb{E}[|Z_m|^p|Z_n|^p] = \mathbb{E}[|Z_m|^p]\mathbb{E}[|Z_n|^p] = G_p^2$ and the

variance of W_j becomes

$$\begin{aligned}\sigma^2_{W_j} &= MG_{2p} - M^2G_p^2 + M(M-1)G_p^2 \\ &= M(G_{2p} - G_p^2). \end{aligned} \tag{9.8}$$

Therefore, we can write mean μ_0 and variance σ_0^2 of W under the hypothesis H_0 as $\mu_0 = MNG_p$ and $\sigma_0^2 = MN(G_{2p} - G_p^2)$, respectively.

Under H_1

The mean μ_1 is given by

$$\mu_1 = N\mathbb{E}[W_j|H_1] = MNr^pG_p, \tag{9.9}$$

where r is $\sqrt{\gamma+1}$. The variance σ_1^2 of W is

$$\sigma_1^2 = N\left(r^{2p}(MG_{2p} - M^2G_p^2) + \sum_{m,n,m\neq n} \mathbb{E}\left[|Z_m|^p|Z_n|^p\right]\right), \tag{9.10}$$

where $\mathbb{E}\left[|Z_m|^p|Z_n|^p\right]$ is given by

$$\begin{aligned}\mathbb{E}\left[|Z_m|^p|Z_n|^p\right] = \frac{r^{2p}}{\pi}&\Gamma(p+1)(1-c^2)^{p+(1/2)}\mathcal{B}\left(\frac{1}{2}, p+1\right) \\ &\times\left[F_1\left(\left(p+1, p+1, \frac{1}{2}, p+\frac{3}{2}; c, -1\right)\right)\right. \\ &\left.+ F_1\left(\left(p+1, p+1, \frac{1}{2}, p+\frac{3}{2}; -c, -1\right)\right)\right], \end{aligned} \tag{9.11}$$

where $\mathcal{B}(\cdot,\cdot)$ is the beta function (please see [107, 8.380]) and F_1 is the hypergeometric function of two variables (please see [107, 9.180]). The derivation of (9.11) is relegated to the Appendix E.1.

Similar to H_0 case, for no correlation under H_1, Z_m and Z_n become independent. Then, the variance $\sigma^2_{1_{nc}}$ of W under H_1 can be given by a closed-form expression as

$$\sigma^2_{1_{nc}} = MN(1+\gamma)^p(G_{2p} - G_p^2). \tag{9.12}$$

The probability of detection P_D and the probability of false alarm P_F are given by $\mathbb{P}(H_1|H_1)$ and $\mathbb{P}(H_1|H_0)$, respectively. The probability of miss detection P_m is $1 - P_D$ and

the total error rate P_t is given by $P_m + P_F$. From the test statistic given in (9.2) and using its Gaussian approximation, we can write the probability of detection as

$$P_D = \int_T^\infty \mathcal{N}(\mu_1, \sigma_1)\mathrm{d}x = Q\left(\frac{T-\mu_1}{\sigma_1}\right), \tag{9.13}$$

where T is the threshold, $\mathcal{N}(m, \sigma)$ represents Gaussian distribution with mean m and variance σ^2, $Q(\cdot)$ is given as $Q(t) = \frac{1}{\sqrt{2\pi}} \int_t^\infty \exp(-x^2/2)\mathrm{d}x$. μ_1 and σ_1 are given by (9.9) and (9.10), respectively. Similarly, we can write the probability of false alarm as

$$P_F = \int_T^\infty \mathcal{N}(\mu_0, \sigma_0)\mathrm{d}x = Q\left(\frac{T-\mu_0}{\sigma_0}\right), \tag{9.14}$$

where μ_0 and σ_0^2 denote mean and variance of W under H_0, respectively.

9.3.3 Joint Computation of Optimum p and Optimum Threshold

As shown in [160], the improved energy detector enhances the detection performance, by suitably choosing the power operation p. We will show in Sect. 9.4 that the optimum power operation p_{opt} may change with the correlation among multiple antennas. From (9.13) and (9.14), the expressions relating P_D and P_F independent of threshold T can be written as

$$P_D = Q\left(\frac{\sigma_0 Q^{-1}(P_F) + \mu_0 - \mu_1}{\sigma_1}\right), \tag{9.15}$$

$$P_F = Q\left(\frac{\sigma_1 Q^{-1}(P_D) + \mu_1 - \mu_0}{\sigma_0}\right). \tag{9.16}$$

We consider p_{opt} for three cases as follows: 1) p_{opt} that maximizes P_D for a fixed P_F. Numerical simulations are used to find p_{opt} using (9.15). 2) p_{opt} that minimizes P_F for a fixed P_D. Numerical simulations are used to find p_{opt} using (9.16). 3) p_{opt} along with the optimum threshold T_{opt} that minimizes the total error rate. from (9.15) and (9.16), we can notice that for the first two criteria, finding p_{opt} is independent of the value of the threshold. However, third criterion, that is, the total error rate, depends on the value of p as well as the value of the threshold. Thus, to minimize the total error rate, the optimum value of p and the optimum value of threshold have to be computed jointly.

The total error rate P_t can be given by using (9.13) and (9.14) as

$$P_t \;=\; 1 - Q\left(\frac{T-\mu_1}{\sigma_1}\right) + Q\left(\frac{T-\mu_0}{\sigma_0}\right). \tag{9.17}$$

On differentiating (9.17) with respect to T for a fixed p, and equating to zero as

$$\frac{\partial P_t}{\partial T} = \frac{\exp\left(-\frac{1}{2}\left(\frac{T-\mu_1}{\sigma_1}\right)^2\right)}{\sigma_1} - \frac{\exp\left(-\frac{1}{2}\left(\frac{T-\mu_0}{\sigma_0}\right)^2\right)}{\sigma_0} = 0$$

yields the optimum threshold T_{opt}

$$T_{opt} = \frac{\mu_0\sigma_1^2 - \mu_1\sigma_0^2 + D\sigma_0\sigma_1}{\sigma_1^2 - \sigma_0^2}, \tag{9.18}$$

where $D = \sqrt{(\mu_1 - \mu_0)^2 + 2(\sigma_1^2 - \sigma_0^2)\log_e(\sigma_1/\sigma_0)}$. It can be shown that the second derivative of P_t is positive at the optimum value of T. Substituting (9.18) in (9.17), p_{opt} can be obtained as follows:

$$\begin{aligned} p_{opt} &= \arg\min_p \left\{ 1 - Q\left(\frac{(\mu_0 - \mu_1)\sigma_1 + D\sigma_0}{\sigma_1^2 - \sigma_0^2}\right) \right. \\ &\quad \left. + Q\left(\frac{(\mu_0 - \mu_1)\sigma_0 + D\sigma_1}{\sigma_1^2 - \sigma_0^2}\right) \right\}. \end{aligned} \tag{9.19}$$

From (9.19), we can see that the two variables problem of finding p_{opt} and T_{opt} is effectively reduced to a single variable problem of finding p_{opt} only. The computation of (9.19) depends on (9.11) due to the presence of the term σ_1. Given the complex nature of (9.11), the optimum p, i.e., p_{opt} can be easily found numerically.

9.3.4 Low and high SNR Approximations

From (9.7), where $c = \frac{\gamma\rho^{|m-n|}}{1+\gamma}$, we can see that, for exponential correlation, c approaches 0 at low SNR, that is, the samples at different antennas tend to become uncorrelated. The system behaves as if it has independent multiple antennas even though the antennas are correlated. Thus, in low SNR regime, the effect of correlation among multiple antennas diminishes. From (9.10), (9.11), and (9.19), it can be shown that the optimum value of p becomes independent of c, and thus, of the correlation coefficient ρ.

At high SNR, it can be seen from (9.7) that c approaches $\rho^{|m-n|}$. Therefore, the correlation among multiple antennas affects the optimum value of p. The analysis is supported by the numerical results shown in Fig. 9.5.

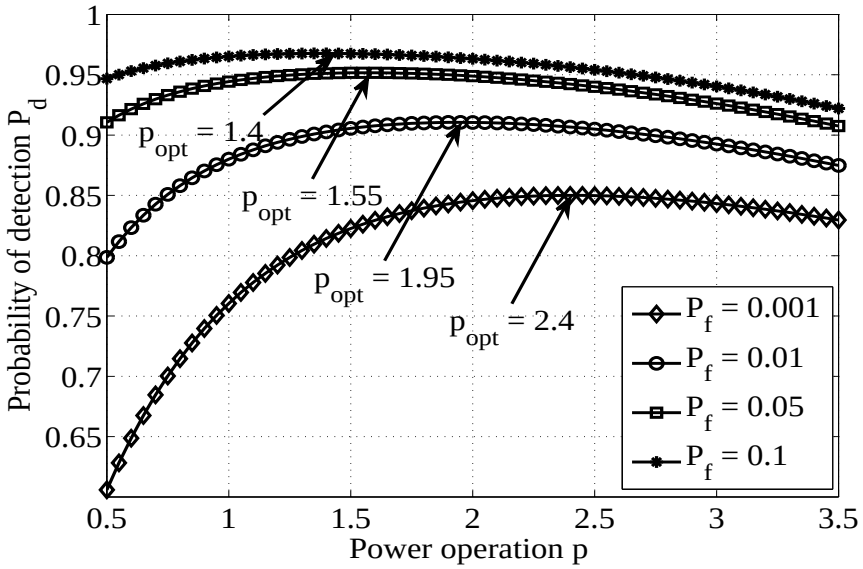

Figure 9.1: P_D versus p for different probability of false alarm P_F, $\rho = 0.5$, $M = 3$, $N = 20$, $\sigma_n^2 = 1$, SNR = 0 dB.

9.4 Results and Discussions

In this section, we present numerical results to show the effect of a number of antennas M, antenna correlation ρ, and average SNR on the optimum power operation p_{opt} that corresponds to following three criteria to measure the detection performance.

1. Maximization of P_D keeping P_F constant.

2. Minimization of P_F keeping P_D constant.

3. Minimization of the total error rate $P_m + P_F$.

The first two criteria are independent of the threshold T, and we only need to find the optimum p for given system parameters. In Figs. 9.1-9.6, we shall study the effect of aforementioned system parameters on the optimum p for the first two detection performance criteria. However, the third criterion is dependent on both p and threshold jointly. Thus, we need the optimum p and optimum threshold jointly that minimize the total error rate. In Figs. 9.7-9.9, we shall numerically find the optimum pair of p and threshold jointly for given

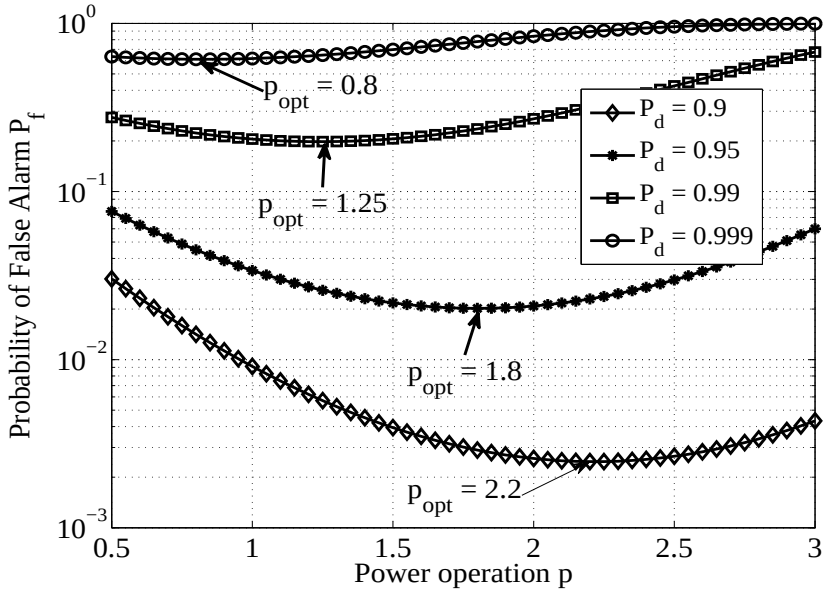

Figure 9.2: P_F versus p for different probability of detection P_D, $\rho = 0.5$, $M = 3$, $N = 20$, $\sigma_n^2 = 1$, SNR = 0 dB.

system parameters, and study the effects of them on the joint computation of p_{opt} and T_{opt}. The system parameters considered are given along with respective figures.

9.4.1 Effect of p on the detection performance

Fig. 9.1 shows P_D versus p for a fixed P_F with three correlated multiple antennas. The correlation coefficient ρ is set to 0.5. We can see that there exists an optimum value p_{opt} of $p \neq 2$ that maximizes P_D for a given P_F. Also, p_{opt} that maximizes P_D changes with P_F; in particular, as the target P_F decreases, making constraint more stringent, p_{opt} that maximizes P_D increases. Also, note that the maximum value of P_D achieved falls as the target P_F is set to a lower value. Similarly, p_{opt} that minimizes P_F for a fixed P_D can be obtained, and is shown in Fig. 9.2. Here, as the target P_D increases, making constraint more stringent, p_{opt} that minimizes P_F reduces, while the minimum value of P_F that can be obtained increases.

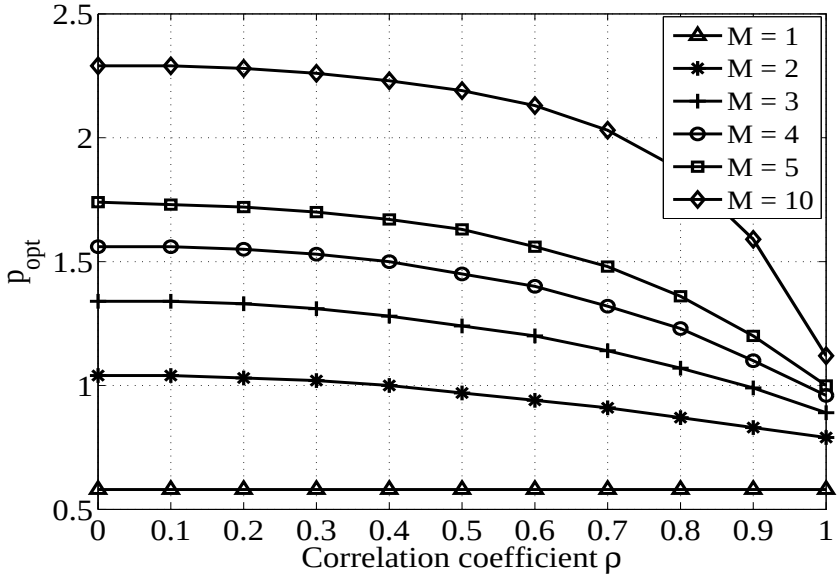

Figure 9.3: p_{opt} versus ρ. Minimizing P_F for a fixed P_D for multiple antennas M, $P_D = 0.99$, $N = 20$, $\sigma_n^2 = 1$, SNR = 0 dB. For $M = 1$, the correlation is not applicable and p_{opt} remains constant.

9.4.2 Effect of the correlation coefficient on the optimum p

Figs. 9.3 and 9.4 show the variation of p_{opt} with antenna correlation coefficient ρ for different number of antennas M. In Fig. 9.3, for a fixed P_D, p_{opt} is calculated that minimizes P_F. As the correlation among antennas increases, p_{opt} that minimizes P_F decreases. Fig. 9.4 shows the variation of p_{opt} against ρ that maximizes P_D when P_F is fixed to 0.01. It can also be noticed from Figs. 9.3 and 9.4 that for the case of maximizing P_D while keeping P_F constant, the optimum value of p remains almost the same irrespective of the correlation coefficient for a given number of antennas; while the optimum p changes significantly with the correlation coefficient when we try to minimize P_F for a given P_D.

Figs. 9.5 and 9.6 show the effect of average received SNR on p_{opt}, and corresponding maximized P_D and minimized P_F, respectively, for different ρ and $M = 3$. As discussed in Sect. 9.3.4, at low SNR, the antennas become almost independent and ρ has no effect on p_{opt}. This can be seen in Fig. 9.5, where the curves corresponding to $\rho = 0$, 0.5, 1 approach each other in low SNR regime. At high SNR, c approaches $\rho^{|m-n|}$, thus ρ affects p_{opt}. This

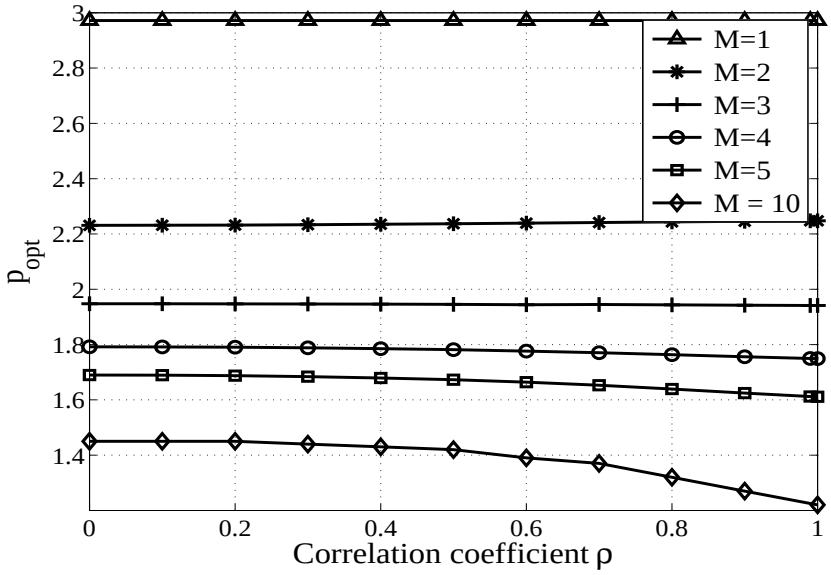

Figure 9.4: Exponential correlation: p_{opt} versus ρ. Maximizing P_D for a fixed P_F for multiple antennas M, $P_F = 0.01$, $N = 20$, $\sigma_n^2 = 1$, SNR = 0 dB. For $M = 1$, the correlation is not applicable and p_{opt} remains constant.

is evident in Fig. 9.5, where at high SNR values, the curves corresponding to $\rho = 0$, 0.5, 1 start diverging from each other. Now, let us pay special attention to the SNR value that corresponds to the intersection of curves for "Maximizing P_D when target $P_F = 0.01$" and "Minimizing P_F when target $P_D = 0.99$" in Fig. 9.5 for a given ρ. We note that, for a given ρ, the point of intersection gives the values of p_{opt} and SNR for which $P_D = 0.99$ and $P_F = 0.01$ at the same time. For example, if we look at both curves for $\rho = 0.5$, we can notice that p_{opt} and SNR at the intersection of curves are 1.47 and 2 dB, respectively, i.e., to achieve $P_D = 0.99$ and $P_F = 0.01$ for $\rho = 0.5$, one should choose p to be 1.47, and the required SNR is 2 dB. Now, for $\rho = 0$, we can see from Fig. 9.5 that, at the point of intersection, $p_{opt} = 1.57$ and SNR = 1.6 dB; while for $\rho = 1$, $p_{opt} = 1.12$ and SNR = 3.35 dB. From aforementioned observations, we remark that, with the increase in ρ, the required SNR to obtain $P_D = 0.99$ and $P_F = 0.01$ increases, while corresponding p_{opt} decreases.

The above discussion can also be validated from Fig. 9.6, which plots "Maximum P_D" and "Minimum P_F" corresponding to p_{opt} in Fig. 9.5 for given ρ and SNR. For example,

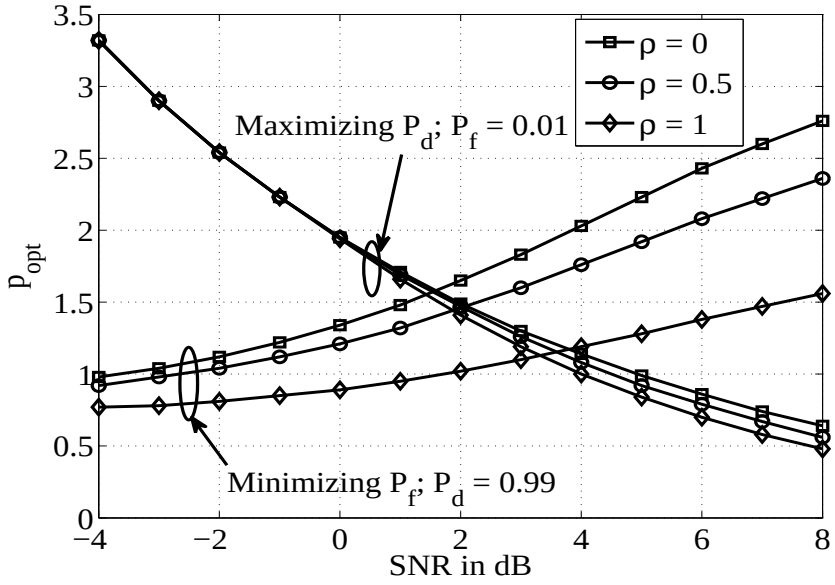

Figure 9.5: Optimum value of p, maximizing P_D against SNR for different values of ρ for a fixed P_F and M, as well as optimum value of p, minimizing P_F against SNR for different values of ρ for a fixed P_D, $M = 3$, $N = 20$.

consider the case when $\rho = 0.5$. In this case, the intersection of the curve for "Maximum P_D" with the dashed line of '0.99' and the intersection of the curve for "Minimum P_F" with the dashed line of '0.01' occur simultaneously at SNR = 2 dB, which is same as the one obtained from Fig. 9.5. We also confirm from Fig. 9.6 that, the required SNR to satisfy $P_D = 0.99$ and $P_F = 0.01$ simultaneously increases with increase in ρ.

From Figs. 9.1-9.6, one can conclude that p_{opt} depends on system parameters like target P_D, target P_F, SNR, M, and ρ. Thus, p_{opt} in an improved energy detector can be determined according to given system parameters, along with the graphs shown in Figs. 9.1-9.6.

9.4.3 Minimizing the total error rate

Let us now look at the minimization of the total error rate P_t. Here, we aim to minimize the overall sensing errors, i.e., $P_m + P_F$, instead of just minimizing only one of the sensing errors (P_m or P_F) keeping other sensing error fixed. Unlike the minimization of only one sensing error (Figs. 9.3-9.6) which requires finding only optimum p for given system parameters, from

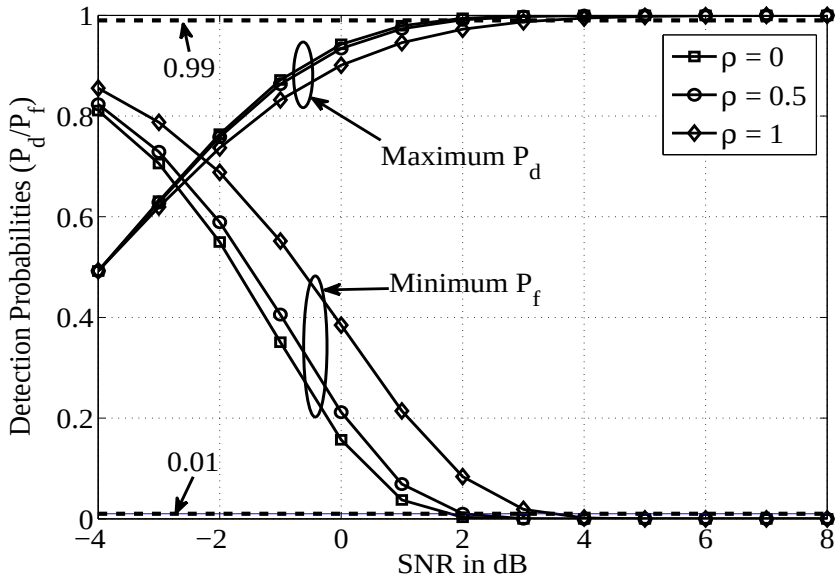

Figure 9.6: Maximized P_D and minimized P_F corresponding to the optimum value of p in Fig. 9.5 versus SNR for different values of ρ, $M = 3$, $N = 20$.

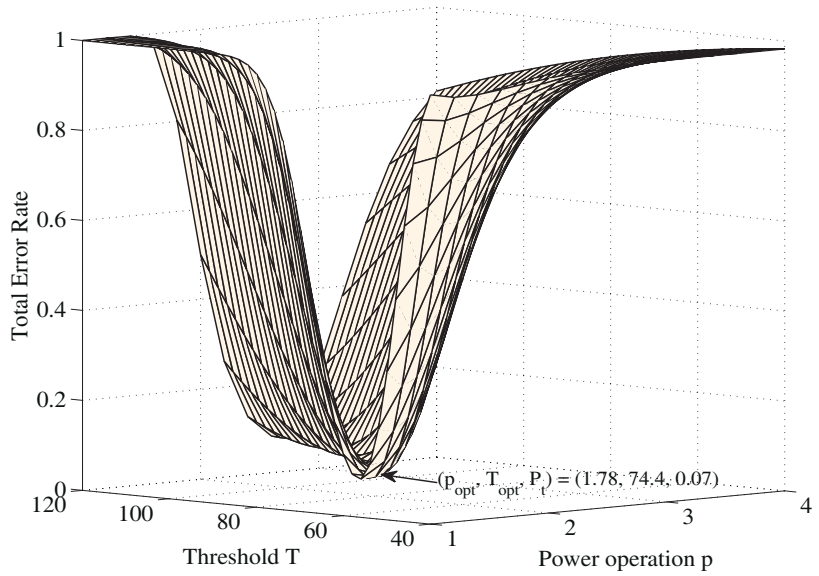

Figure 9.7: Total error rate against the threshold T and the power operation p, $\rho = 0.5$, $M = 3$, SNR = 0 dB, $N = 20$.

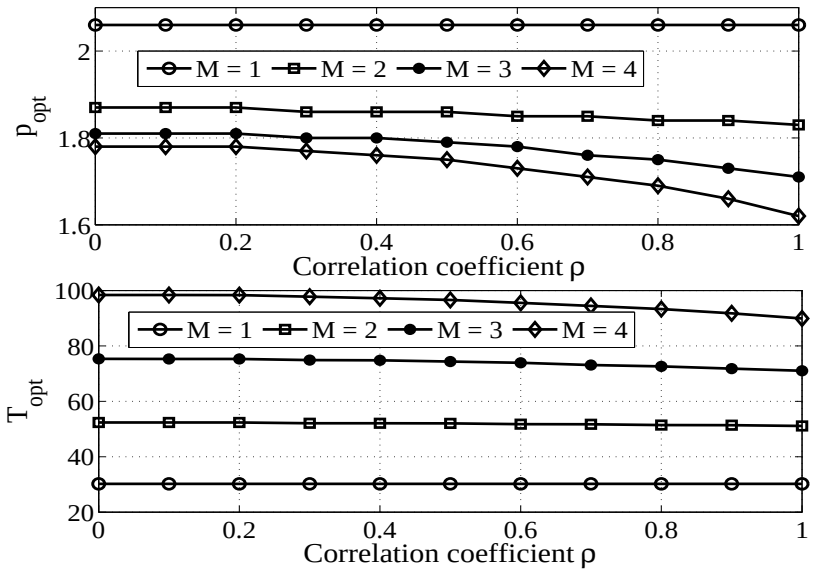

Figure 9.8: Finding p_{opt} and T_{opt} jointly, minimizing $P_t = P_m + P_F$ against different ρ and M, $N = 20$, SNR = 0 dB. For $M = 1$, the correlation is not applicable and p_{opt} remains constant.

(9.13), (9.14), and (9.17), we can see that the minimization of the total error rate P_t is dependent on both p and threshold T. That is, to obtain the minimum total error rate, we have to find corresponding optimum p and T jointly, as discussed in Sect. 9.3.3.

Figure 9.7 shows the joint effect of p and threshold T on the total error rate, where we can see that there exists an optimum pair of p and T that minimizes the total error rate. Figure 9.8 shows the jointly found optimum values of p and threshold that minimize P_t for different number of antennas, against the correlation coefficient ρ; while Fig. 9.9 plots the corresponding values of minimized total error rate. For example, when $\rho = 0.5$ and $M = 3$, the optimum pair (p_{opt}, T_{opt}) that minimizes P_t is found to be (1.78, 74.4), and the corresponding minimized P_t is 0.07. From Fig. 9.8, note that increase in ρ decreases the optimum p as well as the optimum threshold. This trend of the optimum p that minimizes $P_t = P_m + P_F$ is expected as both the optimum p that maximizes P_D (in turn, minimizes P_m) and the optimum p that minimizes P_F, decrease with the increase in ρ (please see Figs. 9.3 and 9.4). Also, from Fig. 9.9, we can observe the deteriorating effect of correlation, i.e.,

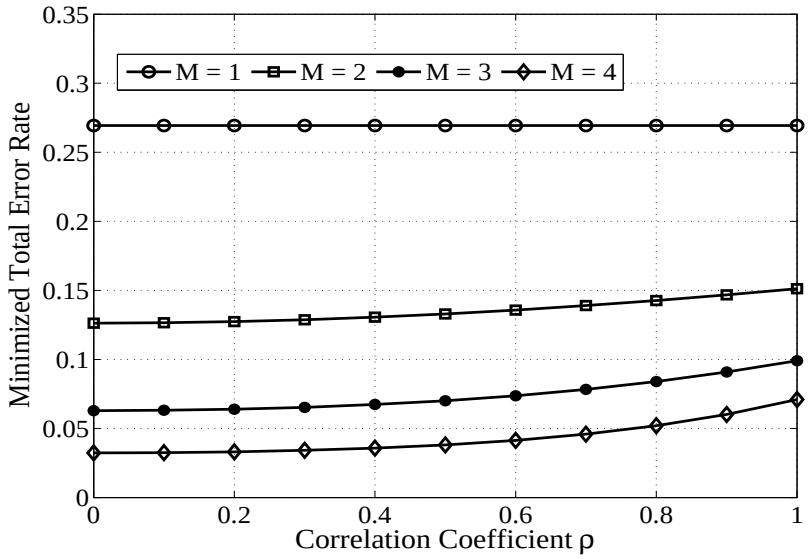

Figure 9.9: Minimized total error rate versus the correlation coefficient ρ and number of antennas M, $N = 20$, SNR = 0 dB. For $M = 1$, the correlation is not applicable, and the minimized total error rate remains constant.

higher correlation among antennas leads to the increase in the minimized total error rate. This is expected as the antenna correlation reduces the degrees of freedom. On the other hand, increase in the number of antennas M improves the detection performance due to the increased spatial diversity, in turn, obtaining lower minimum P_t for a given correlation coefficient.

Figure 9.8 provides guidelines to select p and threshold jointly to minimize the total error rate for given system parameters, so that the opportunity to use the idle spectrum improves (by minimizing the probability of false alarm) while keeping the interference to the primary user below the given limit (by maximizing the probability of detection); Fig. 9.9 shows the minimized total error against the variation of ρ.

9.5 Chapter Summary

The optimum power operation p_{opt} for the improved energy detector changes with the number of antennas M, correlation coefficient ρ among multiple antennas, number of samples and average received SNR, and may be different from $p = 2$ (conventional energy detection). Thus, the value of p should be chosen according to above system parameters. Moreover, we note that maximizing the probability of detection for a given probability of false alarm is more robust to the effect of correlation among multiple antennas than minimizing the probability of false alarm for a given probability of detection; while for minimization of total error rate, the optimum p and threshold are only affected by high correlation values. Numerical results show that in low SNR regime, the effect of correlation on p_{opt} diminishes. We also calculate the optimum pair of p_{opt} and threshold jointly to minimize the total error rate, and show that the optimum pair may change with ρ and M.

Part IV

Conclusions and Appendices

Chapter 10

Conclusions and Future Directions

10.1 Thesis Conclusion

The overarching theme in this thesis is the cognitive radio, where we have focused on cooperation, energy harvesting, and security aspects of spectrum sharing between primary and secondary networks. In general, this thesis has shown that the cooperation among users is always useful in all three modes of spectrum sharing, though we need to be careful of security concerns arising from the interaction between nodes. In this regard, we have addressed two security concerns: spectrum sensing data falsification attack and eavesdropping by an untrusted relay. This thesis has also considered the effects of energy harvesting from the aspects of cooperation and security of cognitive radio. We have shown that the use of interference (prevalent in spectrum sharing) as an energy source subdues its harmful effects due to additional harvested energy.

As punchlines of our works on overlay mode (Chapters 2 and 3), we integrated the inter-network cooperation between primary and secondary networks with the energy harvesting. The main lesson learned from Chapter 2 is that the inter-network cooperation between primary and secondary networks utilizes the spectrum efficiently if careful allocation of energy, time, and users (selection of relaying users) is done. The maximization of the secondary network-level throughput creates unfairness among secondary users in terms of individual throughput. Our proposed optimal resource allocation scheme can be adapted to induce fairness, but at the cost of loss in network-level throughput. The main takeaway from Chapter

3 is that the energy cooperation along with information cooperation provides more spectrum access opportunities to the secondary network and thus improves the overall spectrum usage. But the finite battery size restricts the gains of energy cooperation. The results obtained in Chapters 2 and 3 are applicable to scenarios other than cognitive radio networks. For example, in heterogeneous networks where different networks coexist in the same spectrum, the information and energy cooperation can lead to the better management of resources such as energy and spectrum. Especially, energy cooperation finds applications in ad hoc networks, e.g., wireless sensor networks, where no network structure is present. In this case, nodes can collaborate to share energy to improve the performance and the lifetime of the network.

The crux of our works on the underlay mode (Chapters 4 to 7) is the intra-network cooperation, where an intermediate node, called relay, assists in the communications between SUs. In Chapters 4 to 6, we analyzed the outage performance of the secondary network with EH relays. Chapter 4 reveals the trade-off between the primary's interference constraint and the energy harvesting constraint. In particular, loosening the primary outage constraint may not always be beneficial for the energy-constrained secondary network. Exploiting the primary's interference as a useful energy source, in Chapter 5, the improvement in the secondary network's outage performance is obtained by harvesting extra energy. This highlights the positive aspect of the interference, which has applications in dense wireless networks where the interference is prevalent. Chapter 6 shows that the communication via an energy harvesting untrusted relay can be improved by exploiting the dual role of the jammer as a source of artificial noise as well as RF energy. Chapter 7 provides closed-form expressions for the secondary outage probability, which shows that the direct and the relaying links together improve the outage performance.

Finally, our works on the interweave mode (Chapters 8 and 9) study the intra-network cooperation to detect the presence of the primary user. In Chapter 8, we have shown that an outlier method based on Dixon's test can be used effectively to identify a single malicious user and eliminate it from the cooperation. Chapter 9 shows that one needs to choose the power operation in the improved energy detection carefully in the presence of correlated multiple antenna spectrum sensing to have the optimum spectrum sensing performance.

10.2 Future Directions

Below we conclude with some possible extensions of our works.

- *Imperfect CSI*: We assumed perfect CSI in our works. The CSI acquired can be imperfect due to errors in channel estimation and feedback. The CSI acquisition consumes energy, which could have significant impact on network's performance in energy harvesting scenarios considered in Chapters 2-6, where energy is a scarce resource. For example, corresponding to the work in Chapter 2, the energy consumption in CSI acquisition snatches away a part of energy available for primary data relaying and secondary users' own transmissions, which results in the reduced secondary user throughput. Also, the channel estimation error leads to imperfect cancellation of the jamming signal, causing self-interference at the secondary destination (Chapter 6). Additional investigation about whether the effect of imperfect CSI could be ameliorated is of high interest and important to have a more realistic view of the proposed system.

- *Stochastic geometry-based approach*: Our models consist of two heterogeneous networks with multiple users that share the same spectrum. One can use the powerful mathematical tools from stochastic geometry [175] to analyze our models in a large-scale network. Stochastic geometry characterizes the co-channel interference nicely in wireless networks, which is a key component in our models (Chapters 2, 4-7). For instance, in an energy harvesting setup, the RF interference can be used as an extra energy source, which subsides its deteriorating effects. The analysis of the cooperation between primary and secondary networks from stochastic geometry perspective can bring additional insights that can help in facilitating the efficient spectrum sharing.

- *Sophisticated attacks*: In Chapter 8, we considered the presence of one malicious user in CSS. This raises a natural question: What if multiple malicious users are present? In fact, multiple malicious users can collude with each other to launch a stronger attack. Design of such attacks and propose defence mechanisms against them is important. In addition, we considered attacks where malicious user does not change its characteristics. For example, it always sends the falsified spectrum sensing data. An intelligent

malicious user can act an honest SU occasionally to avoid getting detected as an outlier. Designing such intelligent attack along with the colluded attack can give a more realistic view of the system.

- *Use of game theory*: Game theory studies the interaction among multiple users, their strategies, and the costs involved in interactions. As the inherent nature of cognitive radio includes setups where primary and secondary users share a set of resources and the actions of each user may affect the others, it looks natural that game theory is a viable alternative to depict the cognitive radio taking into account several aspects such as rewards for cooperation, security threats, cost of spectrum sharing in terms of scarce resources (e.g., spectrum and energy), and so on.

References

[1] FCC, "Spectrum policy task force," *ET Docket 02-135*, November 2002.

[2] S. Haykin, "Cognitive radio: Brain-empowered wireless communications," *IEEE Journal on Selected Areas in Communications*, vol. 23, no. 2, pp. 201–220, February 2005.

[3] I. Akyildiz, W.-Y. Lee, M. Vuran, and S. Mohanty, "Next generation/dynamic spectrum access/cognitive radio wireless networks: A survey," *Computer Networks*, vol. 50, no. 13, pp. 2127–2159, September 2006.

[4] Q. Zhao and B. M. Sadler, "A survey of dynamic spectrum access," *IEEE Signal Processing Magazine*, vol. 24, no. 3, pp. 79–89, May 2007.

[5] A. Goldsmith, S. A. Jafar, I. Marić, and S. Srinivasa, "Breaking spectrum gridlock with cognitive radios: An information theoretic perspective," *Proceedings of the IEEE*, vol. 97, no. 5, pp. 894–914, May 2009.

[6] J. Mitola and G. Q. Maguire, "Cognitive radio: Making software more personal," *IEEE Personal Communications*, vol. 6, no. 4, pp. 13–18, August 1999.

[7] N. Devroye, P. Mitran, and V. Tarokh, "Achievable rates in cognitive radio channels," *IEEE Transactions on Information Theory*, vol. 52, no. 5, pp. 1813–1827, May 2006.

[8] A. Sadek, K. J. R. Liu, and A. Ephremides, "Cognitive multiple access via cooperation: Protocol design and performance analysis," *IEEE Transactions on Information Theory*, vol. 53, no. 10, pp. 3677–3696, October 2007.

[9] A. Jovičić and P. Viswanath, "Cognitive radio: An information-theoretic perspective," *IEEE Transactions on Information Theory*, vol. 55, no. 9, pp. 3945–3958, September 2009.

[10] O. Simeone, I. Stanojev, S. Savazzi, Y. Bar-Ness, U. Spagnolini, and R. Pickholtz, "Spectrum leasing to cooperating secondary Ad Hoc networks," *IEEE Journal on Selected Areas in Communications*, vol. 26, no. 1, pp. 203–213, January 2008.

[11] I. Krikidis, J. N. Laneman, J. S. Thompson, and S. McLaughlin, "Protocol design and throughput analysis for multi-user cognitive cooperative systems," *IEEE Transactions on Wireless Communications*, vol. 8, no. 9, pp. 4740–4751, September 2009.

[12] Y. Han, S. H. Ting, and A. Pandharipande, "Cooperative spectrum sharing protocol with secondary user selection," *IEEE Transactions on Wireless Communications*, vol. 9, no. 9, pp. 2914–2923, September 2010.

[13] H. Wang, L. Gao, X. Gan, X. Wang, and E. Hossain, "Cooperative spectrum sharing in cognitive radio networks: A game-theoretic approach," in *Proceedings of IEEE International Conference on Communications (ICC)*, pp. 1–5, 2010.

[14] G. Scutari, D. P. Palomar, and S. Barbarossa, "Cognitive MIMO radio," *IEEE Signal Processing Magazine*, vol. 25, no. 6, pp. 46–59, November 2008.

[15] T. Yucek and H. Arslan, "A survey of spectrum sensing algorithms for cognitive radio applications," *IEEE Communications Surveys and Tutorials*, vol. 11, no. 1, pp. 116–130, First Quarter, 2009.

[16] A. Ghasemi and E. S. Sousa, "Collaborative spectrum sensing for opportunistic access in fading environments," in *Proceedings of IEEE Dynamic Spectrum Access Networks (DySPAN)*, pp. 131–136, 2005.

[17] A. Pandharipande and J. Linnartz, "Performance analysis of primary user detection in a multiple antenna cognitive radio," in *Proceedings of IEEE International Conference on Communications (ICC)*, pp. 6482–6486, 2007.

[18] V. Kuppusamy and R. Mahapatra, "Primary user detection in OFDM based MIMO cognitive radio," in *Proceedings of International Conference on Cognitive Radio Oriented Wireless Networks (CROWNCOM)*, pp. 1–5, 2008.

[19] M. Alamgir, M. Faulkner, J. Gao, and P. Conder, "Signal detection for cognitive radio using multiple antennas," in *Proceedings of IEEE International Symposium on Wireless Communication Systems (ISWCS)*, pp. 488–492, 2008.

[20] S. Kim, J. Lee, H. Wang, and D. Hong, "Sensing performance of energy detector with correlated multiple antennas," *IEEE Signal Processing Letters*, vol. 16, no. 8, pp. 671–674, August 2009.

[21] L. Luo, P. Zhang, G. Zhang, and J. Qin, "Outage performance for cognitive relay networks with underlay spectrum sharing," *IEEE Communications Letters*, vol. 15, no. 7, pp. 710–712, July 2011.

[22] Y. Oohama, "Coding for relay channels with confidential messages," in *Proceedings of 2001 IEEE Information Theory Workshop (ITW'01)*, pp. 87–89, 2001.

[23] R. Chen, J. M. Park, and K. Bian, "Robust distributed spectrum sensing in cognitive radio networks," in *Proceedings of IEEE Conference on Computer Communications (INFOCOM)*, pp. 1876–1884, 2008.

[24] W. Wang, H. Li., Y. L. Sun, and Z. Han, "Attack-proof collaborative spectrum sensing in cognitive radio networks," in *Proceedings of Annual Conference on Information Sciences and Systems (CISS)*, pp. 130–134, 2009.

[25] P. Kaligineedi, M. Khabbazian, and V. K. Bhargava, "Malicious user detection in a cognitive radio cooperative sensing system," *IEEE Transactions on Wireless Communications*, vol. 9, no. 8, pp. 2488–2497, August 2010.

[26] R. K. Sharma and D. B. Rawat, "Advances on security threats and countermeasures for cognitive radio networks: A survey," *IEEE Communications Surveys and Tutorials*, vol. 17, no. 2, pp. 1023–1043, Second Quarter, 2015.

[27] V. Barnett and T. Lewis, *Outliers in Statistical Data*. New York, NY: John Wiley and Sons, 2nd ed., 1985.

[28] A. Sultan, "Sensing and transmit energy optimization for an energy harvesting cognitive radio," *IEEE Wireless Communications Letters*, vol. 1, no. 5, pp. 500–503, October 2012.

[29] S. Park, H. Kim, and D. Hong, "Cognitive radio networks with energy harvesting," *IEEE Transactions on Wireless Communications*, vol. 12, no. 3, pp. 1386–1397, March 2013.

[30] D. Niyato, P. Wang, and D. I. Kim, "Performance analysis of cognitive radio networks with opportunistic RF energy harvesting," in *Proceedings of IEEE Global Communications Conference (GLOBECOM)*, pp. 1096–1101, 2014.

[31] S. Lee, R. Zhang, and K. Huang, "Opportunistic wireless energy harvesting in cognitive radio networks," *IEEE Transactions on Wireless Communications*, vol. 12, no. 9, pp. 4788–4799, September 2013.

[32] J. P. J, S. S. Kalamkar, and A. Banerjee, "Energy harvesting cognitive radio with channel-aware sensing strategy," *IEEE Communications Letters*, vol. 18, no. 7, pp. 1171–1174, July 2014.

[33] M. Usman and I. Koo, "Access strategy for hybrid underlay-overlay cognitive radios with energy harvesting," *IEEE Sensors Journal*, vol. 14, no. 9, pp. 3164–3173, September 2014.

[34] A. E. Shafie, M. Ashour, T. Khattab, and A. Mohamed, "On spectrum sharing between energy harvesting cognitive radio users and primary users," in *Proceedings of International Conference on Computing, Networking and Communications (ICNC)*, pp. 214–220, 2015.

[35] J. A. Paradiso and T. Starner, "Energy scavenging for mobile and wireless electronics," *IEEE Pervasive Computing*, vol. 4, no. 1, pp. 18–27, January 2005.

[36] X. Lu, P. Wang, D. Niyato, D. I. Kim, and Z. Han, "Wireless networks with RF energy harvesting: A contemporary survey," *IEEE Communications Surveys and Tutorials*, vol. 17, no. 2, Second Quarter 2015.

[37] B. Gurakan, O. Ozel, J. Yang, and S. Ulukus, "Energy cooperation in energy harvesting communications," *IEEE Transactions on Communications*, vol. 61, no. 12, pp. 4884–4898, December 2013.

[38] L. R. Varshney, "Transporting information and energy simultaneously," in *Proceedings of IEEE International Symposium on Information Theory (ISIT)*, pp. 1612–1616, 2008.

[39] P. Grover and A. Sahai, "Shannon meets Tesla: Wireless information and power transfer," in *Proceedings of IEEE International Symposium on Information Theory (ISIT)*, pp. 2363–2367, 2010.

[40] H. J. Visser and R. M. Vullers, "RF energy harvesting and transport for wireless sensor network applications: Principles and requirements," *Proceedings of the IEEE*, vol. 101, no. 6, pp. 1410–1423, June 2013.

[41] H. Ju and R. Zhang, "Throughput maximization in wireless powered communication networks," *IEEE Transactions on Wireless Communications*, vol. 13, no. 1, pp. 418–428, January 2014.

[42] S. Bi, C. K. Ho, and R. Zhang, "Wireless powered communication: opportunities and challenges," *IEEE Communications Magazine*, vol. 53, no. 4, pp. 117–125, April 2015.

[43] H. Tabassum, E. Hossain, A. Ogundipe, and D. I. Kim, "Wireless-powered cellular networks: key challenges and solution techniques," *IEEE Communications Magazine*, vol. 53, no. 6, pp. 63–71, June 2015.

[44] X. Zhou, C. K. Ho, and R. Zhang, "Wireless power meets energy harvesting: A joint energy allocation approach," in *Proceedings of IEEE Global Conference on Signal and Information Processing (GLOBALSIP)*, pp. 198–202, 2014.

[45] K. Huang and V. K. N. Lau, "Enabling wireless power transfer in cellular networks: Architecture, modeling and deployment," *IEEE Transactions on Wireless Communications*, vol. 13, no. 2, pp. 902–912, February 2014.

[46] S. Bi and R. Zhang, "Placement optimization of energy and information access points in wireless powered communication networks," *IEEE Transactions on Wireless Communications*, vol. 15, no. 3, pp. 2351–2364, March 2016.

[47] Product Datasheet, P2110-915MHz RF Powerharvester Receiver, Powercast Corporation. [Available online] `http://www.powercastco.com/PDF/P2110-datasheet.pdf`.

[48] Product Datasheet, 2.4 GHz Ultra-Low Power Radio, Interuniversity Microelectronics Centre (IMEC). [Available online] `http://www2.imec.be/be_en/research/wireless-communication/ultralow-power-wireless-communic.html`.

[49] L. Zhao, X. Wang, and K. Zheng, "Downlink hybrid information and energy transfer with massive MIMO," *IEEE Transactions on Wireless Communications*, vol. 15, no. 2, pp. 1309–1322, February 2016.

[50] J. G. Andrews, H. Claussen, M. Dohler, S. Rangan, and M. C. Reed, "Femtocells: past, present, and future," *IEEE Journal on Selected Areas in Communications*, vol. 30, no. 3, pp. 497–508, April 2011.

[51] P. Nintanavongsa, M. Y. Naderi, and K. R. Chowdhury, "Medium access control protocol design for sensors powered by wireless energy transfer," in *Proceedings of IEEE International Conference on Computer Communications (INFOCOM)*, pp. 150–154, 2013.

[52] H. Ju and R. Zhang, "Optimal resource allocation in full-duplex wireless-powered communication network," *IEEE Transactions on Communications*, vol. 62, no. 10, pp. 3528–3540, October 2014.

[53] S.-W. Ko, S. M. Yu, and S.-L. Kim, "The capacity of energy-constrained mobile networks with wireless power transfer," *IEEE Communications Letters*, vol. 17, no. 3, pp. 529–532, March 2013.

[54] X. Kang, C. K. Ho, and S. Sun, "Optimal time allocation for dynamic-TDMA-based wireless powered communication networks," in *Proceedings of IEEE Global Communications Conference (GLOBECOM)*, pp. 3157–3161, 2014.

[55] H. Ju and R. Zhang, "User cooperation in wireless powered communication networks," in *Proceedings of IEEE Global Communications Conference (GLOBECOM)*, pp. 1430–1435, 2014.

[56] H. Chen, Y. Li, J. L. Rebelatto, B. F. Uchoa-Filho, and B. Vucetic, "Harvest-then-cooperate: Wireless-powered cooperative communications," *IEEE Transactions on Signal Processing*, vol. 63, no. 7, pp. 1700–1711, April 2015.

[57] C. Zhong, G. Zheng, Z. Zhang, and G. K. Karagiannidis, "Optimum wirelessly powered relaying," *IEEE Signal Processing Letters*, vol. 22, no. 10, pp. 1728–1732, October 2015.

[58] L. Liu, R. Zhang, and K.-C. Chua, "Wireless information transfer with opportunistic energy harvesting," *IEEE Transactions on Wireless Communications*, vol. 12, no. 1, pp. 288–300, January 2013.

[59] A. A. Nasir, X. Zhou, S. Durrani, and R. A. Kennedy, "Relaying protocols for wireless energy harvesting and information processing," *IEEE Transactions on Wireless Communications*, vol. 12, no. 7, pp. 3622–3636, July 2013.

[60] S. S. Kalamkar, J. Pradha, A. Banerjee, and K. Rajawat, "Resource allocation and fairness in wireless powered cognitive radio networks," *IEEE Transactions on Communications*, vol. 64, no. 8, pp. 3246–3261, August 2016.

[61] J. Pradha J, S. S. Kalamkar, and A. Banerjee, "On information and energy cooperation in energy harvesting cognitive radio," in *Proceedings of IEEE International Symposium on Personal, Indoor and Mobile Communications (PIMRC)*, pp. 943–948, 2015.

[62] S. S. Kalamkar and A. Banerjee, "Outage analysis of spectrum sharing energy harvesting cognitive relays in Nakagami-m channels," in *Proceedings of IEEE Global Communications Conference (GLOBECOM)*, pp. 1–6, 2015.

[63] S. S. Kalamkar and A. Banerjee, "Interference-assisted wireless energy harvesting in cognitive relay network with multiple primary transceivers," in *Proceedings of IEEE Global Communications Conference (GLOBECOM)*, pp. 1–6, 2015.

[64] S. S. Kalamkar and A. Banerjee, "Interference-aided energy harvesting: Cognitive relaying with multiple primary transceivers," *IEEE Transactions on Cognitive Communications and Networking*, vol. 3, no. 3, pp. 313–327, September 2017.

[65] S. S. Kalamkar and A. Banerjee, "Secure communication via a wireless energy harvesting untrusted relay," *IEEE Transactions on Vehicular Technology*, vol. 66, no. 3, pp. 2199–2213, March 2017.

[66] S. Majhi, S. S. Kalamkar, and A. Banerjee, "Secondary outage analysis of amplify-and-forward cognitive relays with direct link and primary interference," in *Proceedings of National Conference on Communications (NCC)*, pp. 1–6, 2015.

[67] S. S. Kalamkar, A. Banerjee, and A. Roychowdhury, "Malicious user suppression for cooperative spectrum sensing in cognitive radio networks using dixon's outlier detection method," in *Proceedings of National Conference on Communications (NCC)*, pp. 1–5, 2012.

[68] S. S. Kalamkar, A. K. Gupta, and A. Banerjee, "Impact of antenna correlation on optimum improved energy detector in cognitive radio," *IEICE Transactions on Communications*, vol. E98-B, no. 8, pp. 1690–1699, August 2015.

[69] W. Su, J. D. Matyjas, and S. Batalama, "Active cooperation between primary users and cognitive radio users in heterogeneous Ad-Hoc networks," *IEEE Transactions on Signal Processing*, vol. 60, no. 4, pp. 1796–1805, April 2012.

[70] Y. Han, A. Pandharipande, and S. H. Ting, "Cooperative decode-and-forward relaying for secondary spectrum access," *IEEE Transactions on Wireless Communications*, vol. 8, no. 10, pp. 4945–4950, October 2009.

[71] R. Manna, R. H. Louie, Y. Li, and B. Vucetic, "Cooperative spectrum sharing in cognitive radio networks with multiple antennas," *IEEE Transactions on Signal Processing*, vol. 59, no. 11, pp. 5509–5522, November 2011.

[72] B. Cao, L. Cai, H. Liang, J. W. Mark, Q. Zhang, H. V. Poor, and W. Zhuang, "Cooperative cognitive radio networking using quadrature signaling," in *Proceedings of IEEE International Conference on Computer Communications (INFOCOM)*, pp. 3096–3100, 2012.

[73] X. Hao, M. H. Cheung, V. Wong, and V. Leung, "A stackelberg game for cooperative transmission and random access in cognitive radio networks," in *Proceedings of IEEE International Symposium on Personal, Indoor and Mobile Communications (PIMRC)*, pp. 411–416, 2011.

[74] Y. Long, H. Li, H. Yue, M. Pan, and Y. Fang, "SUM: Spectrum utilization maximization in energy-constrained cooperative cognitive radio networks," *IEEE Journal on Selected Areas in Communications*, vol. 32, no. 11, pp. 2105–2116, November 2014.

[75] G. Zheng, Z. Ho, E. Jorswieck, and B. Ottersten, "Information and energy cooperation in cognitive radio networks," *IEEE Transactions on Signal Processing*, vol. 62, no. 9, pp. 2290–2303, May 2014.

[76] Z. Wang, Z. Chen, L. Luo, Z. Hu, B. Xia, and H. Liu, "Outage analysis of cognitive relay networks with energy harvesting and information transfer," in *Proceedings of IEEE International Conference on Communications (ICC)*, pp. 4348–4353, 2014.

[77] P. M. Quang, T. T. Duy, and V. N. Q. Bao, "Energy harvesting-based spectrum access model in overlay cognitive radio," in *Proceedings of Advanced Technologies for Communications (ATC)*, 2015.

[78] C. Zhai, J. Liu, and L. Zheng, "Relay based spectrum sharing with secondary users powered by wireless energy harvesting," *Accepted in IEEE Transactions on Communications*, 2016.

[79] S. Yin, E. Zhang, Z. Qu, L. Yin, and S. Li, "Optimal cooperation strategy in cognitive radio systems with energy harvesting," *IEEE Transactions on Wireless Communications*, vol. 13, no. 9, pp. 4693–4707, September 2014.

[80] S. Lee and R. Zhang, "Cognitive wireless powered network: Spectrum sharing models and throughput maximization," *IEEE Transactions on Cognitive Communications and Networking*, vol. 1, no. 3, pp. 335–346, September 2015.

[81] A. Goldsmith, *Wireless Communications*. Cambridge University Press, 2005.

[82] D. P. Bertsekas, *Nonlinear Programming*. Athena Scientific, 2nd ed., 1999.

[83] W. Yu, "Sum-capacity computation for the Gaussian vector broadcast channel via dual decomposition," *IEEE Transactions on Information Theory*, vol. 52, no. 2, pp. 754–759, February 2006.

[84] R. M. Corless, G. H. Gonnet, D. E. G. Hare, D. J. Jeffrey, and D. E. Knuth, "On the Lambert W function," *Advances in Computational Mathematics*, vol. 5, no. 4, pp. 329–359, 1996.

[85] R. K. Jain, D.-M. W. Chiu, and W. R. Hawe, "A quantitative measure of fairness and discrimination for resource allocation in shared systems," Tech. Rep. DEC Res. Rep. TR-301, Eastern Research Lab, Digital Equipment Corporation, 1984.

[86] S. Srinivasa and S. A. Jafar, "The throughput potential of cognitive radio: A theoretical perspective," in *Proceedings of Asilomar Conference on Signals, Systems and Computers (ASILOMER)*, pp. 221–225, 2006.

[87] B. Cao, Q. Zhang, J. W. Mark, L. Cai, and H. Poor, "Toward efficient radio spectrum utilization: user cooperation in cognitive radio networking," *IEEE Network*, vol. 26, no. 4, pp. 46–52, July 2012.

[88] K. Tutuncuoglu and A. Yener, "Cooperative energy harvesting communications with relaying and energy sharing," in *Proceedings of IEEE Information Theory Workshop*, 2013.

[89] J. Xu, Y. Guo, and R. Zhang, "CoMP meets energy harvesting: A new communication and energy cooperation paradigm," in *Proceedings of IEEE Global Communications Conference (GLOBECOM)*, pp. 2508–2513, 2013.

[90] D. P. Palomar and M. Chiang, "A tutorial on decomposition methods for network utility maximization," *IEEE Journal on Selected Areas in Communications*, vol. 24, no. 8, pp. 1439–1451, 2006.

[91] Q. Zhang, J. Jia, and J. Zhang, "Cooperative relay to improve diversity in cognitive radio networks," *IEEE Communications Magazine*, vol. 47, no. 2, pp. 111–117, February 2009.

[92] Y. Guo, G. Kang, N. Zhang, W. Zhou, and P. Zhang, "Outage performance of relay-assisted cognitive-radio system under spectrum-sharing constraints," *Electronics Letters*, vol. 46, no. 2, pp. 182–184, January 2010.

[93] Y. Zou, J. Zhu, B. Zheng, and Y.-D. Yao, "An adaptive cooperation diversity scheme with best-relay selection in cognitive radio networks," *IEEE Transactions on Signal Processing*, vol. 58, no. 10, pp. 5438–5445, October 2010.

[94] B. Medepally and N. Mehta, "Voluntary energy harvesting relays and selection in cooperative wireless networks," *IEEE Transactions on Wireless Communications*, vol. 9, no. 11, pp. 3543–3553, November 2010.

[95] I. Krikidis, T. Charalambous, and J. S. Thompson, "Stability analysis and power optimization for energy harvesting cooperative networks," *IEEE Signal Processing Letters*, vol. 19, no. 1, pp. 20–23, January 2012.

[96] J. Si, Z. Li, X. Chen, B. Hao, and Z. Liu, "On the performance of cognitive relay networks under primary user's outage constraint," *IEEE Communications Letters*, vol. 15, no. 4, pp. 422–424, April 2011.

[97] T. Duong, D. Benevides da Costa, M. Elkashlan, and V. N. Q. Bao, "Cognitive amplify-and-forward relay networks over Nakagami-m fading," *IEEE Transactions on Vehicukar Technology*, vol. 61, no. 5, pp. 2368–2374, June 2012.

[98] K. Tourki, K. Qaraqe, and M.-S. Alouini, "Outage analysis for underlay relay-assisted cognitive networks," in *Proceedings of 2012 Global Communications Conference (GLOBECOM)*, pp. 1248–1253, 2012.

[99] C. Zhong, T. Ratnarajah, and K.-K. Wong, "Outage analysis of decode-and-forward cognitive dual-hop systems with the interference constraint in Nakagami-m fading channels," *IEEE Transactions on Vehicular Technology*, vol. 60, no. 6, pp. 2875–2879, July 2011.

[100] J. Lee, H. Wang, J. G. Andrews, and D. Hong, "Outage probability of cognitive relay networks with interference constraints," *IEEE Transactions on Wireless Communications*, vol. 10, no. 2, pp. 390–395, February 2011.

[101] J. Si, Z. Li, H. Huang, J. Chen, and R. Gao, "Capacity analysis of cognitive relay networks with the PU's interference," *IEEE Communications Letters*, vol. 16, no. 12, pp. 2020–2023, December 2012.

[102] W. Xu, J. Zhang, P. Zhang, and C. Tellambura, "Outage probability of decode-and-forward cognitive relay in presence of primary user's interference," *IEEE Communications Letters*, vol. 16, no. 8, pp. 1252–1255, August 2012.

[103] Y. Gu and S. Aissa, "Interference aided energy harvesting in decode-and-forward relaying systems," in *Proceedings of IEEE International Conference on Communications (ICC)*, pp. 5378–5382, 2014.

[104] S. Mousavifar, Y. Liu, C. Leung, M. Elkashlan, and T. Duong, "Wireless energy harvesting and spectrum sharing in cognitive radio," in *Proceedings of IEEE Vehicular Technology Conference-Fall (VTC-Fall'14)*, pp. 1–5, 2014.

[105] G. Im and J. H. Lee, "Outage probability of underlay cognitive radio networks with SWIPT-enabled relay," in *Proceedings of IEEE Vehicular Technology Conference-Fall (VTC-Fall)*, pp. 1–5, 2015.

[106] V.-D. Nguyen, S. Dinh-Van, and O.-S. Shin, "Opportunistic relaying with wireless energy harvesting in a cognitive radio system," in *Proceedings of IEEE Wireless Communications and Networking Conference (WCNC)*, pp. 87–92, 2015.

[107] I. S. Gradshteyn and I. M. Ryzhik, *Table of Integrals, Series, and Products*. Academic Press, 8th ed., 2015.

[108] B. Medepally, N. Mehta, and C. Murthy, "Implications of energy profile and storage on energy harvesting sensor link performance," in *Proceedings of IEEE Global Communications Conference (GLOBECOM)*, pp. 1–6, 2009.

[109] H. Chen, Y. Li, Y. Jiang, Y. Ma, and B. Vucetic, "Distributed power splitting for SWIPT in relay interference channels using game theory," *IEEE Transactions on Wireless Communications*, vol. 14, no. 1, pp. 410–420, January 2015.

[110] A. A. Nasir, X. Zhou, S. Durrani, and R. A. Kennedy, "Wireless-powered relays in cooperative communications: Time-switching relaying protocols and throughput analysis," *IEEE Transactions on Communications*, vol. 63, no. 5, pp. 1607–1622, May 2015.

[111] A. D. Wyner, "The wire-tap channel," *Bell System Technical Journal*, vol. 54, no. 8, pp. 1355–1387, October 1975.

[112] I. Krikidis, J. S. Thompson, and S. W. McLaughlin, "Relay selection for secure cooperative networks with jamming," *IEEE Transactions on Wireless Communications*, vol. 8, no. 10, pp. 5003–5011, October 2009.

[113] Z. Ding, K. K. Leung, D. L. Goeckel, and D. Towsley, "Opportunistic relaying for secrecy communications: Cooperative jamming vs. relay chatting," *IEEE Transactions on Wireless Communications*, vol. 10, no. 6, pp. 1725–1729, June 2011.

[114] Y. Liu, J. Li, and A. P. Petropulu, "Destination assisted cooperative jamming for wireless physical-layer security," *IEEE Transactions on Information Forensics and Security*, vol. 8, no. 4, pp. 682–694, April 2013.

[115] V. N. Q. Bao, N. Linh-Trung, and M. Debbah, "Relay selection schemes for dual-hop networks under security constraints with multiple eavesdroppers," *IEEE Transactions on Wireless Communications*, vol. 12, no. 12, pp. 6076–6085, December 2013.

[116] Z. Ding, K. K. Leung, D. L. Goeckel, and D. Towsley, "On the application of cooperative transmission to secrecy communications," *IEEE Journal on Selected Areas in Communications*, vol. 30, no. 2, pp. 359–368, February 2012.

[117] L. Dong, Z. Han, A. P. Petropulu, and H. V. Poor, "Improving wireless physical layer security via cooperating relays," *IEEE Transactions on Signal Processing*, vol. 58, no. 3, pp. 1875–1888, March 2010.

[118] X. He and A. Yener, "Cooperation with an untrusted relay: A secrecy perspective," *IEEE Transactions on Information Theory*, vol. 56, no. 8, pp. 3807–3827, August 2010.

[119] X. He and A. Yener, "Two-hop secure communication using an untrusted relay," *EURASIP Journal on Wireless Communications and Networking*, vol. 2009, pp. 1–13, May 2009.

[120] H. Xing, L. Liu, and R. Zhang, "Secrecy wireless information and power transfer in fading wiretap channel," *IEEE Transactions on Vehicular Technology*, vol. 65, no. 1, pp. 180–190, January 2016.

[121] B. He and X. Zhou, "On the placement of RF energy harvesting node in wireless networks with secrecy considerations," in *Proceedings of 2014 IEEE Global Communications Conference (GLOBECOM'14) Workshops*, pp. 1355–1360, December 2014.

[122] D. W. K. Ng, E. S. Lo, and R. Schober, "Robust beamforming for secure communication in systems with wireless information and power transfer," *IEEE Transactions on Wireless Communications*, vol. 13, no. 8, pp. 4599–4615, August 2014.

[123] M. R. A. Khandaker and K.-K. Wong, "Robust secrecy beamforming with energy-harvesting eavesdroppers," *IEEE Wireless Communications Letters*, vol. 4, no. 1, pp. 10–13, February 2015.

[124] R. Feng, Q. Li, Q. Zhang, and J. Qin, "Robust secure transmission in MISO simultaneous wireless information and power transfer system," *IEEE Transactions on Vehicular Technology*, vol. 64, no. 1, pp. 400–405, January 2015.

[125] Q. Shi, W. Xu, J. Wu, E. Song, and Y. Wang, "Secure beamforming for MIMO broadcasting with wireless information and power transfer," *IEEE Transactions on Wireless Communications*, vol. 14, no. 5, pp. 2841–2853, May 2015.

[126] Q. Li, Q. Zhang, and J. Qin, "Secure relay beamforming for simultaneous wireless information and power transfer in nonregenerative relay networks," *IEEE Transactions on Vehicular Technology*, vol. 63, no. 5, pp. 2462–2467, June 2014.

[127] H. Xing, Z. Chu, Z. Ding, and A. Nallanathan, "Harvest-and-jam: Improving security for wireless energy harvesting cooperative networks," in *Proceedings of Global Communications Conference (GLOBECOM)*, pp. 3145–3150, 2014.

[128] H. Xing, K.-K. Wong, and A. Nallanathan, "Secure wireless energy harvesting-enabled AF-relaying SWIPT networks," in *Proceedings of IEEE International Conference on Communications (ICC)*, pp. 2307–2312, 2015.

[129] X. Chen, J. Chen, and T. Liu, "Secure wireless information and power transfer in large-scale MIMO relaying systems with imperfect CSI," in *Proceedings of IEEE Global Communications Conference (GLOBECOM)*, pp. 4131–4136, 2014.

[130] L. Sun, T. Zhang, Y. Li, and H. Niu, "Performance study of two-hop amplify-and-forward systems with untrustworthy relay nodes," *IEEE Transactions on Vehicular Technology*, vol. 61, no. 8, pp. 3801–3807, October 2012.

[131] L. Sun, P. Ren, Q. Du, Y. Wang, and Z. Gao, "Security-aware relaying scheme for cooperative networks with untrusted relay nodes," *IEEE Communications Letters*, vol. 19, no. 3, pp. 463–466, March 2015.

[132] L. Wang, M. Elkashlan, J. Huang, N. H. Tran, and T. Q. Duong, "Secure transmission with optimal power allocation in untrusted relay networks," *IEEE Wireless Communications Letters*, vol. 3, no. 3, pp. 289–292, June 2014.

[133] Y. Liu, L. Li, and M. Pesavento, "Enhancing physical layer security in untrusted relay networks with artificial noise: A symbol error rate based approach," in *Proceedings of IEEE Sensor Array and Multichannel Signal Processing Workshop (SAM)*, pp. 261–264, 2014.

[134] M. Ju, D.-H. Kim, and K.-S. Hwang, "Opportunistic transmission of nonregenerative network with untrusted relay," *IEEE Transactions on Vehicular Technology*, vol. 64, no. 6, pp. 2703–2709, June 2015.

[135] J. Huang, A. Mukherjee, and A. L. Swindlehurst, "Secure communication via an untrusted non-regenerative relay in fading channels," *IEEE Transactions on Signal Processing*, vol. 61, no. 10, pp. 2536–2550, May 2013.

[136] R. Zhang, L. Song, Z. Han, and B. Jiao, "Physical layer security for two-way untrusted relaying with friendly jammers," *IEEE Transactions on Vehicular Technology*, vol. 61, no. 8, pp. 3693–3704, October 2012.

[137] H. Khodakarami and F. Lahouti, "Link adaptation with untrusted relay assignment: Design and performance analysis," *IEEE Transactions on Communications*, vol. 61, no. 12, pp. 4874–4883, December 2013.

[138] J.-B. Kim, J. Lim, and J. M. Cioffi, "Capacity scaling and diversity order for secure cooperative relaying with untrustworthy relays," *IEEE Transactions on Wireless Communications*, vol. 14, no. 7, pp. 3866–3876, July 2015.

[139] J. Y. Ryu, J. Lee, and T. Q. S. Quek, "Trust degree-based cooperative transmission for communication secrecy," in *Proceedings of IEEE Global Communications Conference (GLOBECOM'15)*, 2015.

[140] X. Zhou, R. Zhang, and C. K. Ho, "Wireless information and power transfer: Architecture design and rate-energy tradeoff," *IEEE Transactions on Communications*, vol. 61, no. 11, pp. 4754–4767, November 2013.

[141] M. Bloch, J. Barros, M. R. D. Rodrigues, and S. W. McLaughlin, "Wireless information-theoretic security," *IEEE Transactions on Information Theory*, vol. 54, no. 6, pp. 2515–2534, June 2008.

[142] Y. Liu, L. Wang, S. A. R. Zaidi, M. Elkashlan, and T. Q. Duong, "Secure D2D communication in large-scale cognitive cellular networks: A wireless power transfer model," *Accepted in IEEE Transactions on Communications*, vol. 64, no. 1, pp. 329–342, January 2016.

[143] J. Guo, S. Durrani, X. Zhou, and H. Yanikomeroglu, "Outage probability of Ad Hoc networks with wireless information and power transfer," *IEEE Wireless Communications Letters*, vol. 4, no. 4, pp. 409–412, August 2015.

[144] T. Duong, P. L. Yeoh, V. N. Q. Bao, M. Elkashlan, and N. Yang, "Cognitive relay networks with multiple primary transceivers under spectrum-sharing," *IEEE Signal Processing Letters*, vol. 19, no. 11, pp. 741–744, November 2012.

[145] J. Si, Z. Li, X. Chen, B. Hao, and Z. Liu, "On the performance of cognitive relay networks under primary user's outage constraint," *IEEE Communications Letters*, vol. 15, pp. 422–424, April 2011.

[146] T. Duong, V. Bao, H. Tran, G. Alexandropoulos, and H.-J. Zepernick, "Effect of primary network on performance of spectrum sharing AF relaying," *Electronics Letters*, vol. 48, no. 1, pp. 25–27, January 2012.

[147] P. Yang, L. Luo, and J. Qin, "Outage performance of cognitive relay networks with interference from primary user," *IEEE Communications Letters*, vol. 16, no. 10, pp. 1695–1698, Pctober 2012.

[148] H. Huang, Z. Li, J. Si, and R. Gao, "Outage analysis of underlay cognitive multiple relays networks with a direct link," *IEEE Communications Letters*, vol. 17, pp. 1600–1603, August 2013.

[149] Z. Yan, X. Zhang, and W. Wang, "Exact outage performance of cognitive relay networks with maximum transmit power limits," *IEEE Communications Letters*, vol. 15, no. 12, pp. 1317–1319, December 2011.

[150] S. Ikki and M. Ahmed, "Performance analysis of cooperative diversity wireless networks over Nakagami-m fading channel," *IEEE Communications Letters*, vol. 11, no. 4, pp. 334–336, April 2007.

[151] J. Si, Z. Li, J. Chen, P. Qi, and H. Huang, "Performance analysis of adaptive modulation in cognitive relay networks with interference constraints," in *Proceedings of IEEE Wireless Communications and Networking Conference (WCNC)*, pp. 2631–2636, 2012.

[152] H. Urkowitz, "Energy detection of unknown deterministic signals," *Proceedings of the IEEE*, vol. 55, no. 4, pp. 523–531, April 1967.

[153] F. Digham, M.-S. Alouini, and M. Simon, "On the energy detection of unknown signals over fading channels," *IEEE Transactions on Communications*, vol. 55, no. 1, pp. 21–24, January 2007.

[154] H. V. Le, M. Ohta, K. Inage, T. Fujii, K. Muraoka, and M. Ariyosh, "Outlier detection methods of low SNR nodes for cooperative spectrum sensing," in *Proceedings of International Symposium on Wireless Communication Systems (ISWCS)*, pp. 966–970, 2010.

[155] F. R.Yu, H. Tang, M. Huang, Z. Li, and P. C. Mason, "Defense against spectrum sensing data falsification attacks in mobile ad hoc networks with cognitive radios," in *Proceedings of IEEE Military Communications Conference (MILCOM)*, pp. 1–7, 2009.

[156] S. Verma and A. Quiroz-Ruiz, "Critical values for six dixon tests for outliers in normal samples up to sizes 100, and applications in science and engineering," *Revista Mexicana de Ciencias Geolgicas*, vol. 23, no. 2, pp. 133–161, 2006.

[157] F. Mosteller and J. W. Tukey, *Data Analysis and Regression : A Second Course in Statistics*. Reading: MA: Addison-Wesley, 1st ed., 1977.

[158] D. A. Lax, "Robust estimators of scale: finite-sample performance in log-tailed symmetric distributions," *Journal of American Statistical Association*, vol. 80, no. 391, pp. 736–741, September 1985.

[159] R. McGill, J. W. Tukey, and W. A. Larsen, "Variations of box plots," *The American Statistician*, vol. 32, no. 1, pp. 12–16, February 1978.

[160] Y. Chen, "Improved energy detector for random signals in Gaussian noise," *IEEE Transactions on Wireless Communications*, vol. 9, no. 2, pp. 558–563, February 2010.

[161] J. Song, Z. Feng, P. Zhang, and Z. Liu, "Spectrum sensing in cognitive radios based on enhanced energy detector," *IET Communications*, vol. 6, no. 8, pp. 805–809, May 2012.

[162] V. Sharma Banjade, C. Tellambura, and H. Jiang, "Performance of p-norm detector in AWGN, fading and diversity reception," *IEEE Transactions on Vehicular Technology*, vol. 63, no. 7, pp. 3209–3222, September 2014.

[163] A. Singh, M. R. Bhatnagar, and R. K. Mallik, "Performance analysis of multiple sample based improved energy detector in collaborative CR networks," in *Proceedings of IEEE International Symposium on Personal, Indoor and Mobile Radio Communications (PIMRC'13)*, pp. 2728–2732, 2013.

[164] S. S. Kalamkar and A. Banerjee, "Improved double threshold energy detection for cooperative spectrum sensing in cognitive radio," *Defence Science Journal (Special Issue on Communication Systems and Image Processing Technologies)*, vol. 63, no. 1, pp. 34–40, January 2013.

[165] S. Nallagonda, A. Chandra, S. D. Roy, and S. Kundu, "Performance of improved energy detector based cooperative spectrum sensing over Hoyt and Rician faded channels," *IEICE Communications Express*, vol. 2, no. 7, pp. 319–324, July 2013.

[166] S. S. Kalamkar and A. Banerjee, "On the performance of generalized energy detector under noise uncertainty in cognitive radio," in *Proceedings of National Conference on Communications (NCC)*, pp. 1–5, 2013.

[167] S. S. Kalamkar, A. Banerjee, and A. K. Gupta, "SNR wall for generalized energy detection under noise uncertainty in cognitive radio," in *Proceedings of Asia-Pacific Conference on Communications (APCC)*, pp. 375–380, 2013.

[168] A. Taherpour, M. Nasiri-Kenari, and S. Gazor, "Multiple antenna spectrum sensing in cognitive radios," *IEEE Transactions on Wireless Communications*, vol. 9, no. 2, pp. 814–823, February 2010.

[169] R. Zhang, T. J. Lim, Y.-C. Liang, and Y. Zeng, "Multi-antenna based spectrum sensing for cognitive radios: A GLRT approach," *IEEE Transactions on Communications*, vol. 58, no. 1, pp. 84–88, January 2010.

[170] K. Umebayashi, H. Tsuchiya, and Y. Suzuki, "Analysis of optimal weighted cooperative spectrum sensing with multiple antenna elements," *IEICE Transactions on Communications*, vol. E95.B, no. 10, pp. 3261–3269, October 2012.

[171] A. Singh, M. Bhatnagar, and R. Mallik, "Cooperative spectrum sensing in multiple antenna based cognitive radio network using an improved energy detector," *IEEE Communications Letters*, vol. 16, no. 1, pp. 64–67, January 2012.

[172] A. Papoulis, *Probability, Random Variables and Stochastic Processes.* McGraw-Hill, 3rd ed., 1991.

[173] V. Aalo, "Performance of maximal-ratio diversity systems in a correlated Nakagami-fading environment," *IEEE Transactions on Communications*, vol. 43, no. 8, pp. 2360–2369, August 1995.

[174] S. Loyka, "Channel capacity of MIMO architecture using exponential correlation matrix," *IEEE Communications Letters*, vol. 5, no. 9, pp. 369–371, September 2001.

[175] M. Haenggi, *Stochastic Geometry for Wireless Networks.* NY: Cambridge University Press, 2013.

[176] N. Jacobson, *Basic Algebra I.* W. H. Freeman and Company, 2nd ed., 1996.

Appendix A

Appendices for Chapter 2

A.1 Proof of Proposition 2.1

For notational simplicity, we drop the iteration index l. The optimal primal and dual variables must satisfy the Karush-Kuhn-Tucker (KKT) stationarity conditions. Taking derivatives of $\mathcal{L}_1$ with respect to $(E_{i\mathrm{h}}, E_{i\mathrm{p}})$ and $\mathcal{L}_2$ with respect to (t_0, t_i), we obtain

$$\frac{\gamma_{i\mathrm{h}}}{1+x_i^*} - \mu_i^* = 0, \qquad \forall i, \tag{A.1a}$$

$$\frac{\lambda\gamma_{i\mathrm{p}}}{1+\gamma_{\mathrm{pp}}+y^*} - \mu_i^* = 0, \ \forall i, \tag{A.1b}$$

$$\lambda^* \ln\left(1+\gamma_{\mathrm{pp}}+y^*\right) - \frac{\lambda^* y^*}{1+\gamma_{\mathrm{pp}}+y^*} + \kappa^* Q_2 - 2\nu^* = 0, \tag{A.1c}$$

$$\ln\left(1+x_i^*\right) - \frac{x_i^*}{1+x_i^*} - \nu^* = 0, \qquad \forall i, \tag{A.1d}$$

where $x_i^* = \frac{\gamma_{i\mathrm{h}} E_{i\mathrm{h}}^*}{t_i^*}$, $y^* = \frac{\sum_{\mathrm{SU}_i \in \mathcal{S}_\mathcal{D}} \gamma_{i\mathrm{p}} E_{i\mathrm{p}}^*}{t_0^*}$. The corresponding KKT complementary slackness conditions are

$$\lambda^* \left(\bar{R}_{\mathrm{p}} - t_0^* \ln\left(1+\gamma_{\mathrm{pp}} + \frac{\sum_{\mathrm{SU}_i \in \mathcal{S}_\mathcal{D}} \gamma_{i\mathrm{p}} E_{i\mathrm{p}}^*}{t_0^*}\right)\right) = 0, \tag{A.2a}$$

$$\kappa^* \left(\bar{R}_{\mathrm{p}} - Q_1 t_{\mathrm{e}}^* - Q_2 t_0^*\right) = 0, \tag{A.2b}$$

$$\mu_i^* (E_{i\mathrm{p}}^* + E_{i\mathrm{h}}^* - (P_{\mathrm{e}} + \theta_i) t_{\mathrm{e}}^*) = 0, \ \forall i, \tag{A.2c}$$

$$\nu^* (t_{\mathrm{e}}^* + 2t_0^* + \sum_{i=1}^{N} t_i^* - 1) = 0. \tag{A.2d}$$

We learn from Proposition 2.2 that the primary rate constraint (2.14b), energy neutrality constraint (2.14d), and total time constraint (2.14e) must be satisfied with equality. Therefore, we infer from (A.2a)-(A.2d) that $(\lambda, \boldsymbol{\mu}, \nu) > 0$ and $\kappa \geq 0$. On rearranging the equations (A.1a)-(A.1d) and using (A.2d), we write the optimal solution for the STORA problem as given in Proposition 2.1.

A.2 Proof of Proposition 2.4

The Lagrangian $\mathcal{L}_3$ of the time allocation subproblem of ETA is given by

$$\begin{aligned}\mathcal{L}_3 = &\sum_{i=1}^{N} R_i(E_{i\mathrm{h}}, t_{\mathrm{eq}}) - \lambda\left(\bar{R}_{\mathrm{p}} - R_{\mathrm{p,c}}(\boldsymbol{E}_{\mathbf{sp}}, t_{\mathrm{e}}, t_0)\right) \\ &- \kappa\left(\bar{R}_{\mathrm{p}} - Q_1 t_{\mathrm{e}} - Q_2 t_0\right) - \nu(2t_0 + t_{\mathrm{e}} + \sum_{i=1}^{N} t_i - 1). \end{aligned} \tag{A.3}$$

The optimal t^*_{eq} that maximizes the Lagrangian $\mathcal{L}_3$ can be obtained from

$$\frac{\partial \mathcal{L}_3}{\partial t_{\mathrm{eq}}} = \sum_{i=1}^{N} \ln\left(1 + \frac{\gamma_{i\mathrm{h}} E^*_{i\mathrm{h}}}{t^*_{\mathrm{eq}}}\right) - \frac{\frac{\gamma_{i\mathrm{h}} E^*_{i\mathrm{h}}}{t^*_{\mathrm{eq}}}}{1 + \frac{\gamma_{i\mathrm{h}} E^*_{i\mathrm{h}}}{t^*_{\mathrm{eq}}}} - N\nu^* = 0, \tag{A.4}$$

which forms Proposition 2.4.

A.3 Proof of Proposition 2.5

The energy and time allocation on the access link that maximize (2.52) and (2.53) are found using KKT stationarity conditions. On differentiating (2.52) and (2.53) with respect to $E_{i\mathrm{h}}$ and t_i, we obtain

$$\rho_i \frac{\gamma_{i\mathrm{h}}}{1 + \frac{\gamma_{i\mathrm{h}} E^*_{i\mathrm{h}}}{t^*_i}} - \mu^*_i = 0, \qquad \forall i \tag{A.5}$$

$$\ln\left(1 + \frac{\gamma_{i\mathrm{h}} E^*_{i\mathrm{h}}}{t^*_i}\right) - \frac{\frac{\gamma_{i\mathrm{h}} E^*_{i\mathrm{h}}}{t^*_i}}{1 + \frac{\gamma_{i\mathrm{h}} E^*_{i\mathrm{h}}}{t^*_i}} - \frac{\nu^*}{\rho^*_i} = 0, \quad \forall i. \tag{A.6}$$

The KKT stationarity conditions with respect to $E_{i\mathrm{p}}$ and t_0 are same as that of STORA as given in (A.1b) and (A.1c). The primal variable t_{e} is obtained using KKT complementary

slackness condition (A.2d) and $R_{\min}$ is found using the iterative algorithm discussed in section 2.4.2. On rearranging (A.5) and (A.6), we obtain the results in Proposition 2.5.

A.4 Proof of Proposition 2.6

The Lagrangian $\mathcal{L}_5$ of the energy allocation subproblem for the PTA scheme is

$$\begin{aligned}\mathcal{L}_5 = &\sum_{i=1}^{N} R_i(E_{i\mathrm{h}}, \zeta\gamma_{i\mathrm{p}}E_{i\mathrm{p}}) - \lambda\left(\bar{R}_{\mathrm{p}} - R_{\mathrm{p,c}}(\boldsymbol{E}_{\mathbf{sp}}, t_{\mathrm{e}}, t_0)\right)\\ &- \sum_{i=1}^{N} \mu_i(E_{i\mathrm{p}} + E_{i\mathrm{h}} - (P_{\mathrm{e}} + \theta_i)t_{\mathrm{e}}).\end{aligned}$$

The first order stationarity condition of $\mathcal{L}_5$ with respect to $E_{i\mathrm{h}}$ and $E_{i\mathrm{p}}$ are given by

$$\begin{aligned}\frac{\partial\mathcal{L}_5}{\partial E_{i\mathrm{h}}} &= \frac{\gamma_{i\mathrm{h}}}{1+\frac{\gamma_{i\mathrm{h}}E^*_{i\mathrm{h}}}{\zeta\gamma_{i\mathrm{p}}E^*_{i\mathrm{p}}}} - \mu_i^* = 0,\\ \frac{\partial\mathcal{L}_5}{\partial E_{i\mathrm{p}}} &= \zeta^*\gamma_{i\mathrm{p}}\ln(1+z_i^*) - \frac{z_i^*}{1+z_i^*},\\ &\quad - \frac{\lambda^*\gamma_{i\mathrm{p}}}{1+\gamma_{\mathrm{pp}}+\frac{\sum_{i=1}^{N}\gamma_{i\mathrm{p}}E^*_{i\mathrm{p}}}{t_0^*}} - \mu_i^* - \zeta^*\nu^* = 0,\end{aligned} \tag{A.7}$$

with $z_i^* = \frac{\gamma_{i\mathrm{h}}E^*_{i\mathrm{h}}}{\zeta^*\gamma_{i\mathrm{p}}E^*_{i\mathrm{p}}}$. The solution of t_0 and t_{e} is same as that of STORA scheme. The solution of the above equations and the feasibility condition $t_i^* = \gamma_{i\mathrm{p}}\zeta^*E^*_{i\mathrm{p}}\ \forall i$ form Proposition 2.6.

Appendix B

Appendices for Chapter 4

B.1 Proof of (4.4)

From (4.3), conditioned on $g_{\text{sp}} = x$ we can write

$$\mathrm{P}_{\text{p,out,ST}}\Big|_{g_{\text{sp}}=x} = \mathbb{P}\bigg(g_{\text{pp}} \leq \frac{\theta_{\text{p}}(P_{\text{s}}x + N_0)}{P_{\text{p}}}\bigg). \tag{B.1}$$

Thus, using (4.2), we can write (B.1) as

$$\mathrm{P}_{\text{p,out,ST}}\Big|_{g_{\text{sp}}=x} = \frac{\Upsilon\bigg(m_{\text{pp}}, \alpha_{\text{pp}}\frac{\theta_{\text{p}}(P_{\text{s}}x+N_0)}{P_{\text{p}}}\bigg)}{\Gamma(m_{\text{pp}})}. \tag{B.2}$$

When m_{pp} is a positive integer, we can write the lower incomplete Gamma function as [107, 8.352]

$$\Upsilon(a, b) = (a-1)!\left(1 - \exp(-b)\sum_{k=0}^{a-1}\frac{b^k}{k!}\right). \tag{B.3}$$

Then, using (B.3) in (B.2) and unconditioning over g_{sp}, we can write (4.3) as

$$\begin{aligned}\mathrm{P}_{\text{p,out,ST}}\Big|_{g_{\text{sp}}=x} &= 1 - \exp\left(-\alpha_{\text{pp}}\tfrac{\theta_{\text{p}}(P_{\text{s}}x+N_0)}{P_{\text{p}}}\right)\\ &\quad\times\sum_{k=0}^{m_{\text{pp}}-1}\frac{\left(\alpha_{\text{pp}}\frac{\theta_{\text{p}}(P_{\text{s}}x+N_0)}{P_{\text{p}}}\right)^k}{k!}.\end{aligned} \tag{B.4}$$

Using (4.1) and (B.4), and unconditioning over g_{sp}, we can write (4.3) as

$$\mathrm{P}_{\text{p,out,ST}} = \int_0^\infty \mathrm{P}_{\text{p,out}}\Big|_{g_{\text{sp}}=x}\frac{\alpha_{\text{sp}}^{m_{\text{sp}}}}{\Gamma(m_{\text{sp}})}x^{m_{\text{sp}}-1}\times\exp(-\alpha_{\text{sp}}x)\mathrm{d}x. \tag{B.5}$$

Simplifying (B.5) and using binomial expansion, we get

$$\mathrm{P}_{\mathrm{p,out,ST}} = 1 - \frac{\alpha_{\mathrm{sp}}^{m_{\mathrm{sp}}} \exp\left(\frac{-\alpha_{\mathrm{pp}}\theta_{\mathrm{p}}N_0}{P_{\mathrm{p}}}\right)}{\Gamma(m_{\mathrm{sp}})} \sum_{k=0}^{m_{\mathrm{pp}}-1} \left(\frac{\alpha_{\mathrm{pp}}\theta_{\mathrm{p}}N_0}{P_{\mathrm{p}}}\right)^k \frac{1}{k!} \sum_{t=0}^{k} \binom{k}{t} \left(\frac{P_{\mathrm{s}}}{N_0}\right)^t \times \int_0^{\infty} x^{m_{\mathrm{sp}}+t-1} \exp\left(-x\left(\frac{\alpha_{\mathrm{pp}}\theta_{\mathrm{p}}P_{\mathrm{s}}}{P_{\mathrm{p}}} + \alpha_{\mathrm{sp}}\right)\right) \mathrm{d}x. \tag{B.6}$$

Solving the integral in (B.6), we get the required expression in (4.4).

B.2 Proof of (4.10)

From (4.8), we can see that $\gamma_{i\mathrm{d}}$ and $\gamma_{j\mathrm{s}}$ $(i \neq j, j \in \{1, 2, \ldots, M\})$ contain the common term g_{pd}, which makes them dependent. Thus, conditioned on $g_{\mathrm{pd}} = x$, we can write the CDF of γ_{tot}^N as

$$\mathbb{P}\left(\gamma_{\mathrm{tot}}^N \leq \gamma\big|_{g_{\mathrm{pd}}=x}\right) = \prod_{i=1}^{N}\left[1 - (1 - \mathbb{P}(\gamma_i \leq \gamma)) \underbrace{\left(1 - \mathbb{P}\left(\gamma_{i\mathrm{d}} \leq \gamma\big|_{g_{\mathrm{pd}}=x}\right)\right)}_{\mathcal{I}}\right]. \tag{B.7}$$

Now, we write

$$\begin{aligned} \mathcal{I} &= 1 - \mathbb{P}\left(\gamma_{i\mathrm{d}} \leq \gamma\big|_{g_{\mathrm{pd}}=x}\right) \\ &= 1 - \mathbb{P}\left(g_{i\mathrm{d}} \leq \frac{\gamma(P_{\mathrm{p}}x + N_0)}{P_i}\right). \end{aligned} \tag{B.8}$$

Using (4.2), we can write $\mathcal{I}$ in (B.8) as

$$\mathcal{I} = \frac{\Gamma\left(m_{\mathrm{rd}}, \alpha_{\mathrm{rd}}\frac{\gamma(P_{\mathrm{p}}x+N_0)}{P_{\mathrm{r}}}\right)}{\Gamma(m_{\mathrm{rd}})}. \tag{B.9}$$

Using [107, 8.352]

$$\Gamma(k, t) = (k-1)!\exp(-t)\sum_{n=0}^{k-1}\frac{t^n}{n!}, k = 1, 2, \ldots, \tag{B.10}$$

we can write (B.9) as

$$\mathcal{I} = \exp\left(-\alpha_{\mathrm{rd}}\frac{\gamma(P_{\mathrm{p}}x + N_0)}{P_{\mathrm{r}}}\right) \sum_{k=0}^{m_{\mathrm{rd}}-1} \frac{1}{k!}\left(\alpha_{\mathrm{rd}}\frac{\gamma(P_{\mathrm{p}}x + N_0)}{P_{\mathrm{r}}}\right)^k. \tag{B.11}$$

Now, let

$$\mathcal{A} = 1 - \mathbb{P}(\gamma_i \leq \gamma) = \mathbb{P}\left(\frac{P_{\mathrm{s}}g_{\mathrm{s}i}}{P_{\mathrm{p}}g_{\mathrm{p}i} + N_0} > \gamma\right). \tag{B.12}$$

Using the procedure to derive (4.4), we can write (B.12) as

$$\mathcal{A} = \frac{\alpha_{\rm pr}^{m_{\rm pr}} \exp\left(\frac{-\alpha_{\rm sr}\gamma N_0}{P_{\rm s}}\right)}{\Gamma(m_{\rm pr})} \sum_{k=0}^{m_{\rm sr}-1} \left(\frac{\alpha_{\rm sr}\gamma N_0}{P_{\rm s}}\right)^k \frac{1}{k!} \times \left(\sum_{t=0}^{k} \binom{k}{t} \left(\frac{P_{\rm p}}{N_0}\right)^t \times \frac{\Gamma(m_{\rm pr}+t)}{\left(\frac{\alpha_{\rm sr}\gamma P_{\rm p}}{P_{\rm s}} + \alpha_{\rm pr}\right)^{m_{\rm pr}+t}}\right). \tag{B.13}$$

From (B.11) and (B.13), we can write (B.7) as

$$\mathbb{P}\left((\gamma_{\rm tot}^N \leq \gamma\big|_{g_{\rm pd}=x}\right) = \left[1 - \mathcal{A}\exp\left(-\frac{\alpha_{\rm rd}\gamma N_0}{P_{\rm r}}\right) \sum_{k=0}^{m_{\rm rd}-1} \frac{1}{k!} \times \left(\alpha_{\rm rd}\frac{\gamma N_0}{P_{\rm r}}\right)^k \left(1 + x\frac{P_{\rm p}}{N_0}\right)^k \exp\left(-\alpha_{\rm rd}\frac{\gamma P_{\rm p} x}{P_{\rm r}}\right)\right]^N. \tag{B.14}$$

Now, we use the multinominal theorem [107] given by

$$\left(\sum_{k=0}^{W} a_k\right)^Z = \sum_{r_0=0}^{Z}\sum_{r_1=0}^{r_0}\cdots\sum_{r_{W-1}=0}^{r_{W-2}} \binom{Z}{r_0}\binom{r_0}{r_1}\cdots\binom{r_{W-2}}{r_{W-1}} \times a_0^{Z-r_0} a_1^{r_0-r_1}\ldots a_{W-1}^{r_{W-2}-r_{W-1}} a_W^{r_{W-1}}. \tag{B.15}$$

In accordance with (B.14), we express $\mathbb{P}\left((\gamma_{\rm tot}^N \leq \gamma\big|_{g_{\rm pd}=x}\right)$ as $(-1)^N\left(\sum_{k=0}^{m_{\rm SR-RD}} a_k\right)^N$, where

$$a_k = \mathcal{A}\exp\left(-\frac{\alpha_{\rm rd}\gamma N_0}{P_{\rm r}}\right)\frac{1}{k!}\left(\frac{\alpha_{\rm rd}\gamma N_0}{P_{\rm r}}\right)^k \exp\left(-\frac{\alpha_{\rm ss}\gamma P_{\rm p} x}{P_{\rm r}}\right)\left(1 + \frac{xP_{\rm p}}{N_0}\right)^k,$$

$\forall k = 0,\ldots,m_{\rm SR-RD}-1$ and $a_{m_{\rm SR-RD}} = -1$. Now, using the multinominal theorem given in (B.15) and rearranging, we get

$$\begin{aligned}\mathbb{P}\left(\gamma_{\rm tot}^N \leq \gamma\big|_{g_{\rm pd}=x}\right) = {} & \sum_{r_0=0}^{N}\sum_{r_1=0}^{r_0}\cdots\sum_{r_{m_{\rm rd}-1}=0}^{r_{m_{\rm rd}-2}} \binom{N}{r_0}\binom{r_0}{r_1}\cdots\binom{r_{m_{\rm rd}-2}}{r_{m_{\rm rd}-1}} \mathcal{A}^{N-r_{m_{\rm rd}-1}}(-1)^{N+r_{m_{\rm rd}-1}} \\ & \times \exp\left(-\frac{\alpha_{\rm rd}\gamma N_0(N-r_{m_{\rm rd}-1})}{P_{\rm r}}\right)\left(\frac{\alpha_{\rm rd}\gamma N_0}{P_{\rm r}}\right)^{R_{m_{\rm rd}}} \\ & \times \prod_{k=1}^{m_{\rm rd}-1}\left(\frac{1}{k!}\right)^{r_{k-1}-r_k}\left(1+\frac{xP_{\rm p}}{N_0}\right)^{R_{m_{\rm rd}}} \exp\left(-\frac{\alpha_{\rm rd}\gamma P_{\rm p} x(N-r_{m_{\rm rd}-1})}{P_{\rm r}}\right),\end{aligned} \tag{B.16}$$

where $R_{m_{\mathrm{rd}}} = \sum_{k=1}^{m_{\mathrm{rd}}-1} k(r_{k-1} - r_k)$. In the following step, we use binomial expansion of $\left(1 + \frac{xP_{\mathrm{p}}}{N_0}\right)^{R_{m_{\mathrm{rd}}}}$ and take expectation over g_{pd}. Then, we can write

$$\begin{aligned}
\mathrm{P}_{\mathrm{s,out}}^{N}(\gamma) = & \sum_{r_0=0}^{N} \sum_{r_1=0}^{r_0} \cdots \sum_{r_{m_{\mathrm{rd}}-1}=0}^{r_{m_{\mathrm{rd}}-2}} \binom{N}{r_0} \binom{r_0}{r_1} \cdots \binom{r_{m_{\mathrm{rd}}-2}}{r_{m_{\mathrm{rd}}-1}} \mathcal{A}^{N-r_{m_{\mathrm{rd}}-1}} (-1)^{N+r_{m_{\mathrm{rd}}-1}} \\
& \times \left[\exp\left(-\frac{\alpha_{\mathrm{rd}} \gamma N_0 (N - r_{m_{\mathrm{rd}}-1})}{P_{\mathrm{r}}} \right) \left(\frac{\alpha_{\mathrm{rd}} \gamma N_0}{P_{\mathrm{r}}} \right)^{R_{m_{\mathrm{rd}}}} \prod_{k=1}^{m_{\mathrm{rd}}-1} \left(\frac{1}{k!} \right)^{r_{k-1}-r_k} \right] \\
& \times \left[\sum_{p=0}^{R} \binom{R}{p} \left(\frac{P_{\mathrm{p}}}{N_0} \right)^{p} \int_{x=0}^{\infty} x^{p} \exp\left(-\frac{\alpha_{\mathrm{rd}} \gamma P_{\mathrm{p}} x (N - r_{m_{\mathrm{rd}}-1})}{P_{\mathrm{r}}} \right) \right. \\
& \left. \times \frac{\alpha_{\mathrm{pd}}^{m_{\mathrm{pd}}}}{(m_{\mathrm{pd}} - 1)!} x^{m_{\mathrm{pd}}-1} \exp\left(-\alpha_{\mathrm{pd}} x \right) \mathrm{d}x \right]. \qquad \text{(B.17)}
\end{aligned}$$

Solving the integration in (B.17), we get the required closed-form expression for the secondary outage probability given by (4.10).

Appendix C

Appendices for Chapter 5

C.1 Proof of (5.4)

Let $\mathcal{K}$ be $\Pr\left(\frac{P_{\rm p}g_i}{P_{\rm s}g_{{\rm s}i}} \leq \zeta_{\rm p}\right)$. Then, we can write

$$\mathcal{K} = \int_0^\infty \Pr\left(\frac{P_{\rm p}g_i}{P_{\rm s}y} \leq \zeta_{\rm p}\right) f_{g_{{\rm s}i}}(y){\rm d}y, \tag{C.1}$$

where $f_{g_{{\rm s}i}}(y)$ is the probability density function of $g_{{\rm s}i}$, and is given by $f_{g_{{\rm s}i}}(y) = \frac{1}{\Omega_{\rm sp}} \exp\left(-\frac{y}{\Omega_{\rm sp}}\right)$. Solving (C.1) and then substituting the value of $\mathcal{K}$ in (5.3), we obtain

$$\mathrm{P}_{\rm p,out,ST} = 1 - \left(\frac{P_{\rm p}\Omega_{\rm pp}}{P_{\rm s}\Omega_{\rm sp}\zeta_{\rm p} + P_{\rm p}\Omega_{\rm pp}}\right)^L. \tag{C.2}$$

Solving (C.2) for $P_{\rm s}$, we obtain the required expression in (5.4).

C.2 Proof of Proposition 5.2

From (5.15), we have

$$P_{\rm s,out} = 1 - \mathbb{P}\left(\gamma_{\rm r} \geq \zeta_{\rm s}, \gamma_{\rm d} \geq \zeta_{\rm s}\right), \tag{C.3}$$

where

$$\gamma_{\rm r} = \frac{P_{\rm sm}g_{\rm sr}}{\sum_{i=1}^{L} P_{\rm p}g_{i{\rm r}}} = \frac{P_{\rm sm}X}{U}, \tag{C.4}$$

$$\gamma_{\mathrm{d}} = \frac{\min\left(\frac{2\eta\alpha}{1-\alpha}\left(P_{\mathrm{sm}}g_{\mathrm{sr}} + \sum_{i=1}^{L} P_{\mathrm{p}}g_{i\mathrm{r}}\right), P_{\mathrm{r}}\right) g_{\mathrm{rd}}}{\sum_{i=1}^{L} P_{\mathrm{p}}g_{i\mathrm{s}}} = \frac{\min\left(\theta\left(P_{\mathrm{sm}}X + U\right), P_{\mathrm{r}}\right) Y}{Z}, \tag{C.5}$$

where $\theta = \frac{2\alpha\eta}{1-\alpha}$, $X = g_{\mathrm{sr}}$, $Y = g_{\mathrm{rd}}$, $Z = \sum_{i=1}^{L} P_{\mathrm{p}}g_{i\mathrm{d}}$, and $U = \sum_{i=1}^{L} P_{\mathrm{p}}g_{i\mathrm{r}}$. Then, X and Y are exponentially distributed with means $\Omega_x = \Omega_{\mathrm{sr}}$ and $\Omega_y = \Omega_{\mathrm{rd}}$, respectively, while Z and U are Gamma random variables with the shape parameter L and scale parameters $\Omega_z = P_{\mathrm{p}}\Omega_{\mathrm{pd}}$ and $\Omega_u = P_{\mathrm{p}}\Omega_{\mathrm{pr}}$, respectively. Note that, X, Y, Z, and U are mutually independent random variables, but γ_{r} and γ_{d} are dependent random variables due to the presence of common random variables X and U. Then, we can express the secondary outage probability as

$$P_{\mathrm{s,out}} = 1 - \mathcal{I}, \tag{C.6}$$

where $f_U(u)$, $f_X(x)$, $f_Z(z)$, and $f_Y(y)$ are PDFs of random variables U, X, Z, and Y, respectively, and

$$\mathcal{I} = \int_{u=0}^{\infty} \int_{x=\frac{\zeta_{\mathrm{s}}u}{P_{\mathrm{sm}}}}^{\infty} \int_{z=0}^{\infty} \int_{y=\frac{\zeta_{\mathrm{s}}z}{\min(\theta(P_{\mathrm{sm}}x+u), P_{\mathrm{r}})}}^{\infty} f_U(u) f_X(x) f_Z(z) f_Y(y)\, \mathrm{d}u\, \mathrm{d}x\, \mathrm{d}z\, \mathrm{d}y. \tag{C.7}$$

Then, integrating over Y, we obtain,

$$\mathcal{I} = \int_{u=0}^{\infty} \int_{x=\frac{\zeta_{\mathrm{s}}u}{P_{\mathrm{sm}}}}^{\infty} \int_{z=0}^{\infty} f_U(u) f_X(x) f_Z(z) \exp\left(-\frac{\zeta_{\mathrm{s}}z}{\min(\theta(P_{\mathrm{sm}}x+u), P_{\mathrm{r}})\Omega_{\mathrm{y}}}\right) \mathrm{d}u\, \mathrm{d}x\, \mathrm{d}z. \tag{C.8}$$

Now, let

$$\mathcal{I}_1 = \int_{z=0}^{\infty} f_Z(z) \exp\left(-\frac{\zeta_{\mathrm{s}}z}{\min(\theta(P_{\mathrm{sm}}x+u), P_{\mathrm{r}})\Omega_{\mathrm{y}}}\right) \mathrm{d}z. \tag{C.9}$$

Given Z is a Gamma random variable with the shape parameter L and scale parameter $\Omega_z = P_{\mathrm{p}}\Omega_{\mathrm{pd}}$, we have

$$\mathcal{I}_1 = \int_{z=0}^{\infty} \frac{z^{L-1}\exp\left(-\frac{z}{P_{\mathrm{p}}\Omega_{\mathrm{z}}}\right)}{\Gamma(L)(P_{\mathrm{p}}\Omega_{\mathrm{z}})^L} \exp\left(-\frac{\zeta_{\mathrm{s}}z}{\min(\theta(P_{\mathrm{sm}}x+u), P_{\mathrm{r}})\Omega_{\mathrm{y}}}\right) \mathrm{d}z. \tag{C.10}$$

Let

$$\mathcal{A}(u,x) = \min(\theta(P_{\rm sm}x + u), P_{\rm r})\Omega_{\rm y}. \tag{C.11}$$

Then, we can simplify (C.10) as

$$\mathcal{I}_1 = \frac{1}{\Gamma(L)(P_{\rm p}\Omega_{\rm z})^L} \int_{z=0}^{\infty} z^{L-1} \exp\left(-\left(\frac{1}{P_{\rm p}\Omega_{\rm z}} + \frac{\zeta_{\rm s}}{\mathcal{A}(u,x)}\right) z\right) {\rm d}z. \tag{C.12}$$

Using the definition of Gamma function as $\Gamma(L) = \int_{t=0}^{\infty} t^{L-1}\exp(-t){\rm d}t$, we can finally write (C.12) as

$$\mathcal{I}_1 = \frac{1}{(P_{\rm p}\Omega_{\rm z})^L}\left[\frac{1}{P_{\rm p}\Omega_{\rm z}} + \frac{\zeta_{\rm s}}{\mathcal{A}(u,x)}\right]^{-L}. \tag{C.13}$$

From (C.9) and (C.13), we can write (C.8) as

$$\mathcal{I} = \int_{u=0}^{\infty}\int_{x=\frac{\zeta_{\rm s}u}{P_{\rm sm}}}^{\infty} \frac{1}{(P_{\rm p}\Omega_{\rm z})^L}\left[\frac{1}{P_{\rm p}\Omega_{\rm z}} + \frac{\zeta_{\rm s}}{\mathcal{A}(u,x)}\right]^{-L} \times f_U(u) f_X(x) {\rm d}u\, {\rm d}x. \tag{C.14}$$

Note that, $\mathcal{A}(u,x)$ is minimum of two terms. Thus, we have,

$$\mathcal{A}(u,x) = \begin{cases} \theta(P_{\rm sm}x + u)\Omega_{\rm y}, & \text{if } x \le \frac{P_{\rm r}-\theta u}{\theta P_{\rm sm}} \\ P_{\rm r}\Omega_{\rm y}, & \text{if } x > \frac{P_{\rm r}-\theta u}{\theta P_{\rm sm}}. \end{cases} \tag{C.15}$$

Comparing the threshold $\frac{P_{\rm r}-\theta u}{\theta P_{\rm sm}}$ for x given in (C.15) with the lower limit of x in (C.14), we have following two cases over which we have evaluate the double integral in (C.14).

- Case I: $\frac{P_{\rm r}-\theta u}{\theta P_{\rm sm}} \ge \frac{\zeta_{\rm s}u}{P_{\rm sm}}$. This case corresponds to $u \le \frac{P_{\rm r}}{(1+\zeta_{\rm s}\theta)}$.
- Case II: $\frac{P_{\rm r}-\theta u}{\theta P_{\rm sm}} < \frac{\zeta_{\rm s}u}{P_{\rm sm}}$. This case corresponds to $u > \frac{P_{\rm r}}{(1+\zeta_{\rm s}\theta)}$.

For notational simplicity, let $\delta_1 = \frac{P_{\rm r}}{(1+\zeta_{\rm s}\theta)}$. Thus, Case I happens only when $u \le \delta_1$ and Case II happens only when $u > \delta_1$. Given these two cases define the range of u, we can split (C.14) as follows:

$$\mathcal{I} = \frac{1}{(P_{\rm p}\Omega_{\rm z})^L}(I_1 + I_2 + I_3), \tag{C.16}$$

where

$$I_1 = \int_{u=0}^{\delta_1} \int_{x=\frac{\zeta_s u}{P_{sm}}}^{\frac{P_r-\theta u}{\theta P_{sm}}} f_U(u) f_X(x) \left(\frac{1}{P_p \Omega_z} + \frac{\zeta_s}{\theta(P_{sm}x + u)\Omega_y} \right)^{-L} \mathrm{d}u \, \mathrm{d}x, \tag{C.17}$$

$$I_2 = \int_{u=0}^{\delta_1} \int_{x=\frac{P_r-\theta u}{\theta P_{sm}}}^{\infty} f_U(u) f_X(x) \left(\frac{1}{P_p \Omega_z} + \frac{\zeta_s}{P_r \Omega_y} \right)^{-L} \mathrm{d}u \, \mathrm{d}x, \tag{C.18}$$

and

$$I_3 = \int_{u=\delta_1}^{\infty} \int_{x=\frac{\zeta_s u}{P_{sm}}}^{\infty} f_U(u) f_X(x) \left(\frac{1}{P_p \Omega_z} + \frac{\zeta_s}{P_r \Omega_y} \right)^{-L} \mathrm{d}u \, \mathrm{d}x. \tag{C.19}$$

The double integral in (C.17) cannot be expressed in a closed form; but, we can evaluate it numerically. However, we can derive the double integrals in (C.18) and (C.19) in closed-forms as follows:

$$I_2 = \left(\frac{1}{P_p \Omega_z} + \frac{\zeta_s}{P_r \Omega_y} \right)^{-L} \times I_{21} \tag{C.20}$$

where

$$I_{21} = \int_{u=0}^{\delta_1} \int_{x=\frac{P_r-\theta u}{\theta P_{sm}}}^{\infty} f_U(u) f_X(x) \mathrm{d}u \, \mathrm{d}x. \tag{C.21}$$

Averaging over X, we can write (C.21) as

$$I_{21} = \int_{u=0}^{\delta_1} \exp\left(-\frac{P_r - \theta u}{\theta P_{sm} \Omega_x} \right) \frac{u^{L-1} \exp\left(-\frac{u}{P_p \Omega_u} \right)}{\Gamma(L)(P_p \Omega_u)^L} \mathrm{d}u, \tag{C.22}$$

Using the definition of lower incomplete Gamma function as $\Upsilon(a, b) = \int_0^b t^{a-1} \exp(-t) \mathrm{d}t$, we can write (C.22) as

$$I_{21} = \frac{\Upsilon(L, \omega\delta_1) \exp\left(-\frac{P_r}{\theta P_{sm} \Omega_{sr}} \right)}{\Gamma(L)(P_p \Omega_{pr})^L \omega^L}, \tag{C.23}$$

where $\omega = \frac{1}{P_p \Omega_{pr}} - \frac{1}{P_{sm} \Omega_{sr}}$. Substituting (C.23) in (C.20), we get the closed-form expression of I_2 as in (5.17b). Proceeding in the similar manner to obtain closed-form for I_2, we can obtain a closed-form expression for I_3 as given in (5.17c). Once I_1, I_2, and I_3 are calculated, we can get $\mathcal{I}$ from (C.16), and in turn, we write the secondary outage probability by (C.6).

Appendix D

Appendices for Chapter 6

D.1 Derivation of (6.4)

From (6.3), we have

$$\mathbb{P}\left(P_{\mathcal{I}} g_{\mathrm{rp}} > \mathcal{I}_{\mathrm{p}}\right) \leq \Theta_{\mathrm{p}}. \tag{D.1}$$

Since g_{rp} is exponentially distributed with mean Ω_{rp}, we can write (D.1) as

$$\exp\left(-\frac{\mathcal{I}_{\mathrm{p}}}{P_{\mathcal{I}}\Omega_{\mathrm{rp}}}\right) \leq \Theta_{\mathrm{p}}. \tag{D.2}$$

Note that, at the maximum allowed $P_{\mathcal{I}}$, the inequality in (D.2) becomes an equality. Then, we can write the maximum allowed $P_{\mathcal{I}}$ as given in (6.4).

D.2 Proof of Proposition 6.1

We note that the maximum allowed power P satisfies the primary's interference constraint in (6.2) with equality. That is,

$$\mathbb{P}\left(P(g_{\mathrm{sp}} + g_{\mathrm{dp}}) > \mathcal{I}_{\mathrm{p}}\right) = \Theta_{\mathrm{p}}. \tag{D.3}$$

We can write left hand side of (D.3) as

$$\begin{aligned}\mathbb{P}\left(P(g_{\mathrm{sp}} + g_{\mathrm{dp}}) > \mathcal{I}_{\mathrm{p}}\right) &= 1 - \mathbb{P}\left(P(g_{\mathrm{sp}} + g_{\mathrm{dp}}) \leq \mathcal{I}_{\mathrm{p}}\right) \\ &= 1 - \mathbb{P}\left((g_{\mathrm{sp}} + g_{\mathrm{dp}}) \leq \frac{\mathcal{I}_{\mathrm{p}}}{P}\right).\end{aligned} \tag{D.4}$$

Let $Z = (g_{\rm sp} + g_{\rm dp})$. Since $g_{\rm sp}$ and $g_{\rm dp}$ are exponentially distributed random variables with means $\Omega_{\rm sp}$ and $\Omega_{\rm dp}$, we can write the probability density function of Z as [172]

$$f_Z(z) = \begin{cases} \frac{\exp\left(-\frac{z}{\Omega_{\rm sp}}\right)}{\Omega_{\rm sp}-\Omega_{\rm dp}} + \frac{\exp\left(-\frac{z}{\Omega_{\rm dp}}\right)}{\Omega_{\rm dp}-\Omega_{\rm sp}}, & \text{if } \Omega_{\rm sp} \neq \Omega_{\rm dp} \\ \left(\frac{1}{\Omega_{\rm sp}}\right)^2 z \exp\left(-\frac{z}{\Omega_{\rm sp}}\right), & \text{if } \Omega_{\rm sp} = \Omega_{\rm dp}. \end{cases} \tag{D.5}$$

Note that Z can take only non-negative values as it is the sum of two exponential random variables. Using (D.5) in (D.4), we can write

$$\begin{aligned} \mathbb{P}\left(P(g_{\rm sp} + g_{\rm dp}) > \mathcal{I}_{\rm p}\right) &= \mathbb{P}\left(Z < \frac{\mathcal{I}_{\rm p}}{P}\right) \\ &= \int_0^{\frac{\mathcal{I}_{\rm p}}{P}} f_Z(z)\mathrm{d}z. \end{aligned} \tag{D.6}$$

Evaluating the integral in (D.6), we get the required equality in (6.17).

D.3 Derivation of (6.20)

At high SNR, using the channel reciprocity between SR and SD and substituting $\gamma_{\rm r}$ from (6.9) and $\gamma_{\rm d}$ from (6.22) in (6.16), and then using (6.16) and (6.18), we can write the secrecy outage probability for PS policy as

$$\begin{aligned} P_{\rm out} &= \mathbb{P}\left(\frac{1 + \frac{\eta\beta(1-\beta)Pg_{\rm sr}g_{\rm rd}}{N_0(\eta\beta g_{\rm rd}+(1-\beta))}}{1 + \frac{(1-\beta)Pg_{\rm sr}}{(1-\beta)Pg_{\rm rd}+N_0}} < \delta\right), \\ &= \mathbb{P}\left(\nu(X)g_{\rm sr} < \delta - 1\right)\Big|_{X=g_{\rm rd}}, \end{aligned} \tag{D.7}$$

where

$$\nu(x) = (1-\beta)\left(\frac{\eta\beta Px}{N_0\left(\eta\beta x + (1-\beta)\right)} - \frac{P\delta}{P(1-\beta)x + N_0}\right). \tag{D.8}$$

Based on the sign of $\nu(X)$, we split (D.7) as

$$\begin{aligned} P_{\rm out} = &\mathbb{P}\left(g_{\rm sr} < \frac{\delta-1}{\nu(X)}\middle|\nu(X) \geq 0\right)\mathbb{P}\left(\nu(X) \geq 0\right) \\ &+ \underbrace{\mathbb{P}\left(g_{\rm sr} \geq \frac{\delta-1}{\nu(X)}\middle|\nu(X) < 0\right)}_{=1}\mathbb{P}\left(\nu(X) < 0\right). \end{aligned} \tag{D.9}$$

In (D.9), $\mathbb{P}\left(g_{\rm sr} \geq \frac{\delta-1}{\nu(X)}\middle|\nu(X)<0\right) = 1$, because $g_{\rm sr}$ being an exponential random variable always takes non-negative values. Also, we have

$$\nu(x)\begin{cases} \geq 0, & \text{if } \theta_1 \leq x < \infty \\ < 0, & \text{if } 0 \leq x < \theta_1, \end{cases} \tag{D.10}$$

where

$$\theta_1 = \frac{\frac{\delta-1}{1-\beta} + \sqrt{\left(\frac{\delta-1}{1-\beta}\right)^2 + 4\delta\frac{P}{\eta\beta N_0}}}{2(P/N_0)}. \tag{D.11}$$

Note that θ_1 is the positive root of the equation $\nu(x) = 0$. Using (D.10), we can write (D.9) as

$$\begin{aligned} P_{\rm out} &= \int_{\theta_1}^{\infty}\left(1 - \exp\left(-\frac{\delta-1}{\nu(x)\Omega_{\rm sr}}\right)\right) f_X(x)\,{\rm d}x + \int_0^{\theta_1} f_X(x)\,{\rm d}x, \\ &= \underbrace{\int_0^{\theta_1} f_X(x)\,{\rm d}x + \int_{\theta_1}^{\infty} f_X(x)\,{\rm d}x}_{=1} \\ &\quad - \int_{\theta_1}^{\infty}\left(\exp\left(-\frac{\delta-1}{\nu(x)\Omega_{\rm sr}}\right)\right) f_X(x)\,{\rm d}x. \end{aligned} \tag{D.12}$$

Substituting $f_X(x) = \frac{1}{\Omega_{\rm rd}}\exp\left(-\frac{x}{\Omega_{\rm rd}}\right)$ in the third integral of (D.12), we reach the required expression of $P_{\rm out}$ as in (6.20).

D.4 Proof of Proposition 6.3

We can write the power outage probability as

$$\begin{aligned} P_{\rm p,out} &= \mathbb{P}\left(P_R < \theta_H\right) \\ &= \mathbb{P}\left(P(g_{\rm sr} + g_{\rm rd}) < \theta_H\right) \\ &= \mathbb{P}\left((g_{\rm sr} + g_{\rm rd}) < \frac{\theta_H}{P}\right). \end{aligned} \tag{D.13}$$

Let $Z = (g_{\rm sr} + g_{\rm rd})$. Since $g_{\rm sr}$ and $g_{\rm rd}$ are exponentially distributed random variables with means $\Omega_{\rm sr}$ and $\Omega_{\rm rd}$, we can write the probability density function of Z as [172]

$$f_Z(z) = \begin{cases} \frac{\exp\left(-\frac{z}{\Omega_{\rm sr}}\right)}{\Omega_{\rm sr}-\Omega_{\rm rd}} + \frac{\exp\left(-\frac{z}{\Omega_{\rm rd}}\right)}{\Omega_{\rm rd}-\Omega_{\rm sr}}, & \text{if } \Omega_{\rm sr} \neq \Omega_{\rm rd} \\ \left(\frac{1}{\Omega_{\rm sr}}\right)^2 z\exp\left(-\frac{z}{\Omega_{\rm sr}}\right), & \text{if } \Omega_{\rm sr} = \Omega_{\rm rd}. \end{cases} \tag{D.14}$$

Note that Z can take only non-negative values as it is the sum of two exponential random variables. Using (D.14) in (D.13), we can write

$$\begin{aligned} P_{\text{p,out}} &= \mathbb{P}\left(Z < \frac{\theta_H}{P}\right) \\ &= \int_0^{\frac{\theta_H}{P}} f_Z(z)\mathrm{d}z. \end{aligned} \tag{D.15}$$

Evaluating the integral in (D.15), we get the required expression for the power outage probability as in (6.24).

D.5 Proof of Proposition 6.4

D.5.1 Proof of (6.26a)

We can write the probability of achieving the positive secrecy capacity as

$$\begin{aligned} P_{\text{pos}} &= (1 - P_{\text{p,out}})\mathbb{P}\left(R_{\text{sec}} > 0\right) \\ &= (1 - P_{\text{p,out}})\mathbb{P}\left(\frac{1}{2}\log_2\left[\frac{(1+\gamma_{\text{d}})}{(1+\gamma_{\text{r}})}\right]^+ > 0\right) \\ &= (1 - P_{\text{p,out}})\mathbb{P}\left(\gamma_{\text{d}} > \gamma_{\text{r}}\right). \end{aligned} \tag{D.16}$$

Substituting γ_{r} from (6.9) and γ_{d} from (6.15) in (D.16) , we obtain

$$\begin{aligned} \mathbb{P}\left(\gamma_{\text{d}} > \gamma_{\text{r}}\right) = \mathbb{P}\big[\big(\big(g_{\text{sr}} + g_{\text{rd}}\big) \\ \times P(1-\beta)\big(\eta\beta P g_{\text{rd}}^2 - N_0\big)\big) > N_0^2\big]. \end{aligned} \tag{D.17}$$

Then we can write

$$\begin{aligned} \mathbb{P}\left(\gamma_{\text{d}} > \gamma_{\text{r}}\right) &= \int_0^{\theta_2} F_{g_{\text{sr}}}(\psi(x)) f_{g_{\text{rd}}}(x)\,\mathrm{d}x \\ &+ \int_{\theta_2}^{\theta_3} \left[1 - F_{g_{\text{sr}}}(\psi(x))\right] f_{g_{\text{rd}}}(x)\,\mathrm{d}x \\ &+ \int_{\theta_3}^{\infty} \left[1 - F_{g_{\text{sr}}}(\psi(x))\right] f_{g_{\text{rd}}}(x)\,\mathrm{d}x \\ &= \frac{1}{\Omega_{\text{rd}}} \int_{\theta_2}^{\theta_3} \exp\left(-\left(\frac{\psi(x)}{\Omega_{\text{sr}}} + \frac{x}{\Omega_{\text{rd}}}\right)\right)\mathrm{d}x + \exp\left(-\frac{\theta_3}{\Omega_{\text{rd}}}\right), \end{aligned} \tag{D.18}$$

where

$$\psi(x) = \frac{N_0^2}{P(1-\beta)(\eta\beta P x^2 - N_0)} - x \tag{D.19}$$

with

$$\psi(x) \begin{cases} < 0, & 0 \leq x < \theta_2, \\ \geq 0, & \theta_2 \leq x \leq \theta_3, \\ < 0, & \theta_3 < x < \infty. \end{cases} \tag{D.20}$$

θ_2 is the positive root of the equation $g(x) = \eta\beta P x^2 - N_0 = 0$, and is given as

$$\theta_2 = \sqrt{\frac{N_0}{\eta\beta P}}, \tag{D.21}$$

while θ_3 is the real root of $\psi(x) = 0$ which is a cubic equation given as

$$x^3 - \mathcal{A}x - \mathcal{B} = 0, \tag{D.22}$$

where $\mathcal{A} = \frac{N_0}{\eta\beta P}$ and $\mathcal{B} = \frac{N_0^2}{\eta\beta(1-\beta)P^2}$. We obtain the solution to (D.22) using Cardano's formula [176], which allows us to find the real root of (D.22). The solution is given as

$$\theta_3 = \left(\frac{\mathcal{B}}{2} + \sqrt{\left(\frac{\mathcal{B}}{2}\right)^2 + \left(-\frac{\mathcal{A}}{3}\right)^3}\right)^{\frac{1}{3}} + \left(\frac{\mathcal{B}}{2} - \sqrt{\left(\frac{\mathcal{B}}{2}\right)^2 + \left(-\frac{\mathcal{A}}{3}\right)^3}\right)^{\frac{1}{3}}. \tag{D.23}$$

Substituting (D.18) in (D.16), we get the exact expression of the probability of positive secrecy rate given in (6.26a).

D.5.2 Proof of (6.26b)

Under high SNR approximation of γ_{d} given in (6.22), using (D.16), we can write the probability of positive secrecy rate as

$$P_{\mathrm{pos}} = (1 - P_{\mathrm{p,out}})\mathbb{P}\left(\frac{\eta\beta(1-\beta)P g_{\mathrm{sr}} g_{\mathrm{rd}}}{N_0\left(\eta\beta g_{\mathrm{rd}} + (1-\beta)\right)} > \frac{(1-\beta)P g_{\mathrm{sr}}}{(1-\beta)P g_{\mathrm{rd}} + N_0}\right), \tag{D.24}$$

where we have used γ_{r} from (6.9) with $P_{\mathrm{s}} = P_{\mathrm{d}} = P$ and $h_{\mathrm{dr}} = h_{\mathrm{rd}}$ (channel reciprocity between SR and SD). Simplifying (D.24), we obtain

$$\begin{aligned} P_{\mathrm{pos}} &= (1 - P_{\mathrm{p,out}})\mathbb{P}\left(g_{\mathrm{rd}} > \sqrt{\frac{N_0}{\eta\beta P}}\right) \\ &= (1 - P_{\mathrm{p,out}}) \exp\left(-\sqrt{\frac{\theta_2}{\Omega_{\mathrm{rd}}^2}}\right), \end{aligned} \tag{D.25}$$

where $\theta_2 = \frac{N_0}{\eta\beta P}$.

D.6 Proof of Proposition 6.5

For PS policy, we can write the ergodic secrecy rate as

$$\bar{R}_{\text{sec}} = (1 - P_{\text{p,out}})\mathbb{E}\left[\frac{1}{2}\left[\log_2\left(\frac{1+\gamma_{\text{d}}}{1+\gamma_{\text{r}}}\right)\right]^+\right] \tag{D.26}$$

$$\overset{\text{(a)}}{\geq} (1 - P_{\text{p,out}})\left[\mathbb{E}\left[\frac{1}{2}\log_2\left(\frac{1+\gamma_{\text{d}}}{1+\gamma_{\text{r}}}\right)\right]\right]^+$$

$$\overset{\text{(b)}}{=} (1 - P_{\text{p,out}})\max\left(\frac{1}{2\ln(2)}\left[\underbrace{\mathbb{E}\left[\ln\left(1+\frac{XZ}{Z+1}\right)\right]}_{T_1}\right.\right.$$

$$\left.\left. - \underbrace{\mathbb{E}\left[\ln\left(1+\frac{X}{Y+1}\right)\right]}_{T_2}\right], 0\right), \tag{D.27}$$

where $X = \frac{(1-\beta)Pg_{\text{sr}}}{N_0}$, $Y = \frac{(1-\beta)Pg_{\text{rd}}}{N_0}$, and $Z = \frac{\eta\beta g_{\text{rd}}}{1-\beta}$ are the exponential random variables with means $m_x = \frac{(1-\beta)P\Omega_{\text{sr}}}{N_0}$, $m_y = \frac{(1-\beta)P\Omega_{\text{rd}}}{N_0}$, and $m_z = \frac{\eta\beta\Omega_{\text{rd}}}{1-\beta}$, respectively. The inequality (a) is obtained by using the fact $\mathbb{E}\left[\max(U,V)\right] \geq \max\left(\mathbb{E}\left[U\right], \mathbb{E}\left[V\right]\right)$. Also, to obtain equality (b), we have used γ_{r} from (6.9) and γ_{d} from (6.22). We can further lower bound T_1 as

$$\begin{aligned} T_1 &= \mathbb{E}\left[\ln\left(1+\frac{XZ}{Z+1}\right)\right] \\ &= \mathbb{E}\left[\ln\left(1+\exp\left(\ln\left(\frac{XZ}{Z+1}\right)\right)\right)\right] \\ &\overset{\text{(c)}}{\geq} \ln\left(1+\exp\left(\mathbb{E}\left[\ln\left(\frac{XZ}{Z+1}\right)\right]\right)\right) \\ &= \ln\left(1+\exp\left(\underbrace{\mathbb{E}\left[\ln\left(XZ\right)\right]}_{\mathcal{J}_1} - \underbrace{\mathbb{E}\left[\ln\left(Z+1\right)\right]}_{\mathcal{J}_2}\right)\right), \end{aligned} \tag{D.28}$$

where we have used the convexity of $\ln(1 + t\exp(x))$ for $t > 0$ and Jensen's inequality to obtain inequality (c). We write

$$\mathcal{J}_1 = \mathbb{E}\left[\ln\left(XZ\right)\right] = \int_{x=0}^{\infty}\int_{z=0}^{\infty}\ln(xz)f_X(x)f_Z(z)\,\mathrm{d}x\,\mathrm{d}z,$$

which can be further be written in a compact form using [107, 4.331.1] as

$$\mathcal{J}_1 = -2\phi - \ln\left(\frac{1}{m_x m_z}\right), \tag{D.29}$$

where ϕ is the Euler's constant [107, 9.73]. We can write $\mathcal{J}_2$ as

$$\mathcal{J}_2 = \mathbb{E}\left[\ln\left(Z+1\right)\right] = \int_{z=0}^{\infty} \ln(z+1) f_Z(z)\,\mathrm{d}z, \tag{D.30}$$

which we can write using [107, 4.337.2] as

$$\mathcal{J}_2 = -\exp\left(\frac{1}{m_z}\right) \mathrm{Ei}\left(-\frac{1}{m_z}\right), \tag{D.31}$$

where $\mathrm{Ei}(x)$ is the exponential integral [107, 8.21]. Substituting (D.29) and (D.31) in (D.28), we get the required lower bound for T_1.

We can rewrite T_2 as

$$T_2 = \mathbb{E}\left[\ln\left(1+\gamma_{\mathrm{r}}\right)\right] = \int_{u=0}^{\infty} \ln(1+u) f_{\gamma_{\mathrm{r}}}(u)\,\mathrm{d}u. \tag{D.32}$$

Using the integration by parts method, we can rewrite (D.32) as

$$T_2 = \int_{u=0}^{\infty} \frac{1}{1+u}\left[1 - F_{\gamma_{\mathrm{r}}}(u)\right]\mathrm{d}u, \tag{D.33}$$

where we can write the cumulative distribution function (CDF) $F_{\gamma_{\mathrm{r}}}(u)$ as

$$\begin{aligned} F_{\gamma_{\mathrm{r}}}(u) &= \int_{y=0}^{\infty} F_X((1+y)u) f_Y(y)\,\mathrm{d}y \\ &= \frac{1}{m_y}\int_{y=0}^{\infty} \left[1 - \exp\left(-\frac{(1+y)u}{m_x}\right)\right] \exp\left(-\frac{y}{m_y}\right)\mathrm{d}y \\ &= 1 - \frac{m_x}{m_x + u m_y}\exp\left(-\frac{u}{m_x}\right). \end{aligned} \tag{D.34}$$

Substituting (D.34) in (D.33) and using [107, 3.353.3] and [107, 3.352.4], we finally obtain the required expression for T_2 as in (6.33b).

Appendix E

Appendix for Chapter 9

E.1 Proof of (9.11)

Let I be defined as

$$\begin{aligned} I &= \mathbb{E}\left[|Z_m|^p|Z_m|^p\right] \\ &= \int_0^\infty \int_0^\infty |z_m|^p|z_n|^p f(z_m, z_n)\mathrm{d}z_m\mathrm{d}z_n, \end{aligned} \tag{E.1}$$

where $f(z_m, z_n)$ is the joint probability density function of Z_m and Z_n. $\mathbf{Z}_{mn} = [Z_m\ Z_n]$ is a bivariate distribution with mean $\mathbf{M} = [0\ \ 0]$ and covariance matrix

$$\begin{aligned} \mathbf{V} &= \begin{bmatrix} r^2 & \gamma\rho^{|m-n|} \\ \gamma\rho^{|m-n|} & r^2 \end{bmatrix} \\ &= \begin{bmatrix} r^2 & cr^2 \\ cr^2 & r^2 \end{bmatrix}, \end{aligned} \tag{E.2}$$

where r is $\sqrt{1+\gamma}$ under H_1, and c is given by

$$c = \frac{\gamma\rho^{|m-n|}}{1+\gamma}. \tag{E.3}$$

So $f(z_m, z_n)$ can be written as

$$f(z_m, z_n) = \frac{1}{2\pi r^2\sqrt{1-c^2}} \exp\left(-\frac{1}{2}\frac{1}{1-c^2}\left(\frac{z_m^2}{r^2} - 2c\frac{z_m z_n}{r^2} + \frac{z_n^2}{r^2}\right)\right). \tag{E.4}$$

Thus, the integration I to be solved, is obtained by substituting (E.4) in (E.1). By using transformation of random variables, $U = \frac{Z_m}{r}$ and $V = \frac{Z_n}{r}$, we can write (E.1) as

$$I = \frac{1}{2\pi\sqrt{1-c^2}} r^{2p} \int_0^\infty \int_0^\infty |u|^p |v|^p \exp\left(-\frac{1}{2}\frac{1}{1-c^2}\left(u^2 - 2cuv + v^2\right)\right) \mathrm{d}u\, \mathrm{d}v. \tag{E.5}$$

We again make use of transformation of random variables, $U = A\cos t$ and $V = A\sin t$. Then, we can write (E.5) as

$$I = \frac{1}{2^p}\frac{r^{2p}}{2\pi\sqrt{1-c^2}} \int_0^{2\pi} |\sin 2t|^p \int_0^\infty |a|^{2p+1} \exp\left(-\frac{1}{2}\frac{a^2}{1-c^2}\left(1 - c\sin 2t\right)\right) \mathrm{d}a\, \mathrm{d}t. \tag{E.6}$$

We first solve inner integral I_1 given as

$$I_1 = \int_0^\infty |a|^{2p+1} \exp\left(-\frac{1}{2}\frac{a^2}{1-c^2}\left(1 - c\sin 2t\right)\right) \mathrm{d}a. \tag{E.7}$$

Let $k = \frac{1}{2}\frac{1}{1-c^2}\left(1 - c\sin 2t\right)$. Substituting $ka^2 = w$, the inner integral I_1 becomes

$$\begin{aligned} I_1 &= \frac{1}{2k}\int_0^\infty \left|\frac{w}{k}\right|^p \exp(-w)\mathrm{d}w \\ &= 2^p\Gamma(p+1)\left(\frac{1-c^2}{(1-c\sin 2t)}\right)^{p+1}. \end{aligned} \tag{E.8}$$

Substituting (E.8) in (E.6) and simplifying further, we get

$$I = \frac{1}{2\pi} r^{2p}\Gamma(p+1)(1-c^2)^{p+(1/2)} \int_0^{2\pi} \frac{|\sin t|^p}{(1-c\sin t)^{p+1}}\mathrm{d}t. \tag{E.9}$$

Now, the integral I_2 to be solved is as follows:

$$I_2 = \int_0^{2\pi} \frac{|\sin t|^p}{(1-c\sin t)^{p+1}}\mathrm{d}t. \tag{E.10}$$

Then, we can write (E.10) as

$$I_2 = 2\int_0^{\pi/2} \frac{(\sin t)^p}{(1-c\sin t)^{p+1}}\mathrm{d}t + 2\int_\pi^{3\pi/2} \frac{(-\sin t)^p}{(1-c\sin t)^{p+1}}\mathrm{d}t. \tag{E.11}$$

Putting $-\sin t = x$ in (E.11), we have

$$I_2 = 2\int_0^1 \frac{x^p}{(1-cx)^{p+1}\sqrt{1-x^2}}\mathrm{d}x + 2\int_0^1 \frac{x^p}{(1+cx)^{p+1}\sqrt{1-x^2}}\mathrm{d}x. \tag{E.12}$$

Let the first integral of (E.12) be

$$I_3 = \int_0^1 x^p(1-cx)^{-(p+1)}(1-x^2)^{-1/2}\mathrm{d}x, \tag{E.13}$$

and the second integral of (E.12) be

$$I_4 = \int_0^1 x^p (1+cx)^{-(p+1)} (1-x^2)^{-1/2} \mathrm{d}x. \tag{E.14}$$

Using [107, 3.211], we can write I_3 and I_4 in (E.13) and (E.14) as

$$I_3 = \mathcal{B}\left(\frac{1}{2}, p+1\right) F_1\left(\left(p+1, p+1, \frac{1}{2}, p+\frac{3}{2}; c, -1\right)\right) \tag{E.15}$$

and

$$I_4 = \mathcal{B}\left(\frac{1}{2}, p+1\right) F_1\left(\left(p+1, p+1, \frac{1}{2}, p+\frac{3}{2}; -c, -1\right)\right), \tag{E.16}$$

respectively, where $\mathcal{B}(\cdot,\cdot)$ is the beta function (please see [107, 8.380]) and F_1 is the hypergeometric function of two variables (please see [107, 9.180]). Then, we can write I_2 in (E.12) as

$$\begin{aligned} I_2 = 2\mathcal{B}\left(\frac{1}{2}, p+1\right) \Bigg[& F_1\left(\left(p+1, p+1, \frac{1}{2}, p+\frac{3}{2}; c, -1\right)\right) \\ & + F_1\left(\left(p+1, p+1, \frac{1}{2}, p+\frac{3}{2}; -c, -1\right)\right) \Bigg]. \end{aligned} \tag{E.17}$$

Substituting I_2 from (E.17) in (E.9), we can write (9.11) as follows:

$$\begin{aligned} I = \frac{1}{\pi} r^{2p} \Gamma(p+1) (1-c^2)^{p+(1/2)} \mathcal{B}\left(\frac{1}{2}, p+1\right) \\ \times \Bigg[F_1\left(\left(p+1, p+1, \frac{1}{2}, p+\frac{3}{2}; c, -1\right)\right) \\ + F_1\left(\left(p+1, p+1, \frac{1}{2}, p+\frac{3}{2}; -c, -1\right)\right) \Bigg]. \end{aligned} \tag{E.18}$$